Optimization-Based Finite Element Methods for Evolving Interfaces

Dissertation

zur Erlangung des akademischen Grades eines

Doktors der Naturwissenschaften

(Dr. rer. nat.)

Der Fakultät für Mathematik der

Technischen Universität Dortmund

vorgelegt von

Christopher Basting

im Mai 2017

Dissertation

Optimization-Based Finite Element Methods for Evolving Interfaces

Fakultät für Mathematik
Technische Universität Dortmund

Erstgutachter: Prof. Dr. Dmitri Kuzmin
Zweitgutachter: Prof. Dr. Stefan Turek

Tag der mündlichen Prüfung: 21.07.2017

Mathematics is the art of giving the same name to different things.

Henri Poincaré

Abstract

This thesis is concerned with the development of new approaches to redistancing and conservation of mass in finite element methods for the level set transport equation.
The first proposed method is a PDE- and optimization-based redistancing scheme. In contrast to many other PDE-based redistancing techniques, the variational formulation derived from the minimization problem is elliptic and can be solved efficiently using a simple fixed-point iteration method. Artificial displacements are effectively prevented by introducing a penalty term. The objective functional can easily be extended so as to satisfy further geometric properties.
The second redistancing method is based on an optimal control problem. The objective functional is defined in terms of a suitable potential function and aims at minimizing the residual of the Eikonal equation under the constraint of an augmented level set equation. As an inherent property of this approach, the interface cannot be displaced on a continuous level and numerical instabilities are prevented.
The third numerical method under investigation is an optimal control approach designed to enforce conservation of mass. A numerical solution to the level set equation is corrected so as to satisfy a conservation law for the corresponding Heaviside function. Two different control approaches are investigated.
The potential of the proposed methods is illustrated by a wide range of numerical examples and by numerical studies for the well-known rising bubble benchmark.

Acknowledgements

First and foremost, I would like to express my sincere gratitude to my advisor Prof. Dr. Dmitri Kuzmin. He gave me the opportunity to work on this interesting topic and enabled me to attend many scientific conferences and workshops. Thank you for your continuous support, guidance and encouragement during my PhD studies, and for the many helpful discussions.
I also thank Dr. John N. Shadid from Sandia National Laboratories for the fruitful collaboration on the joint paper and Prof. Dr. Christian Meyer for interesting discussions.
In general, I would like to thank my colleagues at the University of Erlangen-Nuremberg and the TU Dortmund University for the familiar and welcoming atmosphere.
All numerical results presented in this thesis have been computed using the open source computing platform FEniCS. Therefore, I would like to thank the developers for this versatile and stable software.
Special thanks is directed to the following people for carefully proofreading this thesis and providing me with valuable feedback: Christian Wiesel, Dmitri Kuzmin, Steffen Basting, Stefan Turek and Thomas Guess. I would also like to thank Christoph Lohmann for his help on any LaTeX or software problem.
Finally, I would like to express my deepest appreciation to my family for their love and support throughout my life: Thank you Christian, Mama, Papa, Steffen, Melanie, Christine, Anton, Anja and Klaus! Last but not least, I thank Emma who has always been able to put a smile on my face.

Thank you all!

Contents

1 Introduction

Evolving interfaces occur in a large variety of scientific problems and practical applications, such as image processing, medical simulations and multi-phase flows. The shape of these interfaces might be complex and undergo topological changes. In two-phase flow problems for example, two immiscible fluids with different densities and viscosities are separated by an interface. Accurate knowledge of the interface location plays an important role in the modeling of such flows, because density, viscosity and surface tension directly depend on it. Unfortunately, both fluid behavior and interface motion are hard to predict and the use of experiments and measurements is often limited. An appealing alternative is the numerical modeling of free interface problems which gives a deeper insight into the physical phenomena in many cases.

1.1. Objectives

Even though a multitude of numerical algorithms for free interface problems exist, neither of them is perfect and problems such as an unintended loss of volume must be considered. One popular representative of the class of so-called interface-capturing approaches is the level set method. The key idea of this technique boils down to the implicit description of the interface as the zero level set of a scalar function. The motion of the interface is governed by the corresponding level set transport equation. This approach offers several major benefits: the ease of implementation, the possibility to use higher order approximations and the potential to allow for topological changes. Unfortunately, level set methods are generally non-conservative, i.e. volume may be lost or gained. Furthermore, on a discrete level the advection of the level set function and the evaluation of interface related quantities such as normal vector and curvature often rely on the use of level set functions that are close to signed distance functions. Even if the level set function is initialized as signed distance to the interface, this property is not preserved as the interface evolves. In order to compensate for these drawbacks, extensions of the level set method have been developed to improve mass conservation and to correct level set functions so as to approximate signed distance functions. The latter methods are commonly referred to as redistancing schemes.

The primary goal of the present work is to elaborate on the application of level set methods to the simulation of free interface problems. In particular, we consider redistancing schemes and conservative extensions of the level set approach.

In Chapter 5, two optimization-based redistancing techniques are presented and analyzed. The first one is an unconstrained optimization problem, in which the residual of a suitable potential function is minimized so as to approximate a signed distance function [BK13]. An unintended artificial interface displacement is prevented by adding a suitable penalty term. Different potential functions can be employed and offer the possibility to incorporate further design criteria. The resulting numerical scheme is very robust and global, so that only very few iterations are needed for this method to converge. The second approach is based on a constrained optimal control problem [BKS16]. The formulation of the state equation is based on the level set transport equation augmented by a source term, correcting the solution so as to minimize the objective functional. The potentials from the previous approach can be employed for the definition of the objective functional. Since transport equation and redistancing task are solved simultaneously, this is a monolithic approach.

A conservative extension based on an optimal control approach [Kuz13, BK14] is presented in Chapter 6. A numerical solution to the level set equation is corrected so as to satisfy a conservation law for the corresponding Heaviside function. In contrast to many other conservative approaches, the procedure corrects locally and is conservative to machine precision.

1.2. Related Work

Over the past decades, many redistancing techniques have been developed. They can generally be classified into geometric and PDE-based redistancing approaches. Former ones rely on the direct computation of the interface and usually require an explicit localization. PDE-based methods on the other hand build on solving a redistancing equation and mostly avoid the explicit and computationally expensive localization of the interface.

One of the most popular geometric redistancing approaches is the fast-marching method [Tsi94, Set96b, Cho01], which constructs the level set function by using upwind values. This approach is limited to structured meshes and the generalization to higher degree approximations is complicated. However, many redistancing approaches only construct the level set function in immediate vicinity of the interface where accuracy is most crucial and make use of this approach to efficiently extend values to the remaining computational domain. Another interesting geometric redistancing approach was proposed by Ausas et al. in [ADB11]. In a thin interface region, the level set function is computed explicitly to be the signed distance to the interface. To avoid inaccuracies in mass caused by the redistancing procedure, the level set function is corrected by an element-wise shift before the values are extended to the remaining domain.

PDE-based approaches are mostly based on minimizing the residual of the Eikonal equation to obtain a signed distance function. The so-called hyperbolic redistancing approach was introduced by Sussman et al. in [SSO94]. Essentially, a signed distance function is obtained by solving a hyperbolic transport equation to steady state. On a discrete level however, a suitable

regularization of the sign function must be employed and the approach notably depends on this choice [CT08]. The convected level set method proposed by Ville et al. [VSC11] tries to combine the hyperbolic redistancing equation with the level set transport equation. Unfortunately, the resulting numerical approach is very sensitive to the chosen parameters and accuracy might not be satisfactory. Another extension of the hyperbolic redistancing approach was introduced in the paper by Li et al. [LXGF10], in which an energy-minimizing gradient flow problem is considered. However, the approach faces time step restrictions which may lead to significant computational costs. Furthermore, the interface might be moved during redistancing.

Several conservative extensions of the level set method have already been developed. A simple technique is based on shifting the level set function by a suitably chosen constant so as to conserve volume [Smo01]. The constant can efficiently be determined using fixed-point iteration techniques. The major drawback of this approach is that it acts globally and in an unphysical manner, i.e. mass may be redistributed to wrong places. An appealing alternative is the approach originally presented by Olsson and Kreiss [OK05, OKZ07]. Its key idea is to combine the level set method with a volume of fluid technique. For the latter one, conservative advection schemes exist. A similar technique is employed in the dual level set approach proposed by Lesage and Dervieux [LD09], for which a transport equation for a characteristic function is solved in a conservative manner. The coupling with the level set function is achieved by solving the dual level set equation. Unfortunately, this approach faces convergence problems and uniqueness might not be clear. Yet another very similar method was proposed by Kees et al. [KAFB11], in which the transport equation for the corresponding Heaviside function is solved conservatively. Using a variational approach, the level set function is coupled with the Heaviside function. Further conservative level set extensions have been reported in [PSVW05, SP00, DHO+14, DPLFP06].

1.3. Outline

This thesis is organized as follows:

Chapter 2 introduces the generic transport equation, from which many specific models such as the level set equation are deduced. The following section focuses on free interface problems. After a brief introduction, numerical solution strategies are presented and classified. The chapter concludes with three free interface model problems from different scientific disciplines.

Chapter 3 is concerned with an introduction to Galerkin methods. After defining an abstract problem setting, stating fundamental results and studying two model problems, the focus is laid on finite elements as special class of Galerkin approximations. A brief introduction to stability and numerical analysis is provided for the model problems, before investigating the application to hyperbolic problems. To achieve numerical stability in finite element based schemes for hyperbolic problems, the SUPG stabilization technique is presented. The chapter closes with a brief introduction to time-discretization approaches.

Since level set methods are of primary interest in this thesis, an extensive introduction is provided in Chapter 4. Special emphasis is laid on the signed distance function property and the application to modeling the evolution of an interface. Next, the finite element discretization

of the level set approach is discussed and the discrete interface reconstruction is investigated. The last part of the chapter is concerned with time discretizations of the level set equation.

In Chapter 5 the focus is laid on level set redistancing techniques. The chapter begins with an overview of desirable properties of such methods. Redistancing methods can generally be classified as either geometric or PDE-based approaches. The first section provides an overview of commonly used geometric redistancing schemes and discusses their advantages and drawbacks. The following sections focus on PDE-based approaches. First, the well-known hyperbolic redistancing approach developed by Sussman et al. [SSO94] is presented. On this basis, the monolithic convected level set method [VSC11] is introduced. Next, the parabolic redistancing [LXGF10] technique is considered, before turning to the optimization based elliptic redistancing approach [BK13]. This particular approach is investigated thoroughly and the use of different potential functions is motivated, before the corresponding finite element discretization is given. In the next section, an optimal control approach [BKS16] is proposed and analyzed. Discrete optimality conditions are derived and numerical solution strategies are outlined. The chapter concludes with detailed numerical examples to assess the proposed numerical methods.

Chapter 6 deals with conservative level set methods. After providing an a-priori estimate, the level set shifting approach is introduced, in which conservation of mass is accomplished by adding a suitable constant to the level set function [Smo01]. The following sections outline more commonly used approaches, which are all essentially based on the combination of the level set method with the conservative volume of fluid technique. Then, an optimal control approach is proposed, in which a non-conservative level set function is corrected so as to satisfy a conservation law for the corresponding Heaviside function. Properties and the discretization of the optimal control problem are discussed and a detailed numerical evaluation is provided in the final section.

Chapter 7 introduces a model two-phase flow problem. The first sections address the derivation of the incompressible Navier-Stokes equations from conservation laws. Special emphasis is laid on the coupling conditions and the application of the level set method in the context of two-phase flow problems. The numerical level set approaches proposed and investigated in the previous chapters are then validated for the rising bubble benchmark problem [HTK+07].

1.4. Original publications

Some of the results in this thesis have already been published in the articles listed below and are joint work with the author's advisor Dmitri Kuzmin. The optimal control approach for redistancing was partly developed in collaboration with John N. Shadid.

[Bas12] Basting, Christopher: *Enforcing the Eikonal equation as a constraint in finite element level set methods*, University of Erlangen-Nürnberg, Diplomarbeit, 2012

[BK13] Basting, Christopher ; Kuzmin, Dmitri: A minimization-based finite element formulation for interface-preserving level set reinitialization. In: *Computing* 95 (2013), Nr. 1, 13-25. http://dx.doi.org/10.1007/s00607-012-0259-z. – DOI 10.1007/s00607–012–0259–z. – ISSN 0010–485X

[BK14] Basting, Christopher ; Kuzmin, Dmitri: Optimal control for mass conservative level set methods. In: *Journal of Computational and Applied Mathematics* 270 (2014), 343 - 352. http://dx.doi.org/10.1016/j.cam.2013.12.040. – DOI 10.1016/j.cam.2013.12.040. – ISSN 0377–0427

[BKS16] Basting, Christopher ; Kuzmin, Dmitri ; Shadid, John N.: Optimal control for reinitialization in finite element level set methods. In: *International Journal for Numerical Methods in Fluids* (2016). http://dx.doi.org/10.1002/fld.4348. – DOI 10.1002/fld.4348. – ISSN 1097–0363

The optimal control approach for mass conservation builds on an idea originally presented in

[Kuz13] Kuzmin, Dmitri: An optimization-based approach to enforcing mass conservation in level set methods. In: *Journal of Computational and Applied Mathematics* (2013), -. http://dx.doi.org/10.1016/j.cam.2013.09.009. – DOI 10.1016/j.cam.2013.09.009. – ISSN 0377–0427

The numerical results presented in this thesis are own work of the author. They have all been implemented in the open-source C++ and Python library FEniCS, a computing platform for partial differential equations [KLR+12].[1]

[1] More information on FEniCS can be found online at https://fenicsproject.org

2 Transport Equations and Free Interfaces

Moving interfaces occur in a variety of scientific problems and practical applications ranging from image processing techniques to the simulation of crystal growth and numerical fluid dynamics with multiple phases. Accurate knowledge of the interface position is frequently crucial for the underlying models, but explicit solutions to such problems rarely exist. Many important physical effects such as surface tension take place on the interface. Hence, a multitude of numerical approaches for the approximation of propagating interfaces has been developed in the past decades.

The evolution of general quantities can be described by mathematical models based on differential equations. In fluid dynamics for example, models are derived from physical conservation laws. The Navier-Stokes equations form a well-known model of the motion of fluids and are directly obtained from conservation of mass, momentum and energy, cf. Chapter 7.

In this introductory chapter, we will present basic concepts of (numerical) approaches for free interface problems. In the first section, we will introduce the generic transport equation, from which specific transport problems can be derived. Based on these transport equations, the propagation of an interface can be modeled mathematically. In the subsequent section, we highlight common numerical techniques for the description of an evolving interface. Of particular interest in this thesis is the *level set method*, which will be thoroughly discussed in Chapter 4. The chapter concludes by showing three interface problems from scientific disciplines, to which the presented techniques are commonly applied.

2.1. Transport Equations

Following [KH15, Kuz10], we introduce the *generic transport equation*. Therefore, let us consider a bounded domain $\Omega \subset \mathbb{R}^d$ and a time-dependent conserved quantity $c : (0,T) \times \Omega \to \mathbb{R}$. For an arbitrary control volume $V \subseteq \Omega$ with sufficiently smooth boundary, the temporal variation of c is given by

$$\frac{\mathrm{d}}{\mathrm{d}t} \int_V c(t,\mathbf{x}) \, \mathrm{d}\mathbf{x} + \int_{\partial V} \mathbf{f} \circ c(t,\mathbf{x}) \cdot \mathbf{n} \, \mathrm{d}\sigma = \int_V s(t,\mathbf{x}) \, \mathrm{d}\mathbf{x}, \tag{2.1}$$

where $\mathbf{f}$ denotes the *flux function*, describing the rate at which the mass enters or leaves V and s a source term taking internal sources or sinks into account. Under sufficient regularity assumptions on $c(t, \mathbf{x})$ and $\mathbf{f} \circ c(t, \mathbf{x})$, we can transform the surface integral in (2.1) into a volume integral by application of the divergence theorem:

$$\int_V \left[\frac{\partial}{\partial t} c(t, \mathbf{x}) + \nabla \cdot \big(\mathbf{f} \circ c(t, \mathbf{x}) \big) - s(t, \mathbf{x}) \right] \mathrm{d}\mathbf{x} = 0. \tag{2.2}$$

Since this holds for any control volume V, we obtain the partial differential equation

$$\frac{\partial}{\partial t} c(t, \mathbf{x}) + \nabla \cdot \big(\mathbf{f} \circ c(t, \mathbf{x}) \big) = s(t, \mathbf{x}) \qquad \text{in } \Omega. \tag{2.3}$$

The flux function typically models the transport of c by *convective* and *diffusive* effects:

$$\big(\mathbf{f} \circ c(t, \mathbf{x}) \big) \coloneqq \mathbf{v}(t, \mathbf{x}) c(t, \mathbf{x}) - d(t, \mathbf{x}) \nabla c(t, \mathbf{x}). \tag{2.4}$$

The first term describes the convective transport downstream by the velocity field $\mathbf{v}(t, \mathbf{x})$. The second term takes diffusive effects into account (usually taking place on a molecular level), which are commonly modeled in terms of a diffusion coefficient $d(t, \mathbf{x}) \geq 0$. Substituting (2.4) into (2.3), we obtain the *generic transport equation*

$$\frac{\partial}{\partial t} c + \nabla \cdot (\mathbf{v} c) - \nabla \cdot (d \nabla c) = s \qquad \text{in } \Omega. \tag{2.5}$$

For the well-posedness, we must provide an initial condition

$$c(0, \mathbf{x}) \coloneqq c_0(\mathbf{x}) \qquad \text{in } \Omega, \tag{2.6}$$

and suitable boundary conditions on $\partial\Omega$. From the generic transport equation (2.5), we can deduce models of several types of partial differential equations:

- *Elliptic transport problems*: in the steady-state limit, the time derivative vanishes and the equation reduces to

  $$\nabla \cdot (\mathbf{v} c - d \nabla c) = s \qquad \text{in } \Omega. \tag{2.7}$$

  In absence of convective effects, i.e. for $\mathbf{v} \equiv 0$, the equation further reduces to the (generalized) *Poisson equation*

  $$-\nabla \cdot (d \nabla c) = s \qquad \text{in } \Omega. \tag{2.8}$$

  In particular, for a constant diffusion coefficient and a vanishing right hand side, the Laplace equation is obtained.

- *Parabolic transport problems*: if the fluid is at rest, i.e. $\mathbf{v} \equiv 0$, the generic transport equation reduces to

  $$\frac{\partial}{\partial t} c - \nabla \cdot (d \nabla u) = s \qquad \text{in } \Omega. \tag{2.9}$$

This equation is commonly used to model heat conduction and other diffusive transport processes. At steady state, the Poisson equation is obtained.

- *Hyperbolic transport problems*: when no diffusive effects take place, we obtain

$$\frac{\partial}{\partial t}c + \nabla \cdot (\mathbf{v}c) = s \qquad \text{in } \Omega. \tag{2.10}$$

In the homogeneous case $s \equiv 0$, we obtain the *continuity equation*

$$\frac{\partial}{\partial t}c + \nabla \cdot (\mathbf{v}c) = 0 \qquad \text{in } \Omega, \tag{2.11}$$

which can be derived from conservation laws. In fluid dynamics, it models the evolution of the fluid density.

2.2. Interface Description

We now turn to problems involving free interfaces. In the case of the two-phase flow problem for example, the evolution of two immiscible fluids separated by an evolving interface is considered. Each phase can be modeled using the Navier-Stokes equations, and the interaction between the two phases is accounted for by suitable coupling conditions on the interface. Therefore, accurate knowledge of the position of the interface is of great importance in this setting. This problem is studied in Chapter 7 in more detail.

In this section we will present an overview of numerical methods for free interface problems. Those are commonly classified as follows:

1. *Interface tracking methods* explicitly describe the interface by adding a specific structure to the mesh. The actual movement of the interface is then achieved by moving the associated nodes according to the given velocity field. It is therefore considered to be a Lagrangian approach. Interface tracking methods can be very accurate, but might require an update of the computational mesh as quality deteriorates when nodes are moved with the interface, particularly when interfaces are complex and not smooth.
2. *Interface capturing methods* use an implicit description of the interface and are Eulerian type techniques. They are more flexible than the interface tracking approaches since they do not require re-meshing, but are also less accurate in certain situations. The level set method to be introduced in this chapter is amongst the most popular representatives of interface capturing approaches. Other common choices are the related phase field approaches and volume of fluid methods.

A detailed discussion of different approaches can be found in [Smo01]. The structure of this section is based on the introductory chapter in the thesis of Parolini [Par04].

2.2.1. Interface Tracking Methods

A usual approach in interface tracking methods is to represent the interface by a set of marker points, ideally located on the interface. The interface between these points is usually interpolated. Following [Hym84, HN81, Par04], the marker points can be represented as the height function $h(t, \mathbf{x})$ w.r.t. the mesh. The evolution of this function can then be expressed by the kinematic condition

$$\frac{\partial}{\partial t} h(t, \mathbf{x}) + \mathbf{v} \cdot \nabla h(t, \mathbf{x}) = 0, \tag{2.12}$$

for a given velocity field $\mathbf{v}$. Unfortunately, this approach cannot handle complex interface topologies.

2.2.2. Interface Capturing Methods

Two of the most commonly used representatives of interface capturing approaches are the *level set method* and the *volume of fluid method*. Both methods are based on solving the continuity equation (2.11). In case of the two-phase flow problem, the velocity field $\mathbf{v}$ is obtained from solving the Navier-Stokes equations.

2.2.2.1. Volume of Fluid Method

The volume of fluid method introduced by Hirt and Nichols [HN81] is based on the advection of an indicator function $\psi(t, \mathbf{x})$. The value of ψ in each cell is the volume fraction of one particular phase in this cell. Hence, in cells containing portions of both phases, the value of ψ is between 0 and 1. In all other cells it is either 0 or 1. The evolution of the interface is then governed by the advection of the indicator function ψ:

$$\frac{\partial}{\partial t} \psi(t, \mathbf{x}) + \mathbf{v}(t, \mathbf{x}) \cdot \nabla \psi(t, \mathbf{x}) = 0 \qquad \text{in } \Omega. \tag{2.13}$$

General phase-dependent and piecewise constant quantities $\eta(t, \mathbf{x})$ (for example density or viscosity) can then be expressed by

$$\eta(t, \mathbf{x}) = \psi(t, \mathbf{x})\eta_1 + (1 - \psi(t, \mathbf{x}))\eta_2. \tag{2.14}$$

Note that by design of the method, the interface is not defined sharply but in the range of a cell. From a numerical point of view, special care needs to be taken when solving (2.13) due to the discontinuous function $\psi(t, \mathbf{x})$. The accuracy of the interface location suffers from numerical diffusion or oscillations. Extensive literature on the numerical implementation of volume of fluid methods exist. The interested reader is referred to [Par04].

2.2.2.2. Level Set Method

The level set method is based on an idea introduced by Dervieux and Thomasset [DT80], and was first proposed by Osher and Sethian [OS88]. Similarly to the volume of fluid approach, we introduce an auxiliary function $\varphi : (0,T) \times \Omega$ to describe the evolution of the interface. The two phases are told apart by the sign of the level set function φ, and consequently, the interface is given as the zero level set of φ. Again, the propagation of the interface is governed by the continuity equation

$$\frac{\partial}{\partial t}\varphi(t,\mathbf{x}) + \mathbf{v}(t,\mathbf{x}) \cdot \nabla\varphi(t,\mathbf{x}) = 0 \qquad \text{in } \Omega. \tag{2.15}$$

As we will see in the subsequent chapters, it is advantageous to initialize φ as the *signed distance function* (cf. Definition A.3) to the interface. In contrast to the volume of fluid method, the auxiliary function φ is smooth (sufficient regularity of the interface provided), and therefore better suited for the numerical solution of (2.15). Furthermore, geometrical quantities such as normal vector and curvature can easily be derived from φ as it offers a sharp representation of the interface. In terms of mass conservation, which is an inherent property of volume of fluid methods, special numerical precautions must be taken when applying the level set method. A detailed introduction will be provided in Chapter 4.

More recently, a hybrid approach was proposed in [BW13] to combine the advantages of interface tracking and interface capturing methods. It introduces an implicit level set representation to which the computational mesh is aligned by minimization of a mesh quality functional.

2.3. Free Interface Problems

In this section we present examples of free interface problems from different scientific disciplines. They all share the need for an accurate interface representation, and can be solved numerically using one of the techniques described above. Since the remainder of this thesis focuses on level set methods, we will restrict ourselves to this particular interface capturing technique.

2.3.1. Simulation of Tumor Growth

We illustrate the usage of level set functions for this free boundary problem based on the work presented in [APB00, HMS06]. We consider a domain $\Omega \subset \mathbb{R}^d$, $d \in \{1,2,3\}$, in which the time dependent tumor is contained. The set consisting of all tumor cells is denoted by $\Omega_1(t)$. The tumor growth depends on many variables of the biological system [HMS06]: density of living tumor cells u_T, density of dead tumor cells u_D, density of new capillaries u_C, nutrient concentration u_N, and tumor angiogenic factor concentration u_A. Several model assumptions are made. An increase in u_T requires a sufficient nutrition concentration. Conversely, low nutrition concentration causes a decrease of living tumor cells. Living tumor cells may move to areas of higher nutrition concentration, dead cells cannot move. Living tumor cells increase the concentration u_A, which diffuses also into the domain surrounding the tumor. Nutrition is provided at a linear rate. Putting all assumptions together, a mathematical model is derived,

in which the evolution of the tumor domain Ω_1 is described by a normal velocity field F on the tumor boundary:

$$\frac{\partial}{\partial t}\varphi + F|\nabla\varphi| = 0. \tag{2.16}$$

The velocity F is only defined on $\partial\Omega_1$, which is why it must be extended to Ω. The authors in [HMS06] see several considerable advantages in using the level set approach for this free boundary problem:

- The sign of the level set function tells the tumor domain Ω_1 apart from its surrounding domain Ω_2.
- As a natural attribute of level set functions, geometric properties such as normal vector and curvature on the boundary are readily available.
- The model can be formulated in all space dimensions $d \in \{1, 2, 3\}$.
- A wide range of efficient level set method based algorithms exists.

2.3.2. Mean Curvature Flow

In *mean curvature flow* problems, the interface moves in normal direction with a velocity whose magnitude is directly proportional to the interface curvature. Such flows arise in many physical models such as expansion of flames or growth processes (e.g. crystal growth, tumor growth). Other fields of application can be found in image processing such as image restoration, segmentation or surface reconstruction. In mean curvature flow problems, the velocity $\mathbf{v}$ of the interface $\Gamma(t)$ can be described by

$$\mathbf{v}(t, \mathbf{x}) = -b\kappa(t, \mathbf{x})\hat{\mathbf{n}}(t, \mathbf{x}) \qquad x \in \Gamma(t), \tag{2.17}$$

where $\hat{\mathbf{n}}$ is the interface normal vector and κ the interface curvature. The constant b is a scaling factor and its sign determines the direction of movement (expansion or shrinking). As in (2.16), the evolution of the interface can be described in terms of a level set function governed by the transport equation

$$\frac{\partial}{\partial t}\varphi + V|\nabla\varphi| = 0, \tag{2.18}$$

where V denotes the component of $\mathbf{v}$ normal to the interface. Numerical methods are used to solve this partial differential equation.

2.3.3. Computational Physics

Another wide field of applications of the level set method is computational physics. Particular examples are compressible and incompressible two-phase flows, solid-fluid couplings, liquid-gas interactions and free surfaces. As for the previous problems, the level set method is used to capture the moving interface at which important physical effects take place. In Chapter 4, we

will consider the two-phase problem as a particular example for problems from this scientific discipline.

3 Approximation by Galerkin Methods

In this chapter we study (linear) problems as they usually arise in variational formulations of partial differential equations. In particular, we consider Galerkin approximations, in which the solution space of such problems is replaced by a suitable finite dimensional space. For both, the continuous and the discrete problem, conditions guaranteeing well-posedness of the problem in the sense of Hadamard (cf. Definition 3.1) and stability with respect to the given data can be formulated. As a particular representative of a Galerkin approximation approach, we introduce the finite element method and derive some stability and a priori error estimates for model problems. The underlying theory is very general and can be applied to a wide range of (sub-)problems.

In the first section, an abstract problem setting is formulated. In this setting, we state conditions for stability and well-posedness, and verify these for two model problems. In the following section, the general concept of Galerkin approximations is presented. Subsequently, we introduce the *finite element method* and formulate conditions for stability, solvability and uniqueness. Important concepts for the numerical analysis are briefly reviewed, and stability as well as error estimates are derived for the two model problems under consideration. The *streamline upwind Petrov Galerkin stabilization technique* is presented, applied to the hyperbolic model problem, and a general error bound is quoted. Finally, in the last section of this chapter, we comment on time discretization approaches to obtain fully discrete numerical schemes for time-dependent problems.

The chapter is largely based on the books by Ern and Guermond [EG04], Larsson and Thomée [LT05], Knabner and Angermann [KA03] as well as Quarteroni and Valli [QV08]. The section on stabilization of finite elements follows the book by Gross and Reusken [GR11].

3.1. Abstract Problem Setting

Given two Banach spaces U and V equipped with norms $\|\cdot\|_U$, $\|\cdot\|_V$, a continuous bilinear form $\mathsf{a} : U \times V \to \mathbb{R}$ and a bounded linear form $\mathsf{b} \in V^*$, we consider the following abstract problem:

$$\text{Find } u \in U \text{ such that} \quad \mathsf{a}(u, v) = \mathsf{b}(v) \quad \text{for all } v \in V. \tag{3.1}$$

The function space U is usually referred to as *solution space*, and V as *test space*.

Definition 3.1 (Well-posedness, Hadamard [EG04])
Problem (3.1) is called *well-posed* if it has a unique solution and the solution is stable with respect to the data, i.e.

$$\exists c > 0 \ : \ \forall \mathsf{b} \in V^* \ : \quad \|u\|_U \leq c \, \|\mathsf{b}\|_{V^*} \, . \tag{3.2}$$

The following result provides conditions for the well-posedness of the abstract problem (3.1):

Theorem 3.2 (Banach-Nečas-Babuška [EG04, Theorem 2.6])
Let U and V be Banach spaces and V be reflexive. Further let $\mathsf{a} : U \times V \to \mathbb{R}$ be a continuous bilinear form and $\mathsf{b} \in V^*$ bounded. Then, problem (3.1) is well-posed if and only if the *inf-sup conditions*

$$\exists \alpha > 0 \ : \quad \inf_{u \in U} \sup_{v \in V} \frac{\mathsf{a}(u,v)}{\|u\|_U \, \|v\|_V} \geq \alpha, \tag{3.3a}$$

$$\forall v \in V \ : \quad \big(\forall u \in U, \ \mathsf{a}(u,v) = 0\big) \implies \big(v = 0\big). \tag{3.3b}$$

are satisfied. Moreover, if conditions (3.3a) and (3.3b) are fulfilled, the following a priori estimate holds:

$$\forall \mathsf{b} \in V^* : \qquad \|u\|_U \leq \frac{1}{\alpha} \, \|\mathsf{b}\|_{V^*} \, . \tag{3.4}$$

A proof of this theorem can be found in [EG04]. The Banach-Nečas-Babuška Theorem is sometimes also referred to as "Generalized Lax-Milgram Theorem".

For simplicity, we now assume U and V to be identical Hilbert spaces, even though (reflexive) Banach spaces can be considered in a more general setting. Problem (3.1) then reduces to:

$$\text{Find } u \in V \text{ such that } \quad \mathsf{a}(u,v) = \mathsf{b}(v) \ \text{ for all } v \in V. \tag{3.5}$$

A bilinear form $\mathsf{a}(\cdot,\cdot)$ is said to be V-*coercive*, if

$$\exists C_V > 0 \ : \qquad \mathsf{a}(v,v) \geq C_V \, \|v\|_V^2 \quad \forall v \in V. \tag{3.6}$$

The restriction to Hilbert spaces makes V-coercivity of $\mathsf{a}(\cdot,\cdot)$ a sufficient but not a necessary condition for the well-posedness:

Theorem 3.3 (Lax-Milgram [EG04])
Let V be a Hilbert space ($U := V$), $\mathsf{a} : V \times V \to \mathbb{R}$ be a continuous, coercive bilinear form and $\mathsf{b} \in V^*$. Then, problem (3.5) is well-posed and

$$\|u\|_V \leq \frac{1}{C_V} \, \|\mathsf{b}\|_{V^*} \, , \tag{3.7}$$

where C_V is the V-coercivity constant from (3.6).

A proof of this theorem can be found in [LT05]. The theorem is also a direct consequence of Theorem 3.2. Note that if the bilinear form $\mathsf{a}(\cdot,\cdot)$ is symmetric and coercive, problem (3.5) is equivalent to the minimization problem

$$\min_{u\in V}\left(\frac{1}{2}\mathsf{a}(u,u)-\mathsf{b}(u)\right).$$

This characterization is sometimes referred to as *Dirichlet's principle*; the interested reader is referred to [LT05, Chapter 3].

3.1.1. Poisson's Problem

Let Ω be an open domain and $U = V = H_0^1(\Omega)$. The homogeneous Dirichlet problem for the Poisson equation is given by: find $u \in C^2(\Omega)$ such that

$$-\Delta u = f \qquad \text{in } \Omega, \tag{3.8a}$$
$$u = 0 \qquad \text{on } \partial\Omega, \tag{3.8b}$$

with right hand side $f \in L^2(\Omega)$. After multiplying (3.8a) by a test function $v \in H_0^1(\Omega)$, integrating over Ω, applying the integration by parts formula and invoking the homogeneous boundary condition (3.8b), we obtain the *weak form* of the problem:

$$\text{Find } u \in H_0^1(\Omega) \text{ such that} \tag{3.9a}$$
$$\int_\Omega \nabla u\cdot\nabla v\,\mathrm{d}\mathbf{x} = \int_\Omega fv\,\mathrm{d}\mathbf{x} \qquad \forall v\in H_0^1(\Omega). \tag{3.9b}$$

Introducing the bilinear form

$$\mathsf{a}(u,v) \coloneqq \int_\Omega \nabla u\cdot\nabla v\,\mathrm{d}\mathbf{x}, \tag{3.10}$$

and the linear form

$$\mathsf{b}(v) \coloneqq \int_\Omega fv\,\mathrm{d}\mathbf{x}, \tag{3.11}$$

equation (3.9a) can be rewritten as

$$\mathsf{a}(u,v) = \mathsf{b}(v) \qquad \forall v\in H_0^1(\Omega). \tag{3.12}$$

The forms $\mathsf{a}(\cdot,\cdot)$ and $\mathsf{b}(\cdot)$ are both continuous and by application of Poincaré's inequality (A.9),

$$\mathsf{a}(u,u) = \int_\Omega \nabla u\cdot\nabla u\,\mathrm{d}\mathbf{x} \geq c_\Omega \|u\|_V^2, \tag{3.13}$$

$\mathsf{a}(\cdot,\cdot)$ is also V-coercive. Theorem 3.3 therefore ensures that (3.9a) admits a unique solution u, and the stability estimate

$$\|u\|_{H^1(\Omega)} \leq c\,\|f\|_{V^*} \leq C\,\|f\|_{L^2(\Omega)} \tag{3.14}$$

holds. The last inequality in (3.14) is obtained by application of the Cauchy-Schwarz and Poincaré's inequality (Eq. (A.12))

$$|\mathsf{b}(v)| = \left|(f,v)_{L^2(\Omega)}\right| \leq \|f\|_{L^2(\Omega)}\,\|v\|_{L^2(\Omega)} \leq C\,\|f\|_{L^2(\Omega)}\,\|v\|_{H^1(\Omega)}\,, \tag{3.15}$$

which directly implies

$$\|\mathsf{b}\|_{V^*} \leq C\,\|f\|_{L^2(\Omega)}\,. \tag{3.16}$$

Let us now consider a different boundary condition. We replace the Dirichlet boundary condition in (3.8b) by the homogeneous Neumann boundary condition to obtain the following problem. Let $f \in L^2(\Omega)$ and $g \in L^2(\partial\Omega)$.

$$\text{Find } u \in V = H^1(\Omega) \text{ such that:} \tag{3.17a}$$

$$-\Delta u = f \qquad \text{in } \Omega, \tag{3.17b}$$

$$\partial_n u = g \qquad \text{on } \partial\Omega. \tag{3.17c}$$

Application of the Gauß theorem

$$\int_{\partial\Omega} g \,\mathrm{d}\sigma = \int_{\partial\Omega} \nabla u \cdot \mathbf{n} \,\mathrm{d}\sigma = \int_{\Omega} \Delta u \,\mathrm{d}\mathbf{x} = -\int_{\Omega} f \,\mathrm{d}\mathbf{x}, \tag{3.18}$$

reveals that the data f and g must satisfy the *compability condition*

$$\int_{\Omega} f \,\mathrm{d}\mathbf{x} + \int_{\partial\Omega} g \,\mathrm{d}\sigma = 0. \tag{3.19}$$

Multiplication of (3.17b) by an arbitrary test function $v \in H^1(\Omega)$ and integration over Ω gives the variational form of the problem: find $u \in H^1(\Omega)$ such that

$$\mathsf{a}(u,v) = \mathsf{b}(v), \qquad \forall v \in H^1(\Omega). \tag{3.20}$$

with bilinear and linear form

$$\mathsf{a}(u,v) \coloneqq \int_{\Omega} \nabla u \cdot \nabla v \,\mathrm{d}\mathbf{x}, \tag{3.21a}$$

$$\mathsf{b}(v) \coloneqq \int_{\Omega} f v \,\mathrm{d}x + \int_{\partial\Omega} g v \,\mathrm{d}\sigma. \tag{3.21b}$$

The solution of (3.20) is defined uniquely up to a constant. To ensure well-posedness, one therefore commonly requires an additional condition such as the solution having zero mean over Ω, i.e. by using the space

$$H^1_{\int=0}(\Omega) \coloneqq \left\{ v \in H^1(\Omega) \ : \ \int_\Omega v \, \mathrm{d}\mathbf{x} = 0 \right\}. \tag{3.22}$$

Since for constant test functions equation (3.20) is satisfied as a direct consequence of the compatibility condition, test functions can be restricted to $H^1_{\int=0}(\Omega)$.

Lemma 3.4
Let Ω be an open domain with piecewise smooth boundary $\partial\Omega$ and $f \in L^2(\Omega)$, $g \in L^2(\partial\Omega)$ such that (3.19) holds. Then the problem

$$\text{find } u \in H^1_{\int=0}(\Omega) \text{ such that} \tag{3.23a}$$
$$\mathsf{a}(u, v) = \mathsf{b}(v), \qquad \forall v \in H^1_{\int=0}(\Omega), \tag{3.23b}$$

is *well-posed* and the solution u to (3.23) satisfies the stability estimate

$$\|u\|_{H^1(\Omega)} \leq c \left(\|f\|_{L^2(\Omega)} + \|g\|_{L^2(\partial\Omega)} \right). \tag{3.24}$$

Proof. The continuity of $\mathsf{a}(\cdot,\cdot)$ is clear. To show coercivity with respect to $H^1_{\int=0}(\Omega)$, we apply the generalized Poincaré-Friedrich inequality:

$$\mathsf{a}(u, u) = \int_\Omega \nabla u \cdot \nabla u \, \mathrm{d}\mathbf{x} \geq c_\Omega \|u\|_{H^1(\Omega)}.$$

Using the Trace Theorem A.8 we employ the inequality

$$\|v\|_{L^2(\partial\Omega)} \leq C \|v\|_{H^1(\Omega)} \qquad \forall v \in H^1(\Omega),$$

to prove the continuity of $\mathsf{b}(\cdot)$:

$$|\mathsf{b}(v)| \leq \left| \int_\Omega fv \, \mathrm{d}\mathbf{x} \right| + \left| \int_{\partial\Omega} gv \, \mathrm{d}\sigma \right| \leq \|f\|_{L^2(\Omega)} \|v\|_{L^2(\Omega)} + \|g\|_{L^2(\partial\Omega)} \|v\|_{L^2(\partial\Omega)} \leq c \|v\|_{H^1(\Omega)}.$$

Existence and uniqueness of a solution in $H^1_{\int=0}(\Omega)$ can now be concluded by a generalized version of the Lax-Milgram Theorem 3.3 (see, for example, [QV08]) and the stability estimate

$$\|u\|_V \leq \frac{1}{c_\Omega} \|\mathsf{b}\|_{V^*} \leq \frac{1}{c_\Omega} \left(\|f\|_{L^2(\Omega)} + \|g\|_{L^2(\partial\Omega)} \right) \tag{3.25}$$

holds. □

3.1.2. Unsteady Advection-Reaction

Parts of this section are based on the book by Di Pietro and Ern [DPE12, Chapter 3]. We consider the unsteady first-order advection reaction equation in a domain $\Omega \subset \mathbb{R}^d$, $d \in \{2, 3\}$:

$$\frac{\partial}{\partial t} u + \boldsymbol{\beta} \cdot \nabla u + \mu u = f \qquad \text{in } (0,T) \times \Omega, \tag{3.26a}$$

$$u = 0 \qquad \text{on } (0,T) \times \partial\Omega^{\text{in}}, \tag{3.26b}$$

$$u(0) = u_0 \qquad \text{in } \Omega. \tag{3.26c}$$

For the data we make the following assumptions:

- $f \in C^0([0,T]; L^2(\Omega))$,
- $\boldsymbol{\beta}$ and μ are (for simplicity) time-independent,
- $\boldsymbol{\beta} \in \big(\mathrm{Lip}(\Omega)\big)^d$,
- $\mu \in L^\infty(\Omega)$.

We denote

$$\Lambda \coloneqq \mu - \frac{1}{2} \nabla \cdot \boldsymbol{\beta} \tag{3.27}$$

and, by assumption, $\Lambda \in L^\infty(\Omega)$. Assuming the existence of a smooth solution to (3.26), the following energy estimate can be shown.

Lemma 3.5 (Energy Estimate [DPE12, Lemma 3.2])
Let $u \in C^0([0,T]; H^1(\Omega)) \cap C^1([0,T]; L^2(\Omega))$ solve (3.26) and $\varsigma \coloneqq (1/T + 2\,\|\Lambda\|_{L^\infty(\Omega)})^{-1}$. Then the following energy estimate holds:

$$\|u(t)\|^2_{L^2(\Omega)} \leq \exp(t/\varsigma) \left(\|u_0\|^2_{L^2(\Omega)} + \varsigma T \, \|f\|^2_{C^0([0,T];L^2(\Omega))} \right), \tag{3.28}$$

for all $t \in [0,T]$.

The proof of this lemma can be found in [DPE12]. As a direct consequence of the energy estimate, the solution to (3.26) is unique, provided it exists. Under stronger assumptions on Λ, it is possible to prove a much sharper energy estimate without the exponential factor $\exp(t/\varsigma)$. For more details on the theory of unsteady advection-reaction equations, the interested reader is referred to [DPE12, QV08, Eva98].

Let us now consider the simpler case in which $\mu \equiv f \equiv 0$ in (3.26). For the weak formulation, we introduced the so-called *graph space*

$$V^{(\beta)} \coloneqq \{ v \in L^2(\Omega) \ : \ \boldsymbol{\beta} \cdot \nabla v \in L^2(\Omega) \} \tag{3.29}$$

equipped with the norm

$$\|v\|^2_{V^{(\beta)}} \coloneqq \|v\|^2_{L^2(\Omega)} + \|\boldsymbol{\beta} \cdot \nabla v\|^2_{L^2(\Omega)} \,. \tag{3.30}$$

For simplicity we assume $\boldsymbol{\beta} \in \left(H_0^1(\Omega)\right)^d$ and $\operatorname{div}(\boldsymbol{\beta}) = 0$. The weak form in space is simply obtained via multiplication by a test function $\psi \in L^2(\Omega)$ and integration over Ω:

$$\frac{\mathrm{d}}{\mathrm{d}t}\left(u(t), \psi\right)_{L^2(\Omega)} + \left(\boldsymbol{\beta} \cdot \nabla u(t), \psi\right)_{L^2(\Omega)} = 0 \qquad \forall \psi \in L^2(\Omega). \tag{3.31}$$

For this simplified weak problem of (3.26), the existence of a unique solution can be shown:

Theorem 3.6 (Well-posedness of the weak level set equation, [GR11])
Let $u_0 \in V^{(\boldsymbol{\beta})}$. Then for all $t \in [0,T]$ there exists a unique solution $u \in C^1([0,T]; L^2(\Omega)) \cap C^1([0,T]; V^{(\boldsymbol{\beta})})$ such that $u(0,\cdot) = u_0(\cdot)$ and (3.31) holds.

This result is a consequence of the Hille-Yosida Theorem. The interested reader is referred to [EG04, Theorem (6.52)]. Unfortunately, the Theorem cannot be applied to problems with time-dependent velocity fields.

3.2. Galerkin Methods

By choosing *finite dimensional* spaces U_h, V_h and linear forms $\mathsf{a}_h(\cdot,\cdot), \mathsf{b}_h(\cdot)$ to approximate U, V and $\mathsf{a}(\cdot,\cdot), \mathsf{b}(\cdot)$, respectively, the *Galerkin approximation* of problem (3.1) is derived:

$$\text{Find } u_h \in U_h \text{ such that} \qquad \mathsf{a}_h(u_h, v_h) = \mathsf{b}_h(v_h) \qquad \text{for all } v_h \in V_h. \tag{3.32}$$

In the literature, the approximation with solution space U_h different from test space V_h, is sometimes referred to as *Petrov-Galerkin* or *non-standard Galerkin* approximation. For identical solution and test spaces, i.e. $U_h = V_h$, the less general *Ritz-Galerkin* or *Bubnov-Galerkin* approximation is obtained:

$$\text{Find } u_h \in V_h \text{ such that} \qquad \mathsf{a}_h(u_h, v_h) = \mathsf{b}_h(v_h) \qquad \text{for all } v_h \in V_h. \tag{3.33}$$

The discrete spaces U_h and V_h must be equipped with suitable norms $\|\cdot\|_{U_h}$, $\|\cdot\|_{V_h}$. Furthermore, for $U + U_h \coloneqq \operatorname{span}\{u + v \ : \ u \in U, \ v \in V\}$ the following assumption must be made [EG04]:

(i) The space $U + U_h$ can be equipped with a norm $\|\cdot\|_{U+U_h}$.

(ii) For all $u_h \in U_h$, the norm satisfies $\|u_h\|_{U+U_h} = \|u_h\|_{U_h}$.

(iii) U is continuously embedded in $U + U_h$, i.e. $\|u\|_{U+U_h} \leq c\,\|u\|_U$.

The conditions of Theorem 3.2 can directly be transferred to the discrete case:

$$\exists \alpha_h > 0 \ : \quad \inf_{u_h \in U_h} \sup_{v_h \in V_h} \frac{\mathsf{a}(u_h, v_h)}{\|u_h\|_{U_h}\,\|v_h\|_{V_h}} \geq \alpha_h, \tag{3.34a}$$

$$\forall v_h \in V_h \ : \quad \big(u_h \in U_h, \ \mathsf{a}(u_h, v_h) = 0\big) \implies \big(v_h = 0\big). \tag{3.34b}$$

The first condition is then accordingly referred to as *discrete inf-sup condition*.

Definition 3.7 (Conforming Approximation)
The approximation is said to be *conforming* if $U_h \subset U$ and $V_h \subset V$. Otherwise, it is referred to as *non-conforming*.

For many approximations, the analytical solution should also solve the discrete problem. We therefore define:

Definition 3.8 (Consistent Approximation)
The approximation is said to be *consistent*, if a_h can be extended to $(U + U_h) \times V_h$ and the exact solution u to problem (3.1) satisfies the approximate problem (3.32), i.e. if

$$\mathsf{a}_h(u, v_h) = \mathsf{b}_h(v_h) \quad \forall v_h \in V_h. \tag{3.35}$$

The definition of consistency directly implies:

Lemma 3.9 (Galerkin Orthogonality)
A consistent Galerkin approximation satisfies the *Galerkin orthogonality*

$$\mathsf{a}_h(u - u_h, v_h) = 0 \quad \forall v_h \in V_h. \tag{3.36}$$

Based on the Galerkin orthogonality, the following important Lemma gives a bound for the approximation quality.

Lemma 3.10 (Céa [EG04, Lemma 2.28])
Let the Galerkin approximation be consistent and conforming (i.e. $U_h \subset U$ and $V_h \subset V$) with $\dim(U_h) = \dim(V_h)$, and a_h be bounded on $(U + U_h) \times V_h$. Assume that the discrete inf-sup condition (3.34a) holds and that $\mathsf{a}_h = \mathsf{a}$, $\mathsf{b}_h = \mathsf{b}$. Let u_h be a solution of the approximate problem (3.32) and u a solution to (3.1). Then:

$$\|u - u_h\|_U \leq \left(1 + \frac{c}{\alpha_h}\right) \inf_{v_h \in U_h} \|u - v_h\|_U . \tag{3.37}$$

Céa's Lemma implies that, in the context of error analysis, it is sufficient to estimate the best approximation of u in V_h. In the non-conforming and/or non-consistent case, similar and more general results can be shown (cf. [EG04, Strang's Lemma]).

Proof. (cf. [EG04]) Let $w_h \in U_h$ be arbitrary. The Galerkin orthogonality implies

$$\mathsf{a}(u_h - w_h, v_h) = \mathsf{a}(u - w_h, v_h)$$

for all $v_h \in V_h$. By assumption (3.34a), the equivalence of norms in finite dimensions, the Galerkin orthogonality and the continuity of a (with constant c_a),

$$\alpha_h \|u_h - w_h\|_U \leq \sup_{v_h \in V_h} \frac{\mathsf{a}(u_h - w_h, v_h)}{\|v_h\|_V} = \sup_{v_h \in V_h} \frac{\mathsf{a}(u - w_h, v_h)}{\|v_h\|_V} \leq c_\mathsf{a} \|u - w_h\|_U .$$

Application of the triangle inequality yields

$$\|u - u_h\|_U \leq \|u - w_h\|_U + \|u_h - w_h\|_U \leq \left(1 + \frac{c_{\mathsf{a}}}{\alpha_h}\right) \|u - w_h\|_U .$$

Rearranging and taking the infimum over $w_h \in U_h$ concludes the proof. □

Under the stronger assumption of coercivity of $\mathsf{a}(\cdot,\cdot)$ as required in Theorem 3.3, inequality (3.37) holds true with constant $\frac{c}{\alpha_h}$ instead of $1 + \frac{c}{\alpha_h}$. It can be further sharpened if a is symmetric, cf. [EG04].

3.3. Finite Elements

This section briefly follows [QV08] and provides an introduction to the *finite element method*. In the following, let us consider an open domain Ω with Lipschitz-continuous boundary $\partial\Omega$ and an associated family of triangulations $\mathcal{T}_h$ (cf. Definition A.2). A finite dimensional space X_h is defined as the span of piecewise polynomial functions of degree $k \geq 1$,

$$X_h^k \coloneqq \left\{ v_h \in C^0(\overline{\Omega}) \ : \ v_h|_K \in \mathbb{P}^k(K) \ \ \forall K \in \mathcal{T}_h \right\}. \tag{3.38}$$

A useful subspace of X_h^k is the subset of functions with zero boundary values,

$$X_{h,0}^k \coloneqq \left\{ v_h \in X_h^k \ : \ v_h(\mathbf{x}) = 0 \ \ \forall \mathbf{x} \in \partial\Omega \right\}. \tag{3.39}$$

Clearly, the spaces X_h^k and $X_{h,0}^k$ are conforming with respect to $H^1(\Omega)$ and $H_0^1(\Omega)$ (cf. Definition 3.7).

For the case $d = 2$ we have the following setting. In the case of linear finite elements (X_h^1), each polynomial on K is uniquely determined by its values at the three vertices of K. For quadratic finite elements (X_h^2), the polynomial on K is uniquely determined by its values at the three vertices and the middle points of each side. More generally, one can use barycentric coordinates to determine shape functions and degrees of freedom, cf. [KA03].

Generally, the values at the nodes $\mathbf{a}_j$ with which the basis functions are associated, are called *degrees of freedom*. Since $X_h^k \subset C^0(\overline{\Omega})$, the degrees of freedom in a cell K may be shared with the neighboring cells. We can construct a Lagrange nodal basis $\{\psi_i\}_{i=1}^N \subset X_h^k$, i.e.

$$\psi_i(\mathbf{a}_j) = \begin{cases} 1, & i = j, \\ 0, & \text{otherwise}, \end{cases} \tag{3.40}$$

where $i, j = 1, \dots N$. These functions are commonly called *nodal basis functions*. Hence, a function $u_h \in X_h^k$ can be expressed in terms of a coefficient vector $\mathbf{u}_h = [u_i]_{i=1}^N$ and the shape functions:

$$u_h(\mathbf{x}) = \sum_{i=1}^{N} u_i \psi_i(\mathbf{x}). \tag{3.41}$$

By choosing $U_h = V_h = X_h^k$ in (3.32), and using the (bi-)linearity of a_h and b_h, we obtain the system of linear equations

$$\sum_{i=1}^{N} u_i \cdot \mathsf{a}_h(\psi_i, \psi_j) = \mathsf{b}_h(\psi_j), \qquad j = 1, 2, \ldots, N. \tag{3.42}$$

If the bilinear form a is V-coercive, it is also coercive on $V_h \subset V$. Hence, the Lax-Milgram Theorem 3.3 can be used to prove well-posedness and to obtain a similar stability estimate for the discrete problem.

3.3.1. Error Analysis

In this paragraph we provide *a priori estimates* for the approximation error $\|u - u_h\|$ between the analytical solution u and the numerical solution u_h in terms of the mesh size h. As we have already seen in Lemma 3.10, it is sufficient to estimate the error of u_h to its best approximation in V_h.

Definition 3.11 (Interpolation Operator)
Let $v \in C^0(\overline{\Omega})$. The linear operator $\mathcal{I}_h^k : C^0(\overline{\Omega}) \to X_h^k$ defined by

$$\mathcal{I}_h^k(v)(\mathbf{x}) \coloneqq \sum_{i=1}^{N} v(\mathbf{a}_i)\psi_i(\mathbf{x}), \tag{3.43}$$

is called *interpolation operator* of X_h^k, where $\mathbf{a}_i$ are the Lagrange nodes of $\mathcal{T}_h$ and $\{\psi_i\}_{i=1}^N$ the associated nodal shape functions.

Based on local estimates of the interpolation error, it is possible to prove the following global interpolation error estimate:

Theorem 3.12 (Interpolation Error [QV08, Theorem 3.4.2])
"Let $\mathcal{T}_h$ be a family of regular triangulations and assume $m \in \{0, 1\}$, $l = \min\{k, s-1\} \geq 1$. Then there exists a constant C independent of h, such that

$$|v - \mathcal{I}_h^k(v)|_{H^m(\Omega)} \leq C h^{l+1-m} |v|_{H^{l+1}(\Omega)} \qquad \forall v \in H^s(\Omega)." \tag{3.44}$$

The proof of this theorem is based on the well-known Bramble-Hilbert Lemma, and can, for example, be found in [QV08].

3.3.1.1. Poisson's Problem

Using Lemma 3.10 and Theorem 3.12 the following convergence rate estimates for the Poisson problem can be inferred:

Theorem 3.13 (Convergence Rate Estimates)
Under the assumptions of Theorem 3.12 and $d/2 < k+1$, let $u \in H^{k+1}(\Omega)$ be the solution of (3.9a) and $u_h \in X_h^{k+1}$ the solution to the correspondtion Galerkin approximation problem (3.33), respectively. Then, the following *a priori estimates* hold:

$$\|u - u_h\|_{H^1(\Omega)} \leq C h^k \, |u|_{H^{k+1}(\Omega)} \,, \tag{3.45}$$

and in the case $V = H_0^1(\Omega)$

$$\|u - u_h\|_{L^2(\Omega)} \leq C h \, |u - u_h|_{H^1(\Omega)} \,. \tag{3.46}$$

The better error estimate in the $L^2(\Omega)$ norm is obtained by employing a duality argument (Aubin and Nitsche, cf. [KA03, EG04]).

3.3.1.2. Hyperbolic Problems

In this section we will investigate stability and convergence properties for the hyperbolic problem introduced in Section 3.1.2. Let us consider the semi-discrete approximation of (3.26) with $V_h := X_h^k$:

$$\text{For given } u_{0,h} \in V_h, \text{ and } t \in [0,T] \text{ find } u_h(t) \in V_h \text{ such that} \tag{3.47a}$$

$$\frac{\mathrm{d}}{\mathrm{d}t}\,(u_h(t), v_h) + (\boldsymbol{\beta} \cdot \nabla u_h(t), v_h) + (\mu u_h(t), v_h) = (f(t), v_h)\,, \qquad \forall v_h \in V_h^{\text{in}} \tag{3.47b}$$

$$u_h(t) = u_D(t) \qquad \text{on } \partial\Omega^{\text{in}}, \tag{3.47c}$$

$$u_h(0) = u_{0,h} \qquad \text{in } \Omega, \tag{3.47d}$$

where

$$V_h^{\text{in}} := \{v_h \in V_h \;:\; v_h|_{\partial\Omega^{\text{in}}} = 0\}. \tag{3.48}$$

For better readability, we drop the dependence on the spatial coordinate $\mathbf{x}$ where no ambiguity arises, and use the abbreviation $(\cdot,\cdot) := (\cdot,\cdot)_{L^2(\Omega)}$. In contrast to Section 3.1.2, we now also allow for μ to be non-constant in time.

Lemma 3.14 (Stability [QV08])
A solution $u_h(t) \in V_h$ to problem (3.47) satisfies

$$\begin{aligned} &\|u_h(t)\|_{L^2(\Omega)}^2 + \int_0^t \int_{\partial\Omega\setminus\partial\Omega^{\text{in}}} \boldsymbol{\beta} \cdot \mathbf{n}\big(u_h(\tau)\big)^2 \,\mathrm{d}\sigma\,\mathrm{d}\tau \\ &\quad \leq \left(\|u_{0,h}\|_{L^2(\Omega)}^2 + \int_0^t \|f(\tau)\|_{L^2(\Omega)}^2 \,\mathrm{d}\tau\right) \cdot \exp\left(\int_0^t \big(1 + 2\eta^\star(\tau)\big)\,\mathrm{d}\tau\right) \end{aligned} \tag{3.49}$$

for all $t \in [0,T]$ and where

$$\eta^\star(t) \coloneqq \max_{\mathbf{x}\in\overline{\Omega}} \left| -\frac{1}{2}\nabla\cdot\boldsymbol{\beta}(\mathbf{x}) + \mu(t,\mathbf{x}) \right|. \tag{3.50}$$

Proof. For the proof, we follow the general guidelines in [QV08] and use an energy method. For simplicity, let us assume $u_D \equiv 0$. We use the abbreviation

$$\eta(t,\mathbf{x}) \coloneqq -\frac{1}{2}\nabla\cdot\boldsymbol{\beta} + \mu(t,\mathbf{x}).$$

Plugging in the test function $v_h = u_h(t)$, and under consideration of

$$\left(\frac{\partial}{\partial t}u_h(t), u_h(t)\right) = \frac{1}{2}\frac{\mathrm{d}}{\mathrm{d}t}\left\|u_h(t)\right\|^2_{L^2(\Omega)},$$

and

$$\begin{aligned}\int_\Omega (\boldsymbol{\beta}\cdot\nabla u_h(t))u_h(t)\,\mathrm{d}\mathbf{x} &= \frac{1}{2}\int_\Omega \left(\boldsymbol{\beta}\cdot\nabla\big(u_h(t)\big)^2\right)\mathrm{d}\mathbf{x}\\ &= -\frac{1}{2}\int_\Omega (\nabla\cdot\boldsymbol{\beta})\big((u_h(t)\big)^2\,\mathrm{d}\mathbf{x} + \frac{1}{2}\int_{\partial\Omega\setminus\partial\Omega^{\mathrm{in}}} \boldsymbol{\beta}\cdot\mathbf{n}\big(u_h(t)\big)^2\,\mathrm{d}\sigma,\end{aligned}$$

we obtain after multiplication by a factor of 2 and integration over time of (3.47b)

$$\begin{aligned}&\|u_h(t)\|^2_{L^2(\Omega)} - \|u_{0,h}\|^2_{L^2(\Omega)} + \int_{\partial\Omega\setminus\partial\Omega^{\mathrm{in}}} \boldsymbol{\beta}\cdot\mathbf{n}\big(u_h(t)\big)^2\,\mathrm{d}\sigma\\ &\qquad= 2\int_0^t (f(\tau),u_h(\tau))\,\mathrm{d}\tau - 2\int_0^t\int_\Omega \eta(\tau)\big(u_h(\tau)\big)^2\,\mathrm{d}\mathbf{x}\,\mathrm{d}\tau\\ &\qquad\le 2\int_0^t |(f(\tau),u_h(\tau))|\,\mathrm{d}\tau + 2\int_0^t \eta^\star(\tau)\,\|u_h(\tau)\|^2_{L^2(\Omega)}\,\mathrm{d}\tau\\ &\qquad\le \int_0^t \|f(\tau)\|^2_{L^2(\Omega)}\,\mathrm{d}\tau + \int_0^t \big(1+2\eta^\star(\tau)\big)\,\|u_h(\tau)\|^2_{L^2(\Omega)}\,\mathrm{d}\tau.\end{aligned}$$

The last inequality was obtained by application of Young's inequality. Rearranging the terms, we identify

$$\begin{aligned}\|u_h(t)\|^2_{L^2(\Omega)} \le \overbrace{\|u_{0,h}\|^2_{L^2(\Omega)} + \int_0^t \|f(\tau)\|^2_{L^2(\Omega)}\,\mathrm{d}\tau - \int_{\partial\Omega\setminus\partial\Omega^{\mathrm{in}}} \boldsymbol{\beta}\cdot\mathbf{n}\big(u_h(t)\big)^2\,\mathrm{d}\sigma}^{=:G(t)}\\ + \int_0^t \underbrace{\big(1+2\eta^\star(\tau)\big)}_{=:F(t)}\,\|u_h(\tau)\|^2_{L^2(\Omega)}\,\mathrm{d}\tau.\end{aligned}$$

Hence, we can apply Gronwall's Lemma A.6 to obtain

$$\begin{aligned}\|u_h(t)\|_{L^2(\Omega)}^2 \leq \overbrace{\|u_{0,h}\|_{L^2(\Omega)}^2 + \int_0^t \|f(\tau)\|_{L^2(\Omega)}^2 \,\mathrm{d}\tau}^{=:g(t)} - \int_{\partial\Omega\setminus\partial\Omega^{\text{in}}} \boldsymbol{\beta}\cdot\mathbf{n}\big(u_h(t)\big)^2 \,\mathrm{d}\sigma \\ + \int_0^t F(s)\Big[\|u_{0,h}\|_{L^2(\Omega)}^2 + \int_0^s \|f(\tau)\|_{L^2(\Omega)}^2 \,\mathrm{d}\tau \\ \underbrace{- \int_{\partial\Omega\setminus\partial\Omega^{\text{in}}} \boldsymbol{\beta}\cdot\mathbf{n}\big(u_h(t)\big)^2 \,\mathrm{d}\sigma}_{\leq 0}\Big] \exp\left(\int_s^t F(\tau)\,\mathrm{d}\tau\right)\mathrm{d}s,\end{aligned}$$

and, since $g(t)$ is non-decreasing we can further estimate

$$\begin{aligned}\|u_h(t)\|_{L^2(\Omega)}^2 + \int_{\partial\Omega\setminus\partial\Omega^{\text{in}}} \boldsymbol{\beta}\cdot\mathbf{n}\big(u_h(t)\big)^2 \,\mathrm{d}\sigma \\ \leq g(t) + \int_0^T F(s)g(s)\exp\left(\int_s^t F(\tau)\,\mathrm{d}\tau\right)\mathrm{d}s \\ \leq g(t)\left[1 + \int_0^T F(s)\exp\left(\int_s^t F(\tau)\,\mathrm{d}\tau\right)\mathrm{d}s\right].\end{aligned}$$

By the fundamental theorem of calculus,

$$\begin{aligned}\int_0^t F(s)\exp\left(\int_s^t F(\tau)\,\mathrm{d}\tau\right)\mathrm{d}s &= \int_0^t \left[-\frac{\mathrm{d}}{\mathrm{d}s}\exp\left(\int_s^t F(\tau)\,\mathrm{d}\tau\right)\right]\mathrm{d}s \\ &= -\left[\exp(0) - \exp\left(\int_0^t F(\tau)\,\mathrm{d}\tau\right)\right] \\ &= \exp\left(\int_0^t F(\tau)\,\mathrm{d}\tau\right) - 1\end{aligned}$$

and therefore

$$\|u_h(t)\|_{L^2(\Omega)}^2 + \int_{\partial\Omega\setminus\partial\Omega^{\text{in}}} \boldsymbol{\beta}\cdot\mathbf{n}\big(u_h(t)\big)^2 \,\mathrm{d}\sigma \leq g(t)\exp\left(\int_0^t F(\tau)\,\mathrm{d}\tau\right). \qquad \square$$

For the convergence analysis of problem (3.47), it is useful to consider the semi-norm

$$|v|_{\beta,\partial\Omega} \coloneqq \left(\int_{\partial\Omega} |\boldsymbol{\beta}\cdot\mathbf{n}| v^2 \,\mathrm{d}\sigma\right)^{1/2}. \tag{3.51}$$

Theorem 3.15 (Convergence Estimate [QV08])
Let the exact solution satisfy $u \in L^2([0,T]; H^{k+1}(\Omega))$, $\frac{\partial u}{\partial t} \in L^2([0,T]; H^k(\Omega))$ and $u_0 \in H^k(\Omega)$. Then, for $u_h \in X_h^k$, the following convergence estimate for problem (3.47) holds:

$$\max_{t\in[0,T]} \|u(t) - u_h(t)\|_{L^2(\Omega)} + \left(\int_0^T |u(t) - u_h(t)|^2_{\beta,\partial\Omega} \,\mathrm{d}t \right)^{1/2} = \mathcal{O}\left(\|u_0 - u_{0,h}\|_{L^2(\Omega)} + h^k \right). \tag{3.52}$$

For a proof of this theorem, the interested reader is referred to [QV08].

Let us remark that the convergence estimate (3.52) does not provide any control on the first order derivatives, even though a smooth continuous function u was assumed. Also note that the convergence rate in (3.52) is not the highest possible rate of $\mathcal{O}(h^{k+1})$. In the next section, we apply a stabilization technique to obtain a better convergence estimate.

3.3.2. Stabilization

It is well-known that finite element solutions of hyperbolic problems may exhibit numerical artifacts. In particular, spurious oscillations may occur. To avoid these problems, stabilization techniques can be applied. In this section we will give a brief introduction to the streamline-upwind Petrov-Galerkin (SUPG) method. Following section 7.2.1 in [GR11], we consider the hyperbolic model problem

$$\beta u' + u = f \quad \text{in } (0,1), \tag{3.53a}$$
$$u(0) = 0, \tag{3.53b}$$

with constant velocity $\beta > 0$. The weak formulation in $U = H^1((0,1))$ and $V = L^2((0,1))$ is given by

$$\mathsf{a}(u,v) \coloneqq \int_0^1 \beta u' v + uv \,\mathrm{d}x, \tag{3.54a}$$
$$\mathsf{b}(v) \coloneqq \int_0^1 fv \,\mathrm{d}x. \tag{3.54b}$$

By the positivity of β and Theorem 3.2, the well-posedness of the problem

$$\text{find } u \in U \text{ such that} \qquad \mathsf{a}(u,v) = \mathsf{b}(v) \qquad \text{for all } v \in V, \tag{3.55}$$

can be verified. We now consider the conforming linear finite element discretization of problem (3.55) and introduce the discrete space

$$V_h \coloneqq \{v \in C([0,1]) \ : \ v(0) = 0 \text{ and } v|_I \in \mathbb{P}^1(I) \text{ for all } I \in \mathcal{I}_h\}, \tag{3.56}$$

where $\mathcal{I}_h = \{[x_i, x_{i+1}]\}_i$, $x_i = ih$, $0 \leq i \leq n$, and $h = \frac{1}{n}$, $n \in \mathbb{N}$. Note that $V_h \subset U$ and $V_h \subset V$. A discrete approximation problem is given by

$$\text{Find } u \in V_h \text{ such that} \qquad \mathsf{a}(u, v) = \mathsf{b}(v) \qquad \text{for all } v \in V_h. \tag{3.57}$$

To derive a priori error estimates, Céa's Lemma can be employed and the discrete inf-sup condition (3.34) verified. It can be shown that for the inf-sup constant α_h the relation

$$\alpha_h \leq ch \tag{3.58}$$

holds. The inf-sup parameter therefore exhibits the asymptotic behavior $\alpha_h \to 0$ as $h \to 0$, which indicates an unstable numerical approach. The main idea of the stabilization technique to be presented in this section is the following: for any solution $u \in U$ to (3.55) we have

$$\int_0^1 (\beta u' + u)\beta v' \,\mathrm{d}x = \int_0^1 f\beta v' \,\mathrm{d}x \qquad \forall v \in V. \tag{3.59}$$

Therefore, we can add multiples of this equation to (3.55) and obtain the modified forms

$$\mathsf{a}_\delta(u, v) \coloneqq \int_0^1 (u + \beta u')(v + \delta\beta v') \,\mathrm{d}x, \tag{3.60a}$$

$$\mathsf{b}_\delta(v) \coloneqq \int_0^1 f(v + \delta\beta v') \,\mathrm{d}x. \tag{3.60b}$$

The stabilization paramater $\delta \in [0, 1]$ controls how much artificial diffusion is added in this consistent approach. In particular, the original problem is obtained for $\delta = 0$. The added streamline diffusion improves the U-coercivity. For $\mathsf{a}_\delta(\cdot, \cdot)$, the following estimate holds [GR11]:

$$\begin{aligned} \mathsf{a}_\delta(u, u) &= \int_0^1 u^2 \,\mathrm{d}x + \delta\beta^2 \int_0^1 (u')^2 \,\mathrm{d}x + \beta(\delta + 1) \int_0^1 u'u \,\mathrm{d}x \\ &\geq \delta\beta^2 \left|u\right|_{H^1(0,1)} + \|u\|^2_{L^2(0,1)} \qquad \forall u \in U. \end{aligned} \tag{3.61}$$

This enables us to derive a better convergence estimate:

Theorem 3.16 (Streamline Diffusion 1D Convergence Estimate [GR11])
Let $u \in H^2(0, 1)$ and $u_h \in V_h$ be the solutions of (3.55) and (3.57) equipped with the linear forms (3.61). For all $\delta \in [0, 1]$ the error bound

$$\beta\sqrt{\delta}\left|u - u_h\right|_{H^1(0,1)} + \|u - u_h\|_{L^2(0,1)} \leq Ch\left[h + \beta\sqrt{\delta} + b\min\{1, h/\beta\sqrt{\delta}\}\right] \left\|u''\right\|_{L^2(0,1)} \tag{3.62}$$

holds with a constant C independent of h, δ, β and u.

In contrast to the estimate in Theorem 3.15, the error bound (3.62) also provides control of the first derivative of $u - u_h$ w.r.t. $H^1(0, 1)$ (provided $\delta > 0$). The optimal stabilization parameter

in the above theorem is given by the choice $\delta_{\text{opt}} = h/\beta$. In comparison to the error bound in Theorem 3.15, we obtain for the choice $\delta = \delta_{\text{opt}}$ the improved estimates

$$\|u - u_h\|_{L^2(0,1)} \leq ch^{3/2} \|u''\|_{L^2(0,1)} \quad \text{and} \quad |u - u_h|_{H^1(0,1)} \leq ch \|u''\|_{L^2(0,1)}. \tag{3.63}$$

The generalization of this stabilization technique to higher space dimensions and finite element spaces of higher polynomial degrees is straight forward. In the more general setting of (3.47), the stabilized linear forms are given by

$$\begin{aligned} \mathsf{a}_\delta(u_h(t), v_h) &:= (\boldsymbol{\beta} \cdot \nabla u_h(t), v_h) + (\mu u_h(t), v_h) \\ &\quad + \sum_{K \in \mathcal{T}_h} \delta_K \left(\boldsymbol{\beta} \cdot \nabla u_h(t) + \mu(t) u_h(t), \boldsymbol{\beta} \cdot \nabla v_h\right)_{L^2(K)}, \end{aligned} \tag{3.64a}$$

$$\mathsf{b}_\delta(v_h) := (f(t), v_h)_{L^2(\Omega)} + \sum_{K \in \mathcal{T}_h} \delta_K \left(f(t), \boldsymbol{\beta} \cdot \nabla v_h\right)_{L^2(K)}. \tag{3.64b}$$

We use the associated SUPG norm

$$\|u_h(t)\|_\delta := \left(\left\| u_h(t) \sqrt{\mu(t) - \nabla \cdot \boldsymbol{\beta}} \right\|^2_{L^2(\Omega)} + \sum_{K \in \mathcal{T}_h} \delta_K \|\boldsymbol{\beta} \cdot \nabla u_h(t)\|^2_{L^2(K)} \right)^{1/2} \tag{3.65}$$

and

$$\|u_h\|_{t,\delta} := \left(\int_0^t \|u_h(\tau)\|^2_\delta \, \mathrm{d}\tau \right)^{1/2}. \tag{3.66}$$

Here, the SUPG parameter δ_K is set individually for each cell $K \in \mathcal{T}_h$. We conclude this section by quoting a general error bound for this stabilization technique:

Theorem 3.17 (Streamline Diffusion Convergence Estimate [JN11, Th. 5.2])
Let the analytical solution u to (3.26) have the following regularity: $u_t(t) \in H^{k+1}(\Omega)$ for all $t \in [0,T]$ and u, $\frac{\partial}{\partial t} u$, $\frac{\partial^2}{\partial t^2} u \in L^2(0,T; H^{k+1}(\Omega))$. Assume $\mu(t) \geq 0$ and $\eta(t, \mathbf{x}) \geq \eta_0 > 0$ for all $(t, \mathbf{x}) \in [0,T] \times \Omega$. Then, for all $t \in [0,T]$, the following error estimate holds:

$$\begin{aligned} &\|u(t) - u_h(t)\|_{L^2(\Omega)} + \|u - u_h\|_{t,\delta} \\ &\leq C \left[\|e_h(0)\| + \sqrt{\delta} \left(\|\nabla e_h(0)\|_{L^2(\Omega)} + \|(\boldsymbol{\beta} \cdot \nabla e_h)(0)\|_{L^2(\Omega)} + \|(\sqrt{\mu} e_h)(0)\|_{L^2(\Omega)} \right) \right] \\ &\quad + Ch^{k+1/2} \Big[\|u(t)\|_{H^{k+1}(\Omega)} + \sqrt{\delta} \|(\partial_t u)(0)\|_{H^{k+1}(\Omega)} + \|u\|_{L^2(0,t;H^{k+1}(\Omega))} \\ &\quad + \|\partial_t u\|_{L^2(0,t;H^{k+1}(\Omega))} + \sqrt{\delta} \|\partial_{tt} u\|_{L^2(0,t;H^{k+1}(\Omega))} \Big] \end{aligned} \tag{3.67}$$

where $e_h(t) := u_h - \mathcal{I}_h^k u$.

The theorem shows that we gain, in contrast to Theorem 3.15, the power of $\sqrt{h}$ if the analytical solution is sufficiently smooth. Furthermore, one can derive error bounds on the first derivative when using the SUPG stabilized approach. For more information on stability and convergence

analysis, the interested reader is referred to the articles [BGS04, BH04, JN11, Zho97] and the book [QV08].

3.4. Fully-Discrete Approximation

So far we have only applied the finite element method for spatial approximation. Even though the use of space-time elements is an option, many algorithms usually separate temporal and spatial discretization for various reasons. Let us now turn to temporal discretization. Therefore, consider a semi-discrete problem of the form (cf. [QV08])

$$\frac{\mathrm{d}}{\mathrm{d}t}\left(u_h(t), v_h\right) + \mathsf{a}_h(u_h(t), v_h) = \mathsf{b}_h(t, v_h) \qquad \forall v_h \in V_h,\ t \in (0, T), \tag{3.68a}$$

$$u_h(0) = u_0. \tag{3.68b}$$

For simplicity, we restrict ourselves to a *finite difference approach* for the *temporal discretization*. Problem (3.68) is an ordinary differential equation in time. Therefore, Taylor expansion can be applied to approximate the time derivative:

$$\begin{aligned}\frac{\left(u_h(t+\Delta t) - u_h(t), v_h\right)}{\Delta t} + \mathsf{a}_h\Big(\theta u_h(t+\Delta t) + (1-\theta)u_h(t), v_h\Big) \\ \approx \theta \mathsf{b}_h(t+\Delta t, v_h) + (1-\theta)\mathsf{b}_h(t, v_h),\end{aligned} \tag{3.69}$$

where $\theta \in [0,1]$. Let the time interval $[0,T]$ be partitioned into N equidistant subintervals $[t_i, t_{i+1}]$ of length $\Delta t = {}^{T}/_{N}$. The solution to (3.68) at time level t_n is then denoted by u_h^n. Applying the Taylor expansion from (3.69) to (3.68), we obtain the *θ-scheme*:

$$\frac{\left(u_h^{n+1} - u_h^n, v_h\right)}{\Delta t} + \mathsf{a}_h(\theta u_h^{n+1} + (1-\theta)u_h^n, v_h) \approx \theta \mathsf{b}_h(u_h^{n+1}, v_h) + (1-\theta)\mathsf{b}_h(u_h^n, v_h), \tag{3.70}$$

for $n = 0, ..., N-1$ and $v_h \in V_h$. For $\theta = 0$, the explicit *forward Euler method* is obtained. On the other hand, for $\theta = 1$, the scheme is fully implicit and defines the *backward Euler method*. Both methods are first order accurate in time. For $\theta = {}^{1}/_{2}$, we obtain the unconditionally stable and second order accurate *Crank-Nicolson* method.

Other approaches for discretization in time include fractional step and operator-splitting methods [QV08, Chapter 5.7], or (discontinuous) finite elements. In Section 4.4 the second order accurate *Lax-Wendroff method* is presented, in which time derivatives are replaced by the space derivatives arising in the level set equation [DH03].

4 Level Set Methods

A vast range of literature on level set methods and their numerical implementation exists. This chapter is partly based on the books by Gross and Reusken [GR11], Osher and Fedkiw [OF03] and Donea and Huerta [DH03], as well as on the manuscripts [Bas12, Set96b]. It is organized as follows. In the first section, the mathematical concept of level set methods is introduced and basic properties as well as essential results are reviewed. The level set transport equation is derived and analyzed. In the subsequent section, we look at the finite element discretization of the level set equation, the quality of interface approximation and possible stabilization techniques. In the last section, we comment on two possible time discretization approaches.

4.1. Level Set Functions

The level set method is an interface capturing approach. Its essential idea is to implicitly describe an interface in terms of a scalar indicator function, the so-called *level set function* which will be denoted further on by φ. Generally, an interface Γ associated with such a function $\varphi : (0,T) \times \Omega \to \mathbb{R}$ is then defined as the *zero level set* of φ, i.e.

$$\Gamma(t) = \{\mathbf{x} \in \Omega \ : \ \varphi(t,\mathbf{x}) = 0\}. \tag{4.1}$$

In the remainder of this thesis, we restrict ourselves to the two-dimensional case. The general setting defined below is illustrated in Fig. 4.1.

Definition 4.1 (General Setting)
Let $\Omega \subset \mathbb{R}^2$ be a domain with piecewise smooth boundary $\partial\Omega$. In the time interval $[0,T]$, we consider an evolving interface $\Gamma(t) \subset \Omega$ with the following properties:

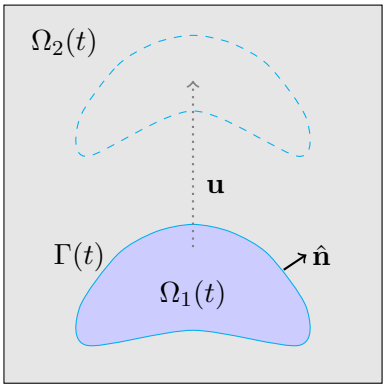

Figure 4.1.: An illustration of a domain Ω containing an evolving interface Γ separating two subdomains Ω_1 and Ω_2.

i) For all $t \in [0,T]$, $\Gamma(t)$ separates two phases $\Omega_1(t)$ and $\Omega_2(t)$, where $\Omega_1(t)$ and $\Omega_2(t)$ are finite unions of domains in Ω such that the following properties are fulfilled:

$$\Omega_1(t) \cap \Omega_2(t) = \emptyset, \tag{4.2a}$$
$$\Gamma(t) = \overline{\Omega}_1(t) \cap \overline{\Omega}_2(t), \tag{4.2b}$$
$$\overline{\Omega}_1(t) \cup \overline{\Omega}_2(t) = \overline{\Omega}, \tag{4.2c}$$
$$\exists c_U > 0 \ : \ U(t) \coloneqq \{\mathbf{x} \in \mathbb{R} \ : \ \operatorname{dist}(\mathbf{x}, \Gamma(t)) < c_U\} \subset \Omega. \tag{4.2d}$$

ii) $\Gamma(t)$ is a finite union of continuous curves in Ω.

iii) In particular, $\operatorname{meas}_2(\Gamma(t)) = 0$ and $\operatorname{meas}_1(\Gamma(t)) > 0$.

In this setting we can now give a more precise definition of level set functions.

Definition 4.2 (Level set function)
In the setting of Definition 4.1, a continuous function $\varphi : [0,T] \times \mathbb{R}^2 \to \mathbb{R}$ associated with the interface $\Gamma(t)$ that satisfies

$$\varphi(t,\mathbf{x}) \begin{cases} > & 0 \quad \text{for } \mathbf{x} \in \Omega_1(t), \\ = & 0 \quad \text{for } \mathbf{x} \in \Gamma(t), \\ < & 0 \quad \text{for } \mathbf{x} \in \Omega_2(t), \end{cases} \tag{4.3}$$

is called *level set function* of $\Gamma(t)$.

This definition is very general and imposes only few requirements on φ. However, for the purpose of interface capturing, several properties are desirable. The level set function should at least be continuous, so that it can be evaluated pointwise and the interface can be numerically reconstructed. In many applications the normal vector to the interface is required. This can easily be accomplished when the level set function is (or approximates) the *signed distance function* to the level set.

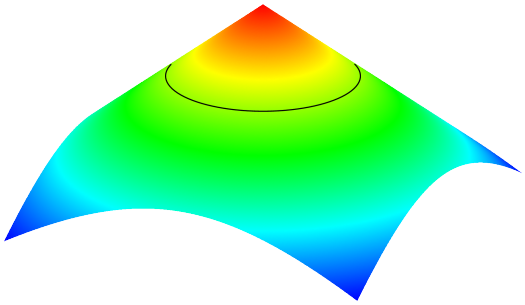

Figure 4.2.: An illustration of a signed distance function and its zero level set curve.

Definition 4.3 (Signed distance function)
In the setting of Definition 4.1, the *signed distance function* (SDF) to $\Gamma(t)$ is the function $\varphi : [0,T] \times \Omega \to \mathbb{R}$ defined by:

$$\varphi(t,\mathbf{x}) = \begin{cases} \operatorname{dist}(\mathbf{x},\Gamma(t)) & \text{for } \mathbf{x} \in \Omega_1(t), \\ 0 & \text{for } \mathbf{x} \in \Gamma(t), \\ -\operatorname{dist}(\mathbf{x},\Gamma(t)) & \text{for } \mathbf{x} \in \Omega_2(t), \end{cases} \tag{4.4}$$

where $\operatorname{dist}(\cdot,\cdot)$ denotes the distance function as defined in Definition A.3.

Fig. 4.2 shows an illustration of the signed distance function with respect to a circle-shaped interface. Clearly, the signed distance function is also a level set function that offers several additional useful properties.

Theorem 4.4 (Properties of signed distance functions)
In the setting of Definition 4.1 at time $t^* \in [0,T]$, the signed distance function $\varphi : \Omega \to \mathbb{R}$ of $\Gamma = \Gamma(t^*)$

i) is Lipschitz continuous with constant 1 and differentiable almost everywhere,

ii) satisfies the so-called Eikonal equation

$$|\nabla\varphi(\mathbf{x})| = 1, \tag{4.5}$$

where φ is differentiable,

iii) is differentiable at any point $\mathbf{x} \in \Gamma$, and

$$\nabla\varphi(\mathbf{x}) = \hat{\mathbf{n}}(\mathbf{x}), \tag{4.6}$$

where $\hat{\mathbf{n}}(\mathbf{x})$ is the unit normal vector to Γ.

(iv) yields a direct way to compute the curvature $\kappa(\mathbf{x})$ of Γ:

$$\kappa(\mathbf{x}) = \nabla \cdot \nabla\varphi(\mathbf{x}), \tag{4.7}$$

for $\mathbf{x} \in \Gamma$ and sufficiently smooth interface Γ.

Proof. i) φ being 1-Lipschitz is a direct consequence of the triangle inequality of the distance function. It is first shown, that the distance function $\operatorname{dist}(\cdot, \Gamma)$ is Lipschitz continuous with constant $L = 1$. Following [Vin10, proposition 4.8.1], for any $\mathbf{y} \in \Omega$ and $\mathbb{R} \ni \epsilon > 0$ sufficiently small, there exists by definition a $\mathbf{z} \in \Gamma$ s.t. $\operatorname{dist}(\mathbf{y}, \Gamma) \geq |\mathbf{y} - \mathbf{z}| - \epsilon$. Consequently, for any $\mathbf{x} \in \Omega$, $\mathbf{x} \neq \mathbf{y}$, we have

$$\operatorname{dist}(\mathbf{x}, \Gamma) \leq |\mathbf{x} - \mathbf{z}| \leq |\mathbf{x} - \mathbf{y}| + |\mathbf{y} - \mathbf{z}| \leq |\mathbf{x} - \mathbf{y}| + \operatorname{dist}(\mathbf{y}, \Gamma) + \epsilon,$$

and, since ϵ was chosen arbitrarily,

$$\operatorname{dist}(\mathbf{x}, \Gamma) - \operatorname{dist}(\mathbf{y}, \Gamma) \leq |\mathbf{x} - \mathbf{y}|.$$

Now, by interchanging $\mathbf{x}$ and $\mathbf{y}$, we obtain

$$|\operatorname{dist}(\mathbf{x}, \Gamma) - \operatorname{dist}(\mathbf{y}, \Gamma)| \leq |\mathbf{x} - \mathbf{y}|,$$

and the Lipschitz-continuity with constant $L = 1$ of $\operatorname{dist}(\mathbf{x}, \Gamma)$ follows. Without loss of generality, for any $\mathbf{x} \in \Omega_1$, $\mathbf{y} \in \Omega_2$, there exists a $\lambda \in [0, 1]$ and $\mathbf{z} \in \Gamma$ with $\mathbf{z} = \lambda\mathbf{x} + (1 - \lambda)(\mathbf{y} - \mathbf{x})$, and since

$$|\varphi(\mathbf{x}) - \varphi(\mathbf{y})| \leq |\operatorname{dist}(\mathbf{x}, \Gamma)| + |\operatorname{dist}(\mathbf{y}, \Gamma)| \leq |\operatorname{dist}(\mathbf{x}, \mathbf{z})| + |\operatorname{dist}(\mathbf{y}, \mathbf{z})| = |\mathbf{x} - \mathbf{y}|,$$

φ is also 1-Lipschitz continous. As a direct consequence of φ being 1-Lipschitz continuous, it is also differentiable almost everywhere, cf. Rademacher's Theorem A.7.

ii) For $\mathbf{x} \in \Omega \setminus \Gamma$, the proposition follows directly from the differentiability of the distance function, see Theorem A.4.

iii) Let $\gamma(s) = (x_i(s))_{i=1,\dots,d}$ be a parametrization of the at least C^1-continuous curve Γ and $\mathbf{x}_0 = \gamma(s_0)$ an arbitrary but fixed-point on Γ. By definition

$$\varphi(s) \coloneqq \varphi(\gamma(s)) = 0 \qquad \text{(for all } s\text{)}.$$

Differentiating this equation with respect to s by the chain rule yields

$$0 = \frac{\mathrm{d}\gamma}{\mathrm{d}s}(s_0) = \sum_{i=1}^{d} \frac{\partial \varphi}{\partial x_i}\bigg|_{\mathbf{x}_0} \frac{\partial x_i}{\partial s}\bigg|_{s_0} = \nabla\varphi(\mathbf{x}_0) \cdot \gamma'(s_0).$$

Hence, the gradient is normal to the tangent of the curve and the normal vector can be expressed as:

$$\hat{\mathbf{n}}(\mathbf{x}_0) = \frac{\nabla\varphi(\mathbf{x}_0)}{|\nabla\varphi(\mathbf{x}_0)|}.$$

If additionally $\varphi(\mathbf{x})$ is the signed distance of $\mathbf{x}$ to Γ, then

$$\hat{\mathbf{n}}(\mathbf{x}_0) = \nabla\varphi(\mathbf{x}_0).$$

iv) See [AD99] or [GR11]. □

Hence, when having a signed distance function at hand, geometric variables such as normal vector and curvature can be computed from φ without actually localizing the implicitly defined interface. In the case of a general level set function that does not satisfy the signed distance

function property, the curvature must be expressed in terms of the tangential derivative (cf. (7.43)) as follows:

$$\kappa(\mathbf{x}) = \underline{\nabla} \cdot \nabla\varphi(\mathbf{x}). \tag{4.8}$$

As shown in Theorem 4.4, signed distance functions are solutions to the Eikonal equation (4.5). The equation holds almost everywhere but at points that are closest to more than one point on Γ. The set of these points is often called *skeleton* in literature and is of zero measure provided Γ is smooth. However, as classical solutions to PDEs may fail to exist, it is useful to consider the viscosity solution of the Eikonal equation instead, cf. [GR11, CIL92].

4.2. Evolution of an Interface

The evolution of an interface in time can be driven by different processes. We have already seen the derivation of transport equations from conservation laws in Chapter 2. More generally, we can subdivide the causes of interface propagation into externally and internally generated motions [OF03]. For former ones, an externally provided velocity field describes the motion of the interface, while for the latter ones, the interface movement is based on the interface itself, for example mean curvature flow (cf. Section 2.3.2). Within the scope of this thesis, we will only consider externally generated motion. Therefore, we assume a sufficiently smooth velocity field $\mathbf{v} : \Omega \to \mathbb{R}^d$, or, in the time dependent case, $\mathbf{u} : (0, T) \times \Omega \to \mathbb{R}^d$. We will now derive the *level set transport equation* directly by application of the chain rule.

To determine the movement of an evolving interface, a virtual particle $\mathbf{X}$ with Eulerian coordinates $\mathbf{x}(t) \in \Gamma(t)$ is observed (cf. Section 7.1). As time goes by, the particle moves along its characteristics $\mathbf{x}(t, \mathbf{X})$ where the value of φ remains constant:

$$\varphi(t, \mathbf{x}(t, \mathbf{X})) = \varphi(t_0, \mathbf{X}). \tag{4.9}$$

Differentiation with respect to t yields the transport equation

$$\frac{\partial\varphi(t, \mathbf{x})}{\partial t} + \mathbf{v}(t) \cdot \nabla\varphi(t, \mathbf{x}) = 0 \tag{4.10}$$

in Ω and for $t \geq 0$, where

$$\mathbf{v}(t) = \frac{\partial}{\partial t}\mathbf{x}(t, \mathbf{X}). \tag{4.11}$$

Equation (4.10) is referred to as *level set equation* and forms the basis of many numerical techniques for interface capturing. This partial differential equation is of hyperbolic type. Hence, boundary conditions must only be prescribed on the inflow portion $\partial\Omega^{\text{in}}$ of the outer

boundary $\partial\Omega$, that is for $\mathbf{x} \in \partial\Omega$ with $\mathbf{n}(\mathbf{x}) \cdot \mathbf{v}(\mathbf{x}) < 0$. The full level set problem with Dirichlet boundary condition reads:

$$\frac{\partial}{\partial t}\varphi(t,\mathbf{x}) + \mathbf{v} \cdot \nabla\varphi(t,\mathbf{x}) = 0 \qquad \text{in } (0,T) \times \Omega, \tag{4.12a}$$

$$\varphi(0,\mathbf{x}) = \varphi_0(\mathbf{x}) \qquad \text{in } \Omega, \tag{4.12b}$$

$$\varphi(t,\mathbf{x}) = g(t,\mathbf{x}) \qquad \text{on} (0,T) \times \partial\Omega^{\text{in}}. \tag{4.12c}$$

Since the level set function is not a physical quantity per se, the prescription of meaningful or natural boundary conditions is unclear. In many applications however, no such boundary conditions are required, or arbitrary boundary conditions can be set temporarily before applying a redistancing procedure (cf. Chapter 5). Note that given a divergence free velocity field, equation (4.10) can be cast into *conservative form*:

$$\frac{\partial\varphi}{\partial t} + \nabla \cdot (\mathbf{v}\varphi) = 0. \tag{4.13}$$

The following theorem shows that the transport equation preserves an interface in the sense that its d-measure remains zero:

Theorem 4.5
Let the velocity field $\mathbf{v} \in \big(\text{Lip}(\Omega)\big)^d$ and an initial condition $\varphi_0(\mathbf{x})$ be given such that

$$\text{meas}_d(\Gamma(t_0)) = 0. \tag{4.14}$$

Then the interface $\Gamma(t)$ associated with the solution of (4.12) possesses the property

$$\text{meas}_d(\Gamma(t)) = 0, \qquad t \in (t_0, T). \tag{4.15}$$

For details on this theorem and its proof, the interested reader is referred to [GR11, CIL92].

Phase field approach

For completeness, let us briefly comment on the related phase field approach. The level set method captures a sharp interface. In the *phase field approach*, instead of the sharp interface, a diffusive narrow band along the interface is considered. The densities of the two phases are constant except in this region. For more information, the interested reader is referred to [DMAW98, GR11].

In [OK05, OKZ07], a conservative level set algorithm is presented. It uses features from both, the level set and the phase field approach. A brief summary of the method is provided in Section 6.3.

4.3. Space Discretization

As in Chapter 3, we consider the following weak formulation in space of the level set equation (4.12):

$$\text{For any } t \in [0,T] \text{ find } \varphi_h(t) \in V^{(\mathbf{v})} \text{ such that} \tag{4.16a}$$

$$\frac{\mathrm{d}}{\mathrm{d}t}\left(\varphi(t), v\right)_{L^2(\Omega)} + \left(\mathbf{v}\cdot\nabla\varphi, v\right)_{L^2(\Omega)} = 0 \qquad \forall v \in V^{(\mathbf{v})}, \tag{4.16b}$$

$$\varphi(t,\mathbf{x}) = g(t,\mathbf{x}) \qquad \text{on } \partial\Omega^{\text{in}}, \tag{4.16c}$$

$$\varphi(0,\mathbf{x}) = \varphi_0(\mathbf{x}) \qquad \text{in } \Omega. \tag{4.16d}$$

We have already seen that one can prove the existence of a unique solution to this problem, cf. Theorem 3.6. This section is devoted to the numerical approximation of problem (4.16) in space. At first, we consider the spatial finite element discretization. In particular, we assess the quality of the interface approximation when using linear and quadratic finite elements for $d = 2$.

4.3.1. Finite Element Approximation

For the semi-discretization in space, we employ the finite element approach introduced in Section 3.3. We only consider the two-dimensional case $\Omega \subset \mathbb{R}^2$ and the finite element spaces $V_h := X_h^k$ for $k \in \{1,2\}$ on a given triangulation $\mathcal{T}_h$ of Ω, cf. (3.38). We consider the Dirichlet boundary condition $\varphi|_{\partial\Omega^{\text{in}}} = g$, and incorporate it into the test space $V_{h,0} := \{v \in X_h^k \,:\, v|_{\partial\Omega^{\text{in}}} = 0\}$. For a given initial datum $\varphi_{0,h} \in V_h$ and a velocity field $\mathbf{v} \in \left(H_0^1(\Omega)\right)^2$, the finite element semi-discretization of problem (4.16) is given by:

$$\text{Find } \varphi_h(t) \in V_h \text{ for all } t \in [0,T] \text{ such that} \tag{4.17a}$$

$$\frac{\mathrm{d}}{\mathrm{d}t}\left(\varphi_h(t), v_h\right)_{L^2(\Omega)} + \left(\mathbf{v}\cdot\nabla\varphi_h(t), v_h\right)_{L^2(\Omega)} = 0 \qquad \forall v_h \in V_{h,0}, \tag{4.17b}$$

$$\varphi(t,\mathbf{x}) = g(t,\mathbf{x}) \qquad \text{on } (0,T)\times\partial\Omega^{\text{in}}, \tag{4.17c}$$

$$\varphi(0,\mathbf{x}) = \varphi_0(\mathbf{x}) \qquad \text{in } \Omega. \tag{4.17d}$$

From the more general problem (3.47), we directly transfer the stability estimate (Lemma 3.14)

$$\|\varphi_h(t)\|_{L^2(\Omega)}^2 + \int_0^t \int_{\partial\Omega\setminus\partial\Omega^{\text{in}}} \mathbf{v}\cdot\mathbf{n}\left(\varphi_h(\tau)\right)^2 \mathrm{d}\tau \le \|\varphi_{0,h}\|_{L^2(\Omega)}^2 \cdot \exp\left(\int_0^t \max_{\mathbf{x}\in\overline{\Omega}} \frac{1}{2}\left|\nabla\cdot\mathbf{v}\right|\right), \tag{4.18}$$

and the convergence estimate (Theorem 3.15)

$$\max_{t\in[0,T]} \|\varphi(t) - \varphi_h(t)\|_{L^2(\Omega)} + \left(\int_0^T |\varphi(t) - \varphi_h(t)|_{\mathbf{v},\partial\Omega}\,\mathrm{d}t\right)^{1/2} = \mathcal{O}\left(\|\varphi_0 - \varphi_{0,h}\|_{L^2(\Omega)} + h^k\right), \tag{4.19}$$

assuming sufficient regularity of the exact solution φ.

As explained in Section 3.3.2, the finite element discretization of the hyperbolic level set problem can be unstable. For stabilization, we add *streamline diffusion* acting only in the direction of $\mathbf{v}$:

$$\forall K \in \mathcal{T}_h \ : \qquad v_h^\delta|_K \coloneqq v_h + \delta_K \mathbf{v} \cdot \nabla v_h \qquad v_h \in V_{h,0}, \tag{4.20}$$

where δ_K is a cell dependent stabilization parameter. The stabilized semi-discrete problem reads

$$\text{Find } \varphi_h \in V_h \text{ such that for all } t \in [0,T] \tag{4.21a}$$

$$\frac{\mathrm{d}}{\mathrm{d}t}(\varphi_h(t), v_h^\delta)_{L^2(\Omega)} + (\mathbf{v} \cdot \nabla \varphi_h(t), v_h^\delta)_{L^2(\Omega)} = 0 \qquad \forall v_h \in V_{h,0}, \tag{4.21b}$$

$$\varphi(t) = g(t) \qquad \text{on } \partial\Omega^{\text{in}}, \tag{4.21c}$$

$$\varphi(0) = \varphi_0 \qquad \text{in } \Omega. \tag{4.21d}$$

Since $v_h^\delta \in L^2(\Omega)$, the stabilized scheme is consistent. In what follows we will only consider this stabilized discretization, since the unstabilized form is contained as special case with parameter $\delta = 0$ anyway. Based on numerical experiments, Gross and Reusken suggest in [GR11] the element-wise choice

$$\delta_K \coloneqq c \frac{h_K}{\max\{\varepsilon_0, \|\mathbf{v}\|_{\infty,K}\}}, \tag{4.22}$$

where $\varepsilon_0 > 0$ is a small positive constant, $c = \mathcal{O}(1)$ and h_K the diameter of element $K \in \mathcal{T}_h$.

4.3.2. Interface Approximation

In some applications, explicit knowledge of the interface is required. This section presents explicit results on the interface approximation quality of a finite element level set function. It is largely based on results collected in [GR11] and introduces a simple method for extracting the zero isocontour from the level set function.

Definition 4.6 (Approximation of Γ by Γ_h)
For a given interface $\Gamma(\varphi)$ implicitly defined by a finite element level set function $\varphi_h \in V_h$, and an interpolation operator $\mathcal{I}$, the discrete interface approximation Γ_h is defined by

$$\Gamma_h \coloneqq \{\mathbf{x} \in \Omega \ : \ \mathcal{I}(\varphi_h)(\mathbf{x}) = 0\}. \tag{4.23}$$

For $V_h = X_h^1$, we use the linear interpolation operator and the resulting approximation Γ_h^1 is just a polygonal line. It is determined by the intersections of the interface with edges of the triangulation. For $V_h = X_h^2$, we also employ a linear interpolation operator but on the triangulation $\mathcal{T}_{h'}$ obtained after one regular refinement of $\mathcal{T}_h$. In particular, the degrees of freedom of X_h^2 on $\mathcal{T}_h$ coincide with those of X_h^1 on the refined triangulation $\mathcal{T}_{h'}$. The resulting numerical approximation of the interface Γ_h^2 may, in contrast to Γ_h^1, not coincide with the exact interface Γ on edge intersections of Γ with $\mathcal{T}_{h'}$. Fig. 4.3 illustrates the construction of Γ_h^1 and Γ_h^2.

For a successful numerical interface construction, several assumptions must be made on the triangulation $\mathcal{T}_h$:

- at most two edges of each cell $K \in \mathcal{T}_h$ are intersected by Γ,
- every edge edge is either intersected at exactly one point or not intersected at all.

A detailed listing of assumptions and counter-examples for invalid triangulations is given in [GR11, Sec. 7.3]. In essence, the assumptions ensure that the triangulation is fine enough to resolve interfaces with large curvature. Special treatment is required if the interface touches cells or coincides with triangle edges.

In this section we analyze the approximation quality of Γ_h^1 and Γ_h^2. Let h_Γ be the largest diameter of triangles adjacent to the interface. From φ_h an approximation Γ_h on Γ is obtained as described in Definition 4.6. Quantities of interest are the distance between Γ and its approximation Γ_h, as well as the quality of the numerical normal vector $\hat{\mathbf{n}}_h$. For the remainder of this section we drop the time dependence and write $\varphi(\mathbf{x}) = \varphi(t, \mathbf{x})$ to simplify notation.

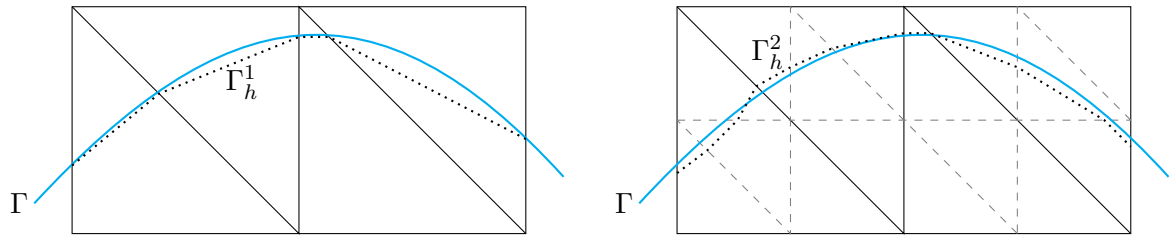

Figure 4.3.: Illustration of numerical interface construction in X_h^1 (left) and X_h^2 (right).

The following Theorem is a collection of various approximation results collected from [RL11].

Theorem 4.7 (Level Set Approximation Errors [RL11])
In the setting of Definition 4.1 at fixed time $t \in [0, T]$, let $\varphi : \Omega \to \mathbb{R}$ be smooth and the associated interface Γ be a connected C^2-curve. For the discrete approximation $\varphi_h \in V_h$, let

$$\|\varphi - \varphi_h\|_{L^2(\Omega)} \leq c h^{k+1/2}. \tag{4.24}$$

For the associated interface Γ_h we assume:

i) $\Gamma_h \subset U$,

ii) $\forall \mathbf{x} \in \Gamma : \ \exists! \, \mathbf{y} \in \Gamma_h : \ \exists! \, \alpha \in \mathbb{R} : \ \mathbf{y} = \mathbf{x} + \alpha \hat{\mathbf{n}}(\mathbf{x})$,

iii) $\hat{\mathbf{n}} \cdot \hat{\mathbf{n}}_h > 0$ on Γ_h.

Furthermore, let $|\nabla \varphi|$ be bounded below and above, i.e.

$$c_0 \leq |\nabla \varphi(\mathbf{x})| \leq c_1 \qquad \text{for almost all } \mathbf{x} \in U. \tag{4.25}$$

Then the following estimate holds:

$$\|\mathrm{dist}(\mathbf{x},\Gamma) - \varphi_h\|_{L^2(\Gamma_h)} \leq ch^k. \tag{4.26}$$

If furthermore there exists a constant $c_{0,h}$ such that

$$c_{0,h} \leq |\nabla\varphi_h(\mathbf{x})|\,, \qquad \text{for all } \mathbf{x} \in U, \tag{4.27}$$

the following error bound for the normal vectors holds:

$$\|\hat{\mathbf{n}} - \hat{\mathbf{n}}_h\|_{L^2(\Gamma_h)} \leq ch^{k-1}. \tag{4.28}$$

The interested reader can find the proofs of this theorem in [RL11], Theorem 4.1 to Theorem 4.2. Note that assumptions (4.25) and (4.27) already indicate the need for using redistancing schemes, which will ensure $|\nabla\varphi| \approx 1$ at least in vicinity of the zero level set. From the interpolation error bound in Theorem 3.12, assumption (4.24) can be verified for X_h^1 and X_h^2.

When using the above interpolation procedure for functions in X_h^2 on a refined triangulaton (see also Fig. 4.3), the following theorem holds:

Theorem 4.8 (Approximation error of Γ_h [GR11, Theorem 7.3.1])
Let $\varphi \in H^2_\infty(\Omega)$ and

$$c_0 \leq |\nabla\varphi| \leq c_1 \tag{4.29}$$

for some constants $c_0, c_1 > 0$. Assume that Γ is contained in the sufficiently small neighborhood $U \coloneqq \{\mathbf{x} \in \mathbb{R}^d \;:\; \mathrm{dist}(\mathbf{x},\Gamma) < c_U\}$ of Γ and that the approximation $\varphi_h \in V_h = X_h^2$ of φ satisfies

$$\|\varphi - \varphi_h\|_{L^\infty(U)} + h_\Gamma \|\varphi - \varphi_h\|_{H^1_\infty(U)} \leq ch_\Gamma^m \|\varphi\|_{H^m_\infty(U)}\,, \tag{4.30}$$

for $m = 1, 2$. Furthermore suppose that the linear interpolation operator on the refined mesh (see above) is employed for Γ_h. Then the following estimates hold for all $\mathbf{x} \in \Gamma_h$:

$$\mathrm{dist}(\mathbf{x},\Gamma) \leq ch_\Gamma^2, \tag{4.31a}$$

$$\|\hat{\mathbf{n}}(\mathbf{x}) - \hat{\mathbf{n}}_h(\mathbf{x})\| \leq ch_\Gamma. \tag{4.31b}$$

4.4. Time Discretization

In this last section we will briefly comment on the time discretization. In the numerical examples to be presented in the chapters below, we have mainly used the θ-scheme combined with linear SUPG-stabilized finite elements.

4.4.1. Finite Difference Scheme

To obtain a fully discrete problem for the level set equation, let us first consider the θ-scheme introduced in Section 3.4. Given the usual partition of $[0,T]$ into N discrete time levels, we obtain a fully discrete version of (4.21):

$$\frac{(\varphi_h^{n+1}-\varphi_h^n, v_h^\delta)}{\Delta t} + \theta\left(\nabla\varphi_h^{n+1}\cdot\mathbf{v}, v_h^\delta\right) + (1-\theta)\left(\nabla\varphi_h^n\cdot\mathbf{v}, v_h^\delta\right) = 0, \tag{4.32a}$$

$$\varphi_h^0 = \varphi_0. \tag{4.32b}$$

For this approach the following convergence estimate holds:

Theorem 4.9 (Convergence Estimate [Bur10, Theorem 13], [RL11])
Let φ be a sufficiently smooth solution to (4.12) and $\{\varphi_h^n\}_{n=0}^N$ the numerical solution to (4.32) with $\theta = 1/2$ (Crank-Nicolson) and $V_h = X_h^k$. Then the following estimate holds:

$$\|\varphi_h^N - \varphi(T)\|_{L^2(\Omega)} \le c\big(h^{k+1/2} + (\Delta t)^2\big), \tag{4.33}$$

where the constant c depends on the smoothness of the data but not on T, h or Δt.

The proof of this theorem, precise regularity assumptions, and the concrete choice of the SUPG parameter δ_K can be found in [Bur10].

4.4.2. Lax-Wendroff-Method

A different approach which is second-order accurate in time, is given by the Lax-Wendroff method. It is based on the Taylor expansion

$$\varphi(t^{n+1}) = \varphi(t^n) + \Delta t\frac{\partial}{\partial t}\varphi(t^n) + \frac{(\Delta t)^2}{2}\frac{\partial^2}{\partial t^2}\varphi(t^n) + \mathcal{O}((\Delta t)^3). \tag{4.34}$$

The higher order time derivatives are replaced by space derivatives using relation (4.10) (cf. [DH03, Section 3.4]):

$$\frac{\partial}{\partial t}\varphi(t^n) = -\mathbf{v}\cdot\nabla\varphi(t^n), \tag{4.35}$$

$$\frac{\partial^2}{\partial t^2}\varphi(t^n) = -\frac{\partial}{\partial t}\big(\mathbf{v}\cdot\nabla\varphi(t^n)\big) = (\mathbf{v}\cdot\nabla)^2\varphi(t^n). \tag{4.36}$$

Substituting these relations into (4.12) we obtain:

$$\varphi(t^{n+1}) \approx \varphi(t^n) - \Delta t\mathbf{v}\cdot\nabla\varphi(t^n) + \frac{(\Delta t)^2}{2}(\mathbf{v}\cdot\nabla)^2\varphi(t^n). \tag{4.37}$$

The second order term introduces numerical diffusion and therefore has a stabilizing effect. In contrast to the streamline diffusion technique, no parameter needs to be adjusted.

5 Level Set Redistancing Methods

Many applications rely not only on an accurate interface location but also on a precise reconstruction of geometrical properties such as normal vector and curvature. As we have seen in Chapter 4, for the numerical reconstruction of these quantities from a level set function φ it is advantageous if φ is a sufficiently good approximation of the signed distance function. Furthermore, in the context of the level set transport equation, numerical schemes also benefit if φ_h is a good approximation to the signed distance function. In particular, this implies $|\nabla\varphi_h| \approx 1$, which is why steepening or flattening effects can be avoided.

Consequently, it is common practice in many numerical applications to initialize the level set function as the signed distance to the initial interface. In the context of evolving interfaces, numerical methods generally fail to preserve the signed distance function property. Therefore, so-called *reinitialization* or *redistancing* techniques are applied to correct the distorted level set function to become a good approximation of a signed distance function. Such approaches should possess three essential properties (cf. [BKS16]):

1. The redistancing process should not displace the interface, since many important physical phenomena may take place on or be influenced by the interface, making the accuracy of its numerical approximation crucial.
2. The result should be a good approximation to the signed distance function of the interface. As consequence of Theorem 4.4, the residual of the Eikonal equation $|\nabla\varphi_h| = 1$ can indicate the approximation accuracy, and consequently, the minimization of this residual forms the basis of many numerical redistancing schemes.
3. The computational costs of the redistancing technique should be reasonable in relation to the expected benefits.

Over the past decades, many redistancing approaches have been developed. One can generally distinguish between two types:

(i) *Geometric redistancing approaches* compute the distance to the interface directly. Thus, they generally require the localization of the interface, which can be a complex task (cf. Section 4.3.2), in particular for higher order polynomial approximations of the level set function and higher space dimensions. On the other hand, it is possible to construct

high accuracy schemes that have the same asymptotic approximation quality as the nodal interpolation of the exact distance function [EG14].

Many geometric approaches consist of two steps. First, redistancing is performed in the immediate vicinity of the interface with a high accuracy algorithm. In the second step, the results are extended to the surrounding region, using an approach aiming for efficiency.

The idea of redistancing was first proposed by Chopp in [Cho93] and led to the developement of the well-known geometric fast marching reinitialization technique by Tsitsiklis and Sethian [Set96a, Set99a, Tsi94]. In the last years, more efficient and more accurate techniques were developed.

(ii) *PDE-based redistancing approaches* build on solving a redistancing equation that minimizes the residual of the Eikonal equation. Many are based on a technique originally presented by Sussman et al. [SSO94], in which the distance function to a given interface can be computed by evolving a hyperbolic advection equation to steady state.

In contrast to geometric approaches, no actual knowledge of the interface position is required. Hence, one can easily employ higher order polynomials for the approximation of the level set function. As an inherent property of a finite element discretization in PDE-based approaches, the application to unstructured meshes is possible while most geometric approaches rely on Cartesian grids. However, in many algorithms it is necessary to use sufficiently stable discretization techniques and to evaluate the discontinuous sign function. Numerical implementations often induce artificial diffusion which may negatively influence the accuracy of the interface approximation.

In this thesis we focus on PDE-based redistancing approaches, which is why we only provide a brief presentation of two popular geometric redistancing techniques in the first section. In the subsequent sections, we introduce PDE-based approaches before proposing an optimal control approach. The chapter concludes with a detailed numerical evaluation of the presented methods and schemes.

5.1. Geometric Redistancing

Geometric redistancing techniques are based on the direct computation of the distance to the interface. The most intuitive approach is the so-called *brute-force* redistancing, in which for each degree of freedom of the discrete level set function the actual distance to the interface is computed. Even though the numerical costs can be reduced by a suitable subdivision of the interface, one still has to face a complexity of $\mathcal{O}(M \cdot N)$, where N is the number of grid points and M the number of interface segments [Hys07]. Many approaches build on brute-force redistancing but are commonly used only in the immediate interface vicinity.

5.1.1. Fast Marching Method

One of the most popular geometric redistancing approaches is the *fast-marching method*, proposed in [Tsi94, Set96b, Cho01]. As explained in [Bas12], the key idea boils down to construct-

ing the level set function φ by using upwind values, i.e. information is only propagated from smaller to larger values of φ. Sethian presented the following algorithm in [Set99b]:

1. On a discrete grid, for grid points in immediate vicinity of the interface, the distance to the interface is directly computed. Those points are then marked as "known".
2. For grid points adjacent to a "known" grid point, the distance is determined approximately by computing the distance to the closest "known" point. Each of these points is then marked as "trial".
3. All other grid points are tagged as "far" and the value at those points is initialized by a value bigger than the largest possible distance to the interface.
4. From the set of "trial" points, we pick the point p with minimal distance value, and tag it as "known".
5. For all "far" grid points adjacent to p, the distance is recomputed and the points are tagged as "trial".
6. While the set of "trial" points is not empty, go back to step 4.

For the actual computation of the distance of a "trial" point to the interface, an upwind finite difference scheme is applied to discretize the Eikonal equation. This results in a quadratic equation to be solved. For efficiency, an adequate algorithm for finding the point with minimal distance in the "trial" set is required. For a detailed description and more information, the interested reader is referred to [OF03, Set99b].

Even though the computational costs of $\mathcal{O}(N \log(N))$ are less than for brute-force redistancing, the sorting of the trial set is expensive. Furthermore, the approach requires at least two grid points in which the correct value of the signed distance function is known in advance. However, in many techniques the Fast Marching approach is employed in the extension phase after redistancing has been accomplished in a narrow interface band.

5.1.2. Geometric Mass-Preserving Scheme

An interesting approach was proposed by Ausas et al. in [ADB11] which is based on [MBD06]. It introduces a finite element based redistancing algorithm that also works on unstructured meshes and conserves mass.

The method consists of the following steps:

1. *Initialization*
   Given a level set function $\tilde{\varphi}_h$ to be reinitialized, reconstruct the interface Γ_h from $\tilde{\varphi}_h$.
2. *Local redistancing*
   Let $\mathcal{K}$ denote the set of cells intersected by the interface and $\mathcal{P}$ the set of nodes of these cells. For all nodes in $\mathcal{P}$, we compute the nodal values of the intermediate level set function φ_h^* to be the exact distance w.r.t. Γ_h, i.e.

$$\varphi_h^*(\mathbf{x}) = \operatorname{dist}(\mathbf{x}, \Gamma_h) \qquad \forall \mathbf{x} \in \mathcal{P}. \tag{5.1}$$

This brute force approach can be performed element-wise and therefore be efficiently implemented in parallel.

3. *Mass Correction*
   The mass of φ_h^*

$$\mathrm{m}_{\mathcal{K}}(\varphi_h^*) \coloneqq \int_{\mathcal{K}} \mathrm{H}\left(\varphi_h^*(\mathbf{x})\right) \,\mathrm{d}\mathbf{x} \tag{5.2}$$

   may suffer loss or gain, and therefore in general $\mathrm{m}_{\mathcal{K}}(\tilde{\varphi}_h^*) \neq \mathrm{m}_{\mathcal{K}}(\tilde{\varphi}_h)$. This is why we seek a correction function ψ_h such that

$$\mathrm{m}_{\mathcal{K}}(\varphi_h^* + \psi_h) = \mathrm{m}_{\mathcal{K}}(\tilde{\varphi}). \tag{5.3}$$

   Therefore, one computes element-wise the piecewise constant function η_h such that

$$\mathrm{m}_K(\varphi_h^* + \eta_h) = \mathrm{m}_K(\tilde{\varphi}_h) \qquad \forall K \in \mathcal{K}. \tag{5.4}$$

   This requires solving a non-linear problem in each cell $K \in \mathcal{K}$, for which a simple secant procedure is suggested. Based on η_h, one computes the continuous L^2-projection ξ_h of η_h. Finally, by solving a non-linear equation again, a constant C is determined such that

$$\psi_h = C\xi_h. \tag{5.5}$$

   corrects φ_h^* such that (5.3) holds.

4. *Extension Phase*
   In the last step, the values of the conservative level set function $\varphi_h^* + \psi_h$ are extended to the remaining mesh nodes. This can be performed by applying other redistancing approaches. In [ADB11], the authors suggest to use a geometric approach developed by Mut et al. [MBD06].

Let us remark that in contrast to the level set shifting approach for mass conservation (introduced below in Section 6.2) the intermediate level set function is corrected by adding a constant which would correspond to the choice $\xi_h \equiv 1$ here, but may cause a nonphysical distribution of mass (cf. [ADB11]). Furthermore, the scaling of ξ_h by a constant C might have a similar yet less significant effect on the mass distribution and local mass conservation cannot be guaranteed exactly.

In their recent publication [EG14], Esser and Grande extend this approach to piecewise quadratic level set functions. This requires more effort for the computation of the discrete interface Γ_h and the calculation of the exact distance is also more complex.

The presented schemes generally offer good interface approximation accuracy due to the exact computation of the distance values with respect to the discrete representation of the interface. However, they require the complex localization of Γ_h. The numerical implementation therefore becomes more involved and the computational costs increase. Furthermore, the extension to higher degree polynomial approximations of the level set function is difficult.

5.1.3. Further Approaches

We have only shown two general geometric techniques as the focus of this thesis is on PDE-based approaches. However, we want to refer the interested reader to the following publications for more information on geometric redistancing techniques:

- Ausas et al. [ADB11] provide a more general discussion and comparison of geometric and PDE-based approaches (hyperbolic redistancing).
- Elias et al. [EMC07] present an algorithm which computes the distance function in an element-wise manner on unstructured grids. The main idea is similar to the fast marching method. Based on "computable" elements, i.e. elements that have a sufficient number of nodes for which the exact distance value is known to compute it in the remaining nodes, the information is propagated to the adjacent cells. The actual numerical solution of the local Eikonal equation is accomplished by using the discrete gradient operator, resulting in a quadratic form. In addition to the discrete interface localization, this approach requires a suitable mesh structure that provides adjacency information.
- In the recent publication [Reu13], Reusken suggests a variational gradient recovery based approach to compute a continuous finite element approximation of $\nabla\varphi_h$. Based on the recovered gradient, one defines a quasi-normal field to determine the values in grid points close to the interface. In a second step, the values are extended to the entire grid, for example by employing the fast marching method. The author provides a detailed but complex numerical analysis for his approach. In contrast to most other geometric redistancing approaches, the generalization to higher order polynomial degrees is straightforward, but numerical implementation is more involved than for other techniques.

In summary we conclude that geometrical redistancing approaches offer good approximation quality and efficient numerical algorithms exist. A common drawback is the mandatory and possibly complex localization of the interface, in particular when using higher order polynomial approximations to level set functions (cf. 4.3.2).

5.2. Hyperbolic Redistancing

An appealing alternative to geometrical methods is the PDE-based hyperbolic approach introduced by Sussman, Smereka and Osher in [SSO94]. The underlying idea of minimizing the residual of the Eikonal equation forms the basis for many other PDE-based approaches. Given an interface in terms of a level set function $\tilde{\varphi}$, a signed distance function φ with identical zero level set can be obtained by solving the equation

$$\frac{\partial}{\partial\tau}\varphi(\tau,\mathbf{x}) = \operatorname{sign}(\tilde{\varphi}(\mathbf{x}))\big(1 - |\nabla\varphi(\tau,\mathbf{x})|\big) \tag{5.6}$$

to steady state in artificial time τ. By design,

$$\frac{\partial}{\partial\tau}\varphi(\tau,\mathbf{x}) = 0 \qquad \forall\mathbf{x}\in\Gamma(\tilde{\varphi}). \tag{5.7}$$

Hence, any solution to (5.6) cannot displace the interface at a continuous level. On the other hand, $|\nabla\varphi(\tau,\mathbf{x})| \to 1$ as the solution φ to (5.6) approaches the steady state. Where $|\nabla\varphi(\tau,\mathbf{x})| \neq 0$, we can equivalently rewrite equation (5.6) as

$$\frac{\partial}{\partial\tau}\varphi(\tau,\mathbf{x}) + \mathbf{w}(\tau,\mathbf{x})\cdot\nabla\varphi(\tau,\mathbf{x}) = \operatorname{sign}(\tilde{\varphi}(\mathbf{x})) \tag{5.8}$$

using the unit vector

$$\mathbf{w}(\tau,\mathbf{x}) \coloneqq \operatorname{sign}(\tilde{\varphi}(\mathbf{x}))\frac{\nabla\varphi(\tau,\mathbf{x})}{|\nabla\varphi(\tau,\mathbf{x})|}. \tag{5.9}$$

This form reveals the hyperbolic character of the PDE and is very similar to the level set transport equation. Since $\mathbf{w}$ is pointing away from the interface, $\partial\Omega$ does not possess an inflow boundary portion in the case of a convex and sufficiently smooth domain Ω. In numerical applications one naturally uses a regularized sign function such as

$$S_\varepsilon : \mathbb{R} \to \mathbb{R}^+, \qquad S_\varepsilon(f) \coloneqq \frac{f}{\sqrt{f^2+\varepsilon^2}} \tag{5.10}$$

instead of the discontinuous sign function. In [SSO94] a finite difference upwinding scheme is suggested for the numerical approximation of the PDE. An improved approach is presented by Russo and Smereka [RS00] in which the finite difference stencils are restricted to one side of the interface. In contrast to the original formulation, in this method the interface displacement does not depend on the number of pseudo time steps.

Hartmann et al. [HMS08, HMS10] present a further improved finite difference approach based on [SSO94, RS00]. The key idea of their approach is to formulate a least squares problem minimizing displacements of the zero level set in the redistancing process in cells containing the interface. In essence, the original hyperbolic redistancing equation is augmented by a forcing term which acts as a constraint preventing artificial interface displacements. Even though high accuracy can be obtained with this approach, it suffers from general disadvantages of finite difference approaches. In particular, the application to unstructured meshes as well as the approximation of more involved geometries is very complex.

Alternatively, we can apply a stabilized finite element scheme as proposed in [Tor00, TE00]. A possible fully discrete finite element approximation is given by (cf. (4.21) and (4.32)):

$$\frac{(\varphi_h^{n+1}-\varphi_h^n, v_h)}{\Delta t} + (\mathbf{w}_h^n\cdot\nabla\varphi_h^n, v_h + \delta\mathbf{w}_h^n\cdot\nabla v_h) = (S_\varepsilon(\tilde{\varphi}_h), v_h + \delta\mathbf{w}_h^n\cdot\nabla v_h) \qquad \forall v_h \in V_h. \tag{5.11}$$

Tornberg and Enquist [TE00] recommend further stabilization inside the region adjacent to the interface in which $\mathbf{w}_h^n$ might not be a unit vector due to the smearing effect caused by the regularization S_ε. They suggest adding a small diffusive term

$$\alpha(\nabla\varphi_h^{n+1}, \nabla v_h) \tag{5.12}$$

to the left hand side of equation (5.11), with parameter $\alpha = \mathcal{O}(h)$. In contrast to the finite difference approaches for hyperbolic redistancing as presented in [SSO94, RS00, HMS08],

the finite element discretization allows for unstructured meshes and offers better boundary approximation accuracy.

We remark that due to the numerically inevitable replacement of $\operatorname{sign}(\cdot)$ by the continuous approximation $S_\varepsilon(\cdot)$, additional numerical diffusion is introduced which may cause interface displacements. In particular, given a large parameter ε, the displacement can become significant. Inordinately small values of the parameter ε tend to degrade the rate of convergence. In general, the approach notably depends on the particular choice of this regularization parameter. The interested reader is further referred to [CT08].

5.2.1. Convected Level Set Method

The hyperbolic redistancing scheme (5.6) as well as the geometric approaches from the previous section are predictor-corrector algorithms. Based on a given initial function $\tilde{\varphi}$, they construct an approximation of a signed distance function with respect to the interface provided by $\tilde{\varphi}$.

In many applications the interface evolves over time (as, for example, in two-phase flow problems). Even if the provided initial data is (close to) a signed distance function, numerical schemes generally fail to preserve this property as time evolves. Gradients of the level set function may become very flat or steep, which increases numerical inaccuracies. Therefore one usually applies a redistancing scheme to a tentative solution of the level set equation at each time step or when necessary. Alternatively, it is possible to use a monolithic scheme that embeds the numerical solution process of the transport equation and a redistancing technique into a single method.

The *convected level set method* proposed by Ville et al. [VSC11] is such a monolithic approach which combines the hyperbolic redistancing scheme from the previous section with the solution of the transport equation. The *convected redistancing equation*

$$\frac{\partial}{\partial t}\varphi(t,\mathbf{x}) + (\mathbf{v}(t,\mathbf{x}) + \lambda\mathbf{w}(t,\mathbf{x}))\cdot\nabla\varphi(t,\mathbf{x}) = \lambda \operatorname{sign}\big(\varphi(t,\mathbf{x})\big) \tag{5.13}$$

is obtained as follows (cf. [VSC11]). At a fixed time t, we seek, based on the hyperbolic redistancing approach, an approximation $\Phi(\tau,\mathbf{x})$ in virtual time τ such that

$$\frac{\partial}{\partial \tau}\Phi(\tau,\mathbf{x}) + \operatorname{sign}\big(\varphi(t,\mathbf{x})\big)\,(|\nabla\Phi(\tau,\mathbf{x})| - 1) = 0, \tag{5.14a}$$

$$\Phi(0,\mathbf{x}) = \varphi(t,\mathbf{x}). \tag{5.14b}$$

In a hyperbolic approach, we would replace the predictor $\varphi(t,\mathbf{x})$ by the corrector, which is the steady state limit of (5.14). Similarly as in (5.9), the unit vector

$$\mathbf{w}(\tau,\mathbf{x}) \coloneqq \operatorname{sign}(\varphi(t,\mathbf{x}))\frac{\nabla\Phi(\tau,\mathbf{x})}{|\nabla\Phi(\tau,\mathbf{x})|}, \tag{5.15}$$

is defined, and problem (5.14) is rewritten into the advection equation

$$\frac{\partial}{\partial\tau}\Phi(\tau,\mathbf{x}) + \mathbf{w}(\tau,\mathbf{x})\cdot\nabla\Phi(\tau,\mathbf{x}) = \operatorname{sign}\big(\varphi(t,\mathbf{x})\big), \tag{5.16a}$$

$$\Phi(0,\mathbf{x}) = \varphi(t,\mathbf{x}). \tag{5.16b}$$

Ville et al. [VSC11] then introduce the parameter

$$\lambda = \frac{\partial\tau}{\partial t}, \tag{5.17}$$

to relate the virtual time τ with the physical time t:

$$\frac{\partial}{\partial t}\Phi(\tau,\mathbf{x}) = \lambda\frac{\partial}{\partial\tau}\Phi(\tau,\mathbf{x}). \tag{5.18}$$

From (5.14) we obtain

$$\frac{\partial}{\partial t}\Phi(\tau,\mathbf{x}) + \lambda\operatorname{sign}\big(\varphi(t,\mathbf{x})\big)\left(|\nabla\Phi(\tau,\mathbf{x})| - 1\right) = 0. \tag{5.19}$$

The key idea presented in [VSC11] is to change the partial time derivative of Φ into the total time derivative, since the domain is moving in a Eulerian context. This motivates the hyperbolic redistancing task

$$\frac{\mathrm{d}}{\mathrm{d}t}\Phi(\tau,\mathbf{x}) + \lambda\operatorname{sign}\big(\varphi(t,\mathbf{x})\big)\left(|\nabla\Phi(\tau,\mathbf{x})| - 1\right) = 0, \tag{5.20a}$$

$$\Phi(0,\mathbf{x}) = \varphi(t,\mathbf{x}), \tag{5.20b}$$

in a moving reference frame driven by the velocity field $\mathbf{v}$. Ville et al. [VSC11] further propose the heuristic approach to replace Φ by the main level set variable φ:

$$\frac{\mathrm{d}}{\mathrm{d}t}\varphi(t,\mathbf{x}) + \lambda\operatorname{sign}\big(\tilde{\varphi}(t,\mathbf{x})\big)\left(|\nabla\varphi(t,\mathbf{x})| - 1\right) = 0, \tag{5.21a}$$

$$\varphi(0,\mathbf{x}) = \tilde{\varphi}(t,\mathbf{x}), \tag{5.21b}$$

where $\tilde{\varphi}$ is a provisional solution to the level set equation. Substituting the material derivative (see (7.2))

$$\frac{\mathrm{d}}{\mathrm{d}t}\varphi(t,\mathbf{x}) = \frac{\partial}{\partial t}\varphi(t,\mathbf{x}) + \mathbf{v}\cdot\nabla\varphi(t,\mathbf{x}), \tag{5.22}$$

we obtain the convected level set equation (5.13). In a discrete setting with mesh size h, physical time step size Δt and virtual time increment $\Delta\tau$, Ville et al. suggest setting

$$\lambda = \frac{h}{\Delta t}. \tag{5.23}$$

The convected level set equation is of hyperbolic type. As before, the utilization of a suitable stabilization technique is therefore strongly recommended. Ville et al. [VSC11] propose to use streamline diffusion technique introduced above with a cell-dependent stabilization parameter

$$\delta = \frac{h}{D|\mathbf{v}|}, \tag{5.24}$$

where D denotes the number of nodes per element (for $d = 2$ and linear finite elements on a triangular mesh we have $D = 3$). Note that the problem at hand is non-linear. A suitable linearization can be obtained by employing a simple fixed-point iteration or by applying Newton's method. Furthermore, the sign function should be replaced by a smooth version such as $S_\varepsilon(\cdot)$ in (5.10). This however may cause a smearing of the interface and a significant loss in accuracy. As for the hyperbolic approach, numerical accuracy, stability and convergence behavior may significantly depend on the choice of ε (cf. [CT08]). Let us remark that in our numerical experiments we found the scheme to be quite sensitive w.r.t. the specific choice of λ. Smaller values than suggested in (5.23) often result in a significant increase of the number of required virtual time steps, while larger values lead to stronger numerical inaccuracies. Finally, let us remark that the approach is a heuristic algorithm that is not obtained from a rigorous mathematical derivation.

5.3. Parabolic Redistancing

Based on the hyperbolic redistancing approach (5.6), Li et al. [LXGF10] proposed a technique in which the corrected level set equation is obtained by solving the energy-minimizing gradient flow problem

$$\frac{\partial}{\partial \tau}\varphi + \frac{\partial}{\partial \varphi}\mathcal{R}_p(\varphi) = 0 \tag{5.25}$$

to steady state. Here, $\frac{\partial}{\partial \varphi}$ denotes the variational derivative. The level set regularization term

$$\mathcal{R}_p(\varphi) \coloneqq \int_\Omega p(|\nabla \varphi|)\, \mathrm{d}\mathbf{x}, \tag{5.26}$$

is defined in terms of a suitable *potential function* $p : [0, \infty) \to \mathbb{R}$. For example, the least squares solution to the Eikonal equation (4.5) can be obtained by setting $p(s) \coloneqq 1/2\,(s-1)^2$, which gives rise to the following regularization term:

$$\mathcal{R}_p(\varphi) = \frac{1}{2}\int_\Omega \left(|\nabla \varphi| - 1\right)^2 \mathrm{d}\mathbf{x} = \frac{1}{2}\left\||\nabla \varphi| - 1\right\|^2_{L^2(\Omega)}. \tag{5.27}$$

Other choices for the potential function can be found in the original publication and in Section 5.4. It can easily be seen [LXGF10, BK13] that in the particular case of the level set regularization term from (5.27), equation (5.25) simplifies to the non-linear heat equation

$$\frac{\partial}{\partial \tau}\varphi - \nabla \cdot \left(\nabla\varphi - \frac{\nabla\varphi}{|\nabla\varphi|} \right) = 0. \tag{5.28}$$

Li et al. [LXGF10] suggest a fully explicit finite difference scheme for discretization. Let us remark that even though the method is easy in terms of implementation, computational costs may be significant due to time step restrictions [BK13]. Furthermore, the internal boundary condition

$$\varphi = 0 \qquad \text{on } \Gamma \tag{5.29}$$

may be violated.

5.4. Elliptic Redistancing

In this section we consider an extension of the parabolic redistancing approach proposed by Li et al. [LXGF10] to a finite element discretization. It is based on the work presented in [BK13]. The internal boundary condition (5.29) is enforced by adding a penalty term

$$\mathcal{P}_\Gamma(\varphi) = \frac{\alpha}{2} \int_\Gamma \varphi^2 \, \mathrm{d}\sigma \tag{5.30}$$

to (5.26). Furthermore, the minimization problem

$$\min_{\varphi \in V} \big(\mathcal{R}_p(\varphi) + \mathcal{P}_\Gamma(\varphi) \big) \tag{5.31}$$

can be solved without resorting to pseudo-time stepping:

$$\frac{\partial}{\partial \varphi} \big(\mathcal{R}_p(\varphi) + \mathcal{P}_\Gamma(\varphi) \big) = 0. \tag{5.32}$$

The minimization problem is consistent in the sense that the (signed) distance function $\bar{\varphi}(\mathbf{x}) \coloneqq \operatorname{dist}(\mathbf{x}, \Gamma)$ (cf. Definition A.3) is a global minimum. In particular, $\mathcal{P}_\Gamma(\bar{\varphi}) = 0$ by definition and due to Theorem 4.4, the Eikonal equation is satisfied almost everywhere, i.e. $\mathcal{R}(\bar{\varphi}) = 0$. It is also the unique solution to (5.31), provided the sign of $\bar{\varphi}$ is fixed with respect to Ω_1 and Ω_2. For a sufficiently large penalty parameter $\alpha > 0$, the interface displacements are negligible. Furthermore, this is a global approach and no time iteration is required.

5.4.1. Existence of a Solution in the Finite-Dimensional Setting

To show the existence of a solution to a discrete approximation of minimization problem (5.31), we need the following auxiliary result:

Lemma 5.1 (Poincaré-like Inequality)
Let $\tilde{\varphi} \in H^1(\Omega)$ be such that $\Gamma = \Gamma(\tilde{\varphi}) \coloneqq \{\mathbf{x} \in \Omega \mid \tilde{\varphi}(\mathbf{x}) = 0\}$ has non-zero $(d-1)$ measure. Then there exist constants $c > 0$ and $C(\Gamma, \gamma) > 0$ such that for all $\gamma > 0$ and $\varphi \in H^1(\Omega)$ with $\mathcal{P}_\Gamma(\varphi) < \alpha\gamma$

$$\|\varphi\|_{H^1(\Omega)} \leq c \|\nabla\varphi\|_{L^2(\Omega)} + C(\Gamma, \gamma). \tag{5.33}$$

holds.

Proof. The proof is based on the Poincaré-Friedrichs inequality, see Theorem A.10. By definition of $\mathcal{P}_\Gamma$, cf. (5.30), and by assumption the inequality

$$\left| \int_\Gamma \varphi \, \mathrm{d}\sigma \right| \leq \sqrt{|\Gamma|} \left(\int_\Gamma \varphi^2 \, \mathrm{d}\sigma \right)^{1/2} \leq \sqrt{|\Gamma|}\sqrt{\gamma}$$

holds. Consider the linear form

$$f(v) \coloneqq \frac{1}{|\Gamma|} \int_\Gamma v \, \mathrm{d}\sigma,$$

from Theorem A.10. Inequality (A.12) yields

$$\|\varphi - f(\varphi)\|_{H^1(\Omega)} \leq c \|\nabla\varphi\|_{L^2(\Omega)},$$

and an application of the triangle inequality concludes the proof:

$$\|\varphi\|_{H^1(\Omega)} \leq c \|\nabla\varphi\|_{L^2(\Omega)} + \|f(\varphi)\|_{H^1(\Omega)} \leq c \|\nabla\varphi\|_{L^2(\Omega)} + \frac{\sqrt{\gamma}}{\sqrt{|\Gamma|}}.$$

□

Lemma 5.2 (Existence of a Solution)
Let $V_h \subset H^1(\Omega)$ be a closed subspace, $\tilde{\varphi}_h \in V_h$ satisfying the assumptions of Lemma 5.1 and defining $\Gamma = \Gamma(\tilde{\varphi})$. Let $p(s) \coloneqq \frac{1}{2}(s-1)^2$ in the definition of the level set regularization term $\mathcal{R}_p(\cdot)$. Then the minimization problem (5.32) has a global solution in V_h.

Proof. We roughly follow the proof of Theorem 4.1 in [Vex12]. Since $\tilde{\varphi}_h \in V_h$, the set is obviously nonempty. Furthermore, the objective functional is non-negative by definition:

$$J(\varphi) = \mathcal{R}_p(\varphi) + \mathcal{P}_\Gamma(\varphi) = \| |\nabla\varphi| - 1 \|^2_{L^2(\Omega)} + \frac{\alpha}{2} \int_\Gamma \varphi^2 \, \mathrm{d}\sigma \geq 0.$$

This implies the existence of

$$j \coloneqq \inf_{\varphi \in V_h} J(\varphi),$$

and of a sequence $\{\varphi_n\} \subset V_h$ with

$$J(\varphi_n) \to j, \qquad \text{as } n \to \infty$$

such that

$$J(\varphi_n) < j + \frac{1}{n}.$$

In light of Lemma 5.1 (set $\gamma := \frac{j+1/2}{\alpha}$), we can conclude that the sequence $\{\varphi_n\}$ is bounded in $H^1(\Omega)$:

$$\begin{aligned}\|\varphi_n\|_{H^1(\Omega)} &\leq c\,\|\nabla\varphi_n\|_{L^2(\Omega)} + C(\Gamma,\gamma) = c\,\||\nabla\varphi_n| - 1 + 1\|_{L^2(\Omega)} + C(\Gamma,\gamma)\\ &\leq c\,\||\nabla\varphi_n| - 1\|_{L^2(\Omega)} + c|\Omega|^{1/2} + C(\Gamma,\gamma) \leq c\sqrt{2\mathcal{R}_p(\varphi_n)} + \hat{C}\\ &\leq c\sqrt{2J(\varphi_n)} + \hat{C} \leq c\sqrt{2j+1} + \hat{C}.\end{aligned}$$

Since V_h is finite-dimensional, the Theorem of Bolzano-Weierstraß ensures the existence of a convergent subsequence $\{\varphi_{n_k}\} \subset V_h$,

$$\varphi_{n_k} \to \bar{\varphi}_h \in V_h,$$

with $\bar{\varphi}_h \in V_h$, since V_h is closed. The continuity of $J(\varphi)$ can be shown very similarly to Lemma 5.3, and finally yields

$$J(\varphi_{n_k}) \to J(\bar{\varphi}_h). \qquad \square$$

Unfortunately, the proof cannot be carried out for functions $\varphi \in H^1(\Omega)$, since we could only deduce the existence of a weakly convergent subsequence $\{\varphi_{n_k}\}$, $\varphi_{n_k} \rightharpoonup \bar{\varphi}$ in the infinite dimensional case. The continuity of the objective function is not sufficient to conclude $J(\varphi_{n_k}) \to J(\bar{\varphi})$. We would need $J(\varphi)$ to be weakly lower semi-continuous. This is true for continuous and convex functionals, however $J(\varphi)$ is not convex.

The usual approach to show uniqueness by employing the convexity of the objective functional (5.32) is not applicable here. Uniqueness can not generally be expected in $H^1(\Omega)$ without adding a suitable regularization term as the one-dimensional example in Fig. 5.1 shows. Both depicted functions satisfy the Eikonal equation almost everywhere in Ω, but only one is a signed distance function. In practice however, good initial guesses for the fixed-point iteration (5.35) prevent such deteriorated functions. In the context of transport equations, a temporary solution or the solution from the previous time step can directly provide a suitable initial guess. We remark that this behavior can mostly be avoided when adding an additional continuous interior penalty (CIP) term, cf. (5.51).

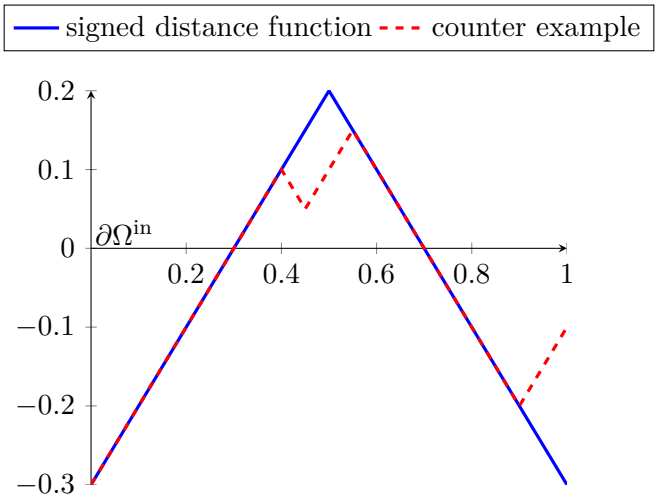

Figure 5.1.: Illustration of a counter example for the uniqueness of the solution.

5.4.2. Weak Formulation

For the regularization term defined in (5.27) and a sufficiently smooth test function v, we obtain the variational form of (5.32):

$$\int_\Omega \left(1 - \frac{1}{|\nabla\varphi|}\right) \nabla\varphi \cdot \nabla v \, \mathrm{d}\mathbf{x} + \alpha \int_\Gamma \varphi v \, \mathrm{d}\sigma = 0. \tag{5.34}$$

The problem is non-linear in φ. Therefore, we employ the iterative solution strategy presented in [BK13]: Based on an initial guess $\varphi^{(0)}$, successive approximations are computed using the fixed-point iteration

$$\mathsf{a}(\varphi^{(m)}, v) = \mathsf{b}(\varphi^{(m-1)}, v) \qquad \forall v, \tag{5.35}$$

where the bilinear forms $a(\cdot,\cdot)$ and $b(\cdot,\cdot)$ are defined by

$$\mathsf{a}(\varphi, v) \coloneqq \int_\Omega \nabla\varphi \cdot \nabla v \, \mathrm{d}\mathbf{x} + \alpha \int_\Gamma \varphi v \, \mathrm{d}\sigma, \tag{5.36a}$$

$$\mathsf{b}(\tilde{\varphi}, v) \coloneqq \int_\Omega \frac{\nabla\tilde{\varphi}}{|\nabla\tilde{\varphi}|} \cdot \nabla v \, \mathrm{d}\mathbf{x}. \tag{5.36b}$$

More generally, different level set regularization terms can be considered. In [LXGF10, BK13], the generic term

$$\mathcal{R}_p(\varphi) \coloneqq \int_\Omega p(|\nabla\varphi|) \, \mathrm{d}\mathbf{x} \tag{5.37}$$

for a given potential function $p : [0, \infty) \to \mathbb{R}$ is defined. Enough regularity provided, the variational derivative of $\mathcal{R}_p(\varphi)$ with respect to φ in direction v is given by

$$\delta\mathcal{R}_p(\varphi, v) = \int_\Omega d_p(|\nabla\varphi|)\nabla\varphi \cdot \nabla v \, \mathrm{d}\mathbf{x}, \tag{5.38}$$

where

$$d_p(s) = \frac{p'(s)}{s}. \tag{5.39}$$

denotes the *diffusion rate* associated with p. In the strong form we have

$$\frac{\partial}{\partial\varphi}\mathcal{R}_p(\varphi) = \nabla \cdot \big(d_p(|\nabla\varphi|)\nabla\varphi\big), \tag{5.40}$$

which shows that the level set regularization term creates forward diffusion where $d_p(|\nabla\varphi|) > 0$ and backward diffusion where $d_p(|\nabla\varphi|) < 0$. For consistency, we define the potential used in (5.27) as

$$p_1(s) \coloneqq \frac{1}{2}(s-1)^2. \tag{5.41}$$

The associated diffusion rate is

$$d_1(s) = 1 - \frac{1}{s}. \tag{5.42}$$

5.4.3. Different Potential Functions

Unfortunately, for flat gradients of φ, the diffusion rate detoriates since $d_1(s) \to -\infty$ as $s \searrow 0$ (cf. Fig. 5.2). As alternative potential to p_1, Li et al. [LXGF10] therefore propose the *double-well* potential

$$p_2(s) \coloneqq \begin{cases} \frac{1}{4\pi^2}\big(1 - \cos(2\pi s)\big) & \text{if } s \le 1, \\ \frac{1}{2}(s-1)^2 & \text{if } s > 1. \end{cases} \tag{5.43}$$

In contrast to p_1, the double well potential has an additional minimum at $s = 0$ and the diffusion rate

$$d_2(s) = \begin{cases} \frac{1}{2\pi s}\sin(2\pi s) & \text{if } s \le 1, \\ 1 - \frac{1}{s} & \text{if } s > 1, \end{cases} \tag{5.44}$$

is bounded below. For flat gradients, i.e. where $|\nabla\varphi(\mathbf{x})| < \frac{1}{2}$, the diffusion rate is positive, forcing φ to become constant. However, the non-linear stationary problem associated with $\mathcal{R}_{p_2}$

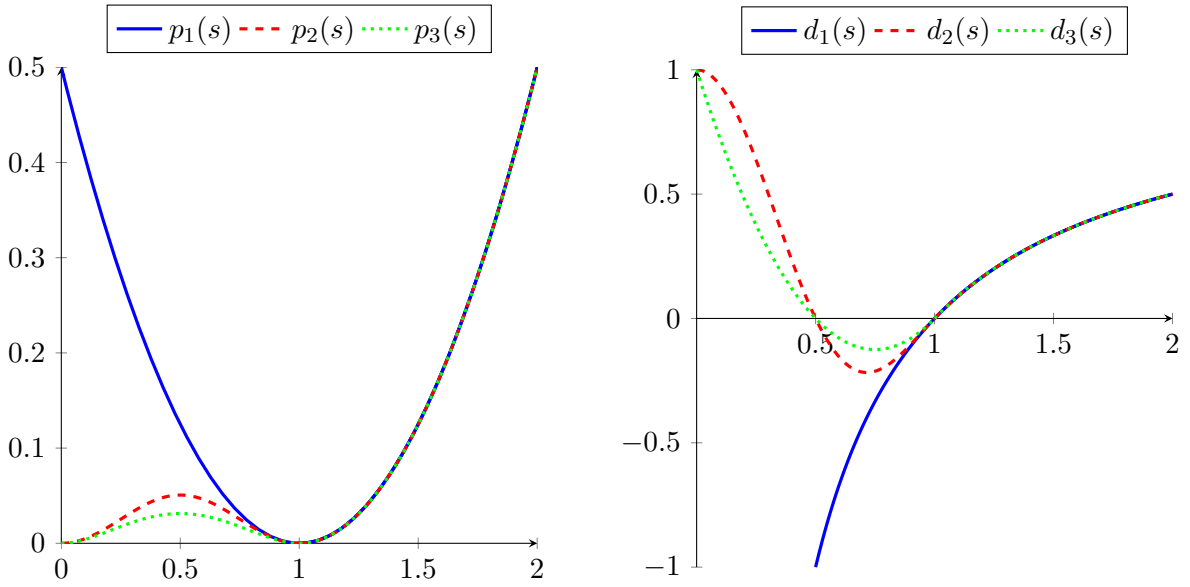

Figure 5.2.: Illustration of potential functions and associated diffusion rates.

cannot be solved by a fixed-point iteration of the form (5.35) any more. For that reason, in [BK13] an improved double-well potential is proposed:

$$p_3(s) := \begin{cases} \frac{s^2}{2}(s-1)^2 & \text{if } s \leq 1, \\ \frac{1}{2}(s-1)^2 & \text{if } s > 1. \end{cases} \tag{5.45}$$

The corresponding diffusion rate is given by

$$d_3(s) := \begin{cases} 2s^2 - 3s + 1 & \text{if } s \leq 1, \\ 1 - \frac{1}{s} & \text{if } s < 1. \end{cases} \tag{5.46}$$

All three potential functions and their associated diffusion rates are depicted in Fig. 5.2. Even though the potentials p_2 and p_3 are quite similar, the latter one is better suited for the proposed elliptic redistancing technique (5.32). Note that p_2 and p_3 share the same minimum points and their diffusion rates have the same roots. Furthermore, d_3 is continuously differentiable in $s = 1$. In contrast to d_2, it contains an additive constant of 1 also for $s < 1$. Therefore, the same fixed-point iteration technique as in (5.35) can be applied to solve the elliptic redistancing problem associated with $\mathcal{R}_{p_3}$. While the bilinear form $\mathsf{a}(\cdot,\cdot)$ remains the same, the linear form $\mathsf{b}(\cdot,\cdot)$ changes to

$$\mathsf{b}(\varphi, v) := \int_\Omega \big(d_3(|\nabla\varphi|) - 1\big)\nabla\varphi \cdot \nabla v \, \mathrm{d}\mathbf{x}. \tag{5.47}$$

Such double-well potentials are also very useful when using higher order finite element discretizations, in which oscillations may occur at the skeleton of the distance function (i.e. at points that are closest to more than one point on the interface). The advantages of this approach are discussed in [UKO16].

5.4.4. Discretization

As introduced in Chapter 3, for a triangulation $\mathcal{T}_h$ of Ω, the linear finite element approximation of the problem is obtained by replacing the function space V with the finite-dimensional space $V_h := V_h^1$ with nodal basis $\{\psi_i\}_{i=1}^N$. The system matrix of the algebraic system obtained from this discretization applied to fixed-point iteration (5.35)

$$A_{i,j} = \int_\Omega \nabla\psi_i \cdot \nabla\psi_j \, \mathrm{d}\mathbf{x} \tag{5.48}$$

is a classical *stiffness matrix* and must only be assembled once. The right hand side vector associated with (5.36b) or (5.47) requires an update at each iteration. In particular, the gradient of the finite element function φ_h needs to be evaluated at quadrature points for the computation of the right hand side. We remark that $\nabla\varphi_h$ is discontinuous, which can make the use of a gradient recovery technique worthwhile. For example, the recovered gradient $\mathbf{g}_h$ of $\nabla\varphi_h$ can be determined using the simple L^2-projection

$$\int_\Omega \mathbf{g}_h\psi_i \, \mathrm{d}\mathbf{x} = \int_\Omega \nabla\varphi_h\psi_i \, \mathrm{d}\mathbf{x}, \qquad i = 1, \dots, N_h^1. \tag{5.49}$$

The mass matrix that arises in the left hand side can be replaced by the diagonal *lumped mass matrix*, since accuracy is not crucial in this setting. The solution of the linear system is therefore trivial and the additional computational costs reduce to two matrix-vector multiplications and the one-time assembly of mass and discrete gradient matrix.

In any case, the arising linear system can be solved using the efficient CG-method combined with a suitable preconditioner such as Incomplete Cholesky Factorization (ICC).

For the numerical computation of the surface integral arising in (5.30), different techniques can be used. Based on the level set function, the interface can be reconstructed (cf. Section 4.3.2), and a numerical quadrature formula applied. An approach easier to implement is the use of adaptive quadrature formulas. Elements containing the interface are suitably subdivided, and a quadrature formula is applied to the transformed volume integral

$$\int_{\Gamma_h} \varphi_h^2 \, \mathrm{d}\sigma \approx \int_\Omega \delta(\Gamma_h, \mathbf{x})\varphi_h^2 \, \mathrm{d}\mathbf{x} \tag{5.50}$$

on the refined mesh. Here, $\delta(\Gamma_h, \mathbf{x})$ denotes the Delta distribution localizing the interface [Hys07]. A third possibility is presented in Section 5.4.5.

The behavior of φ converging to a (local) minimum of the Eikonal equation in which the signed distance function property is violated can be avoided in many scenarios when adding the continuous interior penalty (CIP) term

$$\mathcal{P}_{\mathrm{CIP}}(\varphi_h) = \frac{\gamma}{2} \sum_{K\in\mathcal{T}_h} \int_{\partial K} [\![\mathbf{n} \cdot \nabla\varphi_h]\!] \, [\![\mathbf{n} \cdot \nabla v_h]\!] \, \mathrm{d}\sigma \tag{5.51}$$

presented in [BH04]. In Fig. 5.3 the elliptic redistancing scheme is applied to the perturbed signed distance function Φ_{10} introduced in (5.83). Without the CIP stabilization term the

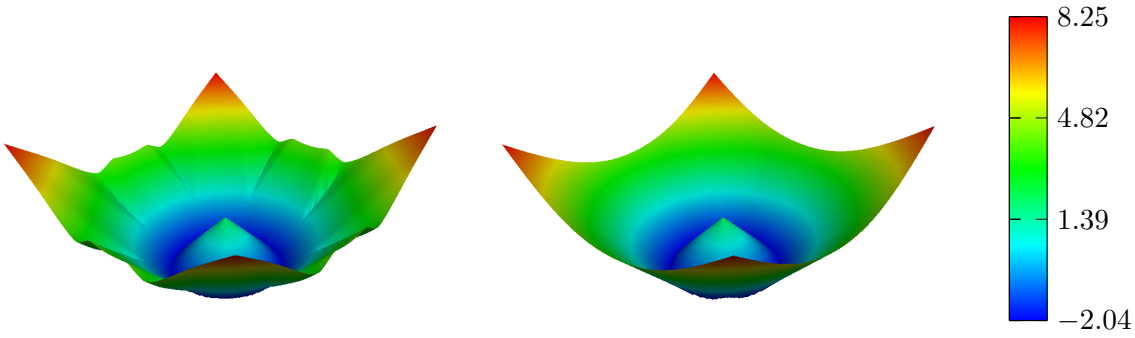

Figure 5.3.: Elliptic redistancing without (left) and with CIP (right) for a perturbed distance function.

solution fails to converge to the correct signed distance function. In terms of the increased cost, an additional matrix needs to be assembled once. In our numerical experiments we found that with the CIP term the rate of convergence could be slightly accelerated, even though this term is only required when dealing with heavily distorted distance functions.

In [UKO16], Utz et al. use a discontinuous Galerkin finite element method for the spatial discretization of the elliptic redistancing problem. This approach shows comparable numerical results, but offers better properties in the context of a parallel implementation. It is closely related to the finite element approach with CIP penalty term.

5.4.5. Interface Local Projection Approach

In [BKS16] an alternative approach to enforcing the internal boundary condition $\varphi|_\Gamma = 0$ was presented. It is based on a *local projection* technique by Parolini [Par04], and easier to implement as it does not require an exact localization of the interface.

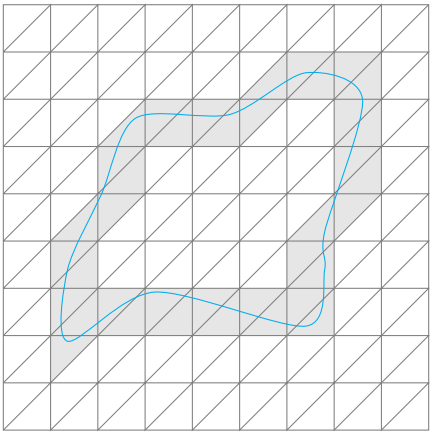

Figure 5.4.: Illustration of interface region Ω^{int} (shaded) in the local projection approach.

The key idea is to define a desired state locally in the immediate vicinity of the interface Ω^{int} (cf. Fig. 5.4). This state can be computed from the auxiliary solution $\tilde{\varphi}$, which we assume to implicitly define the interface Γ. Since the redistanced reconstruction of $\tilde{\varphi}$ can be discontinuous across element boundaries, a local L^2-projection is employed to compute the local target state φ_{int}:

$$\int_{\Omega^{\text{int}}} \varphi_{\text{int}} v \, \mathrm{d}\mathbf{x} = \int_{\Omega^{\text{int}}} \frac{\tilde{\varphi}}{|\nabla \tilde{\varphi}|} v \, \mathrm{d}\mathbf{x}. \tag{5.52}$$

The penalty term (5.30) is then replaced by

$$\tilde{\mathcal{P}}(\varphi) = \frac{\alpha}{2} \int_{\Omega^{\text{int}}} (\varphi - \varphi_{\text{int}})^2 \, \mathrm{d}\mathbf{x}, \tag{5.53}$$

and the level set regularization term (5.26) is updated to

$$\tilde{\mathcal{R}}(\varphi) = \int_{\Omega \setminus \Omega^{\text{int}}} p(|\nabla \varphi|) \, \mathrm{d}\mathbf{x}. \tag{5.54}$$

Let us emphasize that even though this approach seems similar to the technique by [ADB11] presented in Section 5.1.2, it does not require explicit knowledge of the interface. Therefore, the numerical implementation is much simpler and the approach can easily be extended to higher order polynomial finite element functions.

We remark that the required local L^2-projection introduces an additional discretization error that may negatively influence interface accuracy. In our numerical studies we could not observe advantages over the interface penalty term (5.30) in terms of convergence behavior or interface accuracy.

5.5. Optimal Control Approach for Redistancing

In this section we present a new monolithic advection scheme with built-in redistancing, which was first presented in [BKS16]. In essence, a level set regularization term $\mathcal{R}(\varphi)$ such as (5.26) is minimized under the constraint of an augmented level set transport equation. The general optimization problem reads as follows:

$$\min_{\varphi \in V,\, q \in Q} J(\varphi, q) \coloneqq \frac{1}{2} \int_0^T \mathcal{R}_p(\varphi(t, \mathbf{x})) \, \mathrm{d}t + \frac{\beta}{2} \int_0^T \|q(t, \mathbf{x})\|_Q^2 \, \mathrm{d}t, \tag{5.55}$$

subject to

$$\frac{\partial}{\partial t}\varphi + \mathbf{v} \cdot \nabla \varphi + \varphi q = 0 \qquad \text{in } (0, T) \times \Omega, \tag{5.56a}$$

$$\varphi(t, \mathbf{x}) = \varphi_D(t, \mathbf{x}) \qquad \text{on } (0, T) \times \partial\Omega^{\text{in}}, \tag{5.56b}$$

$$\varphi(0, \cdot) = \varphi_0(\cdot) \qquad \text{in } \Omega. \tag{5.56c}$$

The initial level set function defining the interface at time $t = 0$ is given in terms of the function $\varphi_0 : \Omega \to \mathbb{R}$. The Dirichlet boundary condition on the inflow portion of the boundary, if any, is specified by $\varphi_D : (0,T) \times \partial\Omega^{\text{in}} \to \mathbb{R}$. In the context of an optimal control problem, we refer to φ as the *state variable* and to q as the *control variable*. The control q is sought in a suitable function space Q and corrects the solution so as to minimize the objective functional (5.55). In particular, on the zero level set of φ the source term vanishes regardless of the values of q. As a direct consequence, the interface cannot be artificially displaced. The second term in the cost functional $J(\cdot,\cdot)$ is a so-called *Tikhonov*-regularization term, ensuring that the control q remains sufficiently smooth and bounded. In contrast to the hyperbolic schemes which rely on a well-chosen regularization parameter for the approximation of the sign function, no such parameter is needed here. Instead, the regularization parameter β controls how much corrections of the level set function are tolerated.

Unfortunately, the objective functional $J(\varphi, q)$ is highly non-linear in $\mathcal{R}_p(\cdot)$ and non-convex. Furthermore, considering a solution φ to the state equation (5.56a) for given q, one can only expect $\varphi \in \{v \in L^2(\Omega) \ : \ \mathbf{v} \cdot \nabla v \in L^2(\Omega)\}$ (see, for example, [DPE12]), which is insufficient with respect to the objective (5.55). For these reasons, the application of the usual analysis framework is not possible in the continuous setting. Furthermore, depending on the choice of p in the regularization term $\mathcal{R}_p(\varphi)$, the solution space V must be carefully chosen.

In the following we consider a simplified and time independent version of the general minimization problem (5.55)-(5.56) with potential function $p = s - 1$:

$$\min_{\varphi \in V,\, q \in Q} J(\varphi, q) \coloneqq \frac{1}{2} \left\| |\nabla\varphi| - 1 \right\|^2_{L^2(\Omega)} + \frac{\beta}{2} \|q\|^2_Q \,, \tag{5.57}$$

subject to

$$\frac{\partial}{\partial t}\varphi + \mathbf{v} \cdot \nabla\varphi + \varphi q = 0 \qquad \text{in } (0,T) \times \Omega, \tag{5.58a}$$

$$\varphi(0, \mathbf{x}) = \varphi_0(\mathbf{x}) \qquad \text{in } \Omega. \tag{5.58b}$$

For this particular choice of $J(\varphi, q)$, we can show continuity in (φ, q).

Lemma 5.3
The functional

$$J(\varphi, q) = \frac{1}{2} \left\| |\nabla\varphi| - 1 \right\|^2_{L^2(\Omega)} + \frac{\beta}{2} \|q\|^2_{H^1(\Omega)} \tag{5.59}$$

is continuous in $(\varphi, q) \in H^1(\Omega) \times H^1(\Omega)$.

This result is to be expected, as compositions of continuous mappings are continuous. We provide the proof for completeness.

Proof. The continuity of $\|q\|^2_{H^1(\Omega)}$ is obvious. It remains to show the continuity of

$$f(\varphi) \coloneqq \left\| |\nabla\varphi| - 1 \right\|^2_{L^2(\Omega)} .$$

For $\varepsilon > 0$, $\delta > 0$, $\varphi \in H^1(\Omega)$ and $\psi \in H^1(\Omega)$ such that $\|\varphi - \psi\|_{H^1(\Omega)} \leq \delta$ we have

$$\begin{aligned} |f(\varphi) - f(\psi)| &\leq \int_\Omega \left| (|\nabla\varphi| - 1)^2 - (|\nabla\psi| - 1)^2 \right| \mathrm{d}\mathbf{x} \\ &= \| (|\nabla\varphi| - |\nabla\psi|) \cdot (|\nabla\varphi| + |\nabla\psi| - 2) \|_{L^1(\Omega)} \\ &\overset{\text{Hölder}}{\leq} \| |\nabla\varphi| - |\nabla\psi| \|_{L^2(\Omega)} \cdot \| |\nabla\varphi| + |\nabla\psi| - 2 \|_{L^2(\Omega)} . \end{aligned}$$

For the first term, the reverse triangle inequality yields

$$\| |\nabla\varphi| - |\nabla\psi| \|_{L^2(\Omega)} \leq \|\nabla(\varphi - \psi)\|_{L^2(\Omega)} < \delta,$$

and the second term is bounded by

$$\begin{aligned} \| |\nabla\varphi| + |\nabla\psi| - 2 \|_{L^2(\Omega)} &\leq \| |\nabla\varphi| \|_{L^2(\Omega)} + \| |\nabla\psi| \|_{L^2(\Omega)} + 2 \|1\|_{L^2(\Omega)} \\ &= \|\nabla\varphi\|_{L^2(\Omega)} + \|\nabla\psi\|_{L^2(\Omega)} + 2|\Omega| \\ &\leq 2 \|\nabla\varphi\|_{L^2(\Omega)} + \delta + 2|\Omega|. \end{aligned}$$

This proves the continuity of f in φ:

$$|f(\varphi) - f(\psi)| \leq \delta \cdot \left(\|\nabla\varphi\|_{L^2(\Omega)} + \delta + 2|\Omega| \right) < \varepsilon,$$

for all $\delta < \frac{-\gamma + \sqrt{\gamma^2 + 4\varepsilon}}{2}$, $\gamma \coloneqq \|\nabla\varphi\|_{L^2(\Omega)} + 2|\Omega|$. Consequently, $J(\varphi, q)$ is a continuous functional in (φ, q). □

5.5.1. Existence of a Solution in the Finite-Dimensional Setting

When we replace the non-linear source term φq in (5.57) with the linear source term $\tilde{\varphi} q$, the resulting simplified minimization problem can be interpreted as predictor-corrector scheme. We consider a discrete version obtained by using the finite-dimensional spaces $V_h \subset H^1(\Omega)$ and $Q_h \subset H^1(\Omega)$. In particular, the Dirichlet boundary condition shall be embedded into V_h, so that Poincaré's inequality (cf. Theorem A.10) can be applied in V_h. The simplified state equation (5.58a) then can be written in terms of the discrete operators $\tilde{\mathsf{A}}_h = \tilde{\mathsf{A}}_h(\tilde{\varphi})$ and B_h, and the right hand side f_h:

$$\mathsf{B}_h \varphi_h + \tilde{\mathsf{A}}_h q_h = \mathsf{f}_h. \tag{5.60}$$

The generic discrete operators can be obtained, for example, by applying the θ time splitting scheme and finite elements for spatial discretization. Note that the operator B_h and the right hand side f_h contain contributions from both spatial and temporal discretization. Let us consider the following *discrete minimization problem*

$$\min_{\varphi_h \in V_h,\, q_h \in Q_h} J(\varphi_h, q_h) \coloneqq \frac{1}{2} \| |\nabla\varphi| - 1 \|^2_{L^2(\Omega)} + \frac{\beta}{2} \|q_h\|^2_{H^1(\Omega)} \tag{5.61}$$

subject to

$$\mathsf{B}_h\varphi_h + \tilde{\mathsf{A}}_h q_h = \mathsf{f}_h. \tag{5.62}$$

In this setting, the existence of a solution can be shown:

Lemma 5.4 (Existence of a Solution)
For the two finite-dimensional spaces V_h and Q_h specified above, each equipped with $\|\cdot\|_{H^1(\Omega)}$, let the predictor $\tilde{\varphi} \in V_h$ be such that $\tilde{\mathsf{A}}$ is invertible. Then the minimization problem (5.61)-(5.62) has a global solution for all $\beta > 0$.

Proof. The proof uses a standard technique for finite-dimensional optimization problems. It is roughly based on the proof of [Vex12, Theorem 4.1], but with interchanged roles of state and control.
For any $\varphi_h \in V_h$ exists one and only one

$$q_h = q_h(\varphi_h) = \tilde{\mathsf{A}}_h^{-1}\big(\mathsf{f}_h - \mathsf{B}_h\varphi_h\big),$$

because $\tilde{\mathsf{A}}_h$ is invertible by assumption. Since $\tilde{\varphi}_h \in V_h$, the set

$$W_h \coloneqq \{(\varphi_h, q_h) \in V_h \times Q_h \ : \ \mathsf{B}_h\varphi_h + \tilde{\mathsf{A}}_h q_h = \mathsf{f}_h\}$$

is not empty. The objective functional satisfies

$$J(\varphi_h, q_h) \geq 0, \qquad \forall (\varphi_h, q_h) \in W_h,$$

and therefore the infimum j exists:

$$j \coloneqq \inf_{(\varphi_h, q_h) \in W_h} J(\varphi_h, q_h).$$

By definition, there is a sequence $\{(\varphi_n, q_n)\} \subset W_h$ such that

$$j \leq J(\varphi_n, q_n) \leq j + \frac{1}{n},$$

and

$$J(\varphi_n, q_n) \to j, \qquad \text{as } n \to \infty.$$

The sequence $\{q_n\}$ is bounded by definition:

$$\|q_n\|^2_{H^1(\Omega)} \leq \frac{2}{\beta} J(\varphi_n, q_n) \leq \frac{2}{\beta}\left(j + \frac{1}{n}\right).$$

For the boundedness of $\{\varphi_n\}$, we use Young's inequality $\|a+b\|^2 \leq 2\|a\|^2 + 2\|b\|^2$ with $a = |\nabla\varphi_n| - 1$ and $b = 1$ to get:

$$2\,\||\nabla\varphi| - 1\|^2_{L^2(\Omega)} + 2\,\|1\|^2_{L^2(\Omega)} \geq \|\,|\nabla\varphi|\,\|^2_{L^2(\Omega)} = \|\nabla\varphi\|^2_{L^2(\Omega)} \geq \frac{1}{c_\Omega}\,\|\varphi\|^2_{H^1(\Omega)}\,.$$

The last inequality is a direct consequence of Poincaré's inequality, which is applicable by definition of V_h. Hence, $\{\varphi_n, q_n\}$ is a bounded sequence, and by application of the Bolzano–Weierstraß Theorem, there exists a convergent subsequence $\{(\varphi_{n_k}, q_{n_k})\}$ with

$$(\varphi_{n_k}, q_{n_k}) \to (\bar{\varphi}_h, \bar{q}_h),$$

where $(\bar{\varphi}_h, \bar{q}_h) \in V_h \times Q_h$.

$$0 = \mathsf{B}_h \varphi_{n_k} + \tilde{\mathsf{A}}_h q_{n_k} - f, \qquad \forall n_k,$$

and, since $\tilde{\mathsf{A}}_h$ and B_h are linear continuous operators,

$$0 = \lim_{n_k \to \infty} B_h \varphi_{n_k} + \tilde{\mathsf{A}}_h q_{n_k} - f = \mathsf{B}_h \bar{\varphi}_h + \tilde{\mathsf{A}}_h \bar{q}_h - f = 0, \qquad \Longrightarrow \qquad (\bar{\varphi}_h, \bar{q}_h) \in W_h.$$

Finally, as shown in Lemma 5.3, the objective functional $J(\cdot,\cdot)$ is continuous in $V_h \times Q_h$ w.r.t. $\|\cdot\|_{H^1(\Omega)}$, and therefore

$$J(\varphi_{n_k}, q_{n_k}) \to J(\bar{\varphi}, \bar{q}) \qquad \Longrightarrow \qquad J(\bar{\varphi}, \bar{q}) = j. \qquad \square$$

The assumption that the discrete operator $\tilde{\mathsf{A}}$ is invertible is reasonable in the sense that the interface associated with $\tilde{\varphi}$ must not be degenerate. In particular, there must not be elements in which $\tilde{\varphi}$ has zero values in all degrees of freedom. The matrix can be considered as a mass matrix scaled by $\tilde{\varphi}$.

5.5.2. Weak Formulation

Similarly to the level set equation, the weak form of state equation (5.58a) can be obtained, thus:

$$\int_\Omega \left(\frac{\partial}{\partial t}\varphi + \mathbf{v} \cdot \nabla \varphi + \varphi q \right) v \, \mathrm{d}\mathbf{x} \qquad \forall v \in V. \tag{5.63}$$

As trial space for φ we may use $V \coloneqq H^1(\Omega)$ to ensure sufficient regularity of the level set regularization term $\mathcal{R}_p(\cdot)$. For the control space Q, we pick $Q = L^2(\Omega)$ based on numerical experience but also $Q = H^1(\Omega)$ is feasible. Let us consider the associated generic semi-discrete problem:

$$\min_{\varphi_h \in V_h,\, q_h \in Q_h} J(\varphi_h, q_h) \coloneqq \mathcal{R}_p(\varphi_h) + \frac{\beta}{2} \|q_h\|_Q \tag{5.64}$$

subject to

$$\mathsf{a}(\varphi_h, v_h) + \mathsf{b}(\varphi_h, q_h, v_h) = \mathsf{l}(v_h) \qquad \forall v_h \in V_h, \tag{5.65a}$$

$$\varphi_h(0, \mathbf{x}) = \varphi_{0,h}(\mathbf{x}). \tag{5.65b}$$

Even though the convection-dominated state equation calls for the use of stabilized numerical schemes, the standard Galerkin discretization may also be employed. The additonal source term has a stabilizing effect on the solution. Furthermore, continuously applied redistancing will prevent steep or flat gradients, which generally cause instabilities to arise. Nevertheless, a stabilized discretization technique can easily be employed. Let us consider three different discretization approaches (cf. [BKS16]):

1. θ-scheme and linear finite elements:

$$\mathsf{a}_1(\varphi_h, v_h) = \int_\Omega \varphi_h v_h + \Delta t \theta \mathbf{v}_h \cdot \nabla \varphi_h v_h \, \mathrm{d}\mathbf{x}, \tag{5.66a}$$

$$\mathsf{b}_1(\varphi_h, q_h, v_h) = \int_\Omega \Delta t \varphi_h q_h v_h \, \mathrm{d}\mathbf{x}, \tag{5.66b}$$

$$\mathsf{l}_1(v_h) = \int_\Omega \varphi_h^n v_h - \Delta t (1-\theta) \mathbf{v}_h \cdot \nabla \varphi_h^n \, \mathrm{d}\mathbf{x}; \tag{5.66c}$$

2. θ-scheme and streamline diffusion stabilized linear finite elements:

$$\mathsf{a}_2(\varphi_h, v_h) = \int_\Omega \big(\varphi_h + \Delta t \theta \mathbf{v}_h \cdot \nabla \varphi_h\big)(v_h + \delta \mathbf{v}_h \cdot \nabla v_h) \, \mathrm{d}\mathbf{x}, \tag{5.67a}$$

$$\mathsf{b}_2(\varphi_h, q_h, v_h) = \int_\Omega \Delta t \varphi_h q_h (v_h + \delta \mathbf{v}_h \cdot \nabla v_h) \, \mathrm{d}\mathbf{x}, \tag{5.67b}$$

$$\mathsf{l}_2(v_h) = \int_\Omega \big(\varphi_h^n - \Delta t (1-\theta) \mathbf{v}_h \cdot \nabla \varphi_h^n\big)(v_h + \delta \mathbf{v}_h \cdot \nabla v_h) \, \mathrm{d}\mathbf{x}; \tag{5.67c}$$

3. semi-implicit Lax-Wendroff scheme and linear finite elements:

$$\mathsf{a}_3(\varphi_h, v_h) = \int_\Omega \left(\varphi_h v_h + \frac{(\Delta t)^2}{2} (\mathbf{v}_h \cdot \nabla \varphi_h)(\mathbf{v}_h \cdot \nabla v_h)\right) \mathrm{d}\mathbf{x}, \tag{5.68a}$$

$$\mathsf{b}_3(\varphi_h, q_h, v_h) = \int_\Omega \Delta t \varphi_h u q_h v_h \, \mathrm{d}\mathbf{x}, \tag{5.68b}$$

$$\mathsf{l}_3(v_h) = \int_\Omega -\Delta t \mathbf{v}_h \cdot \nabla \varphi_h^n v_h \, \mathrm{d}\mathbf{x}. \tag{5.68c}$$

For the θ-scheme, the source term $\varphi_h q_h v_h$ is treated fully implicitly regardless of θ. This can be justified by the fact that the evolution of the control in time does not have to be smooth. In many optimal control settings, in particular when the admissible set of controls is bounded above and below, the control exhibits a *bang-bang* structure, jumping between the upper and lower bound.

For the streamline diffusion approach, the stabilization parameter δ is commonly chosen to be element-wise constant, cf. (4.22). Also note that the semi-implicit Lax-Wendroff scheme as introduced in Section 4.4 can be considered as a parameter-free stabilization technique.

5.5.3. Discrete Optimality Conditions

To derive first order optimality conditions for the generic discrete minimization problem (5.64)-(5.65), we introduce the associated *discrete Lagrange functional*

$$\mathcal{L}_h(\varphi_h, q_h, \lambda_h) \coloneqq J(\varphi_h, q_h) + \mathsf{a}(\varphi_h, \lambda_h) + \mathsf{b}(\varphi_h, q_h, \lambda_h) - \mathsf{l}(\lambda_h). \tag{5.69}$$

Differentiating $\mathcal{L}_h$ with respect to the state variable φ_h, the control variable q_h and the *Lagrange multiplier* λ_h yields the system of first order optimality conditions

$$\delta\mathcal{R}(\varphi_h, \psi) + \mathsf{a}(\psi, \lambda_h) + \mathsf{b}(\psi, q_h, \lambda_h) = 0 \qquad \forall \psi \in V_h, \tag{5.70a}$$

$$\mathsf{b}(\varphi_h, \eta, \lambda_h) + \beta\,(q_h, \eta)_Q = 0 \qquad \forall \eta \in Q_h, \tag{5.70b}$$

$$\mathsf{a}(\varphi_h, v_h) + \mathsf{b}(\varphi_h, q_h, v_h) = \mathsf{l}(v_h) \qquad \forall v_h \in V_h. \tag{5.70c}$$

The derivative of $\mathcal{R}_p$ can be computed as shown in (5.38).

5.5.4. Linearization

As we have seen, neither $\mathcal{R}_p$ nor its variational derivative are linear functions in φ. For the numerical solution of system (5.70), we must employ a suitable linearization technique. A straight-forward approach is based on the fixed-point iteration introduced in (5.35), in which

$$\delta\mathcal{R}_{p_1}(\varphi_h, v_h) \approx \int_\Omega \nabla\varphi_h^{(m+1)} \cdot \nabla v_h \,\mathrm{d}\mathbf{x} - \int_\Omega \frac{\nabla\varphi_h^{(m)} \cdot \nabla v_h}{|\nabla\varphi_h^{(m)}|} \,\mathrm{d}\mathbf{x}, \tag{5.71}$$

and, for the trilinear form

$$\mathsf{b}(\varphi_h, q_h, \lambda_h) \approx \mathsf{b}(\varphi_h^{(m)}, q_h^{(m+1)}, \lambda_h^{(m+1)}). \tag{5.72}$$

In each iteration, the vector

$$\big(r(\varphi_h)\big)_i = \int_\Omega \frac{\nabla\varphi_h \cdot \nabla\psi_i}{|\nabla\varphi_h|} \,\mathrm{d}\mathbf{x} \tag{5.73}$$

and the weighted mass matrix

$$\big(M(\varphi_h)\big)_{i,j} = \int_\Omega \varphi_h\,\psi_i\,\psi_j \,\mathrm{d}\mathbf{x} \tag{5.74}$$

must be assembled.

An alternative linerization approach is obtained by application of Newton's method. The second derivative of $\mathcal{R}_p$ can be computed to be

$$\begin{aligned}\delta^2\mathcal{R}_p(\varphi, v, w) &= \int_\Omega p''(|\nabla\varphi|)\frac{\nabla\varphi\cdot\nabla w}{|\nabla\varphi|}\frac{\nabla\varphi\cdot\nabla v}{|\nabla\varphi|}\,\mathrm{d}\mathbf{x}\\ &\quad+\int_\Omega p'(|\nabla\varphi|)\left(\frac{\nabla w\cdot\nabla v}{|\nabla\varphi|}-\frac{\nabla\varphi\cdot\nabla v}{|\nabla\varphi|^2}\frac{\nabla w\cdot\nabla\varphi}{|\nabla\varphi|}\right)\mathrm{d}\mathbf{x}\\ &= \int_\Omega \frac{p''(|\nabla\varphi|)}{|\nabla\varphi|^2}(\nabla\varphi\cdot\nabla w)(\nabla\varphi\cdot\nabla v)\,\mathrm{d}\mathbf{x}\\ &\quad+\int_\Omega \frac{p'(|\nabla\varphi|)}{|\nabla\varphi|}\left(\nabla w\cdot\nabla v-\frac{(\nabla\varphi\cdot\nabla v)(\nabla\varphi\cdot\nabla w)}{|\nabla\varphi|^2}\right)\mathrm{d}\mathbf{x}.\end{aligned}\tag{5.75}$$

Let $\mathbf{z}_h \coloneqq (\varphi_h, q_h, \lambda_h)$ and $F(\mathbf{z}_h)$ denote the residual of the optimality system (5.70). The Jacobian matrix $J_F(\mathbf{z})$ of F is given by

$$(J_F(\mathbf{z}))_{i,j} \coloneqq \left(\frac{\partial F_i}{\partial z_{h,j}}\right)(\mathbf{z}).\tag{5.76}$$

The partial derivatives of F are:

$$\frac{\partial F_1}{\partial \varphi_h} = \delta^2\mathcal{R}_p(\varphi_h, \delta\varphi_h, \psi),\tag{5.77a}$$
$$\frac{\partial F_1}{\partial q_h} = \mathsf{b}(\psi, \delta q_h, \lambda_h),\tag{5.77b}$$
$$\frac{\partial F_1}{\partial \lambda_h} = \mathsf{a}(\psi, \delta\lambda_h) + \mathsf{b}(\psi, q_h, \delta\lambda_h),\tag{5.77c}$$
$$\frac{\partial F_2}{\partial \varphi_h} = \mathsf{b}(\delta\varphi_h, \eta, \lambda_h),\tag{5.77d}$$
$$\frac{\partial F_2}{\partial q_h} = (\delta q_h, \eta)_U,\tag{5.77e}$$
$$\frac{\partial F_2}{\partial \lambda_h} = \mathsf{b}(\varphi_h, \eta, \delta\lambda_h),\tag{5.77f}$$
$$\frac{\partial F_3}{\partial \varphi_h} = \mathsf{a}(\delta\varphi_h, v_h) + \mathsf{b}(\delta\varphi_h, q_h, v_h),\tag{5.77g}$$
$$\frac{\partial F_3}{\partial q_h} = \mathsf{b}(\varphi_h, \delta q_h, v_h),\tag{5.77h}$$
$$\frac{\partial F_3}{\partial \lambda_h} = 0.\tag{5.77i}$$

The Newton update can be formulated as follows: for given $\mathbf{z}^{(0)}$, compute

$$\mathbf{z}_h^{(m+1)} \coloneqq \mathbf{z}_h^{(m)} - \left(J_F(\mathbf{z}_h^{(m)})\right)^{-1} F(\mathbf{z}_h^{(m)}), \qquad m = 0, 1, \ldots.\tag{5.78}$$

In our numerical experience we could not observe a significant difference between the two linearization approaches. For good approximations to signed distance functions we observed fast

convergence. When stronger deformations occur, the required number of fixed-point iterations increases. In addition to the presented algorithm we also considered an extension by using a CIP penalty term as in the elliptic-redistancing approach. Furthermore, we replaced the gradient of φ by a smooth counterpart obtained from variational gradient recovery based on the idea presented in [Reu13]. However, we could not observe any significant improvement for these extensions.

Let us conclude this section with a remark on the inf-sup condition associated with the problem. The optimization problem does not impose any restrictions on the choice of the finite element spaces per se, but an inf-sup condition could be introduced when solving the first-order optimality conditions. Due to the non-linearity of the problem, we were not able to show that such an inf-sup condition is satisfied automatically. However, based on our numerical experience, we assume that the inherent inf-sup conditions holds for the employed finite element spaces.

5.6. Numerical Results

In the numerical study below, we will use the following abbreviations to keep notation simple:

`[NO-RD]`	no redistancing scheme is applied,
`[HYP-RD]`	hyperbolic redistancing with stabilized linear finite elements, cf. (5.11),
`[CLS-RD]`	convected level set with stabilized linear finite elements, cf. Section 5.2.1,
`[ELP-RD]`	elliptic redistancing with linear finite elements, cf. (5.35),
`[OPC-RD]`	optimal control approach for redistancing as presented in Section 5.5.

The chapter is partly based on results presented in the author's previous publications [Bas12, BK13, BKS16].

We will use the following global and local error measures (cf. [BKS16, Reu13, EG14]):

$$\mathrm{e}_\infty := \max_{K\in\mathcal{T}_h}\left(\max_{x\in K}|\varphi_h(T,\mathbf{x})-\mathrm{d}_{\mathrm{ex}}(\mathbf{x})|\right), \tag{5.79a}$$

$$\mathrm{e}_{\infty,\Gamma} := \max_{K\in\mathcal{T}_h^\Gamma}\left(\max_{x\in K}|\varphi_h(T,\mathbf{x})-\mathrm{d}_{\mathrm{ex}}(\mathbf{x})|\right), \tag{5.79b}$$

$$\mathrm{e}_\infty^\nabla := \max_{K\in\mathcal{T}_h}\sqrt{\frac{1}{K}\left|\int_T\left(|\nabla\varphi_h(T,\mathbf{x})|-1\right)\,\mathrm{d}\mathbf{x}\right|}, \tag{5.79c}$$

$$\mathrm{e}_{\infty,\Gamma}^\nabla := \max_{K\in\mathcal{T}_h^\Gamma}\sqrt{\frac{1}{K}\left|\int_T\left(|\nabla\varphi_h(T,\mathbf{x})|-1\right)\,\mathrm{d}\mathbf{x}\right|}, \tag{5.79d}$$

where $\mathcal{T}_h$ is the computational triangulation of Ω, and $\mathcal{T}_h^\Gamma \subset \mathcal{T}_h$ the subset of elements containing the interface Γ. By $\mathrm{d}_{\mathrm{ex}}(\mathbf{x})$ we denote the exact distance to the interface Γ at final time T. Note that many numerical experiments are designed such that the solution at final time

coincides with the initial data, so that the exact solution $\mathrm{d}_{\mathrm{ex}}(\cdot)$ can easily be provided. More error measures are given in the $L^2(\Omega)$- and $H^1(\Omega)$-norms of $\varphi_h(T,\cdot) - \mathrm{d}_{\mathrm{ex}}(\cdot)$, i.e.

$$\mathrm{e}_{L^2(\Omega)} \coloneqq \|\varphi_h(T,\mathbf{x}) - \mathrm{d}_{\mathrm{ex}}(\mathbf{x})\|_{L^2(\Omega)}\,, \tag{5.80a}$$

$$\mathrm{e}_{H^1(\Omega)} \coloneqq \|\varphi_h(T,\mathbf{x}) - \mathrm{d}_{\mathrm{ex}}(\mathbf{x})\|_{H^1(\Omega)}\,. \tag{5.80b}$$

For all numerical experiments below, we used linear finite elements on uniform, triangular meshes and the second-order accurate Crank-Nicolson time discretization technique.

5.6.1. Pure Redistancing

At first, let us consider pure redistancing problems. For a given perturbed signed distance function $\tilde{\varphi}(\mathbf{x})$, we seek a good correction to approximate the distance function without moving the interface. Naturally, post-processing algorithms can easily be applied. However, for the monolithic approaches `[CLS-RD]` and `[OPC-RD]` which are designed to simultaneously solve the transport equation and perform the redistancing, advection of the interface must be disabled by setting the velocity field to zero. Hence, in this setting monolithic approaches cannot benefit from their more natural embedding of the redistancing procedure.

5.6.1.1. Truncated Distance Functions

This first example is designed to illustrate the capability of using double-well potentials for the level set regularization function $\mathcal{R}_{p_3}(\cdot)$ in the `[ELP-RD]` approach. Let $\tilde{\varphi}$ be given by

$$\tilde{\varphi}(\mathbf{x}) \coloneqq \sqrt{\sin(\pi x_1)\cdot\sin(\pi x_2)} - \frac{1}{2}. \tag{5.81}$$

In Fig. 5.5 the truncation effect is illustrated. Close to the center $(0.5, 0.5)$ of the domain, the gradients of $\tilde{\varphi}$ are flat and the diffusion rate d_3 becomes positive. This forces the corrected solution φ to become constant in these regions. In all other regions, the diffusion rate adapts itself such that the solution satisfies $|\nabla\varphi| \approx 1$. The computations are carried out on a numerical mesh with 101×101 nodes and the penalty parameter is set to $\alpha = 10^5$. The depicted result itself was obtained after just one fixed-point iteration. This emphasizes the global character of the `[ELP-RD]` approach and makes it particularly well suited for problems requiring large corrections as well as for applications requiring good signed distance function approximation accuracy also in regions away from the interface.

Based on this example, let us briefly address the numerical solution of the linear system arising in each fixed-point iteration of `[ELP-RD]`. Fig. 5.6 illustrates the dependence of linear solver iterations (CG-method with ICC preconditioning, cf. Section 5.4.4) on the concrete choice of the penalty parameter α for the internal boundary condition. Even though for increasing α more iterations are required, the influence can be regarded as rather insignificant. In practice, we obtained good results for the considered range of α, independently of the mesh size h.

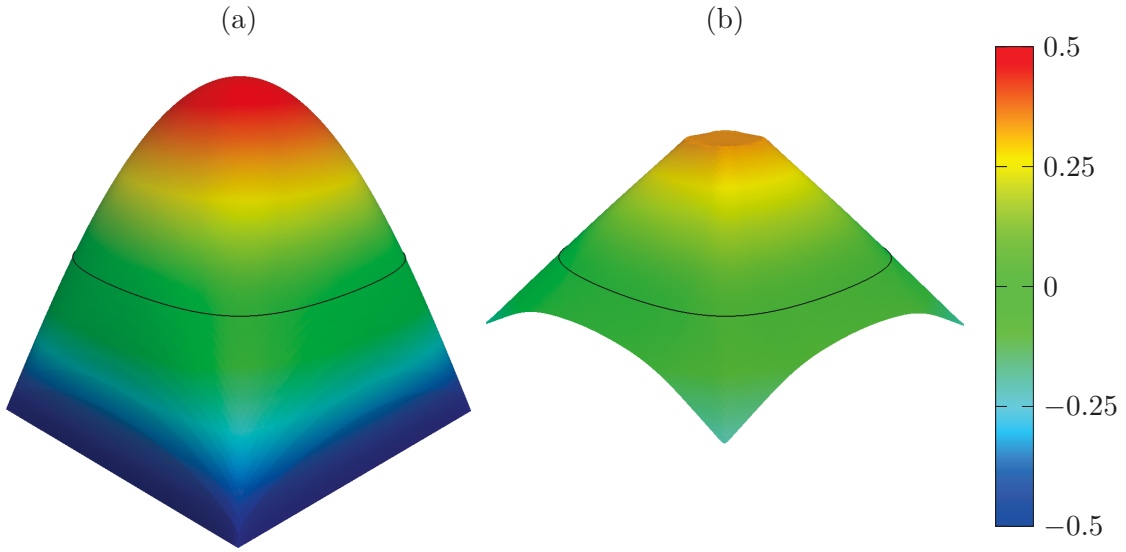

Figure 5.5.: (a) Initial data, (b) solution of `[ELP-RD]` with double-well potential $p = p_3$.

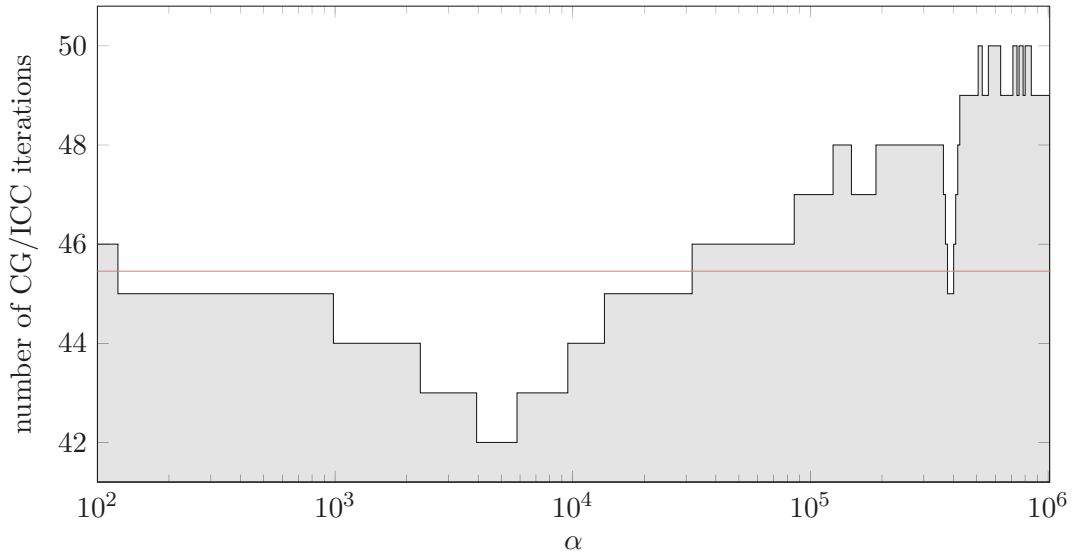

Figure 5.6.: Illustration of dependence of CG/ICC iterations on penalty parameter α. The average number of iterations (45.5) is shown in red (cf. [BK13]).

5.6.1.2. Perturbed Distance Function

The second test case is based on a numerical experiment presented in [Reu13], in which the interface capturing capability and the accuracy of the redistancing method are assessed. Consider the distance function

$$\Phi(\mathbf{x}) \coloneqq \big||x| - R\big| - r \tag{5.82}$$

for radii $R \coloneqq 0.4$ and $r \coloneqq 0.2$ in the domain $\Omega = (-1, 1) \times (-1, 1)$, and the perturbed version

$$\Phi_\iota(\mathbf{x}) \coloneqq \Phi(\mathbf{x}) \cdot \zeta_\iota(\mathbf{x}) \tag{5.83}$$

with the perturbation function

$$\zeta_\iota(\mathbf{x}) \coloneqq 9.0 + 4.0 \cdot \cos\left(\frac{\iota x_1 x_2}{|\mathbf{x}|}\right). \tag{5.84}$$

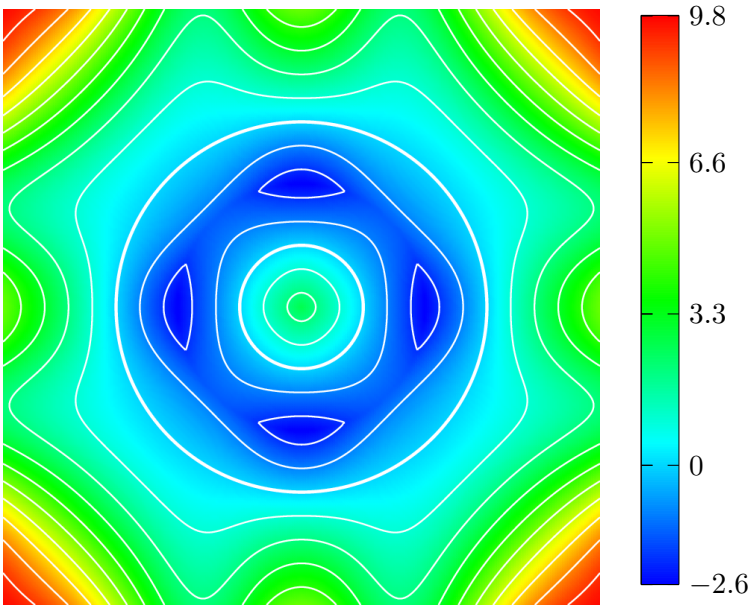

Figure 5.7.: Illustration of Φ_ι for $\iota = 10$. The white isocontours are equidistant, and the zero isocontours are bold.

Note that since $\zeta_\iota(\mathbf{x}) > 0$ for all $\iota > 0$, the zero interfaces of Φ and Φ_ι are identical. The perturbed function Φ_ι challenges redistancing schemes, since it has both, regions with large and flat gradients. As ι increases, Φ_ι becomes less smooth. In Fig. 5.7, equidistant isocontours of Φ_ι are depicted at mesh refinement level $\ell = 6$ and for perturbation parameter $\iota = 10$.

To begin with, we compare the number of iterations of the methods under investigation for the relatively simple test case $\iota = 1$ on a 100×100 mesh. Fig. 5.8 plots the relevant errors vs.

(a) [HYP-RD]

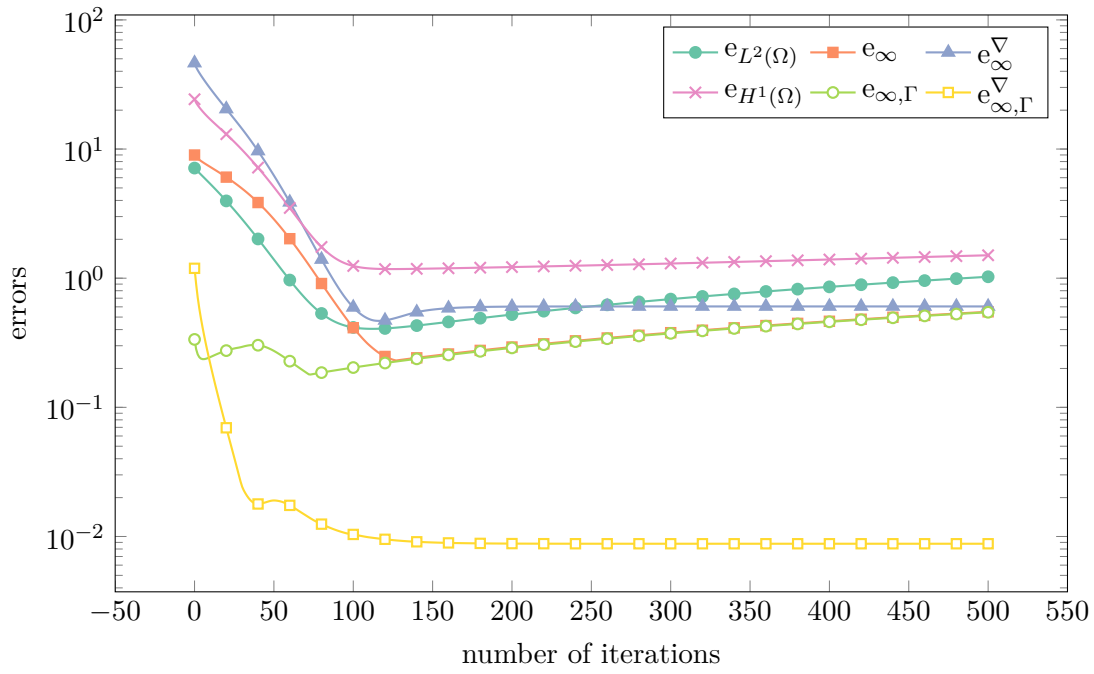

(b) [ELP-RD] with interface penalty parameter $\alpha = 10^4$

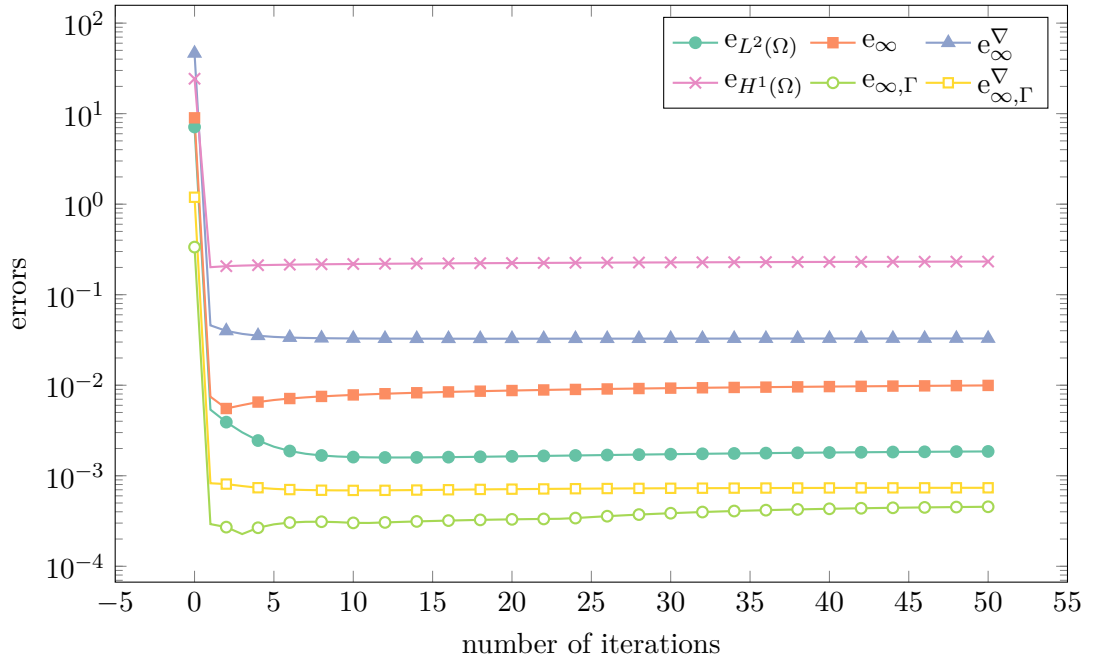

Figure 5.8.: Results for the static redistancing test case with initial data Φ_1.

(c) Rescaling by factor $1/4$ + [CLS-RD]

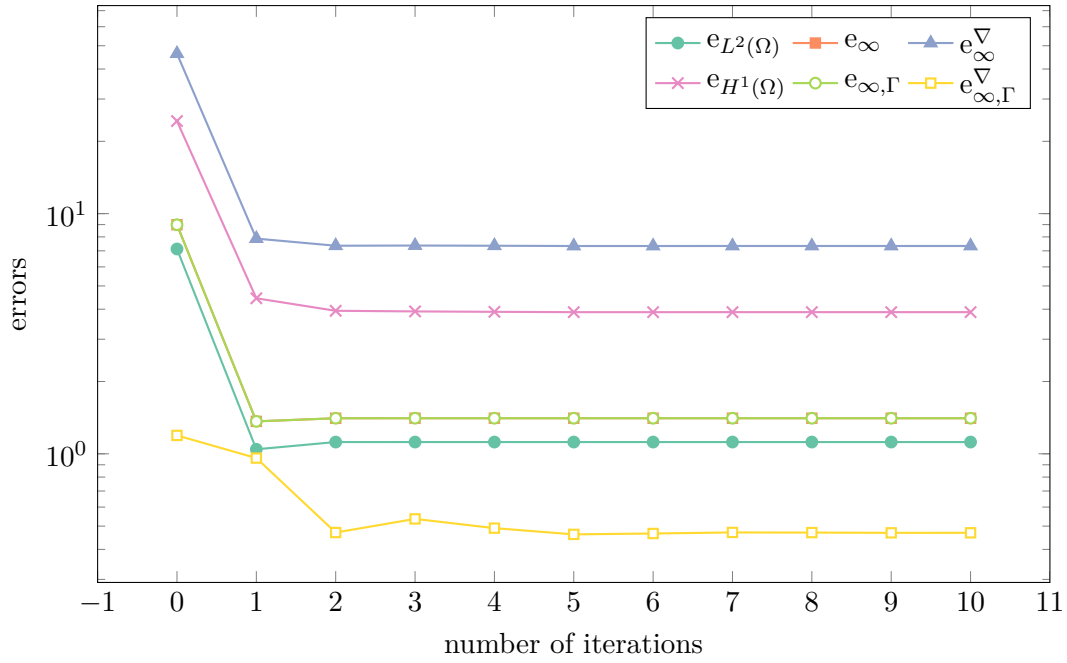

(d) [OPC-RD] with Tikhonov regularization parameter $\beta = 10^{-4}$

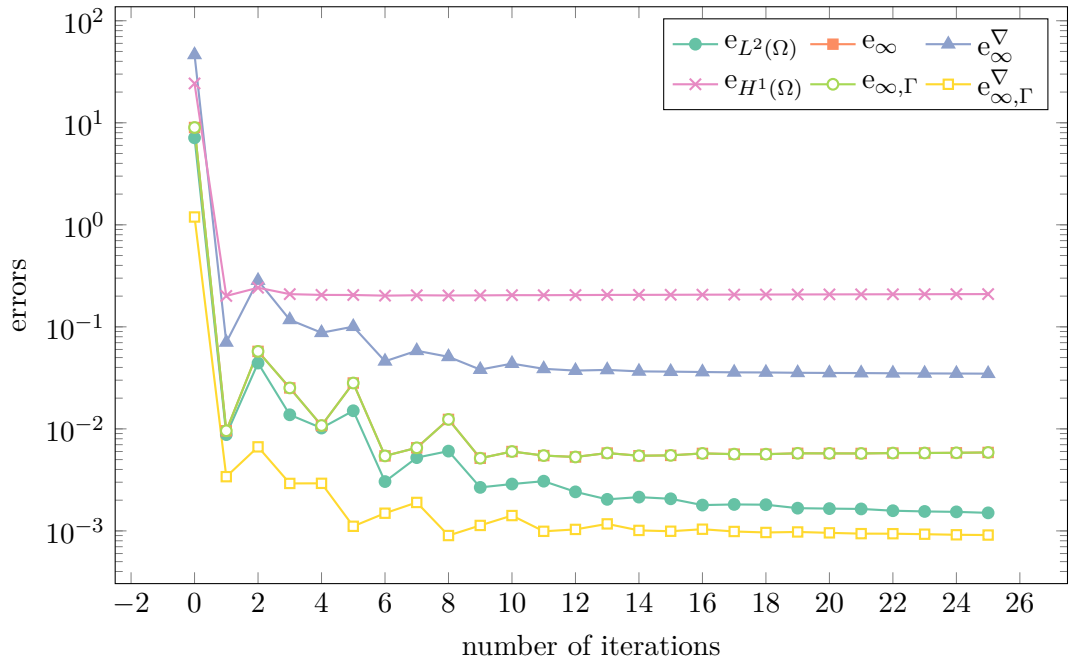

Figure 5.8.: Results for the static redistancing test case with initial data Φ_1.

the number of iterations. For the projection of Φ_1 into the finite element space X_h^1, we have the following initial errors:

$$\|\Phi_1 - \mathcal{I}_h^1(\Phi_1)\|_{L^2(\Omega)} \approx 9.18 \cdot 10^{-4}, \qquad \mathrm{e}_\infty^\nabla \approx 3.62 \cdot 10^{-2},$$
$$\|\Phi_1 - \mathcal{I}_h^1(\Phi_1)\|_{H^1(\Omega)} \approx 1.87 \cdot 10^{-1}, \qquad \mathrm{e}_{\infty,\Gamma}^\nabla \approx 5.80 \cdot 10^{-4}.$$

For the hyperbolic approach `[HYP-RD]` (with SUPG stabilization) to converge, we had to add artificial diffusion of order $\mathcal{O}(h^2)$ as suggested in (5.12). Even though this led to convergence, numerical diffusion caused the method to converge to a solution which only approximates a signed distance function with reasonable accuracy. Let us remark that the perturbation parameter ι controls the oscillations of the perturbation, not the general scaling by a factor between 5 and 13. Even though in this example $\iota = 1$ is chosen rather small, the initial data has steep and flat gradients and requires large corrections. Unfortunately, the diffusive effects prevented the `[HYP-RD]` approach to converge to a satisfactory steady state solution. Generally we observed convergence problems and high sensitivity w.r.t. the regularization parameter ε. This behavior has also been observed in the context of discontinuous Galerkin approximations [UKO16] and finite difference approximations [HMS08, HMS10]. The use of different smoothed versions of the sign function may improve convergence results, see for example [PMO+99].

After only one iteration of the global `[ELP-RD]` approach, all measured errors are reduced significantly. The interface penalty term in (5.30) was set to $\alpha = 10^4$. From the four investigated approaches, `[ELP-RD]` offers the smallest error in terms of displacements of the interface ($\mathrm{e}_{\infty,\Gamma}$), and together with `[OPC-RD]` very good local signed distance function approximation ($\mathrm{e}_{\infty,\Gamma}^\nabla$). Since the method using the local projection approach (5.53) exhibits similar or less accurate performance, we only provide results for `[ELP-RD]` here and below.

The convected redistancing approach `[CLS-RD]` builds on the local hyperbolic approach, and therefore more iterations are to be expected to reach a steady-state solution. Unfortunately, the method is unable to cope with the large gradients of Φ_1, which is why we scale the initial data by the factor of $1/4$ in the first iteration. The general performance of this method for this test case is not satisfactory, however we emphasize that the method is designed as monolithic approach that solves both, the level set equation and the redistancing problem at once. Since deformations per time step are rather small, such strong perturbations hardly occur in the context of advection problems.

Just like `[CLS-RD]`, the optimal control approach `[OPC-RD]` is a monolithic scheme. However it performs quite well for this problem if we choose a sufficiently small Tikhonov regularization parameter $\beta = 10^{-4}$ (which allows for larger corrections). Compared to `[ELP-RD]`, the interface approximation is less accurate. The signed distance function approximation is good. Again, we emphasize that the method is, by design, not suited for pure redistancing tasks. Nevertheless, the results show that `[OPC-RD]` can also be applied to strongly perturbed level set functions and indicate that the approach allows for larger time steps compared to `[CLS-RD]`.

Let us now consider the convergence behavior of the methods applied to Φ_ι for the more challenging case $\iota = 5$, for which the perturbed level set function can still be resolved sufficiently well on the coarsest mesh ($\ell = 3$). We use a uniform family of triangulations of Ω with mesh sizes $h_\ell := 2^{-\ell}$. For the monolithic scheme `[OPC-RD]`, the velocity field is set to zero

and several pseudo time steps are performed in addition to the fixed-point iterations. This allows for larger corrections without artificially increasing the conditioning of the system (as for choosing small values of β). The results and convergence rates for the different error quantities are summarized in Table 5.1. Unfortunately, both `[HYP-RD]` and `[CLS-RD]` failed to converge for this strongly perturbed initial data without further modifications. For the elliptic redistancing approach `[ELP-RD]`, the results with additional CIP-stabilization are less accurate. This can be explained by the fact that `[ELP-RD]` converges to the distance function since deformations are still manageable for $\iota = 5$. However, the accuracy suffers from the additional diffusion introduced by CIP. The results for `[OPC-RD]` are slightly better but incur higher computational costs. The presented test case shows the overall robustness of `[ELP-RD]` and `[OPC-RD]` in contrast to other PDE-based approaches such as `[HYP-RD]` and `[CLS-RD]`.

5.6.2. Vortex Deformation

Let us consider a non-stationary test case in the domain $\Omega = (0,1)^2$, in which the velocity field

$$\mathbf{v}(t,\mathbf{x}) \coloneqq \frac{1}{2}\cos\left(\frac{t\pi}{4}\right)\begin{bmatrix}\sin^2(\pi x_1)\sin(2\pi x_2)\\ -\sin^2(\pi x_2)\sin(2\pi x_1)\end{bmatrix} \tag{5.85}$$

causes strong deformations. As initial data we use the signed distance function of a circle centered at $(0.5, 0.75)$ with radius 0.1. At $t = 2$ the maximum deformation is reached and the direction of motion is reversed. At final time $T = 4$ the exact solution to the level set problem with (5.85) coincides with the initial data. Hence, approximation errors can easily be assessed. Note that $\mathbf{v}(t,\mathbf{x}) = 0$ on $\partial\Omega$ so that no boundary conditions are required.

In the following numerical study, we used linear finite elements on a triangulation $\mathcal{T}_h$ with mesh size $h = 0.1 \cdot 2^{-\ell}$ and Crank-Nicolson time stepping with increment $\Delta t = 0.025 \cdot 2^{-\ell}$ for refinement level $\ell \in \mathbb{N}_0$. Fig. 5.9 shows equidistant level sets of the different methods at time instances $t = {}^{i}/_{4} \cdot T$, $i = 1, 2, 3, 4$.

Naturally, the best results at final time were obtained when no redistancing technique is applied. This is due to the fact that linear finite elements with Crank-Nicolson time stepping yield a reversible scheme. The small deviations from the initial state are caused by the artificial diffusion induced by SUPG. However, at intermediate time steps the level set function has steep gradients (contour lines come closer together) which may cause problems when it comes to recovering interface related quantities.

We emphasize that the deformations caused by the vortex flow are rather strong. The `[CLS-RD]` approach shows real difficulties in approximating a signed distance function and hardly performs better than the approach without redistancing. The inherent diffusion of the method causes significant displacements of the interface. Note that one may obtain better results when tuning this approach to the specific problem setting and we provide this result only for completeness.

The best results in terms of signed distance function approximation are certainly obtained by using the global approach `[ELP-RD]`. At any time level, the isocontours remain equidistant and quite smooth. This approach can easily handle strong deformations and yields good

(a) `[ELP-RD]`

ℓ	$\mathrm{e}_{L^2(\Omega)}$	order	$\mathrm{e}_{H^1(\Omega)}$	order	e_∞	order	$e_{\infty,\Gamma}$	order	e_∞^∇	order	$\mathrm{e}_{\infty,\Gamma}^\nabla$	order
3	3.40e-02		4.40e-01		4.13e-02		1.01e-02		1.68e-01		2.27e-02	
4	1.63e-02	1.06	3.18e-01	0.47	1.98e-02	1.06	5.03e-03	1.01	8.20e-02	1.03	3.89e-03	2.54
5	7.19e-03	1.18	2.34e-01	0.44	9.95e-03	1.00	8.18e-04	2.62	4.14e-02	0.99	8.61e-04	2.18
6	2.82e-03	1.35	1.52e-01	0.63	5.26e-03	0.92	1.19e-04	2.78	1.84e-02	1.17	1.77e-04	2.29

(b) `[ELP-RD]` with CIP-stabilization

ℓ	$\mathrm{e}_{L^2(\Omega)}$	order	$\mathrm{e}_{H^1(\Omega)}$	order	e_∞	order	$e_{\infty,\Gamma}$	order	e_∞^∇	order	$\mathrm{e}_{\infty,\Gamma}^\nabla$	order
3	9.84e-03		4.07e-01		2.50e-02		8.86e-03		1.19e-01		2.15e-02	
4	3.88e-03	1.34	3.13e-01	0.38	1.88e-02	0.41	1.81e-03	2.29	5.73e-02	1.05	3.57e-03	2.59
5	2.73e-03	0.51	2.52e-01	0.31	1.28e-02	0.56	5.29e-04	1.78	3.46e-02	0.73	8.42e-04	2.08
6	1.53e-03	0.84	2.13e-01	0.24	1.19e-02	0.10	1.07e-04	2.30	1.68e-02	1.04	1.86e-04	2.18

(c) `[OPC-RD]`

ℓ	$\mathrm{e}_{L^2(\Omega)}$	order	$\mathrm{e}_{H^1(\Omega)}$	order	e_∞	order	$e_{\infty,\Gamma}$	order	e_∞^∇	order	$\mathrm{e}_{\infty,\Gamma}^\nabla$	order
3	1.25e-02		3.90e-01		2.52e-02		4.82e-03		1.21e-01		1.38e-02	
4	5.51e-03	1.18	2.87e-01	0.44	9.96e-03	1.34	1.86e-03	1.37	6.37e-02	0.92	4.32e-03	1.68
5	2.38e-03	1.21	2.15e-01	0.41	6.56e-03	0.60	4.77e-04	1.96	3.38e-02	0.91	1.22e-03	1.82
6	6.47e-04	1.88	1.44e-01	0.59	3.52e-03	0.90	8.63e-05	2.47	1.51e-02	1.16	2.48e-04	2.30

Table 5.1.: Convergence rates for the redistancing of Φ_5.

	ℓ	$e_{L^2(\Omega)}$	order	$e_{\infty,\Gamma}$	order	$e^{\nabla}_{\infty,\Gamma}$	order
[CLS-RD]	1	2.94e-01		1.38e-01		3.09e-01	
	2	1.68e-01	0.81	6.27e-02	1.14	1.56e-01	0.99
	3	8.53e-02	0.97	2.81e-02	1.16	6.14e-03	4.66
	4	4.42e-02	0.95	1.55e-02	0.86	2.39e-03	1.36
[ELP-RD]	1	5.23e-02		8.98e-02		3.49e-03	
	2	2.56e-02	1.03	3.93e-02	1.19	2.20e-03	0.67
	3	1.12e-02	1.20	2.46e-02	0.67	5.56e-04	1.98
	4	1.31e-03	3.09	3.09e-03	2.99	3.52e-05	3.98
[OPC-RD]	1	7.59e-02		8.26e-02		6.58e-03	
	2	3.88e-02	0.97	3.91e-02	1.08	3.23e-03	1.03
	3	3.29e-02	0.23	1.53e-02	1.36	1.30e-03	1.31
	4	2.41e-02	0.45	4.86e-03	1.65	7.37e-04	0.82

Table 5.2.: Asymptotic results for the vortex flow problem.

approximation accuracy. In this example, we used an interface penalty parameter of $\alpha = 5 \cdot 10^4$ and no CIP stabilization.

The results of [OPC-RD] are quite satisfactory, even though the signed distance function approximation is less accurate than in the case of the [ELP-RD] approach. By the monolithic design of [OPC-RD], the interface seems to be better conserved and lies very close to the solution without redistancing.

Let us remark that in all test cases slightly better results could be obtained when using smaller time step sizes. For the sake of comparison, we used a rather large increment Δt.

Finally, let us comment on the asymptotic behavior. Of particular interest are the errors $e_{\infty,\Gamma}$ and $e^{\nabla}_{\infty,\Gamma}$ which directly reveal the interface approximation quality of the different approaches. The results are summarized in Table 5.2. The best results are obtained for the [ELP-RD] approach. However, note that if [ELP-RD] was applied at every time step (as were [CLS-RD] and [OPC-RD]) the results were significantly less accurate. This can be explained by the fact that the relative error of redistancing can become dominant when the interface region is very thin. In particular, even for the finest mesh $\ell = 4$, the thickness of Ω_1 is of order h in some regions and the penalty term [ELP-RD] will fail to conserve the interface there. Similar problems are encountered for the monolithic approaches [CLS-RD] and [OPC-RD], thus yielding suboptimal convergence rates.

5.6.3. Dependence on Regularization Parameters

In this section we address the dependence of [ELP-RD] and [OPC-RD] on the choices of the penalty parameter α and the Tikhonov regularization parameter β. Therefore, let us consider the vortex deformation example from Section 5.6.2 with velocity field $\mathbf{v}(t, \mathbf{x})$ scaled by a factor of $1/2$.

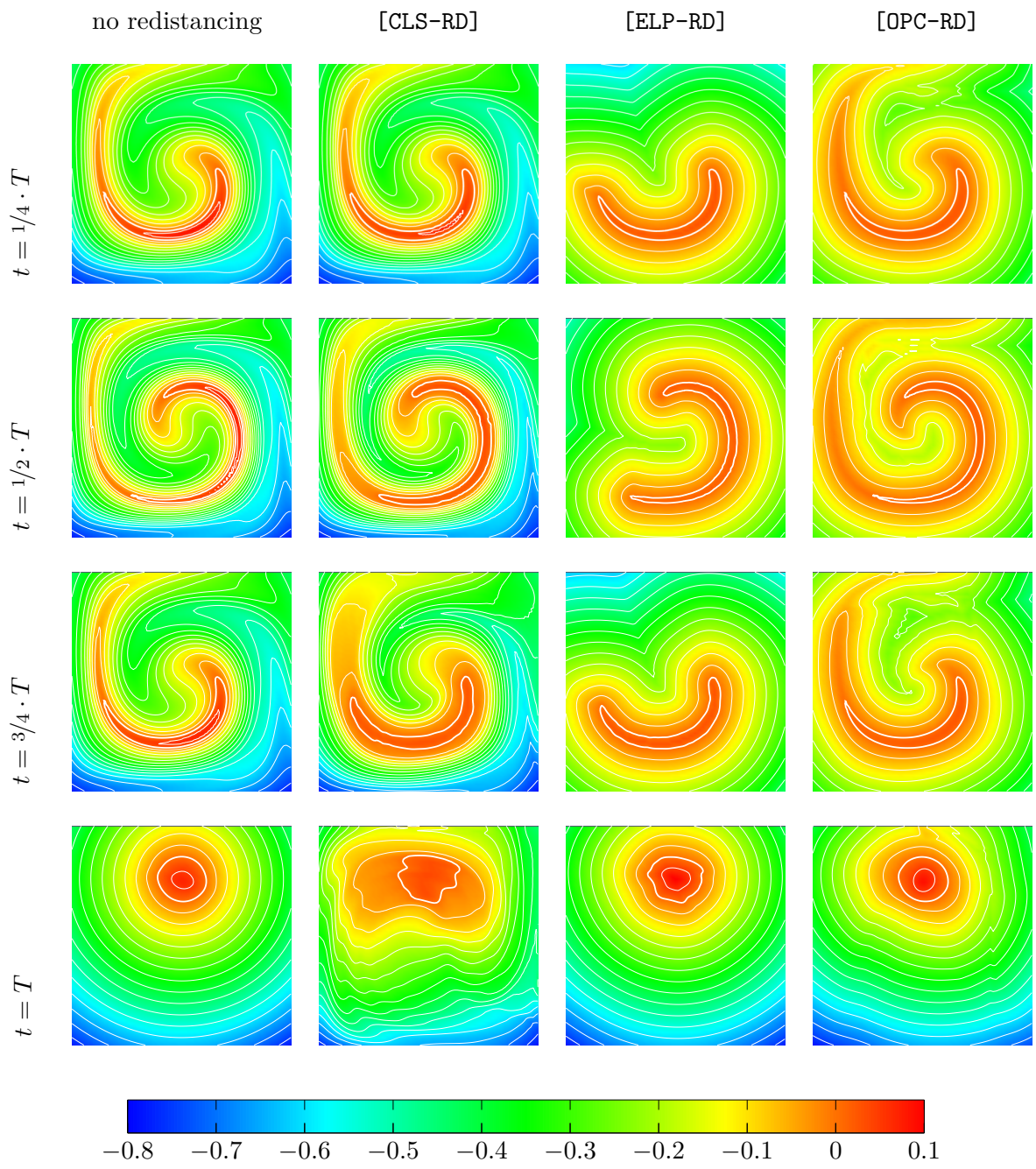

Figure 5.9.: Plots of level set functions subject to vortex flow and different redistancing schemes (columns) at different time instances (rows) and for refinement level $\ell = 3$. Equidistant level set lines are shown in white, the zero level set in bold white.

The error graphs in Fig. 5.10a indicate that the specific choice of the penalty parameter in the [ELP-RD] approach has no significant impact on the results. Similarly, Fig. 5.10b shows the influence of the choice of the Tikhonov regularization parameter β in the [OPC-RD] approach. The oscillating behavior of e_∞ is due to numerical artifacts mostly away from the interface. For increasing values of β, the accuracy of the interface approximation (measured by $\mathrm{e}_{\infty,\Gamma}$) is improved. This is to be expected, as small values of β impose stronger bounds on the control. On the other hand, larger values of β limit the corrections and therefore an increase in $\mathrm{e}_{L^2(\Omega)}$, $\mathrm{e}_{H^1(\Omega)}$ and e_∞^∇ can be observed. However, the increase in $\mathrm{e}_{\infty,\Gamma}^\nabla$ is moderate also for large values of β, and therefore local interface approximation can be considered as relatively robust w.r.t. β.

5.6.4. Stabilization Effect of the Optimal Control Approach

For the discretization of the optimal control approach in Section 5.5 we have already seen that stabilization techniques can be easily embedded into the state equation. However, they may introduce artificial numerical diffusion. As an interesting fact, while enforcing the signed distance function property, the optimal control approach exhibits inherent stabilization properties. This makes the application of an additional stabilization technique unnecessary in many cases.

To demonstrate the stabilization effect, we consider the rotation of the level set function of a circle inside

$$\Omega^\circ \coloneqq \{\mathbf{x} \in \mathbb{R}^2 \ : \ |x| < 1/2\}. \tag{5.86}$$

The velocity is given by

$$\mathbf{v}(t, \mathbf{x}) \coloneqq \pi \begin{bmatrix} x_2 \\ -x_1 \end{bmatrix}. \tag{5.87}$$

and $\varphi_{0,h}$ is set to be the $L^2(\Omega)$-projection of the signed distance function of the circle with radius 0.1 centered at $(0, 0.25)$. Since $\mathbf{v}(t, \mathbf{x}) \cdot \mathbf{n}(\mathbf{x}) = 0$ for all t and $x \in \partial\Omega$, there is no inflow boundary and thus no boundary conditions must be set. The time interval is set to $[0, 2]$, so that the level set function performs one full revolution.

Fig. 5.11 gives an impression of the finite element solution and the [OPC-RD] solution, both without stabilization.

We remark that this result is presented only to illustrate the stabilizing effect of [OPC-RD]. In contrast to these results, the [CLS-RD] approach does not converge or converges at a very poor rate. For post-processing approaches such as [HYP-RD] or [ELP-RD] one observes stronger displacements of the interface caused by oscillations in the predictors. In applications where strong instabilities occur, it might still be necessary to apply a suitable stabilization technique or to choose a sufficiently small Tikhonov regularization parameter.

(a) Errors w.r.t. to the penalty paramter α for `[ELP-RD]`.

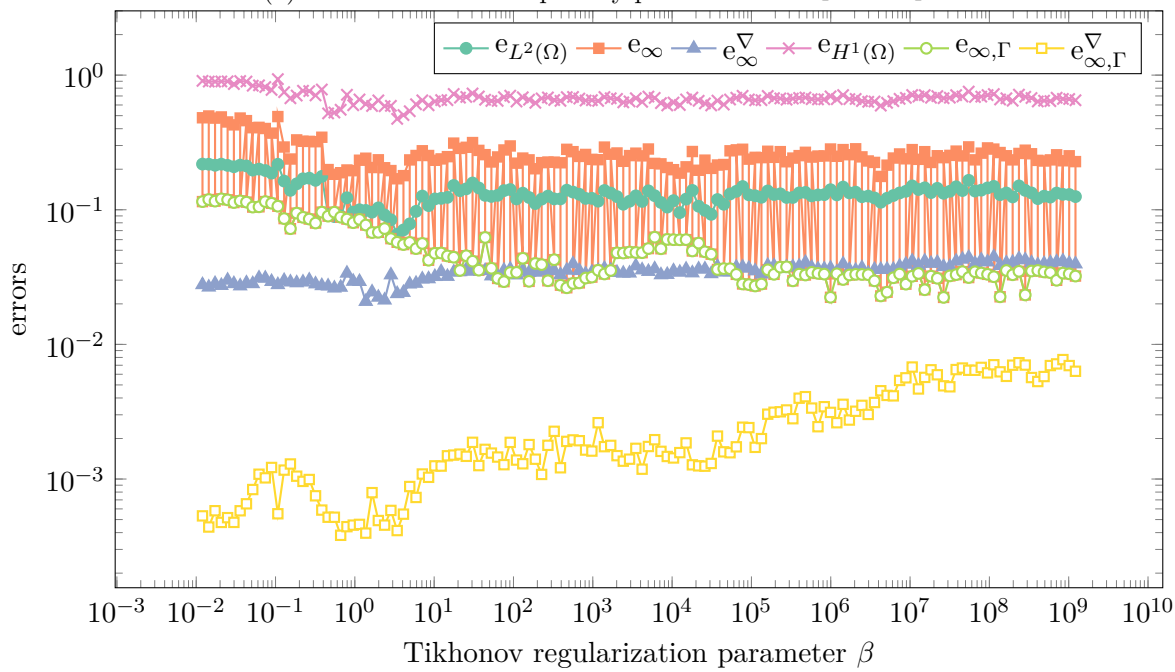

(b) Errors w.r.t. to the regularization paramter β for `[OPC-RD]`.

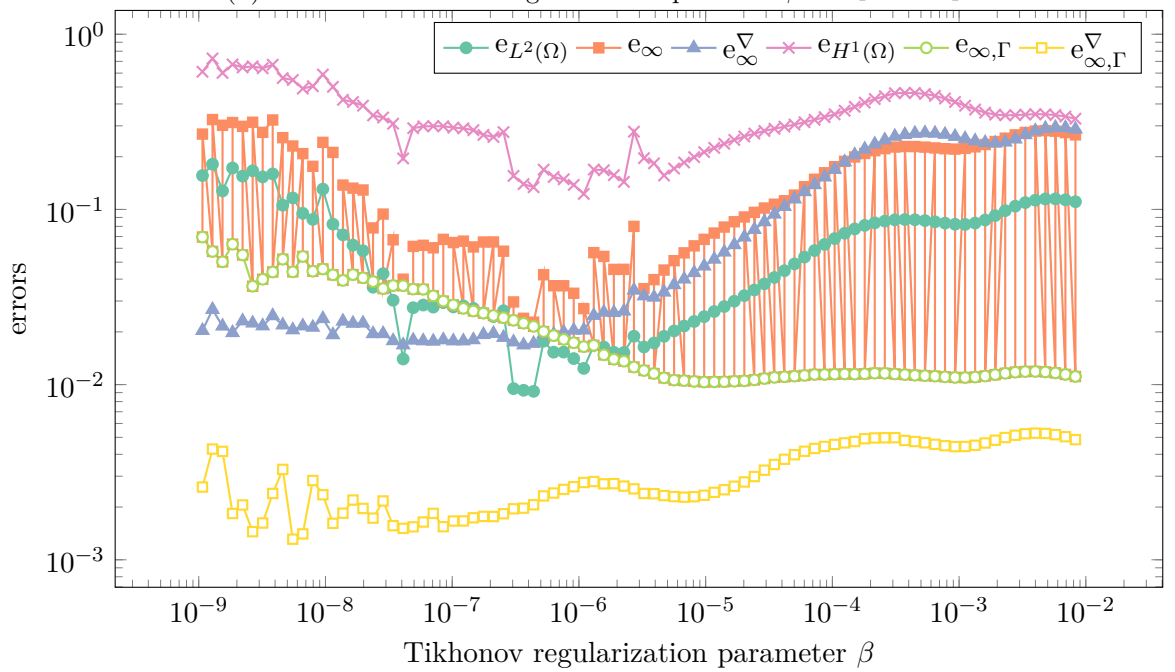

Figure 5.10.: Parameter study for `[ELP-RD]` and `[OPC-RD]`.

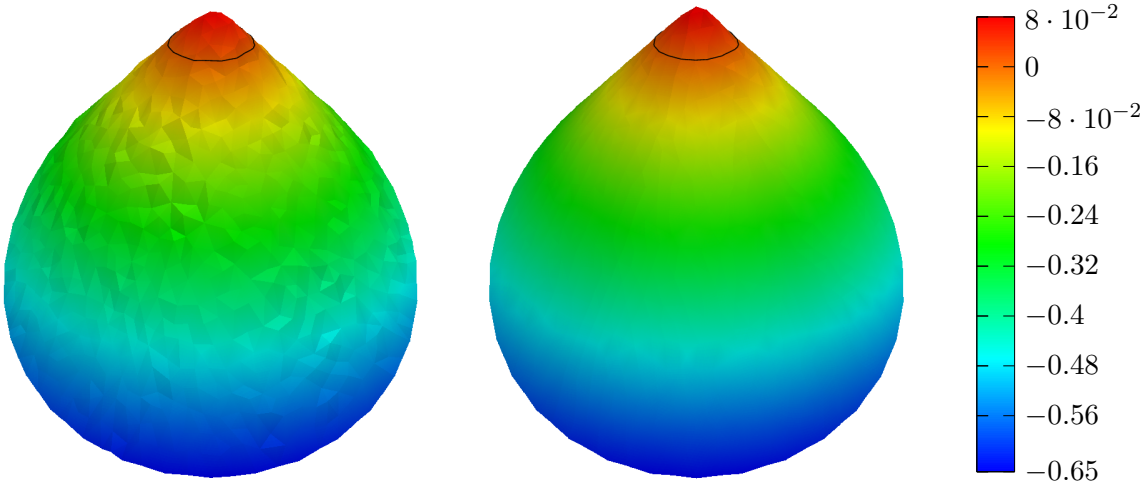

Figure 5.11.: Finite element solution without stabilization and `[OPC-RD]` solution with inherent stabilization.

5.6.5. Other Test Cases

In [BKS16, Section 5.2], results for the rotation of Zalesak's slotted disk are provided. The test case is not challenging in terms of redistancing as the level set function is hardly perturbed and hence the signed distance function property is preserved quite well. Yet it is useful to consider this test case to verify the numerical consistency of the methods under investigation.

Finally, note that the application of the investigated redistancing schemes to the two-phase flow problem is provided in Section 7.6 as further numerical example.

6 Conservative Level Set Methods

One of the major drawbacks of level set methods compared to volume of fluid methods is their inability to conserve mass on a discrete level. Over time, mass is lost or gained, which may negatively influence the overall accuracy and cause nonphysical behavior. This can be explained by several reasons:

1. "The discrete velocity field is not divergence free,
2. The advection of φ in general does not satisfy the conservation of $\mathrm{H}(\varphi)$,
3. Advection of details of the interface that are too small for the mesh will result in numerical clipping these details and will not satisfy conservation,
4. Redistancing does not in general satisfy conservation." [LD09]

Even though it is possible to show in some scenarios that the mass error decreases asymptotically with the mesh size, it can accumulate over time. Unfortunately, theoretical estimates are not always valid in practical applications due to restrictive regularity assumptions.

Although not conservative, level set methods are based on a continuous formulation and consequently, higher order approximations can easily be employed. To achieve better mass conservation properties, several extensions have been developed in the past years.

In this chapter, we review some commonly used conservative extensions of the level set method, before proposing an optimal control based technique. The first section provides a theoretical estimate, showing that under certain assumptions the mass error converges with order k (where k is the degree of the polynomial finite element approximation). In the second section, a simple yet effective global approach is introduced. The following sections briefly outline other commonly used mass conservative extensions of the level set method. In Section 6.6 we introduce an optimal control approach yielding a perfectly conservative scheme. The chapter concludes with a detailed numerical evaluation of the proposed method.

6.1. Theoretical Estimate

Throughout this chapter, we assume that the general setting specified in Definition 4.1 holds. The mass contained in each of the two phases Ω_1 and Ω_2 is given by

$$\mathrm{m}_i \coloneqq |\Omega_i| = \int_{\Omega_i} 1 \, \mathrm{d}\mathbf{x}, \qquad i = 1, 2. \tag{6.1}$$

In particular, we can express m_i by using the associated level set function

$$\mathrm{m}(\varphi) \coloneqq \int_{\Omega} \mathrm{H}(\varphi(\mathbf{x})) \, \mathrm{d}\mathbf{x}, \tag{6.2}$$

which gives $\mathrm{m}_1 = \mathrm{m}(\varphi)$ and $\mathrm{m}_2 = |\Omega| - \mathrm{m}(\varphi)$. We cite the following general estimate on mass errors for continuous finite element level set approximations:

Theorem 6.1 (Mass Error Estimate [RL11])
Under the assumptions of Definition 4.1, the following estimate holds (see [RL11] for details):

$$\left|\mathrm{m}(\varphi_h^N) - \mathrm{m}(\varphi(\cdot, T))\right| \leq c h^k. \tag{6.3}$$

The proof of this theorem and more details can be found in [RL11, Bur10]. We emphasize that this proof requires sufficiently smooth functions and interfaces. However, the signed distance function is generally only in $C(\Omega)$, since at its skeleton it is not continuously differentiable (cf. Section 4.1). In numerical experiments one may thus observe suboptimal convergence rates (cf. Section 6.7), in particular when the skeleton is close to the interface.

Although the error in mass conservation decreases asymptotically, in some applications even small inaccuracies may cause unphysical behavior. Furthermore, these errors can accumulate over time, in particular in long time dependent simulations where $T \gg t_0$.

6.2. Level Set Shifting Approach

A simple computational technique presented by Smolianski in [Smo01] is as follows. At first, the mass w.r.t. the initial data is computed

$$\mathrm{m}_{0,h} = \mathrm{m}(\varphi_{0,h}). \tag{6.4}$$

Note that on a discrete level, the computation of $m(\varphi_h)$ depends on the employed localization technique for the interface. For example, in the case of $\varphi_h \in X_h^1$ the interface can easily be reconstructed in an explicit fashion and $\mathrm{m}_{0,h}$ can be computed exactly with respect to X_h^1. However, for higher polynomial degrees, interface reconstruction can become more involved. In Section 4.3.2 we have introduced a technique to use linear basis functions on a refined mesh for the reconstruction of an interface of a function in X_h^2. Alternatively, one can employ an adaptive quadrature formula to evaluate (6.2) directly. In any case, the discrete mass

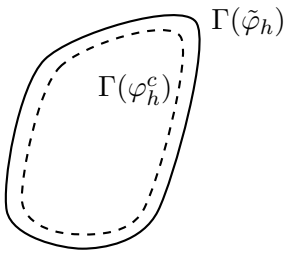

Figure 6.1.: Illustration of level set shifting.

$\mathrm{m}_{0,h}$ significantly depends on the numerical technique employed. Generally, for higher order polynomial degrees we recommend the use of adaptive quadrature techniques (cf. [Vog06]).

Given a provisional solution $\tilde{\varphi}_h$ to the level set equation, the key idea is to correct $\tilde{\varphi}_h$ by shifting the level set function up- or downwards, i.e.

$$\varphi_h^c(\mathbf{x}) \coloneqq \tilde{\varphi}_h(\mathbf{x}) + c. \tag{6.5}$$

The approach is illustrated in Fig. 6.1. To determine the shifting constant c, the problem

$$\text{find } c \in \mathbb{R} \text{ such that } \mathrm{m}(\varphi_h^c) = \mathrm{m}(\varphi_{0,h}) \tag{6.6}$$

needs to be solved. Smolianski [Smo01] uses a first variation formula for volume integrals to derive

$$c = \frac{\mathrm{m}_{0,h} - \mathrm{m}(\tilde{\varphi}_h)}{|\Gamma(\tilde{\varphi})|}. \tag{6.7}$$

The process is repeated iteratively until a sufficiently accurate constant $\hat{c}$ is obtained. The corrected level set function is set to $\varphi_h^{\hat{c}}$ and the temporary solution $\tilde{\varphi}_h$ is discarded. More generally, problem (6.6) can be solved numerically by applying a suitable root-finding technique. For example, Gross and Reusken [GR11] suggest using the Anderson-Björck bracketing method [AB73].

Besides the simplicity in terms of implementation, this approach does not change the gradients of the level set function. In particular, if a redistancing step is applied in advance, the signed distance function approximation is perfectly maintained.

One of the major drawbacks of this approach is that it acts globally. An accurate mass correction scheme should localize the correction to those regions where mass is lost or gained. In this approach however, the redistribution of mass only depends on the nonphysical level set function. In regions where the level set function is rather flat, more mass is redistributed than in regions with steep gradients. This underlines the need of maintaining a good signed distance function approximation. As a consequence of the global correction, mass may be redistributed at wrong locations causing severe nonphysical effects (see for example Section 6.7.3).

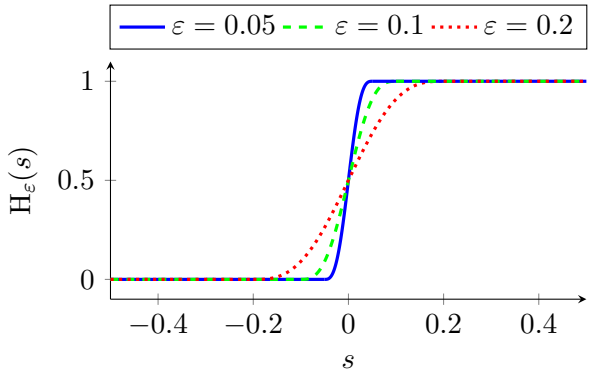

Figure 6.2.: Illustration of H_ε for different values of ε.

In summary, this approach provides an efficient technique to enforce global mass conservation. Local mass conservation however is not guaranteed and the redistribution of mass might heavily depend on the level set function.

6.3. Phase Field - Level Set Hybrid Approach

In this section we present a hybrid approach, that combines the level set approach with a volume of fluid technique. It was originally presented by Olsson and Kreiss in [OK05, OKZ07]. The section is based on these publications. First, the smeared Heaviside function $\mathrm{H}_\varepsilon : \mathbb{R} \to [0,1]$,

$$\mathrm{H}_\varepsilon(s) := \begin{cases} 0 & \text{if } s < -\varepsilon, \\ \frac{1}{2}\left(1 + \frac{s}{\varepsilon} + \frac{1}{\pi}\sin\left(\frac{\pi s}{\varepsilon}\right)\right) & \text{if } -\varepsilon \le s \le \varepsilon, \\ 1 & \text{if } s > \varepsilon, \end{cases} \tag{6.8}$$

is defined (cf. Fig. 6.2). The regularization parameter ε corresponds to the thickness of the interface region. Instead of the signed distance function $\tilde{\varphi}$, one chooses the smeared indicator function

$$\hat{\varphi}(\mathbf{x}) := \mathrm{H}_\varepsilon(\tilde{\varphi}(\mathbf{x})) \tag{6.9}$$

as level set function, that varies smoothly in the interface region and is constant elsewhere. The advection is performed using a conservative scheme which preserves the smoothness of $\hat{\varphi}$. In particular, this implies that $\mathrm{m}(\hat{\varphi})$ will be conserved during advection, and therefore one can expect a good approximation of

$$A_{\hat{\varphi}+1/2} := \mathrm{m}(\hat{\varphi} + 1/2). \tag{6.10}$$

Note that if the sharp Heaviside function was used instead of (6.8), $A_{\hat{\varphi}}$ would be conserved perfectly. To keep the interface shape and width constant, an intermediate step must be applied.

For the conservative advection of the phase field function, Olsson and Kreiss [OK05] suggest to use numerical methods that

1. are conservative,
2. do not introduce spurious oscillations and
3. preserve the profile of $\hat{\varphi}$.

A suitable method that meets these requirements is given by a non-linear TVD (total variation diminishing) method that does not smear discontinuities to preserve the profile of $\hat{\varphi}$. For the temporal discretization a second order Runge-Kutta scheme is suggested.

To maintain an interface thickness of width ε (which is crucial for the accuracy), an intermediate artificial compression procedure must be applied, cf. [OK05, Har77]. This step essentially involves the solution of a conservation law of the form

$$\frac{\partial}{\partial \tau}\hat{\varphi} + \nabla \cdot \mathbf{f}(\hat{\varphi}) = 0, \tag{6.11}$$

where $\mathbf{f}(\hat{\varphi}) \coloneqq \hat{\varphi}(1-\hat{\varphi})\mathbf{n}$ is the compressive flux and τ the artificial time variable. The numerical solution of (6.11) requires suitably stabilized numerical schemes.

The numerical evaluation indicates good (but not perfect) approximation of mass, but slow convergence for refined meshes. In [OKZ07] an improved approach is presented. To obtain a better convergence behavior, the diffusion in the compression step is suggested to be restricted in normal direction with respect to the interface. The good conservation properties however have to be set against a rather complex implementation and significant computational costs.

6.4. Dual Level Set Approach

This section is based on the method presented by Lesage, Dervieux and Guégan in [LD09]. Similarly to the level set equation in conservative form (4.13), we consider the conservation law

$$\frac{\partial}{\partial t}\chi + \nabla \cdot (\mathbf{v}\chi) = 0, \tag{6.12}$$

where χ is the *characteristic function* defined by

$$\chi(t, \mathbf{x}) \coloneqq \begin{cases} 1 & \text{if } \mathbf{x} \in \Omega_1(t), \\ 0 & \text{elsewhere.} \end{cases} \tag{6.13}$$

Unfortunately, this implication does not hold on a discrete level. They key idea of the dual level set approach is to recover (6.12) from the level set equation. In particular, this approach tries to combine the higher accuracy of the level set advection with the local mass conservation

property of the advected characteristic function. This is accomplished as follows. For $V_h := X_h^1$, the *dual level set equation*

$$\int_{\Omega_{\text{int}}} \left(\frac{\partial}{\partial t} \mathrm{H}(\varphi_h) \right) v_h \, \mathrm{d}\mathbf{x} = \int_{\partial\Omega_{\text{int}}} \mathrm{H}(\varphi_h) v_h \mathbf{v} \cdot \mathbf{n} \, \mathrm{d}\sigma - \int_{\Omega_{\text{int}}} \mathrm{H}(\varphi_h) \mathbf{v} \cdot \nabla v_h \, \mathrm{d}\mathbf{x} \qquad \forall v_h \in V_h \tag{6.14}$$

is obtained from the variational form of (6.12) restricted to the subdomain $\Omega_{\text{int}} \subset \Omega$ (i.e. in immediate vicinity of the interface Ω_{int}) and integration by parts. Application of the first-order accurate explicit forward-Euler time-discretization at equidistant time levels $t^n := n \cdot \Delta t$ (cf. Section 3.4) yields for all test functions $v_h \in V_h$:

$$\begin{aligned} \int_{\Omega_{\text{int}}} \mathrm{H}(\varphi_h^{n+1}) v_h \, \mathrm{d}\mathbf{x} \quad = \quad & \int_{\Omega_{\text{int}}} \mathrm{H}(\varphi_h^n) v_h \, \mathrm{d}\mathbf{x} + \Delta t \int_{\partial\Omega_{\text{int}}} \mathrm{H}(\varphi_h^n) v_h \mathbf{v} \cdot \mathbf{n} \, \mathrm{d}\sigma \\ & - \Delta t \int_{\Omega_{\text{int}}} \mathrm{H}(\varphi_h^n) \mathbf{v} \cdot \nabla v_h \, \mathrm{d}\mathbf{x}. \end{aligned} \tag{6.15}$$

Plugging in the admissible test function $v_h \equiv 1$ proves the (local) mass conservation:

$$\int_{\Omega_{\text{int}}} \mathrm{H}(\varphi_h^{n+1}) \, \mathrm{d}\mathbf{x} = \int_{\Omega_{\text{int}}} \mathrm{H}(\varphi_h^n) \, \mathrm{d}x. \tag{6.16}$$

Lesage et al. [LD09] suggest the use of a multi-step Runge-Kutta 3 scheme of second order accuracy to compute φ_h^{n+1}. The system resulting from the discretized dual level set equation is highly non-linear, uniqueness is unclear and special numerical treatment is required. Furthermore, the algorithm only computes the advection in interface vicinity. Therefore, it requires the application of a redistancing scheme (or an alternative extension procedure) after mass correction to extend φ_h to $\Omega \setminus \Omega_{\text{int}}$, which may significantly increase the computational costs. Furthermore, the restriction to Ω_{int} is computationally cumbersome, in particular because affected elements change as time evolves. We remark that the linear system arising from the dual level set equation may not be well posed. Furthermore, the employed Newton method faces convergence problems. The complete algorithm can be found in [LD09].

6.5. Further Approaches

Kees et al. [KAFB11] proposed a method that essentially combines the level set method with the volume of fluid method. We consider the conservation law for the fluid mass

$$\frac{\partial}{\partial t} \big(\rho_1 \, \mathrm{H}(\varphi) \big) + \nabla \cdot \big(\rho_1 \, \mathrm{H}(\varphi) \mathbf{v} \big) = 0. \tag{6.17}$$

Its variational formulation is numerically solved in a conservative manner to obtain a mass-conserving approximate solution $\hat{\mathrm{H}}^{n+1}$ to (6.17). On the other hand, let φ^{n+1} denote the

generally non-conservative solution to the level set equation. The key idea of the approach is to combine φ^{n+1} and $\hat{\mathrm{H}}^{n+1}$ in terms of the variational problem

$$\begin{aligned} &\text{find } \varphi' \in V \text{ such that} \\ &\int_\Omega \big(\mathrm{H}(\varphi^{n+1} - \varphi') - \hat{\mathrm{H}}^{n+1}\big) v \,\mathrm{d}\mathbf{x} + \kappa \int_\Omega \nabla\varphi' \cdot \nabla v \,\mathrm{d}\mathbf{x} = 0 \qquad \forall v \in V. \end{aligned} \tag{6.18}$$

If the test space V admits constant functions, global conservation of mass is guaranteed. In practice, the Heaviside function is replaced by a suitable regularized version such as (6.8) from which a second parameter ε arises. Since the numerical problem to be solved is non-linear, Newton's method is employed for linearization. Unfortunately, the convergence behavior depends on the choices of the free parameters ε and κ. Furthermore, the approach does not guarantee perfect conservation of mass and is not completely local.

The interested reader is referred to [PSVW05] and [SP00] for similar approaches based on combination of the level set and the volume of fluid approximation. A comparative numerical study can be found in [DHO+14], where the induced numerical diffusion is stated as a major drawback.

In [DPLFP06] Di Pietro et al. propose and compare two mass-preserving techniques that are not based on combined strategies as the methods above. The first one builds on a discontinuous Galerkin discretization, while the second one (originally presented in [Par04]) is a continuous Galerkin approximation where gradient jumps on inter-element boundaries are penalized. Both schemes yield better mass-preserving properties than common stabilization technqiues, yet mass is not conserved perfectly. In particular on coarse meshes, the loss or gain in mass can still be significant. However, in particular for coarser meshes, conservative approaches are of particular interest.

6.6. Optimal Control Approach

Let us now consider an optimal control approach to obtain a mass conservative numerical level set scheme. It was first proposed in [Kuz13] and then extended in [BK14]. Similarly to the dual level set method, it is based on the continuity equation for the Heaviside function of φ:

$$\frac{\partial}{\partial t}\mathrm{H}(\varphi) + \nabla \cdot \big(\mathrm{H}(\varphi)\mathbf{v}\big) = 0 \qquad \text{in } \Omega. \tag{6.19}$$

The key idea is to augment this equation by a corrective flux $\mathbf{q} \in \mathbf{Q}$

$$\frac{\partial}{\partial t}\mathrm{H}(\varphi) + \nabla \cdot \big(\mathrm{H}(\tilde{\varphi})\mathbf{v} - \mathbf{q}\big) = 0 \qquad \text{in } \Omega, \tag{6.20}$$

where $\mathbf{Q}$ is a suitable function space. In this equation, $\tilde{\varphi}$ denotes a temporary numerical solution to the level set equation which serves as predictor. We emphasize that this approach is consistent for any flux that satisfies

$$\mathbf{n} \cdot \mathbf{q} = 0 \qquad \text{on } \partial\Omega. \tag{6.21}$$

This can be verified by considering the variational form of (6.20)

$$\int_\Omega \left(\frac{\partial}{\partial t}\,\mathrm{H}(\varphi)\right) v \,\mathrm{d}\mathbf{x} + \int_\Omega \big(\mathbf{q} - \mathrm{H}(\tilde{\varphi})\mathbf{v}\big)\cdot\nabla v \,\mathrm{d}\mathbf{x} = 0 \qquad \forall v \in H^1(\Omega). \tag{6.22}$$

By our general assumptions (cf. Definition 4.1), the domain $\Omega_1(t)$ does not touch (or come close to) $\partial\Omega$, which implies $\tilde{\varphi} < 0$ on $\partial\Omega$ and therefore

$$\int_{\partial\Omega} \mathrm{H}(\tilde{\varphi}) v \hat{\mathbf{n}}\cdot\mathbf{v}\,\mathrm{d}\sigma = 0, \tag{6.23}$$

i.e. the surface integral that arises from integration by parts in (6.22) vanishes. For the admissible test function $v \equiv 1$ we obtain from (6.22) and (6.23) the (local) conservation of mass:

$$\frac{\mathrm{d}}{\mathrm{d}t}\int_\Omega H(\varphi)\,\mathrm{d}x = 0. \tag{6.24}$$

Unfortunately, just like for the dual level set approach, we cannot solve equation (6.20) numerically because the corresponding linear system would be heavily underdetermined. Therefore, we embed the equation as a constraint into the following optimal control approach:

For a given predictor $\tilde{\varphi} \in V$ to the level set equation

$$\min_{\varphi\in V,\ \mathbf{q}\in\mathbf{Q}} J(\varphi,\mathbf{q}) \coloneqq \frac{1}{2}\,\|\varphi - \tilde{\varphi}\|^2_{L^2(\Omega)} + \frac{1}{2}\,\|\beta\mathbf{q}\|^2_{\mathbf{Q}} \tag{6.25a}$$

subject to

$$\int_\Omega \left(\frac{\partial}{\partial t}\,\mathrm{H}(\Phi)\right) v \,\mathrm{d}\mathbf{x} + \int_\Omega \big(\mathbf{q} - \mathrm{H}(\tilde{\varphi})\mathbf{v}\big)\cdot\nabla v \,\mathrm{d}\mathbf{x} = 0 \qquad \forall v \in H^1(\Omega). \tag{6.25b}$$

The Tikhonov regularization parameter β may be non-constant and depend on $\tilde{\varphi}$ but not on φ or $\mathbf{q}$. We refer to this approach as *vector control approach* as the control variable $\mathbf{q}$ is vector valued (cf. [BK14]). In the original publication [Kuz13], the convective flux ∇q of a scalar valued function was used which we refer to as *scalar control approach*. For the latter case we have the augmented continuity equation

$$\frac{\partial}{\partial t}\,\mathrm{H}(\varphi) + \nabla\cdot(\mathrm{H}(\tilde{\varphi})\mathbf{v} - \nabla q) = 0 \qquad \text{in } \Omega \tag{6.26}$$

from which we obtain for controls satisfying the homogeneous Neumann boundary condition

$$\nabla q\cdot\mathbf{n} = 0 \qquad \text{on } \partial\Omega \tag{6.27}$$

the weak form

$$\int_\Omega \left(\frac{\partial}{\partial t}\,\mathrm{H}(\varphi)\right) v \,\mathrm{d}\mathbf{x} + \int_\Omega \big(\nabla q - \mathrm{H}(\tilde{\varphi})\mathbf{v}\big)\cdot\nabla v \,\mathrm{d}\mathbf{x} = 0 \qquad \forall v \in H^1(\Omega) \tag{6.28}$$

and the control problem

$$\min_{\varphi\in V,\ q\in Q} J(\varphi,q) \coloneqq \frac{1}{2}\left\|\varphi-\tilde{\varphi}\right\|^2_{L^2(\Omega)} + \frac{1}{2}\left\|\beta q\right\|^2_Q \tag{6.29a}$$

subject to

$$\int_\Omega \left(\frac{\partial}{\partial t}\,\mathrm{H}(\Phi)\right) v \,\mathrm{d}\mathbf{x} + \int_\Omega \left(\nabla q - \mathrm{H}(\tilde{\varphi})\mathbf{v}\right)\cdot\nabla v \,\mathrm{d}\mathbf{x} = 0 \qquad \forall v\in H^1(\Omega). \tag{6.29b}$$

Different control function spaces must be chosen for problems (6.25) and (6.29). In particular, the scalar approach requires sufficient smoothness for the gradient of q to be well defined. Possible choices are $Q = H^1(\Omega)$ and $\mathbf{Q} = (L^2(\Omega))^d$, which we will assume in what follows. For the level set function space we set $V \coloneqq L^2(\Omega)$. Both approaches are closely related in terms of the *Helmholtz decomposition*: a sufficiently smooth vector field $\mathbf{q}$ in $\mathbb{R}^d$, $d = 2, 3$, can be decomposed into the sum

$$\mathbf{q} = \nabla q + \nabla\times\mathbf{A} \tag{6.30}$$

of a gradient and a curl, where q is a scalar and $\mathbf{A}$ a vector potential (cf. [Gal11]). Note that $\nabla\times\mathbf{A}$ denotes the curl of $\mathbf{A}$.

For simplicity, let us consider the time-discrete versions of problems (6.25) and (6.29):

$$\min_{\varphi^{n+1}\in V,\ \mathbf{q}\in\mathbf{Q}} J(\varphi,\mathbf{q}) \coloneqq \frac{1}{2}\|\varphi^{n+1}-\tilde{\varphi}\|^2_{L^2(\Omega)} + \frac{1}{2}\left\|\beta\mathbf{q}\right\|^2_Q \tag{6.31a}$$

subject to

$$\int_\Omega \frac{\mathrm{H}(\varphi^{n+1})-\mathrm{H}(\varphi^n)}{\Delta t} v \,\mathrm{d}\mathbf{x} + \int_\Omega \left(\mathbf{q} - \theta\,\mathrm{H}(\tilde{\varphi})\mathbf{v} - (1-\theta)\,\mathrm{H}(\varphi^n)\mathbf{v}\right)\cdot\nabla v \,\mathrm{d}\mathbf{x} = 0 \tag{6.31b}$$
$$\forall v\in H^1(\Omega),$$

and

$$\min_{\varphi^{n+1}\in V,\ q\in Q} J(\varphi,q) \coloneqq \frac{1}{2}\|\varphi^{n+1}-\tilde{\varphi}\|^2_{L^2(\Omega)} + \frac{1}{2}\left\|\beta q\right\|^2_Q \tag{6.32a}$$

subject to

$$\int_\Omega \frac{\mathrm{H}(\varphi^{n+1})-\mathrm{H}(\varphi^n)}{\Delta t} v \,\mathrm{d}\mathbf{x} + \int_\Omega \left(\nabla q - \theta\,\mathrm{H}(\tilde{\varphi})\mathbf{v} - (1-\theta)\,\mathrm{H}(\varphi^n)\mathbf{v}\right)\cdot\nabla v \,\mathrm{d}\mathbf{x} = 0 \tag{6.32b}$$
$$\forall v\in H^1(\Omega).$$

6.6.1. Existence of a Solution

To analyze the existence of a solution to the optimal control problem, let us consider the regularized Heaviside function from (6.8). We can associate the *Nemytskii operator* $\mathcal{H}_\varepsilon(\varphi) = \mathrm{H}_\varepsilon(\varphi(\cdot))$ with $\mathrm{H}_\varepsilon(\cdot)$ (cf. Definition A.13) and show its Lipschitz-continuity.

Lemma 6.2 (Lipschitz-Continuity of Regularized Heaviside Function)
Let $\mathcal{H}_\varepsilon$ be the Nemytskii operator associated with H_ε defined in (6.8). Then, $\mathcal{H}_\varepsilon$ is a Lipschitz continuous operator with constant $L_\varepsilon = \frac{\pi+1}{\varepsilon}$.

$$\|\mathrm{H}_\varepsilon(\varphi) - \mathrm{H}_\varepsilon(\psi)\|_{L^r(\Omega)} \leq L_\varepsilon \|\varphi - \psi\|_{L^r(\Omega)} \qquad \forall \varphi, \psi \in L^\infty(\Omega) \tag{6.33}$$

for all $r \in [1, \infty]$.

Proof. The statement is an immediate consequence of Lemma 4.11 in [Trö10], which gives the Lipschitz-continuity of $\mathcal{H}_\varepsilon$ w.r.t. φ, provided that the underlying function H_ε is uniformly bounded and locally Lipschitz continuous. By definition of H_ε we have

$$|\mathrm{H}_\varepsilon(\varphi(\mathbf{x}))| \leq 1 \qquad \forall \varphi \in L^\infty(\Omega) \text{ and } \mathbf{x} \in \Omega$$

so that H_ε is uniformly bounded. Fundamental addition theorems yield

$$|\sin(x) - \sin(y)| = \left|2\cos\left(\frac{x+y}{2}\right)\sin\left(\frac{x-y}{2}\right)\right| \leq 2\left|\sin\left(\frac{x-y}{2}\right)\right| \leq |x-y|$$

and therefore $z : \mathbb{R} \to \mathbb{R}$, $z(x) := \frac{1}{2}\left(1 + \frac{x}{\varepsilon} + \frac{1}{\pi}\sin\left(\frac{\pi x}{\varepsilon}\right)\right)$ can be shown to be Lipschitz-continuous with constant $L_\varepsilon = \frac{\pi+1}{\varepsilon}$:

$$|z(x) - z(y)| \leq \left|\frac{x}{\varepsilon} - \frac{y}{\varepsilon}\right| + \left|\sin\left(\frac{\pi}{\varepsilon}x\right) - \sin\left(\frac{\pi}{\varepsilon}y\right)\right| \leq \frac{1}{\varepsilon}|x-y| + \frac{\pi}{\varepsilon}|x-y| = L_\varepsilon |x-y|. \qquad \square$$

Theorem 6.3 (Existence of a Solution)
Let $\tilde{\varphi} \in V$ be such that $\tilde{\varphi} < 0$ on $\partial\Omega$. If the Heaviside function $\mathrm{H}(\cdot)$ is replaced by a Lipschitz-continuous approximation $\mathrm{H}_\varepsilon(\cdot)$ with Lipschitz constant L_ε, problem (6.32) with $V = H^1(\Omega)$ and $Q = H^1_{\int=0}(\Omega)$ has a solution.

Proof. We use a non-reduced approach for this proof. The admissable set W_{ad} is given by

$$W_{\mathrm{ad}} := \{(\varphi, q) \in V \times Q \ : \ (\varphi, q) \text{ solve (6.32b)}\}.$$

For $\varphi^{n+1} := \varphi^n \subset V$, the compatibility condition (3.19) is satisfied and therefore

$$\int_\Omega \frac{\mathrm{H}_\varepsilon(\varphi^n) - \mathrm{H}_\varepsilon(\varphi^n)}{\Delta t}\,\mathrm{d}\mathbf{x} + \int_\Omega \nabla \cdot \left(\mathrm{H}_\varepsilon(\tilde{\varphi})\mathbf{v}\right)\,\mathrm{d}\mathbf{x} = \int_{\partial\Omega} \mathrm{H}_\varepsilon(\tilde{\varphi})\mathbf{v}\cdot\mathbf{n}\,\mathrm{d}\sigma = 0,$$

because $\mathrm{H}_\varepsilon(\tilde{\varphi}) = 0$ on $\partial\Omega$ by assumption. Hence, we can apply Lemma 3.4 and there exists a unique $q = q(\varphi^n) \in H^1_{\int=0}(\Omega)$ that solves (6.32b). Consequently, W_{ad} is non-empty. Since $J(\varphi, q) \geq 0$, the infimum

$$j := \inf_{(\varphi,q)\in W_{\mathrm{ad}}} J(\varphi, q)$$

exists and, by definition, there is a sequence $\{(\varphi_k, q_k)\} \subset W_{\text{ad}}$ such that

$$\lim_{k\to\infty} J(\varphi_k, q_k) \to j.$$

As before (see proof of Lemma 5.4), it is easy to verify that by definition of the objective functional $J(\cdot,\cdot)$, the sequence $\{\varphi_k, q_k\}$ must be bounded in W_{ad}. This implies the existence of a weakly convergent subsequence $\{\varphi_{k_\ell}, q_{k_\ell}\} \subset W_{\text{ad}}$,

$$(\varphi_{k_\ell}, q_{k_\ell}) \rightharpoonup (\bar\varphi, \bar q) \qquad \text{in } H^1(\Omega) \times H^1(\Omega).$$

We need to check if $(\bar\varphi, \bar q) \in W_{\text{ad}}$. The space $V = H^1(\Omega)$ is closed. Clearly, $H^1_{\int=0}(\Omega)$ is convex and therefore we can apply Mazur's Theorem (see, for example, [Wer09]) to deduce that $H^1_{\int=0}(\Omega)$ is weakly closed in $H^1(\Omega)$, which is why we have $\bar q \in H^1_{\int=0}(\Omega)$.

From the boundedness in $H^1(\Omega)$ and the weak convergence in $L^2(\Omega)$ we can infer the strong convergence of $\varphi_{k_\ell} \to \bar\varphi$ in $L^2(\Omega)$ as well as $q_{k_\ell} \to \bar q$ in $L^2(\Omega)$ (Rellich–Kondrachov Theorem, see [Alt12, Dob10]). Since $H^1_{\int=0}(\Omega)$ is a closed subspace of $H^1(\Omega)$, it is a Hilbert space and we can identify its dual space $H^{-1}_{\int=0}(\Omega)$ by $H^1_{\int=0}(\Omega)$ (cf. Riesz Representation Theorem A.5), i.e. for each $f \in H^{-1}_{\int=0}(\Omega)$ there exists a uniquely determined $v \in H^1_{\int=0}(\Omega)$ such that

$$f(q) = (q, v)_{H^1(\Omega)} = \int_\Omega q \cdot v \,\mathrm{d}\mathbf{x} + \int_\Omega \nabla q \cdot \nabla v \,\mathrm{d}\mathbf{x} \qquad \forall q \in H^1_{\int=0}(\Omega).$$

Hence, by

$$\begin{aligned}
& q_{k_\ell} \rightharpoonup \bar q \quad \text{in } H^1_{\int=0}(\Omega) \\
\iff \quad & f(q_{k_\ell}) \to f(\bar q) \quad \forall f \in H^{-1}_{\int=0}(\Omega) \\
\iff \quad & (q_{k_\ell}, v)_{H^1(\Omega)} \to (\bar q, v)_{H^1(\Omega)} \quad \forall v \in H^1_{\int=0}(\Omega) \\
\iff \quad & \lim_{\ell\to\infty} (\nabla(q_{k_\ell} - \bar q), \nabla v)_{L^2(\Omega)} = -\lim_{\ell\to\infty} (q_{k_\ell} - \bar q, v)_{L^2(\Omega)} \qquad \forall v \in H^1_{\int=0}(\Omega)
\end{aligned}$$

we infer by application of the Cauchy-Schwarz inequality and because of the strong convergence of q_{k_ℓ} in $L^2(\Omega)$:

$$\begin{aligned}
\implies \quad \lim_{\ell\to\infty} \left|(\nabla(q_{k_\ell} - \bar q), \nabla v)_{L^2(\Omega)}\right| &= \lim_{\ell\to\infty} \left|(q_{k_\ell} - \bar q, v)_{L^2(\Omega)}\right| \\
&\le \lim_{\ell\to\infty} \|v\|_{L^2(\Omega)} \cdot \|q_{k_\ell} - \bar q\|_{L^2(\Omega)} = 0 \quad \forall v \in H^1_{\int=0}(\Omega).
\end{aligned}$$

Thus we have

$$(\nabla q_{k_\ell}, \nabla v)_{L^2(\Omega)} \to (\nabla \bar q, \nabla v)_{L^2(\Omega)} \qquad \forall v \in H^1_{\int=0}(\Omega).$$

From the Lipschitz continuity of H_ε we can deduce

$$\|\mathrm{H}_\varepsilon(\varphi_{k_\ell}) - \mathrm{H}_\varepsilon(\bar\varphi)\|_{L^2(\Omega)} \le L_\varepsilon \|\varphi_{k_\ell} - \bar\varphi\|_{L^2(\Omega)}.$$

Together with the strong convergence of φ_{k_ℓ} in $L^2(\Omega)$ we obtain

$$\mathrm{H}_\varepsilon(\varphi_{k_\ell}) \to \mathrm{H}_\varepsilon(\bar{\varphi}) \qquad \text{in } L^2(\Omega),$$

and therefore, by employing the Cauchy-Schwarz inequality as above

$$(\mathrm{H}_\varepsilon(\varphi_{k_\ell}), v)_{L^2(\Omega)} = (\mathrm{H}_\varepsilon(\bar{\varphi}), v)_{L^2(\Omega)} \qquad \forall v \in H^1_{\int=0}(\Omega).$$

Since $(\varphi_{k_\ell}, q_{k_\ell}) \in W_{\mathrm{ad}}$ we have

$$\int_\Omega \frac{\mathrm{H}_\varepsilon(\varphi_{k_\ell}) - \mathrm{H}_\varepsilon(\varphi^n)}{\Delta t} v \,\mathrm{d}\mathbf{x} + \int_\Omega \left(\nabla q_{k_\ell} - \mathrm{H}_\varepsilon(\tilde{\varphi})\mathbf{v}\right) \cdot \nabla v \,\mathrm{d}\mathbf{x} = 0 \qquad \forall v \in H^1_{\int=0}(\Omega) \qquad \forall \ell \in \mathbb{N}$$

from which taking the limit and making use of the previous results we can infer

$$\int_\Omega \frac{\mathrm{H}_\varepsilon(\bar{\varphi}) - \mathrm{H}_\varepsilon(\varphi^n)}{\Delta t} v \,\mathrm{d}\mathbf{x} + \int_\Omega \left(\nabla \bar{q} - \mathrm{H}_\varepsilon(\tilde{\varphi})\mathbf{v}\right) \cdot \nabla v \,\mathrm{d}\mathbf{x} = 0 \qquad \forall v \in H^1_{\int=0}(\Omega).$$

Therefore we have $(\bar{\varphi}, \bar{q}) \in W_{\mathrm{ad}}$. The objective functional $J(\cdot,\cdot)$ is composed of the two functionals

$$J_1(\varphi) \coloneqq \frac{1}{2} \|\varphi - \tilde{\varphi}\|^2_{L^2(\Omega)},$$
$$J_2(q) \coloneqq \frac{\beta}{2} \|q\|^2_Q,$$

which both are continuous and convex. Therefore, $J(\varphi, q) \coloneqq J_1(\varphi) + J_2(q)$ is lower semicontinuous and Theorem A.11 yields

$$J(\bar{\varphi}, \bar{q}) \leq \liminf_{\ell \to \infty} J(\varphi_{k_\ell}, q_{k_\ell}) = j.$$

Since $(\bar{\varphi}, \bar{q}) \in W_{\mathrm{ad}}$, this implies $J(\bar{\varphi}, \bar{q}) = j$ and concludes the proof. □

Even though the cost functional is convex, we cannot conclude uniqueness since the state equation is highly non-linear. We remark that on a continuous level, a (temporary) solution $\tilde{\varphi}$ to the level set equation is conservative. Nevertheless, above theorem shows that a possibly non-conserving variable $\tilde{\varphi}$ can be corrected in its mass while minimizing deviations.

We remark that in the proof we require $V = H^1(\Omega)$, whereas numerically we usually employed $V = L^2(\Omega)$. In particular, a solution to the level set equation can only be expected to be in the graph space $\{v \in L^2(\Omega) \,:\, \mathbf{v} \cdot \nabla v \text{ exists and } \mathbf{v} \cdot \nabla v \in L^2(\Omega)\}$. By application of a redistancing technique however, the required smoothness can easily be gained so that the assumptions in the theorem are reasonable.

6.6.2. Discretization

This section is based on work partly published in [BK14]. We pursue a discretize-then-optimize approach to solve the optimal control problem numerically. First, the problem is discretized in space by the Galerkin approximation. For temporal discretization, we employ the θ scheme introduced in Section 3.4. We recast the discrete constrained optimization problem into an unconstrained optimization problem by introducing the Lagrange functional. Differentiation of this functional then yields a system of necessary optimality conditions which is linearized and numerically solved.

Let us emphasize that in terms of a finite element discretization the evaluation of the Heaviside function requires special care. One can either reconstruct the interface from the level set function and then subdivide Ω into Ω_1 and Ω_2 for exact integration, or one can apply an adaptive quadrature technique. As we have already seen, the latter one is more favorable when using higher polynomial degrees since interface reconstruction gets more involved.

In what follows, we use linear finite elements and exact quadrature with respect to the discrete reconstructed interface (cf. Section 4.3.2). However, the approach is not limited to this interface localization technique and also works for suitable regularizations of the Heaviside function. To keep notation simple, we denote the possibly regularized Heaviside function by $\mathrm{H}(\cdot)$.

As before, let $t^n := n \cdot \Delta t$ denote equidistant time levels from the θ time discretization scheme and $\{\psi_i\}_{i=1}^N$ the set of linear nodal basis functions on the triangulation $\mathcal{T}_h$, i.e. $V_h := X_h^1$. For better readability we omit the time dependence where no ambiguity arises. The discrete level set function can then be written in terms of its nodal values φ_i:

$$\varphi_h(\mathbf{x}) = \sum_{i=1}^{N} \varphi_i \psi_i(\mathbf{x}). \tag{6.34}$$

For the control space, we also employ linear finite elements, i.e. $Q_h := X_h^1$ and $\mathbf{Q}_h := X_h^1 \times X_h^1$, respectively. Hence, we can write the discrete control function in terms of its nodal values q_i and $\mathbf{q}_i$, respectively:

$$q_h(\mathbf{x}) = \sum_{i=1}^{N} q_i \psi_i(\mathbf{x}) \qquad \text{and} \qquad \mathbf{q}_h(\mathbf{x}) = \sum_{i=1}^{N} \mathbf{q}_i \psi_i(\mathbf{x}). \tag{6.35}$$

6.6.2.1. Scalar Control Approach

For the scalar control equation, we obtain the discrete state equation

$$\mathsf{g}(\tilde{\varphi}_h^{n+1}) + \Delta t \mathsf{S} q = \mathsf{g}(\varphi_h^n) + \Delta t \theta \mathsf{f}(\tilde{\varphi}_h) + \Delta t (1-\theta) \mathsf{f}(\varphi_h^n), \tag{6.36}$$

where the components of $\mathsf{f}(\cdot)$, $\mathsf{g}(\cdot)$ are given by

$$\mathsf{f}_i(\varphi_h) \coloneqq \int_\Omega \mathrm{H}(\varphi_h)\mathbf{v}\cdot\nabla\psi_i \,\mathrm{d}\mathbf{x} = \int_{\Omega_1} \mathbf{v}\cdot\nabla\psi_i \,\mathrm{d}\mathbf{x}, \tag{6.37}$$

$$\mathsf{g}_i(\varphi_h) \coloneqq \int_\Omega \mathrm{H}(\varphi_h)\psi_i \,\mathrm{d}\mathbf{x} = \int_{\Omega_1} \psi_i \,\mathrm{d}\mathbf{x}, \tag{6.38}$$

and S denotes the discrete Laplacian operator defined by

$$\mathsf{S}_{i,j} \coloneqq \int_\Omega \nabla\psi_i\cdot\nabla\psi_j \,\mathrm{d}\mathbf{x}. \tag{6.39}$$

Using the partition of unity property of the basis functions

$$\sum_{i=1}^{N} \psi_i(\mathbf{x}) = 1, \tag{6.40}$$

it is easy to verify that the discrete approach also yields a conservative scheme (cf. [BK14, Kuz13]):

$$\begin{aligned}\mathrm{m}(\varphi_h^{n+1}) - \mathrm{m}(\varphi_h^n) &= \int_\Omega \left(\mathrm{H}(\varphi_h^{n+1}) - \mathrm{H}(\varphi_h^n)\right) \mathrm{d}\mathbf{x} = \sum_{i=1}^{n} \left(\mathsf{g}_i(\varphi_h^{n+1}) - \mathsf{g}_i(\varphi_h^n)\right) \\ &= \Delta t\theta \sum_{i=1}^{N} \mathsf{f}_i(\tilde{\varphi}_h) + \Delta t(1-\theta)\sum_{i=1}^{N} \mathsf{f}_i(\varphi_h^n) - \sum_{i=1}^{N} (\mathsf{S}q)_i = 0.\end{aligned} \tag{6.41}$$

For the numerical solution of the constrained optimization problem, we introduce the associated discrete Lagrangian functional

$$\mathcal{L}_h(\varphi_h, q_h, \lambda_h) \coloneqq \frac{1}{2}\left\|\varphi_h - \tilde{\varphi}_h\right\|^2_{L^2(\Omega)} + \frac{\beta}{2}\left\|q_h\right\|^2_{H^1(\Omega)} + \lambda_h^\top r(\varphi_h, q_h, \tilde{\varphi}_h), \tag{6.42}$$

where $r(\varphi_h, q_h, \tilde{\varphi}_h)$ denotes the residual of (6.36). Based on numerical experience, we assume $\lambda_h \in X_h^1$. As for the optimal control problem in Section 5.5, an inf-sup condition could be introduced when solving the first-order optimality conditions. Due to the non-linearity of the problem, we were not able to show that such an inf-sup condition is satisfied automatically.

Differentiation w.r.t. φ_h, q_h and λ_h yields the system of necessary first order optimality conditions:

$$\mathsf{M}\varphi^{n+1} + \mathsf{K}(\varphi_h^{n+1})\lambda = \mathsf{M}\tilde{\varphi}, \tag{6.43a}$$

$$\beta(\mathsf{M}+\mathsf{S})q + S^\top\lambda = 0, \tag{6.43b}$$

$$\mathsf{K}(\varphi_h^{n+1}) + \mathsf{S}q = 0, \tag{6.43c}$$

where φ^{n+1}, q and λ denote the nodal vectors of φ_h^{n+1}, q_h and λ_h, respectively. The mass matrix M and the weighted surface mass matrix $\mathsf{K}(\cdot)$ are defined as

$$\mathsf{M}_{i,j} = \int_\Omega \psi_i \psi_j \, \mathrm{d}\mathbf{x}, \tag{6.44}$$

$$\mathsf{K}(\varphi_h)_{i,j} = \int_\Omega \psi_i \psi_j \, \mathrm{H}'(\varphi_h) \, \mathrm{d}\mathbf{x}. \tag{6.45}$$

The computation of the weighted mass matrix $\mathsf{K}(\cdot)$ involves evaluating the derivative of the Heaviside function $\mathrm{H}'(\varphi_h)$, which is known to be the Dirac delta distribution picking out the interface $\Gamma(\tilde{\varphi})$. Therefore, the volume integral in (6.45) can be transformed into a surface integral by means of the following identity:

$$\int_\Omega \psi_i \psi_j \delta(\varphi_h) |\nabla \varphi_h| \, \mathrm{d}\mathbf{x} = \int_{\Gamma(\varphi_h)} \psi_i \psi_j \, \mathrm{d}\sigma. \tag{6.46}$$

A proof of this identity can be found for example in [JCT07]. When assuming that $\tilde{\varphi}$ is close to a signed distance function and therefore $|\nabla \varphi_h| \approx 1$, we can neglect the additional term $|\nabla \varphi_h|$ and $\mathsf{K}(\cdot)$ simplifies to the mass matrix over $\Gamma(\varphi_h)$, i.e.

$$\mathsf{K}(\varphi_h)_{i,j} \approx \int_{\Gamma(\varphi_h)} \psi_i \psi_j \, \mathrm{d}\sigma. \tag{6.47}$$

The use of this simplification is preferable when the interface is localized exactly on a discrete level and our numerical experience did not indicate any related problems.

Using the approximation

$$g(\varphi_h) \approx \mathsf{K}(\varphi_h)\varphi_h, \tag{6.48}$$

we can write (6.43) in terms of the system block matrix

$$\mathsf{A}(\varphi_h) \coloneqq \begin{bmatrix} \mathsf{M} & 0 & \mathsf{K}(\varphi_h) \\ 0 & \beta(\mathsf{M}+\mathsf{S}) & \mathsf{S} \\ \mathsf{K}(\varphi_h) & \mathsf{S} & 0 \end{bmatrix}. \tag{6.49}$$

We employ the following fixed-point iteration approach for linearization:

1. Initialize: $(\varphi^{(0)}, q^{(0)}, \lambda^{(0)}) \coloneqq (\tilde{\varphi}, 0, 0)$ and $m \coloneqq 0$.
2. Increase m by 1 and compute the residual:

$$\begin{bmatrix} r_\varphi^{(m-1)} \\ r_q^{(m-1)} \\ r_\lambda^{(m-1)} \end{bmatrix} \coloneqq \begin{bmatrix} \mathsf{M}\tilde{\varphi} \\ 0 \\ 0 \end{bmatrix} - \mathsf{A}(\varphi^{(m-1)}) \begin{bmatrix} \varphi^{(m-1)} \\ q^{(m-1)} \\ \lambda^{(m-1)} \end{bmatrix}. \tag{6.50}$$

3. Check if the desired tolerance is reached and stop if so.

4. Update using the preconditioner $\mathsf{A}(\varphi^{(m-1)})$:

$$\begin{bmatrix} \varphi^{(m)} \\ q^{(m)} \\ \lambda^{(m)} \end{bmatrix} \coloneqq \begin{bmatrix} \varphi^{(m-1)} \\ q^{(m-1)} \\ \lambda^{(m-1)} \end{bmatrix} + \mathsf{A}(\varphi^{(m-1)})^{-1} \begin{bmatrix} r_\varphi^{(m-1)} \\ r_q^{(m-1)} \\ r_\lambda^{(m-1)} \end{bmatrix} \tag{6.51}$$

5. Go to step 2.

We remark that instead of computing the actual inverse of $\mathsf{A}(\varphi^{(m-1)})$ one clearly solves the associated linear system.

The following result gives a sufficient condition on the solvability of the arising linear system:

Lemma 6.4 (Invertibility of System Matrix [BK14])
Assuming $\beta > 0$, the matrix of the linear system to be solved within each iteration of the fixed-point linearization technique described above is invertible if $\mathsf{K}(\cdot)$ has strictly positive entries and is non-negative.

Proof. The following proof is taken from [BK14]. Let K have non-zero entries. Consider the blocks

$$D \coloneqq \begin{bmatrix} \mathsf{M} & 0 \\ 0 & \beta(\mathsf{M}+\mathsf{S}) \end{bmatrix} \qquad \text{and} \qquad E \coloneqq \begin{bmatrix} \mathsf{K} \\ \mathsf{S} \end{bmatrix}$$

of A. Since $\beta > 0$, D is clearly positive definite and consequently invertible. The stiffness matrix is symmetric positive semi-definite and (in accordance with the fact that a solution to the Laplace problem with homogeneous Neumann boundary condition is uniquely defined up to a constant) the kernel has dimension 1, i.e.

$$\operatorname{Ker}(\mathsf{S}) = \operatorname{span}(1, 1, \ldots, 1)^\top.$$

To conclude the non-singularity of

$$\mathsf{A} = \begin{bmatrix} D & E \\ E^\top & 0 \end{bmatrix},$$

we apply Theorem 3.2 from [BGL05], which states that for symmetric positive semi-definite D and matrices E of full rank, a necessary and sufficient condition for the existence of A^{-1} is given by the condition $\operatorname{Ker}(D) \cap \operatorname{Ker}(E) = \{0\}$. By assumption, K has at least one strictly positive entry, thus

$$\operatorname{Ker}(E) = \operatorname{Ker}(\mathsf{K}) \cap \operatorname{Ker}(\mathsf{S}) = \{0\}.$$

Furthermore, E is of full rank which can be seen by application of the dimension formula (see, for example, [KB13])

$$\dim\big(\operatorname{Ker}(E)\big) + \dim\big(\operatorname{Im}(E)\big) = N.$$

Hence, all conditions of Theorem 3.2 in [BGL05] are fulfilled and we can conclude that A is invertible. □

The required condition on $\mathsf{K}(\cdot)$ to have at least one strictly positive entry means that the interface $\Gamma(\varphi_h^{(m-1)})$ does not vanish, i.e. that the problem does not degenerate. In practice we have never observed any problems related to this condition.

6.6.2.2. Vector Control Approach

Similarly to the scalar control approach, we obtain the discrete vector control state equation

$$\mathsf{g}(\tilde{\varphi}_h^{n+1}) + \Delta t \mathsf{C}\mathbf{q} = \mathsf{g}(\varphi_h^n) + \Delta t \theta \mathsf{f}(\tilde{\varphi}_h) + \Delta t (1-\theta)\mathsf{f}(\varphi_h^n), \tag{6.52}$$

where the skew-symmetirc matrix C is defined by

$$\mathsf{C}\mathbf{q} \coloneqq \begin{bmatrix} \mathsf{C}_1 & 0 \\ 0 & \mathsf{C}_2 \end{bmatrix} \mathbf{q} = \mathsf{C}_1 q_1 + \mathsf{C}_2 q_2, \tag{6.53}$$

and

$$(\mathsf{C}_i)_{j,k} \coloneqq \int_\Omega \left(\frac{\partial}{\partial x_i} \psi_j \right) \psi_k \, \mathrm{d}\mathbf{x}. \tag{6.54}$$

As in the scalar control case, one can easily verify that the discrete approach yields a conservative scheme.

For the numerical solution of the constrained optimization problem, we introduce the associated discrete Lagrangian functional

$$\mathcal{L}_h(\varphi_h, \mathbf{q}_h, \lambda_h) \coloneqq \frac{1}{2} \|\varphi_h - \tilde{\varphi}_h\|^2_{L^2(\Omega)} + \frac{\beta}{2} \|\mathbf{q}_h\|^2_{(L^2(\Omega))^2} + \lambda_h^\top r(\varphi_h, \mathbf{q}_h, \tilde{\varphi}_h), \tag{6.55}$$

where $r(\varphi_h, \mathbf{q}_h, \tilde{\varphi}_h)$ denotes the residual of (6.52). As before, differentiation w.r.t. φ_h, $\mathbf{q}_h$ and λ_h yields the system of necessary first order optimality conditions:

$$\mathsf{M}\varphi^{n+1} + \mathsf{K}(\varphi_h^{n+1})\lambda = \mathsf{M}\tilde{\varphi}, \tag{6.56a}$$

$$\beta \mathsf{M} q_1 - \mathsf{C}_1^\top \lambda = 0, \tag{6.56b}$$

$$\beta \mathsf{M} q_2 - \mathsf{C}_2^\top \lambda = 0, \tag{6.56c}$$

$$\mathsf{K}(\varphi_h^{n+1}) + \mathsf{C}_1 q_1 + \mathsf{C}_2 q_2 = 0, \tag{6.56d}$$

where φ^{n+1}, $\mathbf{q}$ and λ denote the nodal vectors of φ_h^{n+1}, $\mathbf{q}_h$ and λ_h, respectively. The mass matrix M and the weighted mass matrix $\mathsf{K}(\cdot)$ are defined as in (6.44) and (6.45).

Using the same linearization as for the scalar control case, we obtain the system matrix

$$\mathsf{A}(\varphi_h) \coloneqq \begin{bmatrix} \mathsf{M} & 0 & 0 & \mathsf{K}(\varphi_h) \\ 0 & \beta\mathsf{M} & 0 & -\mathsf{C}_1^\top \\ 0 & 0 & \beta\mathsf{M} & -\mathsf{C}_2^\top \\ \mathsf{K}(\varphi_h) & \mathsf{C}_1 & \mathsf{C}_2 & 0 \end{bmatrix} \tag{6.57}$$

and the following fixed-point iteration procedure:

1. Initialize: $(\varphi^{(0)}, \mathbf{q}^{(0)}, \lambda^{(0)}) \coloneqq (\tilde{\varphi}, 0, 0)$ and $m \coloneqq 0$.
2. Increase m by 1 and compute the residual:

$$\begin{bmatrix} r_\varphi^{(m-1)} \\ r_{q_1}^{(m-1)} \\ r_{q_2}^{(m-1)} \\ r_\lambda^{(m-1)} \end{bmatrix} \coloneqq \begin{bmatrix} \mathsf{M}\tilde{\varphi} \\ 0 \\ 0 \\ 0 \end{bmatrix} - \mathsf{A}(\varphi^{(m-1)}) \begin{bmatrix} \varphi^{(m-1)} \\ q_1^{(m-1)} \\ q_2^{(m-1)} \\ \lambda^{(m-1)} \end{bmatrix}. \tag{6.58}$$

3. Check if the desired tolerance is reached and stop if so.
4. Update using the preconditioner $\mathsf{A}(\varphi^{(m-1)})$:

$$\begin{bmatrix} \varphi^{(m)} \\ q_1^{(m)} \\ q_2^{(m)} \\ \lambda^{(m)} \end{bmatrix} \coloneqq \begin{bmatrix} \varphi^{(m-1)} \\ q_1^{(m-1)} \\ q_2^{(m-1)} \\ \lambda^{(m-1)} \end{bmatrix} + \mathsf{A}(\varphi^{(m-1)})^{-1} \begin{bmatrix} r_\varphi^{(m-1)} \\ r_{q_1}^{(m-1)} \\ r_{q_2}^{(m-1)} \\ r_\lambda^{(m-1)} \end{bmatrix} \tag{6.59}$$

5. Go to step 2.

6.7. Numerical Results

In this section we assess the quality of the simple level set shifting approach and the optimal control approach in terms of mass conservation. We consider the following error measures:

$$\mathrm{e}_{L^2(\Omega)} \coloneqq \|\varphi_h - \varphi_{\mathrm{ex}}\|_{L^2(\Omega)}, \tag{6.60a}$$

$$\mathrm{e}_{H^1(\Omega)} \coloneqq \|\varphi_h - \varphi_{\mathrm{ex}}\|_{H^1(\Omega)}, \tag{6.60b}$$

$$\mathrm{e}_{\infty,\Gamma} \coloneqq \max_{K \in \mathcal{T}_h^\Gamma} \left(\max_{x \in K} |\varphi_h(T, \mathbf{x}) - \varphi_{\mathrm{ex}}(\mathbf{x})| \right), \tag{6.60c}$$

$$\mathrm{e}_{\mathrm{m}} \coloneqq |\mathrm{m}(\varphi_h) - \mathrm{m}_{\mathrm{ex}}|, \tag{6.60d}$$

$$\mathrm{e}_{\mathrm{m},h} \coloneqq |\mathrm{m}(\varphi_{0,h}) - \mathrm{m}(\varphi_h)|, \tag{6.60e}$$

where φ_{ex} denotes the exact solution, $\mathrm{m}_{\mathrm{ex}} \coloneqq \mathrm{m}(\varphi_{\mathrm{ex}})$ the exact mass and $\mathcal{T}_h^\Gamma$ the subsets of elements containing the interface $\Gamma_h(t)$ (cf. Section 5.6). Conservative approaches should

exhibit a very low error in $\mathrm{e}_{\mathrm{m},h}$, while e_{m} depends on the projection of the initial data into the discrete finite element space.

For the numerical computation of interface related quantities we employ the approximation technique presented in Section 4.3.2, i.e. the interface is explicitly localized. We emphasize that the optimal control approach does not require an explicit localization. Alternatively, one can use a sufficiently accurate quadrature technique such as the adaptive approach presented in [Vog06].

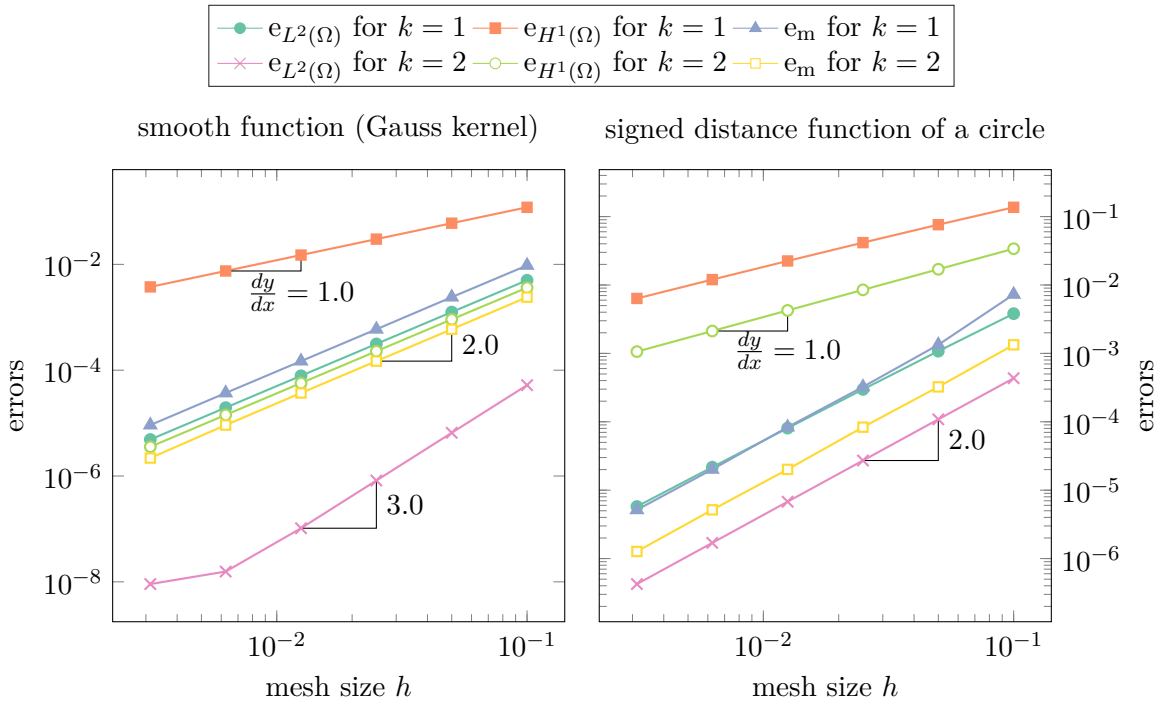

Figure 6.3.: Finite element approximation quality for $k = 1, 2$.

First, let us consider the initial approximation errors that arise when the initial data φ_0 is projected into the finite element space. The errors for a $C^\infty(\Omega)$ function (Gauss kernel) and the signed distance function of a circle (which is in $C(\Omega)$ but not in $C^1(\Omega)$) are depicted in Fig. 6.3.

For the signed distance function we obtain suboptimal convergence rates for quadratic basis functions. This is due to the kink at the center of the circle and the missing regularity of the signed distance function at this point. We recall that a signed distance function is smooth only almost everywhere. In particular, it is not differentiable at its skeleton, leading to suboptimal convergence results when measuring the error in the entire domain Ω. If we restrict ourselves to a narrow band along the interface, optimal convergence rates become visible.

One can easily verify that the mass error results for $k = 2$ correspond to those for $k = 1$ on a one step coarser mesh. This is to be expected because the localization of the interface from a $\mathbb{P}^2$ level set function is performed by considering the $\mathbb{P}^1$ projection on a refined mesh (cf. Fig. 6.3). Even though this interface approximation technique does not provide better mass

conservation, it improves the approximation of interface related quantities (such as surface tension, cf. Chapter 7). The interested reader is referred to [GR11, RL11] for further details.

As in the previous chapter, we use abbreviations for the different numerical schemes to keep notation simple:

`[NO-MC]`	no mass correction is applied,
`[SH-MC]`	shifting approach, cf. Section 6.2,
`[OSC-MC]`	optimal control approach with scalar control, cf. Section 6.6,
`[OVC-MC]`	optimal control approach with vector control, cf. Section 6.6.

In the following test cases we assess the accuracy in mass preservation of the proposed numerical scheme `[OSC-MC]` and compare it to `[NO-MC]` and `[SH-MC]`. Note that the results obtained by `[OSC-MC]` and `[OVC-MC]` are qualitatively very similar, which is why we only present results for `[OSC-MC]` in the first sections. A comparison between the two optimal control approaches is presented later on in Section 6.7.4.

6.7.1. Rotation of a Slotted Disk

In a given circular-shaped domain

$$\Omega^\circ := \{\mathbf{x} \in \mathbb{R}^2 \ : \ |x| < 1/2\}, \tag{6.61}$$

we define the slotted disk (often also referred to as Zalesak's disk, cf. [Zal79]) centered at $(0, 0.25)$ in terms of radius r and slot width s by

$$\begin{aligned} \Gamma_Z := &\{\mathbf{x} \in \mathbb{R}^2 \ : \ |x| = r \ \wedge \ \neg(|x_1| < s/2 \ \wedge \ x_2 < 0)\} \\ &\cup \{\mathbf{x} \in \mathbb{R}^2 \ : \ |x_1| = s/2 \ \wedge \ -\sqrt{r^2 - s^2/4} \leq x_2 \leq \tfrac{2r}{3}\} \\ &\cup \{\mathbf{x} \in \mathbb{R}^2 \ : \ |x_1| \leq s/2 \ \wedge \ x_2 = \tfrac{2r}{3}\}. \end{aligned} \tag{6.62}$$

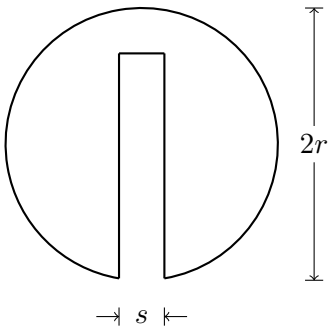

Figure 6.4.: Zalesak's disk.

As initial data one uses the signed distance function Φ_Z with respect to Γ_Z. The slotted disk is depicted in Fig. 6.4. The velocity field is given by

$$\mathbf{v}(t, \mathbf{x}) \coloneqq \pi \begin{bmatrix} x_2 \\ -x_1 \end{bmatrix}. \tag{6.63}$$

and forces the slotted disk to rotate counter-clockwise about the origin. At the end of the time interval $[0, 10]$, the slotted disk has performed 5 rotations about $(0, 0)$. As before, we can compare results with the initial data for the numerical evaluation. Note that there is no inflow boundary because $\mathbf{v} \cdot \mathbf{n} = 0$ on $\partial\Omega^\circ$, i.e. $\partial\Omega^{\text{in}} = \emptyset$.

This is a commonly chosen and challenging test case to assess mass conservation properties, see for example [BK14, KAFB11, LD09, PSVW05]. Numerical methods tend to smear the slot and the sharp reentrant corners, which causes inaccuracies in mass. For all evaluated methods we used SUPG stabilization.

Fig. 6.5a illustrates the evolution of mass for the methods under investigation. Even though initially the mass error for the standard Galerkin approach `[NO-MC]` seems negligible, it significantly accumulates over time to a relative mass error of $\approx 12.87\%$ at $t = T$. Both, `[SH-MC]` and `[OSC-MC]` yield numerical schemes that keep the absolute mass error almost in the machine precision region and the relative mass error remains below 10^{-10}. The Tikhonov regularization parameter was set to the constant 10^2 for `[OSC-MC]`.

The zero level sets at final time are depicted in Fig. 6.5b. For the non-corrected standard Galerkin approach the slot is smeared out more strongly resulting in a significant gain in mass. Best approximation results of the slot are obtained when using the `[OSC-MC]` approach. The accuracy of the simpler `[SH-MC]` technique suffers from stronger diffusion which can be explained by the global correction approach (rather than the local flux based correction) that redistributes mass evenly.

The average number of iterations for the mass correction techniques at refinement level $\ell = 2$ are 22.59 for `[SH-MC]` and 13.37 for `[OSC-MC]`. Naturally, one `[OSC-MC]` iteration is more expensive because a higher dimensional KKT system needs to be solved. For either method, in each iteration the interface must be relocalized (or a sufficiently accurate quadrature formula must be applied to evaluate the Heaviside function integrals). In both cases, the number of required iterations decreases on finer meshes. This can be explained by the higher accuracy on finer meshes calling for less correction.

The quantitative results of the particular methods are listed in Table 6.1. Both conservative approaches preserve the asymptotic properties of the standard and non-conservative Galerkin approach `[NO-MC]`. We emphasize that this is an academic test problem free of interface related couplings. Even though the benefit of mass corrected schemes may not seem significant, the results in Section 7.6 will show the severe losses in numerical accuracy when mass is not conserved.

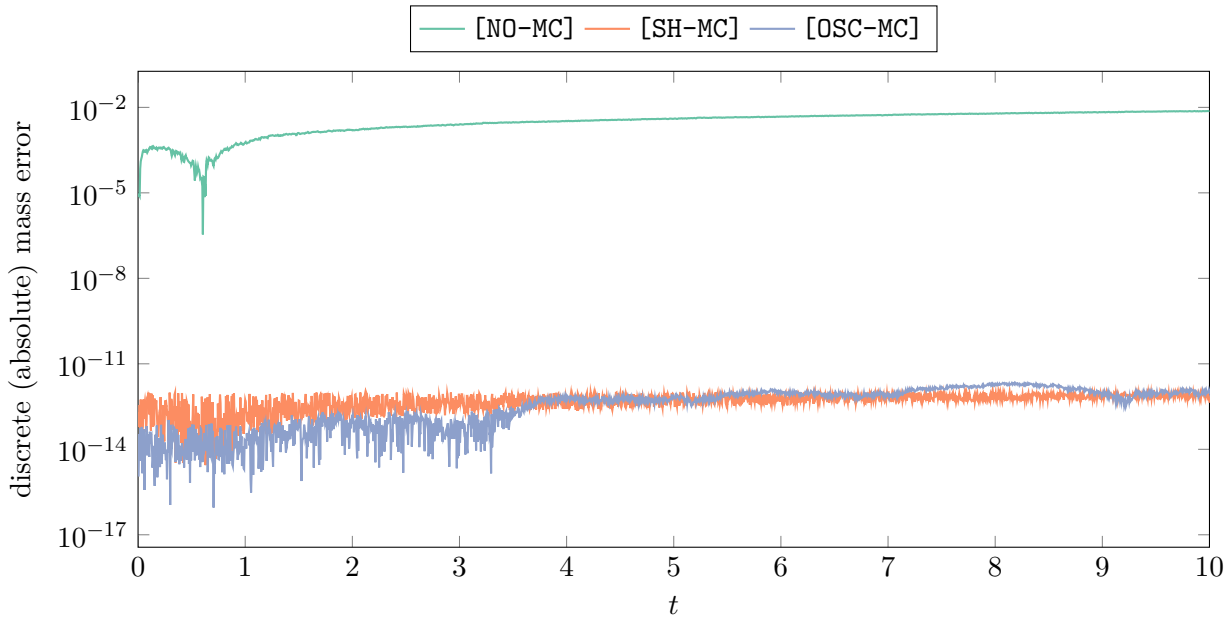

(a) Mass error evolution.

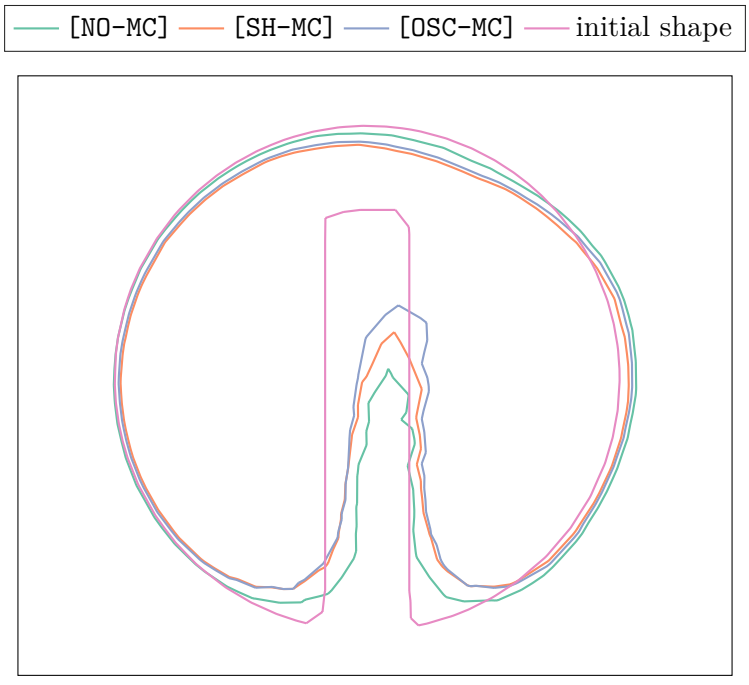

(b) Zero isocontours at final time $t = 10$.

Figure 6.5.: Results for Zalesak's disk test case at refinement level $\ell = 2$.

	ℓ	$e_{m,h}$	$e_{L^2(\Omega)}$	order	$e_{\infty,\Gamma}$	order	$e_{H^1(\Omega)}$	order
[NO-MC]	1	1.28e-05	6.31e-03		5.53e-02		2.53e-01	
	2	7.48e-03	3.48e-03	0.86	3.53e-02	0.65	1.94e-01	0.38
	3	8.38e-04	1.37e-03	1.34	1.72e-02	1.04	1.40e-01	0.46
	4	4.80e-04	6.49e-04	1.08	9.22e-03	0.90	1.25e-01	0.18
[SH-MC]	1	6.71e-13	6.36e-03		5.67e-02		2.54e-01	
	2	1.08e-11	5.16e-03	0.30	3.47e-02	0.71	1.96e-01	0.37
	3	1.80e-14	1.58e-03	1.71	1.69e-02	1.04	1.42e-01	0.46
	4	4.59e-15	7.15e-04	1.14	9.62e-03	0.81	1.25e-01	0.19
[OSC-MC]	1	1.51e-12	7.29e-03		5.21e-02		2.63e-01	
	2	9.09e-13	3.55e-03	1.04	3.36e-02	0.63	1.94e-01	0.44
	3	7.12e-15	1.36e-03	1.38	1.71e-02	0.97	1.41e-01	0.46
	4	8.33e-15	6.47e-04	1.07	9.57e-03	0.84	1.25e-01	0.18

Table 6.1.: Asymptotic results for Zalesak's disk test case.

6.7.2. Vortex Flow

In this section we consider the vortex flow test case that has already been presented in Section 5.6.2 and in which strong interface deformations occur. The results of this test case at refinement level $\ell = 2$ are plotted in Fig. 6.6. While the non-conservative approach `[NO-MC]` exhibits a significant loss of mass, `[SH-MC]` and `[OSC-MC]` (with Tikhonov regularization parameter $\beta = 10^2$) preserve mass very well. Even though the absolute error in mass conservation is slightly better for `[SH-MC]`, the `[OSC-MC]` approach shows better asymptotic results, cf. Table 6.2. Furthermore, when considering the final isocontours, `[OSC-MC]` seems to be closer to the inital data than `[SH-MC]` and `[NO-MC]`.

	ℓ	$e_{m,h}$	$e_{L^2(\Omega)}$	order	$e_{\infty,\Gamma}$	order	$e_{H^1(\Omega)}$	order
[NO-MC]	1	3.01e-02	1.93e-02		8.83e-02		3.08e-01	
	2	9.23e-03	8.07e-03	1.26	3.34e-02	1.4	1.63e-01	0.92
	3	8.78e-04	3.40e-03	1.25	1.57e-02	1.09	9.26e-02	0.82
	4	1.09e-03	1.38e-03	1.3	9.28e-03	0.76	5.27e-02	0.81
[SH-MC]	1	3.54e-02	6.70e-02		8.69e-02		3.39e-01	
	2	5.86e-13	1.41e-02	2.25	2.88e-02	1.59	1.74e-01	0.97
	3	3.74e-14	3.84e-03	1.88	1.51e-02	0.93	9.92e-02	0.81
	4	1.55e-15	2.44e-03	0.65	8.13e-03	0.9	5.63e-02	0.82
[OSC-MC]	1	7.62e-10	1.78e-02		5.46e-02		3.21e-01	
	2	1.38e-11	7.56e-03	1.23	2.53e-02	1.11	1.68e-01	0.93
	3	2.15e-11	3.49e-03	1.12	1.41e-02	0.84	9.27e-02	0.86
	4	2.69e-11	1.33e-03	1.39	7.17e-03	0.98	5.06e-02	0.87

Table 6.2.: Asymptotic results for the vortex flow test case.

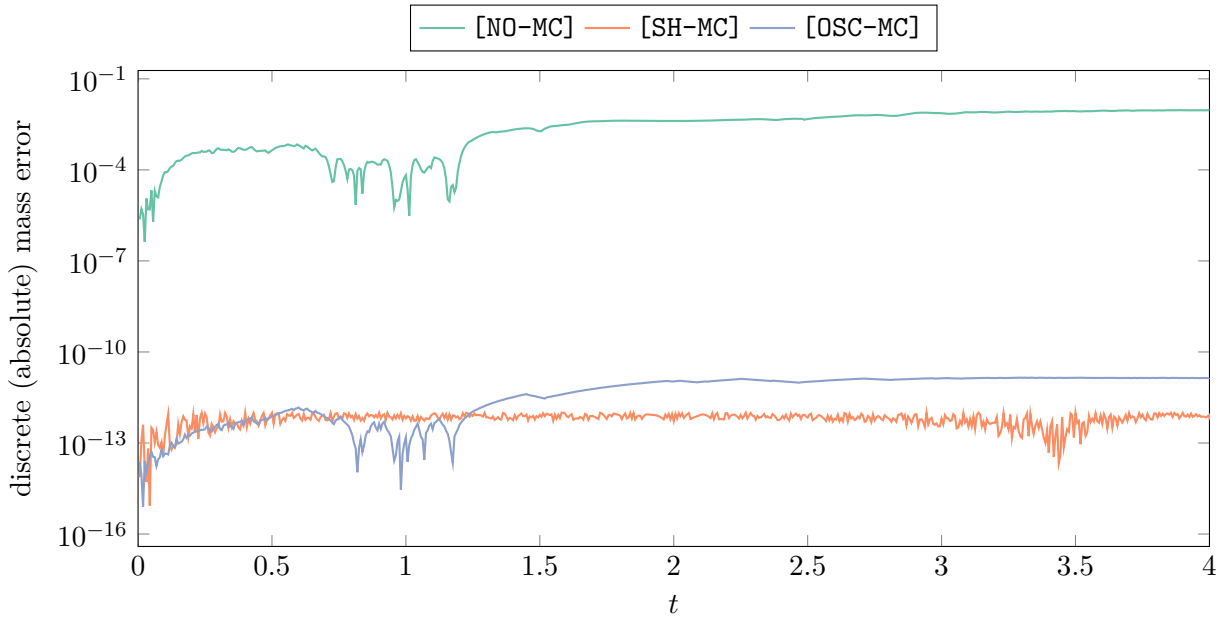

(a) Mass error evolution.

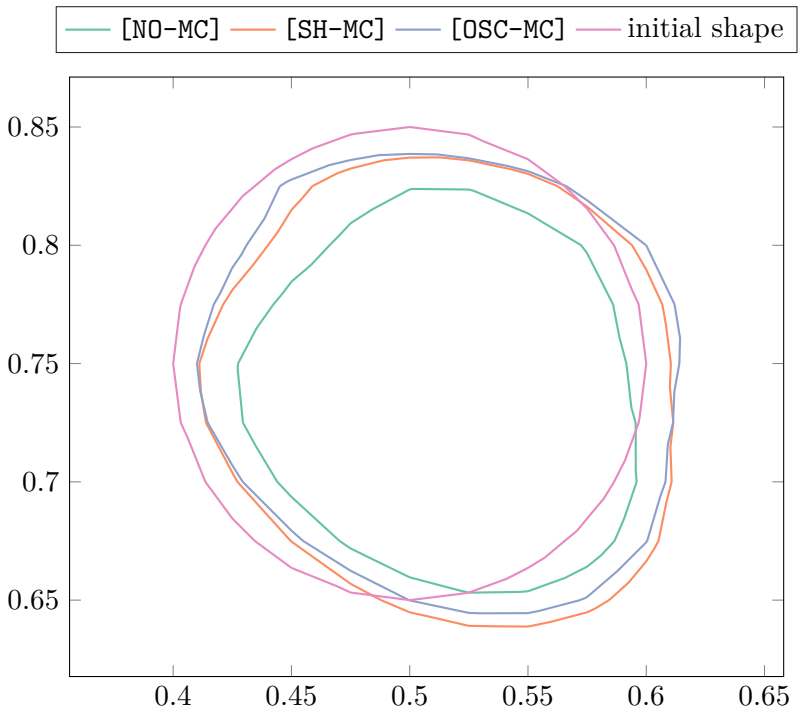

(b) Zero isocontours at final time $t = 4$.

Figure 6.6.: Results for vortex flow test case at refinement level $\ell = 2$.

6.7.3. Multiple Bubbles

For the vortex flow problem, [SH-MC] and [OSC-MC] have shown no significant difference in performance. In this test case, we assess the local conservation properties of the two methods by considering a non-connected domain Ω_1. This is a situation that frequently occurs in practical applications, for example when more than one bubble is considered.

Based on the vortex flow example from the previous section, we modify the initial data to be the signed distance function w.r.t. three disjoint circles as depicted in Fig. 6.7b.

By design, [SH-MC] requires a good signed distance function approximation, which is why elliptic redistancing was periodically applied. For visualization, numerical computations were carried out on a rather coarse mesh ($\ell = 1$), and the vortex flow velocity field is scaled by 0.15 to ensure that details can be resolved sufficiently well on the mesh.

The relative mass conservation errors of the medium sized bubble results are plotted in Fig. 6.7a. We used the following non-constant Tikhonov regularization function

$$\tilde{\beta}(\mathbf{x}) \coloneqq \beta \cdot \left(\frac{\tilde{\varphi}(\mathbf{x})}{h} \right)^2 . \tag{6.64}$$

This choice leads to a strong penalization of corrective fluxes far from the interface. The local conservation accuracy depends on the magnitude of β. Smaller values of β lead to insufficiently accurate results, while for $\beta \approx 10^{-7}$ the accuracy comes close to machine precision. The increase in number of iterations can be explained by the following fact. The desired tolerance for the fixed-point iteration is kept constant. However, for larger values of β, the residual increases (as does mass accuracy). Consequently, to still meet the prescribed tolerance, more iterations are required. In the provided academic examples we used a rather challenging tolerance of 10^{-12}. When instead using mass accuracy as a threshold, only a very mild increase in the average iteration number was observed.

For the globally conservative [SH-MC] approach, the local relative mass error dramatically increases as time evolves. As a consequence, one bubble unphysically expands while the other two bubbles shrink. In contrast, for [OSC-MC] with $\beta \approx 10^5$ the final isocontour almost coincides with the initial data.

The isocontours at final time $t = 4$ show the strong influence of local mass conservation on the interface approximation quality.

6.7.4. Scalar versus Vector Control

Finally let us briefly comment on numerical results for the two different optimal control approaches. In the vector control case, the linear system to be solved can be written in block notation as

$$\begin{bmatrix} \mathsf{A} & -\mathsf{B}^\top \\ \mathsf{B} & 0 \end{bmatrix} \begin{bmatrix} \mathbf{q} \\ p \end{bmatrix} = \begin{bmatrix} f \\ g \end{bmatrix} , \tag{6.65}$$

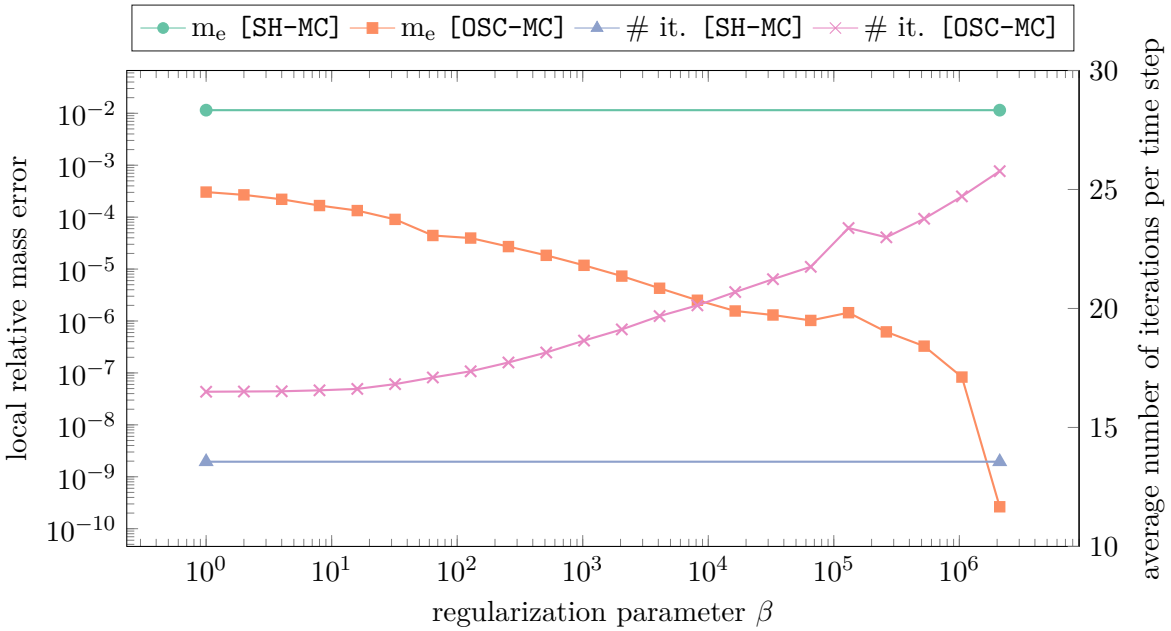

(a) Local mass error vs. regularization parameter β for [OSC-MC].

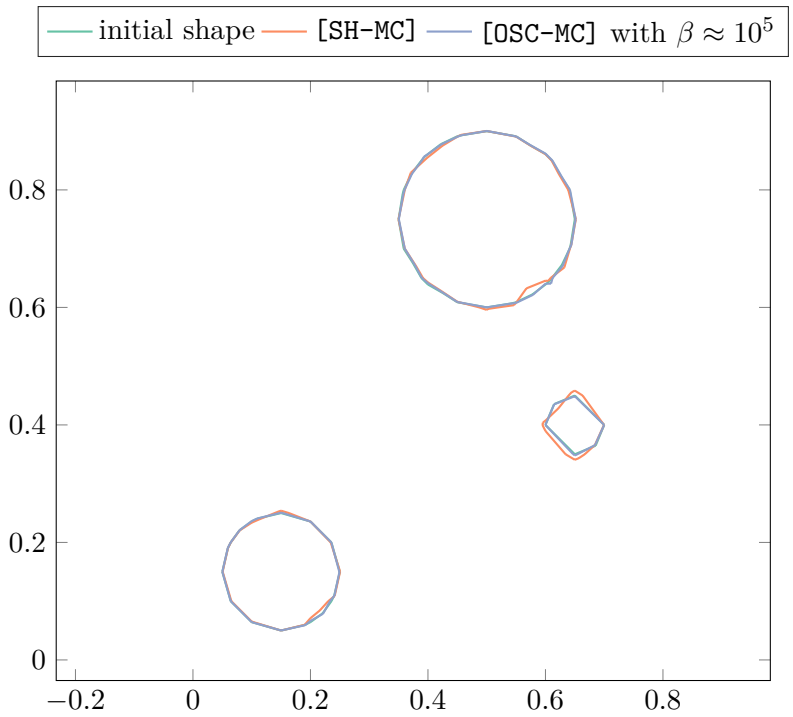

(b) Zero isocontours at final time $t = 4$ on coarse mesh ($\ell = 1$).

Figure 6.7.: Results for multiple bubbles subject to vortex flow.

where $\mathsf{A} = \operatorname{diag}(M, \beta M, \beta M)$ is essentially a scaled block-diagonal mass matrix and $\mathsf{B} = \begin{bmatrix} K, C_x, C_y \end{bmatrix}$. Using the Schur complement

$$\mathsf{S} \coloneqq \mathsf{B}\mathsf{A}^{-1}\mathsf{B}^\top = KM^{-1}K^\top + \frac{1}{\beta}C_x M^{-1} C_x + \frac{1}{\beta}C_y M^{-1} C_y, \tag{6.66}$$

in each fixed-point iteration we need to solve

$$\Delta p^{(m-1)} \coloneqq \mathsf{S}^{-1}(g - \mathsf{B}\mathsf{A}^{-1} f) - p^{(m-1)}, \tag{6.67a}$$

$$p^{(m)} \coloneqq p^{(m-1)} + \Delta p^{(m-1)}, \tag{6.67b}$$

$$\mathbf{q}^{(m)} \coloneqq A^{-1}(f - \mathsf{B}^\top p^{(m)}). \tag{6.67c}$$

Obviously inverse matrices are not explicitly computed but linear systems solved instead. The linear system for the update of p can be solved using the preconditioned CG-method with the preconditioner

$$\mathsf{P}^{-1} = \mathsf{B}\operatorname{diag}(\mathsf{A})^{-1}\mathsf{B}. \tag{6.68}$$

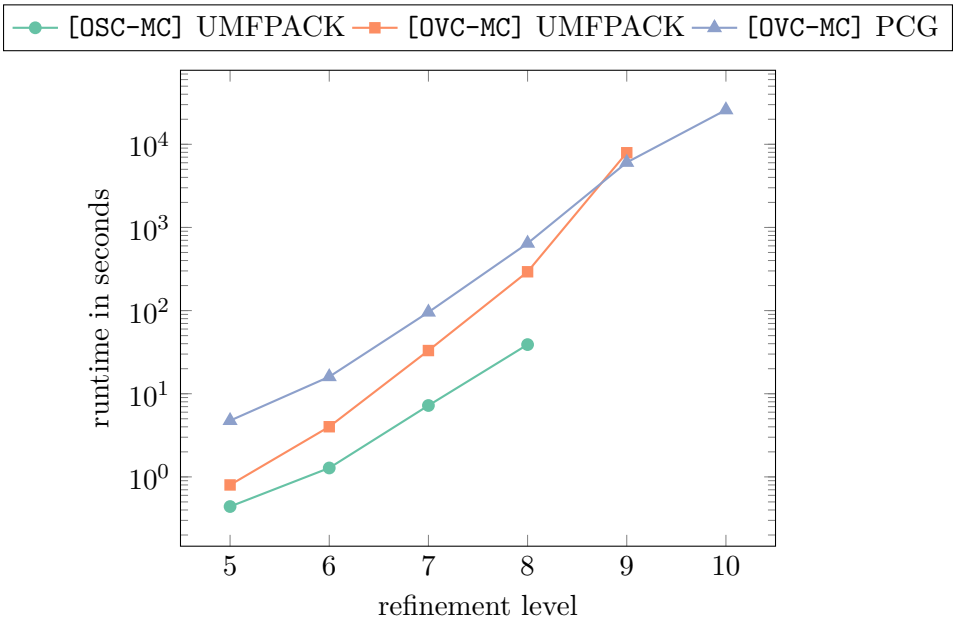

Figure 6.8.: Runtime comparison for scalar and vector control approaches.

In Fig. 6.8, the computational runtimes for the two approaches are illustrated. On coarser meshes, the scalar control approach is faster. This can easily be explained by the fact that in the vector control approach the number of degrees of freedom double compared to the scalar control approach. On fine meshes, the direct UMFPACK solver fails due to insufficient memory. Furthermore, at refinement level $\ell = 9$, the preconditioned Schur-complement approach pays off compared to a direct solver and is also capable of handling finer meshes.

7 Two-Phase Flows

The first part of this chapter introduces the underlying mathematical model of two-phase flow problems. It is based on conservation principles of physical quantities such as mass and momentum. The resulting partial differential equations are often very complex, and the existence and uniqueness of an analytical solution is mostly unclear. However, many of these problems have successfully been solved numerically and are of great interest in many practical applications.

A common way to solve two-phase flow problems computationally is to employ a finite element discretization. To account for the evolving interface separating the two fluids, several approaches can be applied. One popular choice is the level set method, that is easy to implement on the one hand, and easy to extend to higher order polynomial degrees on the other hand. This chapter focuses on the application of the level set method extensions presented above to two-phase flow problems. The numerical evaluation is based on a well-known benchmark [HTK+07] and shows the potential of the proposed schemes in a practical application.

The chapter is organized as follows. The first section addresses kinematics, based on which general conservation laws are derived in the following sections. Next, the incompressible Navier-Stokes equations are derived and a finite element discretization is introduced. In the last section we consider a two-phase flow benchmark problem to assess the quality of the numerical solutions. The chapter is mainly based on the books by Gross and Reusken [GR11], Eck, Garcke and Knabner [EGK11], but also on the text by Kuzmin [Kuz10] and the thesis of Hysing [Hys07], as well as the publication [HTK+07] by Hysing et al., in which the bubble dynamics benchmark is specified.

7.1. Kinematics

We consider a connected, open and bounded reference domain $\hat{\Omega} \subset \mathbb{R}^d$ (i.e. a connected, open and bounded set, cf. Definition A.1), $d \in \{1, 2, 3\}$ and a time interval $[t_0, T)$. A *material point* at time t_0 is given by its position in $\mathbf{X} \in \hat{\Omega}$ and the mapping

$$t \mapsto \boldsymbol{\chi}(t, \mathbf{X}) \tag{7.1}$$

describes its *trajectory*. If we observe different particles pass through a fixed-point $\mathbf{x} \in \hat{\Omega}$, we speak of *Eulerian coordinates*. If instead we follow the trajectory $\boldsymbol{\chi}(t, \mathbf{X})$, we refer to *Lagrangian coordinates*. For a prototypical scalar quantity $c : (t_0, T) \times \hat{\Omega} \to \mathbb{R}$, the *material derivative* is obtained by application of the chain rule:

$$\mathrm{D}_t c(t, \mathbf{X}) \coloneqq \frac{\mathrm{d}}{\mathrm{d}t} c(t, \mathbf{X}) = \frac{\partial}{\partial t} c(t, \boldsymbol{\chi}(t, \mathbf{X})) + \mathbf{u}(t, \mathbf{X}) \cdot \nabla c(t, \boldsymbol{\chi}(t, \mathbf{X})), \tag{7.2}$$

where $\mathbf{u}(t, \mathbf{X}) \coloneqq \frac{\partial}{\partial t} \boldsymbol{\chi}(t, \mathbf{X})$ is the velocity field in Eulerian coordinates. Of particular interest in the remainder of this thesis are free boundary problems, where we consider the evolution of an open domain $\Omega(t)$ in $\hat{\Omega}$, defined in terms of the initial domain $\Omega_0 \subset \hat{\Omega}$ at $t = t_0$, i.e.

$$\Omega(t) = \{\boldsymbol{\chi}(t, \mathbf{X}) \mid \mathbf{X} \in \Omega_0\}. \tag{7.3}$$

In what follows, let us assume (cf. [EGK11]):

1. $(t, \mathbf{X}) \mapsto \boldsymbol{\chi}(t, \mathbf{X})$ is continuously differentiable,
2. $\Omega \ni \mathbf{X} \mapsto \boldsymbol{\chi}(t, \mathbf{X})$ is invertible for all $t \geq t_0$,
3. $\det \left(\frac{\partial x_i}{\partial X_j}(t, \mathbf{X}) \right)_{i,j=1}^{d} > 0$ for all $t \geq t_0$,

The determinant $J(t, \mathbf{X}) \coloneqq \det \left(\frac{\partial x_i}{\partial X_j}(t, \mathbf{X}) \right)_{i,j=1}^{d}$ describes the change of volume

$$|\Omega(t)| = \int_{\Omega(t)} 1 \, \mathrm{d}\mathbf{x} = \int_{\Omega_0} J(t, \mathbf{X}) \, \mathrm{d}\mathbf{X}. \tag{7.4}$$

The following Theorem provides a fundamental result on how to move a time derivative into an integral over a moving domain $\Omega(t)$:

Theorem 7.1 (Reynolds' Transport Theorem [EGK11])
Let $\boldsymbol{\chi}(t, \mathbf{X})$ satisfy the assumptions stated above and let the quantity $c : [t_0, T) \times \hat{\Omega} \to \mathbb{R}$ be sufficiently smooth. Then the following identity holds:

$$\frac{\mathrm{d}}{\mathrm{d}t} \int_{\Omega(t)} c(t, \mathbf{x}) \, \mathrm{d}\mathbf{x} = \int_{\Omega(t)} \left[\frac{\partial}{\partial t} c(t, \mathbf{x}) + \nabla \cdot \big(c(t, \mathbf{x}) \, \mathbf{u}(t, \mathbf{x}) \big) \right] \mathrm{d}\mathbf{x}. \tag{7.5}$$

7.2. Conservation Laws

Based on Reynolds' Transport Theorem 7.1, so-called *conservation laws* can be derived for evolving domains. Instead of the prototypical quantity $c(\cdot, \cdot)$, let us now consider the *density* function $\rho(\cdot, \cdot)$. As before, we assume $\Omega(t) \subset \hat{\Omega}$ to be an open domain. The quantity

$$m(t) = \int_{\Omega(t)} \rho(t, \mathbf{x}) \, \mathrm{d}\mathbf{x} \tag{7.6}$$

then describes the *mass* at time t. If mass is conserved in $\Omega(t)$, i.e. $\frac{\mathrm{d}}{\mathrm{d}t}m(t) = 0$, application of Reynolds' Transport Theorem yields

$$0 = \frac{\mathrm{d}}{\mathrm{d}t}m(t) = \frac{\mathrm{d}}{\mathrm{d}t}\int_{\Omega(t)} \rho(t,\mathbf{x})\ \mathrm{d}\mathbf{x} = \int_{\Omega(t)} \frac{\partial}{\partial t}\rho(t,\mathbf{x}) + \nabla\cdot\big(\rho(t,\mathbf{x})\mathbf{u}(t,\mathbf{x})\big)\ \mathrm{d}\mathbf{x}. \tag{7.7}$$

Since (7.7) holds for any $\Omega(t)$ (in particular also for every subdomain of $\Omega(t)$), the pointwise differential equation

$$\frac{\partial}{\partial t}\rho(t,\mathbf{x}) + \nabla\cdot\big(\rho(t,\mathbf{x})\mathbf{u}(t,\mathbf{x})\big) = 0, \tag{7.8}$$

can be derived if ρ and $\mathbf{u}$ are sufficiently smooth (cf. [EGK11]). This equation is also commonly referred to as *continuity equation*. In the particular case of a constant density function $\rho(t,\mathbf{x}) =$ const, the continuity equation simplifies to

$$\nabla\cdot\mathbf{u}(t,\mathbf{x}) = 0. \tag{7.9}$$

The *momentum* is given by

$$\mathbf{M}(t) = \int_{\Omega(t)} \rho(t,\mathbf{x})\mathbf{u}(t,\mathbf{x}). \tag{7.10}$$

Any change in $\mathbf{M}(t)$ is equal to the sum of all forces $\mathbf{F}(t)$ acting on $\Omega(t)$. Generally, one must distinguish between volume forces such as gravity

$$\int_{\Omega(t)} \rho(t,\mathbf{x})\mathbf{g}\ \mathrm{d}\mathbf{x}, \tag{7.11}$$

and boundary forces acting on the boundary of $\Omega(t)$. Let us assume that the boundary $\Gamma(t)$ of $\Omega(t)$ is continuously differentiable in time and space. $\Omega(t)$ may exert forces onto the surrounding fluid across $\partial\Omega(t)$ and vice versa. In *Cauchy's Theorem*, these internal forces are modeled to be linear, i.e. the resulting boundary force can be written in terms of the *Cauchy stress tensor* $\boldsymbol{\sigma}(t,\mathbf{x}) \in \mathbb{R}^{d\times d}$ as follows:

$$\int_{\partial\Omega(t)} \boldsymbol{\sigma}(t,\mathbf{x})\cdot\mathbf{n}(t,\mathbf{x})\,\mathrm{d}\sigma = \int_{\Omega(t)} \operatorname{div}\big(\boldsymbol{\sigma}(t,\mathbf{x})\big)\ \mathrm{d}\mathbf{x}. \tag{7.12}$$

By application of the Gauss theorem, the surface integral has been transformed into a volume integral in (7.12). For simplicity, we only consider gravitation as a volume force. Adding up the forces exerted in $\Omega(t)$ and on $\partial\Omega(t)$, *conservation of momentum* can be expressed as

$$\frac{\mathrm{d}}{\mathrm{d}t}\mathbf{M}(t) = \frac{\mathrm{d}}{\mathrm{d}t}\int_{\Omega(t)} \rho(t,\mathbf{x})\mathbf{u}(t,\mathbf{x})\ \mathrm{d}\mathbf{x} = \int_{\Omega(t)} \rho(t,\mathbf{x})\mathbf{g} + \operatorname{div}\big(\boldsymbol{\sigma}(t,\mathbf{x})\big)\ \mathrm{d}\mathbf{x}. \tag{7.13}$$

Finally, by application of Reynolds' Transport Theorem 7.1 and by employing Eq. (7.8) we obtain

$$\frac{\mathrm{d}}{\mathrm{d}t}\mathbf{M}(t) = \int_{\Omega(t)} \rho(t,\mathbf{x})\frac{\partial}{\partial t}\mathbf{u}(t,\mathbf{x}) + \rho(\mathbf{u}(t,\mathbf{x})\cdot\nabla)\mathbf{u}(t,\mathbf{x})\ \mathrm{d}\mathbf{x}, \tag{7.14}$$

where we use the differential operator

$$(\mathbf{u}\cdot\nabla)(\cdot) = \sum_{i=1}^{d} u_i \partial_{x_i}(\cdot). \tag{7.15}$$

As before, because $\Omega(t)$ can be chosen arbitrarily the partial differential equation

$$\rho\frac{\partial}{\partial t}\mathbf{u} + \rho(\mathbf{u}\cdot\nabla)\mathbf{u} = \rho\mathbf{g} + \mathrm{div}(\boldsymbol{\sigma}) \tag{7.16}$$

holds (we omit the dependence on time and space variable when no ambiguity arises). It is often referred to as *momentum equation*.

7.3. Navier-Stokes Equations

Based on the conservation laws derived in the previous sections, the incompressible Navier-Stokes equations can be obtained. We therefore consider a fluid in $\hat{\Omega}$ with the following properties:

1. The fluid is *Newtonian*, i.e. shear stresses are linearly dependent on the velocity gradients. For non-Newtonian fluids, applied stress causes changes in the viscosity. The stress tensor thus can be modeled by

   $$\boldsymbol{\sigma} = -p\mathbf{I} + 2\mu\mathbf{D}(\mathbf{u}), \tag{7.17}$$

   where p denotes the pressure, $\mathbf{I}$ the identity tensor, $\mathbf{D}$ the *deformation tensor*

   $$\mathbf{D}(\mathbf{u}) \coloneqq \frac{1}{2}\left(\nabla\mathbf{u} + (\nabla\mathbf{u})^{\top}\right), \tag{7.18}$$

   and μ the *dynamic viscosity* of the fluid. We made use of the operator

   $$\nabla\mathbf{u} \coloneqq \begin{bmatrix}\nabla u_1 & \cdots & \nabla u_d\end{bmatrix}. \tag{7.19}$$

   Many common fluids including water and air can be modeled as Newtonian. In contrast, blood is a non-Newtonian fluid.
2. The fluid is incompressible. As a direct consequence, $\rho = \text{const}$ in $\hat{\Omega}$ and the continuity equation (7.8) simplifies to (7.9).
3. The fluid is isotropic.

Under the given assumptions, the *Navier-Stokes equations for incompressible fluid flow* are obtained by combining the coninuity equation (7.9) and the momentum equation (7.16). Using the constitutive relation (7.17) for the stress tensor [EGK11, GR11], we obtain:

$$\rho\frac{\partial}{\partial t}\mathbf{u} + \rho(\mathbf{u}\cdot\nabla)\mathbf{u} = -\nabla p + \operatorname{div}(2\mu\mathbf{D}(\mathbf{u})) + \rho\mathbf{g}, \tag{7.20a}$$

$$\operatorname{div}(\mathbf{u}) = 0. \tag{7.20b}$$

Note that the non-linear term in (7.20a) makes the solution of the problem particularly challenging. Even though existence and uniqueness of a solution to (7.20) is still unclear, numerical methods have been developed and successfully applied to a wide range of applications.

In the framework of this thesis, we are interested in incompressible two-phase flows where two immiscible fluids are considered. The modeling begins with formulating the incompressible Navier-Stokes equations for each phase as before. The two phases are then related to each other by an additional coupling condition imposed on the interface.

The Navier-Stokes equations (7.20) can also be transferred into a dimensionless form, which can be helpful in terms of determining the characteristic flow regime. Let V denote the characteristic velocity, and ℓ the typical length scale, and define the dimensionless variables

$$\tilde{t} = \frac{V}{\ell}t, \qquad \tilde{\mathbf{x}} = \frac{\mathbf{x}}{\ell}, \qquad \tilde{\mathbf{u}} = \frac{\mathbf{u}}{V}, \qquad \tilde{p} = \frac{p}{\rho V^2} \qquad \text{and} \qquad \tilde{\mathbf{g}} = \frac{\ell}{V^2}\mathbf{g}. \tag{7.21}$$

Introducing the dimensionless *Reynolds number*

$$\mathrm{Re} = \frac{\rho\ell V}{\mu}, \tag{7.22}$$

the dimensionless Navier-Stokes equations for incompressible two phase flow are written as:

$$\frac{\partial}{\partial\tilde{t}}\tilde{\mathbf{u}} + (\tilde{\mathbf{u}}\cdot\nabla)\tilde{\mathbf{u}} = -\nabla\tilde{p} + \frac{2}{\mathrm{Re}}\operatorname{div}(\mathbf{D}(\tilde{\mathbf{u}})) + \tilde{\mathbf{g}}, \tag{7.23a}$$

$$\operatorname{div}(\tilde{\mathbf{u}}) = 0. \tag{7.23b}$$

For low Reynolds numbers, viscous forces are dominant (laminar flow) while for high Reynolds numbers convective terms dominate (turbulent flow).

7.3.1. Two Phase Flow Modeling

Let us now consider two incompressible Newtonian fluids in a domain Ω. In addition to the previous assumptions, we require the fluids to be *immiscible*, i.e. no phase transitions occur. The two phases are contained in the disjoint open subdomains $\Omega_1(t) \subset \Omega$ and $\Omega_2(t) \subset \Omega$, respectively, such that $\overline{\Omega_1(t)} \cup \overline{\Omega_2(t)} = \overline{\Omega}$ for all $t \in [t_0, T)$. Each fluid has different material properties specified by the densities ρ_i and the dynamic viscosities μ_i, $i = 1, 2$. The interface separating the two phases $\Omega_1(t)$ and $\Omega_2(t)$ is therefore given by

$$\Gamma(t) \coloneqq \overline{\Omega_1(t)} \cap \overline{\Omega_2(t)}. \tag{7.24}$$

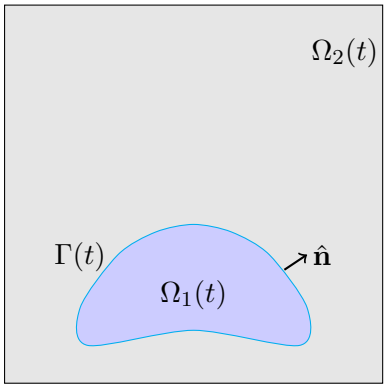

Figure 7.1.: Illustration of two-phase flow setting.

The setting is depicted in Fig. 7.1. By $\hat{\mathbf{n}}(t, \mathbf{x})$ we denote the unit normal vector at the interface pointing into $\Omega_2(t)$. Note that this vector is only defined on the interface Γ and not in $\Omega_1(t)$ or $\Omega_2(t)$.

For the implicit interface description of $\Gamma(t)$ we employ the level set method. Therefore, let φ be the corresponding level set function such that $\varphi > 0$ in $\Omega_1(t)$ and $\varphi < 0$ in $\Omega_2(t)$.

The conservation laws derived in the previous section can be applied to each subdomain separately, and therefore the Navier-Stokes equations can be formulated for each subdomain Ω_i, $i = 1, 2$, as follows:

$$\rho_i \frac{\partial}{\partial t}\mathbf{u} + \rho_i(\mathbf{u} \cdot \nabla)\mathbf{u} = -\nabla p + \operatorname{div}(\mu_i \mathbf{D}(\mathbf{u})) + \rho_i \mathbf{g}, \qquad \text{in } \Omega_i, \tag{7.25a}$$

$$\operatorname{div}(\mathbf{u}) = 0, \qquad \text{in } \Omega_i. \tag{7.25b}$$

7.3.2. Coupling Conditions

For the modeling of the complete problem in Ω, we must also take internal forces between the two phases into account. On a molecular level, due the different material properties of the two fluids, cohesive forces are exerted across the interface. These forces pull the surface so as to contract it to minimal circumference ($d = 2$) or area ($d = 3$), and are therefore summarized as the so-called *surface tension* force. A common way of modeling this force is

$$\mathbf{f}_{\mathrm{st}}(t) \coloneqq -\tau \int_{\Gamma(t)} \kappa \hat{\mathbf{n}} \, \mathrm{d}\sigma, \tag{7.26}$$

where $\kappa(t, \mathbf{x})$ is the mean curvature of $\Gamma(t)$ and τ is the surface tension coefficient. Even though τ can be variable in general, we restrict ourselves to constant surface tension coefficients that only depend on the material properties of the two adjacent fluids. From (7.26) one can derive (see [GR11] for details) the coupling condition

$$[\![\boldsymbol{\sigma}]\!]\, \hat{\mathbf{n}} = -\tau\kappa\hat{\mathbf{n}} \qquad \text{on } \Gamma. \tag{7.27}$$

In the absence of phase transitions due to the assumed immiscibility of the fluids, the velocity jump across the interface must be zero:

$$[\![\mathbf{u}]\!] = 0 \qquad \text{on } \Gamma. \tag{7.28}$$

From (7.25) and under consideration of the coupling conditions (7.27) and (7.28), the following *two-phase flow problem* is obtained:

$$\rho_i \frac{\partial}{\partial t}\mathbf{u} + \rho_i(\mathbf{u}\cdot\nabla)\mathbf{u} = -\nabla p + \operatorname{div}(\mu_i \mathbf{D}(\mathbf{u})) + \rho_i \mathbf{g} \qquad \text{in } \Omega_i, \tag{7.29a}$$

$$\operatorname{div}(\mathbf{u}) = 0 \qquad \text{in } \Omega_i, \tag{7.29b}$$

$$[\![\mathbf{u}]\!] = 0 \qquad \text{on } \Gamma, \tag{7.29c}$$

$$[\![\boldsymbol{\sigma}\hat{\mathbf{n}}]\!] = -\tau\kappa\hat{\mathbf{n}} \qquad \text{on } \Gamma, \tag{7.29d}$$

$$(\hat{\mathbf{u}} - \mathbf{u})\cdot\hat{\mathbf{n}} = 0 \qquad \text{on } \Gamma. \tag{7.29e}$$

Note that the additional last condition (7.29e) is a natural constraint ensuring that the normal velocity of the interface $\hat{\mathbf{u}}\cdot\hat{\mathbf{n}}$ equals the velocity $\mathbf{u}\cdot\hat{\mathbf{n}}$. If the interface $\Gamma(t)$ touches the boundary of Ω, the model must be extended to take the resulting contact forces into account. More information on contact forces can be found, for example, in [SOW05, GR11].

7.4. Discretization of the Incompressible Navier-Stokes Equations

To obtain the finite element discretization in two space dimensions, we first derive the weak formulation of problem (7.20). Therefore, let us consider the Sobolev spaces

$$\mathbf{U} \coloneqq H_0^1(\Omega) \times H_0^1(\Omega), \tag{7.30a}$$

$$P \coloneqq L_0^2(\Omega). \tag{7.30b}$$

Let $\partial\Omega_D$ denote the boundary portion of $\partial\Omega$ on which Dirichlet boundary conditions for $\mathbf{u}$ are prescribed by $\mathbf{u}_D$. For simplicity, we assume $\mathbf{u}_D \equiv 0$. Following [GR11, QV08], we define the bi- and trilinear forms

$$\mathsf{m} : \mathbf{U}\times\mathbf{U} \to \mathbb{R}, \qquad \mathsf{m}(\mathbf{u},\mathbf{v}) \coloneqq \int_\Omega \rho\mathbf{u}\cdot\mathbf{v}\,\mathrm{d}\mathbf{x}, \tag{7.31a}$$

$$\mathsf{a} : \mathbf{U}\times\mathbf{U} \to \mathbb{R}, \qquad \mathsf{a}(\mathbf{u},\mathbf{v}) \coloneqq \int_\Omega \mu \sum_{i,j=1}^{d} \big(\mathbf{D}(\mathbf{u})\big)_{i,j}\big(\mathbf{D}(\mathbf{v})\big)_{i,j}\,\mathrm{d}\mathbf{x}, \tag{7.31b}$$

$$\mathsf{b} : \mathbf{U}\times P \to \mathbb{R}, \qquad \mathsf{b}(\mathbf{v},q) \coloneqq -\int_\Omega q\operatorname{div}(\mathbf{v})\,\mathrm{d}\mathbf{x}, \tag{7.31c}$$

$$\mathsf{c} : \mathbf{U}\times\mathbf{U}\times\mathbf{U} \to \mathbb{R}, \qquad \mathsf{c}(\mathbf{u};\mathbf{v},\mathbf{w}) \coloneqq \int_\Omega \rho(\mathbf{u}\cdot\nabla\mathbf{v})\cdot\mathbf{w}\,\mathrm{d}\mathbf{x}. \tag{7.31d}$$

The *weak formulation of the incompressible Navier-Stokes equations* is given by

$$\text{Find } \mathbf{u} \in \mathbf{U}, p \in P, \text{such that for almost all } t \in [t_0, T]:$$

$$\mathsf{m}\left(\frac{\partial}{\partial t}\mathbf{u}, \mathbf{v}\right) + \mathsf{c}(\mathbf{u}; \mathbf{u}, \mathbf{v}) + \mathsf{a}(\mathbf{u}, \mathbf{v}) + \mathsf{b}(\mathbf{v}, p) = (\rho \mathbf{g}, \mathbf{v})_{L^2(\Omega)}, \qquad \forall \mathbf{v} \in \mathbf{U}, \tag{7.32a}$$

$$\mathsf{b}(\mathbf{u}, q) = 0, \qquad \forall q \in P, \tag{7.32b}$$

$$\mathbf{u}(0, \cdot) = \mathbf{u}_0(\cdot), \qquad \text{a.e. in } \Omega. \tag{7.32c}$$

Under stronger smoothness assumptions, it is possible to prove existence and uniqueness of a solution for $d = 2$. For more information, the interested reader is referred to [QV08, Section 13.2].

7.4.1. Finite Element Approximation

For the Galerkin approximation of problem (7.32) we consider the finite-dimensional subspaces $\mathbf{U}_h := X_h^2(\Omega) \times X_h^2(\Omega) \subset \mathbf{U}$ and $P_h := X_h^1(\Omega) \subset P$ for $t \in [0, T]$. This choice for $(\mathbf{U}_h, P_h)$ is commonly referred to as *Taylor-Hood* and is inf-sup stable [GR11], i.e. it satisfies the discrete inf-sup condition (also often called *LLB stability condition*)

$$\sup_{\mathbf{u}_h \in \mathbf{U}_h} \frac{\mathsf{b}(\mathbf{u}_h, p_h)}{\|\mathbf{u}_h\|_{H^1(\Omega)}} \geq \hat{\beta} \|p_h\|_{L^2(\Omega)} \qquad \forall p_h \in P_h. \tag{7.33}$$

Therefore, for given initial data $\mathbf{u}_0 \in U_h$, the problem

$$\text{Find } \mathbf{u}_h \in \mathbf{U}_h, p_h \in P_h, \text{such that for } t \in [0, T]:$$

$$\mathsf{m}\left(\frac{\partial \mathbf{u}_h}{\partial t}, \mathbf{v}_h\right) + \mathsf{c}(\mathbf{u}_h; \mathbf{u}_h, \mathbf{v}_h) + \mathsf{a}(\mathbf{u}_h, \mathbf{v}_h) + \mathsf{b}(\mathbf{v}_h, p_h) = (\rho \mathbf{g}, \mathbf{v}_h)_{L^2(\Omega)} \quad \forall \mathbf{v}_h \in \mathbf{U}_h, \tag{7.34a}$$

$$\mathsf{b}(\mathbf{u}_h, q_h) = 0 \quad \forall q_h \in P_h, \tag{7.34b}$$

$$\mathbf{u}_h(0, \cdot) = \mathbf{u}_0(\cdot) \quad \text{in } \Omega, \tag{7.34c}$$

can be shown to be well-posed (cf. [QV08]). As in (3.3), the algebraic form of (7.34) is given by

$$\text{Find } \mathbf{u}_h \in \mathbf{U}_h, p_h \in P_h, \text{such that for } t \in [0, T]:$$

$$\mathsf{M}\frac{\mathrm{d}}{\mathrm{d}t}\mathbf{u}_h(t) + \mathsf{C}(\mathbf{u}_h(t))\mathbf{u}_h(t) + \mathsf{A}\mathbf{u}_h(t) + \mathsf{B}^\top p_h(t) = \mathbf{f}_h(t), \tag{7.35a}$$

$$\mathsf{B}\mathbf{u}_h(t) = 0, \tag{7.35b}$$

$$\mathbf{u}_h(0) = \mathbf{u}_0, \tag{7.35c}$$

where $\{\boldsymbol{\psi}_i\}_{i=1}^{N_h^2}$ denotes the basis of $\mathbf{U}_h$, $\{\omega_i\}_{i=1}^{N_h^1}$ denotes the basis of P_h, and $\mathbf{u}_h(t)$, $p_h(t)$ are the associated coefficient vectors. The matrices in (7.35) are given by

$$(\mathsf{M})_{i,j} = (\boldsymbol{\psi}_i, \boldsymbol{\psi}_j)_{L^2(\Omega)}, \tag{7.36a}$$

$$(\mathsf{A})_{i,j} = \mathsf{a}\left(\boldsymbol{\psi}_i, \boldsymbol{\psi}_j\right), \tag{7.36b}$$

$$(\mathsf{B})_{i,j} = \mathsf{b}\left(\boldsymbol{\psi}_i, \omega_j\right), \tag{7.36c}$$

$$(\mathsf{C}(\mathbf{w}_h))_{i,j} = \mathsf{c}(\mathbf{w}_h; \boldsymbol{\psi}_i, \boldsymbol{\psi}_j), \tag{7.36d}$$

$$\mathbf{f}_h(t) = (\rho \mathbf{g}, v_h)_{L^2(\Omega)}. \tag{7.36e}$$

In order to obtain a linear system of equations, the convective term must be suitably linearized. For discretization in time we apply the finite difference θ-scheme introduced in Section 3.4 to the algebraic system (7.35).

7.4.2. Numerical Solution

The fully discrete algebraic system to be solved at each time step can be written in block matrix form as follows:

$$\begin{bmatrix} \mathbf{A} & \mathbf{B}^\top \\ \mathbf{B} & 0 \end{bmatrix} \begin{bmatrix} \mathbf{u} \\ p \end{bmatrix} = \begin{bmatrix} \mathbf{f} \\ 0 \end{bmatrix}, \tag{7.37}$$

The blocks $\mathbf{A}$, $\mathbf{B}$ and the right hand side $\mathbf{f}$ can easily be determined from (7.35). One generally distinguishes between two solution strategies. The obvious approach is to simultaneously solve system (7.37) for velocity and pressure. Unfortunately, this requires solving large, poorly conditioned algebraic systems. The second strategy is based on the decoupling of the equations, i.e. velocity and pressure are computed separately. This can significantly reduce the computational costs, as the linear systems are smaller. However, the application of a splitting technique may have impacts on accuracy, stability and robustness. For a thorough discussion, the interested reader is referred for example to the books [KH15, Tur99] and the thesis [Smo01], which provides a good overview on splitting techniques.

In the numerical experiments carried out below, we employed an integrated solution approach (i.e. solving for velocity and pressure simultaneously). Even though computations could have been carried out much more efficiently, the objective was to assess the performance of the underlying level set methods and avoid inaccuracies and stability problems arising from the discretization of the Navier-Stokes equations.

7.5. Application of the Level Set Method

We have already seen that a coupling condition on the interface is required to combine the two phases in the two-phase flow setting. The level set method is a suitable approach to provide the interface location and describe interface evolution.

Let $\varphi(t, \mathbf{x})$ be the level set function associated with the evolving interface $\Gamma(t)$, cf. Chapter 4. Consider a piecewise constant density function $\rho : (0, T) \times \Omega \to \mathbb{R}$ and a piecewise constant viscosity function $\mu : (0, T) \times \Omega \to \mathbb{R}$ defined w.r.t. the level set function φ by

$$\rho(\varphi)(t, \mathbf{x}) \coloneqq \begin{cases} \rho_1(t, \mathbf{x}) & \text{if } \varphi(t, \mathbf{x}) > 0, \\ \rho_2(t, \mathbf{x}) & \text{if } \varphi(t, \mathbf{x}) < 0, \end{cases} \tag{7.38a}$$

$$\mu(\varphi)(t, \mathbf{x}) \coloneqq \begin{cases} \mu_1(t, \mathbf{x}) & \text{if } \varphi(t, \mathbf{x}) > 0, \\ \mu_2(t, \mathbf{x}) & \text{if } \varphi(t, \mathbf{x}) < 0. \end{cases} \tag{7.38b}$$

For a meaningful definition of ρ and μ in the Lebesgue sence, we again assume $\operatorname{meas}_d(\Gamma(t)) = 0$ for a.e. $t \in (0, T)$.

Using the level set approach, the two-phase flow problem (7.29) can be formulated as follows:

$$\rho(\varphi)\frac{\partial}{\partial t}\mathbf{u} + \rho(\varphi)(\mathbf{u} \cdot \nabla)\mathbf{u} = -\nabla p + \operatorname{div}(2\mu(\varphi)\mathbf{D}(\mathbf{u})) + \rho(\varphi)\mathbf{g} \text{ in } \Omega_1 \cup \Omega_2, \tag{7.39a}$$

$$\operatorname{div}(\mathbf{u}) = 0 \qquad \text{in } \Omega_1 \cup \Omega_2, \tag{7.39b}$$

$$[\![\mathbf{u}]\!] = 0 \qquad \text{on } \Gamma = \Gamma(\varphi), \tag{7.39c}$$

$$[\![\boldsymbol{\sigma}\mathbf{n}]\!] = -\tau\kappa\hat{\mathbf{n}} \qquad \text{on } \Gamma = \Gamma(\varphi), \tag{7.39d}$$

$$\frac{\partial}{\partial t}\varphi + \mathbf{u} \cdot \nabla\varphi = 0 \qquad \text{in } \Omega, \tag{7.39e}$$

$$\varphi = g \qquad \text{on } \partial\Omega^{\text{in}}. \tag{7.39f}$$

For the evolution of the interface $\Gamma(t)$, the level set equation replaces the former propagation condition (7.29e).

Note that if Ω has an inflow boundary portion $\partial\Omega^{\text{in}}$, a suitable boundary condition for the level set equation is required. When prescribing a Dirichlet boundary condition as, the particular choice of the boundary data g is in our setting circumstantial because only a narrow band around the interface is of interest. Imprecise or unphysical choices of g can readily be corrected by the occasional application of a redistancing procedure.

7.5.1. Surface Tension

The surface tension term (7.39d) can be transformed into the following force term:

$$f_\Gamma : \mathbf{U} \to \mathbb{R}, \qquad f_\Gamma(\mathbf{v}) \coloneqq -\tau \int_\Gamma \kappa\hat{\mathbf{n}} \cdot \mathbf{v} \, \mathrm{d}\sigma. \tag{7.40}$$

Note that $f_\Gamma \in \mathbf{U}^*$ if the curvature κ is bounded (cf. [GR11]). As usual, we incorporate any Dirichlet boundary conditions on $\partial\Omega_D$ into the spaces $\mathbf{U}_0 \coloneqq \{\mathbf{v} \in \mathbf{U} \ : \ \mathbf{v} = 0 \text{ on } \partial\Omega_D\}$ and

$\mathbf{U}_D \coloneqq \{\mathbf{v} \in \mathbf{U} \ : \ \mathbf{v} = \mathbf{u}_D \text{ on } \partial\Omega_D\}$. Similarly to (7.32), the *weak formulation of the two-phase flow problem* is obtained (cf. [GR11]):

$$\text{Find } \mathbf{u} \in \mathbf{U}_D, p \in P, \varphi \in V_D^{(\mathbf{u})} \text{ such that for almost all } t \in [0,T]: \tag{7.41a}$$

$$\mathsf{m}\left(\frac{\partial \mathbf{u}}{\partial t}, \mathbf{v}\right) + \mathsf{c}(\mathbf{u};\mathbf{u},\mathbf{v}) + \mathsf{a}(\mathbf{u},\mathbf{v}) + \mathsf{b}(\mathbf{v},p) = (\rho\mathbf{g},\mathbf{v})_{L^2(\Omega)} + f_\Gamma(\mathbf{v}) \quad \forall \mathbf{v} \in \mathbf{U}_0, \tag{7.41b}$$

$$\mathsf{b}(\mathbf{u},q) = 0 \quad \forall q \in P, \tag{7.41c}$$

$$\mathbf{u}(0,\mathbf{x}) = \mathbf{u}_0(\mathbf{x}) \quad \text{a.e. in } \Omega, \tag{7.41d}$$

$$\left(\frac{\partial}{\partial t}\varphi, \psi\right)_{L^2(\Omega)} + (\mathbf{u}\cdot\nabla\varphi,\psi)_{L^2(\Omega)} = 0 \quad \forall \psi \in L^2(\Omega). \tag{7.41e}$$

Note that the (homogeneous) Dirichlet boundary condition (7.29e) is absorbed into $V_D^{(\mathbf{u})} \coloneqq \{\psi \in V^{(\mathbf{u})} \ : \ \varphi = g \text{ on } \partial\Omega^{\text{in}}\}$ (to be understood in the trace sense) and that the interface Γ directly depends on the level set function φ.

In many applications for the numerical treatment of the source f_Γ representing surface tension the surface integral is transformed into a volume integral by means of a (regularized) Dirac delta function for the localization of Γ_h [Hys07]. Closely following [GR11], we will use a different approach based on the work of Dziuk and Bänsch [Dzi90, Bän01] that computes the source term on the localized interface. The key idea is to use an alternative, equivalent way to express the curvature term, known as *Laplace-Beltrami operator* $\underline{\Delta}$:

$$-\underline{\Delta}\mathbf{x} = \kappa(\mathbf{x})\hat{\mathbf{n}}(\mathbf{x}), \qquad \mathbf{x} \in \Gamma. \tag{7.42}$$

The operator is defined in terms of the *tangential gradient*

$$\underline{\nabla} f(\mathbf{x}) \coloneqq \underbrace{\left(\mathrm{Id} - \hat{\mathbf{n}}(\mathbf{x})\hat{\mathbf{n}}(\mathbf{x})^\top\right)}_{=:\mathbf{P}(\mathbf{x})} \nabla f(\mathbf{x}). \tag{7.43}$$

Note that

$$\mathrm{Id}(\mathbf{x}) \coloneqq \mathbf{x} \tag{7.44}$$

denotes the identity operator. Analogously, the *tangential divergence* is defined by $\underline{\mathrm{div}}(\mathbf{f}) \coloneqq \underline{\nabla}\cdot\mathbf{f}$, as is the Laplace Beltrami operator $\underline{\Delta} f \coloneqq \underline{\mathrm{div}}(\underline{\nabla} f)$. The advantage of formulation (7.42) is the possibility of applying the integration by parts formula:

$$-\tau \int_\Gamma \kappa\hat{\mathbf{n}}\cdot\mathbf{v}\,\mathrm{d}\sigma = -\tau\int_\Gamma \underline{\nabla}\hat{\mathrm{Id}}\cdot\underline{\nabla}\mathbf{v}\,\mathrm{d}\sigma. \tag{7.45}$$

On a discrete level, we find that

$$f_{\Gamma_h}(\mathbf{v}_h) = -\tau\int_{\Gamma_h} \underline{\nabla}_h\mathbf{x}\cdot\underline{\nabla}_h\mathbf{v}_h\,\mathrm{d}\sigma = -\tau\int_{\Gamma_h}\mathbf{P}_h\nabla\mathbf{x}\cdot\mathbf{P}_h\nabla\mathbf{v}_h\,\mathrm{d}\sigma. \tag{7.46}$$

It can be shown that using the improved projection

$$\tilde{\mathbf{P}}_h \coloneqq \mathrm{Id} - \left(\frac{\nabla\varphi_h(\mathbf{x})}{|\nabla\varphi_h(\mathbf{x})|}\right)\left(\frac{\nabla\varphi_h(\mathbf{x})}{|\nabla\varphi_h(\mathbf{x})|}\right)^\top, \tag{7.47}$$

with the associated source term

$$\tilde{f}_{\Gamma_h} = -\tau \int_{\Gamma_h} \tilde{\mathbf{P}}_h \nabla\mathbf{x} \cdot \tilde{\mathbf{P}}_h \nabla\mathbf{v}_h \,\mathrm{d}\sigma \tag{7.48}$$

provides better accuracy properties (with $V_h = X_h^2 \times X_h^2$ we have $\mathcal{O}(\sqrt{h})$ for $\mathbf{P}_h$ and $\mathcal{O}(h)$ for $\tilde{\mathbf{P}}_h$, cf. [GR11, Section 7.7]). In the context of the discrete system, better stability is to be expected when using the semi-discrete formulation

$$f_{\Gamma_h}(\mathbf{v}_h) = -\tau \int_{\Gamma_h} \underline{\nabla}_h \mathbf{x}^n \cdot \underline{\nabla}_h \mathbf{v}_h \,\mathrm{d}\sigma - \tau\Delta t \int_{\Gamma_h} \underline{\nabla}\mathbf{u}^{n+1} \cdot \underline{\nabla}\mathbf{v}_h \,\mathrm{d}\sigma, \tag{7.49}$$

motivated by $\mathbf{x}^{n+1} \approx \mathbf{x}^n + \Delta t \mathbf{u}^{n+1}$, cf. [Bän01]. Using an explicit representation of f_{Γ_h} may cause severe instabilities.

7.5.2. Spurious Velocities

Insufficiently accurate treatment of the surface tension may lead to numerical oscillations at the interface, commonly referred to as *spurious velocities* or *spurious currents*. Ganesan et al. [GMT07] investigated this phenomenon numerically and observed that spurious velocities do not vanish with the expected order of convergence. Two main reasons are identified: inaccurate approximation of the curvature and the free boundary. This is why an accurate treatment of the level set function is of great importance in this setting. In particular, redistancing helps obtaining good curvature and interface approximations.

7.6. Rising Bubble Benchmark

The focus of this thesis lies on level set methods. Therefore, in the numerical examples below, we solved the coupled system arising from the discretized Navier-Stokes equations using a direct solver. Even though this approach is computationally expensive, we can circumvent operator splitting related problems and focus on the evaluation of the extensions of the level set methods for interface handling.

Let us finally complete the numerical study of the methods presented in Chapter 5 and Chapter 6 by applying them to a well-known two-phase flow benchmark. The configuration was proposed in [HTK+07] and computational reference data from different research groups is available at

`http://www.featflow.de/en/benchmarks.html`.

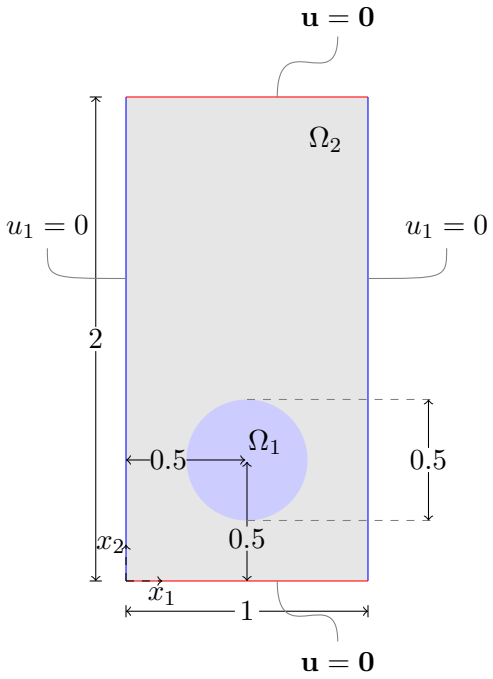

Figure 7.2.: General setting of the rising bubble benchmark, cf. [HTK+07]. No-slip boundary condition at the top and bottom (red) and free slip boundary condition at both sides (blue).

The general setting of this benchmark is depicted in Fig. 7.2. In a domain $\Omega = (0,1) \times (0,2)$ we consider two immiscible fluids $\Omega_1 = B_{0.25}(0.5)$ and $\Omega_2 = \Omega \setminus \overline{\Omega}_1$. The density ρ_1 in Ω_1 is set smaller than the density ρ_2 in the surrounding fluid Ω_2 which causes the bubble to rise. At the top and bottom boundary parts of Ω, denoted by $\partial\Omega_{\text{NS}}$, the no-slip boundary condition

$$\mathbf{u} = 0 \qquad \text{on } \partial\Omega_{\text{NS}} \tag{7.50}$$

is imposed, whereas on the left and right wall $\partial\Omega_{\text{FS}}$ the free slip boundary condition

$$\mathbf{u} \cdot \mathbf{n} = 0 \quad \text{and} \quad \boldsymbol{\tau} \cdot \left(\nabla \mathbf{u} + (\nabla \mathbf{u})^\top\right) \cdot \mathbf{n} = 0 \qquad \text{on } \partial\Omega_{\text{FS}} \tag{7.51}$$

is set, where $\boldsymbol{\tau}$ denotes the tangential vector. The acting forces can be related to each other through the dimensionless Reynolds and Eötvös numbers

$$\text{Re} = \frac{\rho_1 \sqrt{g} (2r_0)^{3/2}}{\mu_1}, \tag{7.52a}$$

$$\text{Eo} = \frac{4\rho_1 g r_0^2}{\sigma}, \tag{7.52b}$$

where μ_1 and μ_2 are the viscosities in Ω_1 and Ω_2, g the gravitational constant, σ the surface tension coefficient and $r_0 = 1/4$ the radius of the initial bubble. The benchmark specifies two test cases which are listed in Table 7.1.

test case	ρ_1	ρ_2	μ_1	μ_2	g	σ	Re	Eo	σ_2/σ_1	μ_2/μ_1
1	100	1000	1	10	0.98	24.5	35	10	10	10
2	1	1000	0.1	10	0.98	1.96	35	125	1000	100

Table 7.1.: Benchmark test case configuration, cf. [HTK+07].

For numerical evaluation, the benchmark defines the following reference quantities:

Center of Mass The center of mass of the bubble, given by

$$\mathbf{x}_c = \frac{1}{|\Omega_1|} \int_{\Omega_1} \mathrm{d}\mathbf{x}. \tag{7.53}$$

Circularity The circularity is defined as

$$\not\epsilon = \frac{2\pi r_a}{P}, \tag{7.54}$$

where P denotes the perimeter of the bubble, and r_a the radius of a circle having the same area as the bubble.

Rise Velocity We consider the mean velocity of the bubble's motion, i.e.

$$\mathbf{u}_c = \frac{1}{|\Omega_1|} \int_{\Omega_1} \mathbf{u} \, \mathrm{d}\mathbf{x}. \tag{7.55}$$

We compare our numerical results to those obtained with the TP2D code `[REF]` at the highest refinement level $\ell = 7$. It is based "on finite element discretizations in space with non-conforming $\widetilde{\mathbb{Q}}_1\mathbb{Q}_0$ basis functions for the flow variables and a conforming $\mathbb{Q}_1$ bilinear approximation for the level set function" [HTK+07]. For time discretization, the second-order accurate Crank-Nicolson scheme is used in TP2D.

In this section, we consider the finite element level set approach as presented above with the following extensions:

`[NO-EXT]`	no extension,
`[HYP-RD]`	hyperbolic redistancing, cf. Section 5.2,
`[ELP-RD]`	elliptic redistancing, cf. Section 5.4,
`[OPC-RD]`	optimal control based redistancing, cf. Section 5.5,
`[SH-MC]`	level set shifting approach, cf. Section 6.2,
`[OSC-MC]`	scalar optimal control approach for mass preservation, cf. Section 6.6.

It is also possible to combine redistancing and mass correction techniques. First, an auxiliary solution to the level set equation is computed. Occasionally this solution is improved by a redistancing technique. Alternatively, one may use a monolithic approach such as `[OPC-RD]`. Based on this intermediate solution, a mass correction scheme is applied.

7.6.1. Test Case 1

The first test case can be considered rather mild as the bubble deforms smoothly and slowly. Yet one might encounter numerical instabilities when using `[NO-EXT]`. We have already seen that there are two major sources for this problem: decreasing smoothness of the level set function and the inability to conserve mass. In fact, without the application of a redistancing scheme, strong spurious currents occured and the numerical simulation failed in many cases. The numerical results of the various approaches for this benchmark problem are depicted in Figures 7.3 and 7.4. The benchmark quantities specified above as well as the mass of the rising bubble are plotted against the fine-scale TP2D reference solution `[REF]` in Figures 7.5, 7.6 and 7.7.

ℓ	`[HYP-RD]`	`[ELP-RD]`	`[OPC-RD]`
1	35.32 %	12.71 %	55.39 %
2	22.36 %	6.06 %	34.70 %
3	15.07 %	2.96 %	22.37 %

Table 7.2.: Share of redistancing in computational costs per time step.

First, let us comment on `[NO-EXT]`. At the upper boundary of the bubble, the level set function becomes very steep in interface vicinity when no redistancing is applied. At the same time, it becomes very flat on the lower boundary of the interface. As a dramatic consequence, strong spurious velocities occur and cause artificial displacements of the interface. In contrast, when a redistancing scheme was applied, the level set function and the interface remained smooth and only mild spurious currents could be observed. These remaining spurious velocities can be explained by the continuous finite element approximation for the discontinuous pressure. Better results can be obtained when using an interface adapted mesh and a discretization that allows for the pressure jump across the interface, see for example [Bas16].

Hyperbolic redistancing `[HYP-RD]` shows a significant loss of mass which can be explained by the numerical diffusion induced by the regularization of the sign function. As explained in Chapter 5, the particular choice of the regularization parameter ε has a direct influence on the numerical accuracy and the additional computational costs. For the approximation Eq. (5.10), small values of $\varepsilon \ll h^2$ caused a significant increase in the number of iterations or the method failed to converge at all. On the other hand, for choices $\varepsilon \gg h$ we observed strong numerical diffusion and poor interface accuracy. In this example, we found $\varepsilon \sim h^{3/2}$ to provide most accurate results. Even though the scheme effectively reduces spurious currents, the interface inaccuracy leads to errors in the rise velocity and the position of the center of mass. Good agreement with the reference data is achieved for the circularity, which indicates that the bubble shape is preserved quite well.

Similarly, we could observe a (less significant) loss of mass for the elliptic redistancing approach `[ELP-RD]`. It is caused by the non-conservative solution of the level set equation. The error from the redistancing procedure can be neglected for sufficiently large interface penalty parameters α. In the numerical computations shown in this chapter, we used $\alpha = 10^6$. Spurious velocities were well damped. Compared to `[HYP-RD]`, the overall accuracy is better and `[ELP-RD]` is more efficient, cf. Table 7.2.

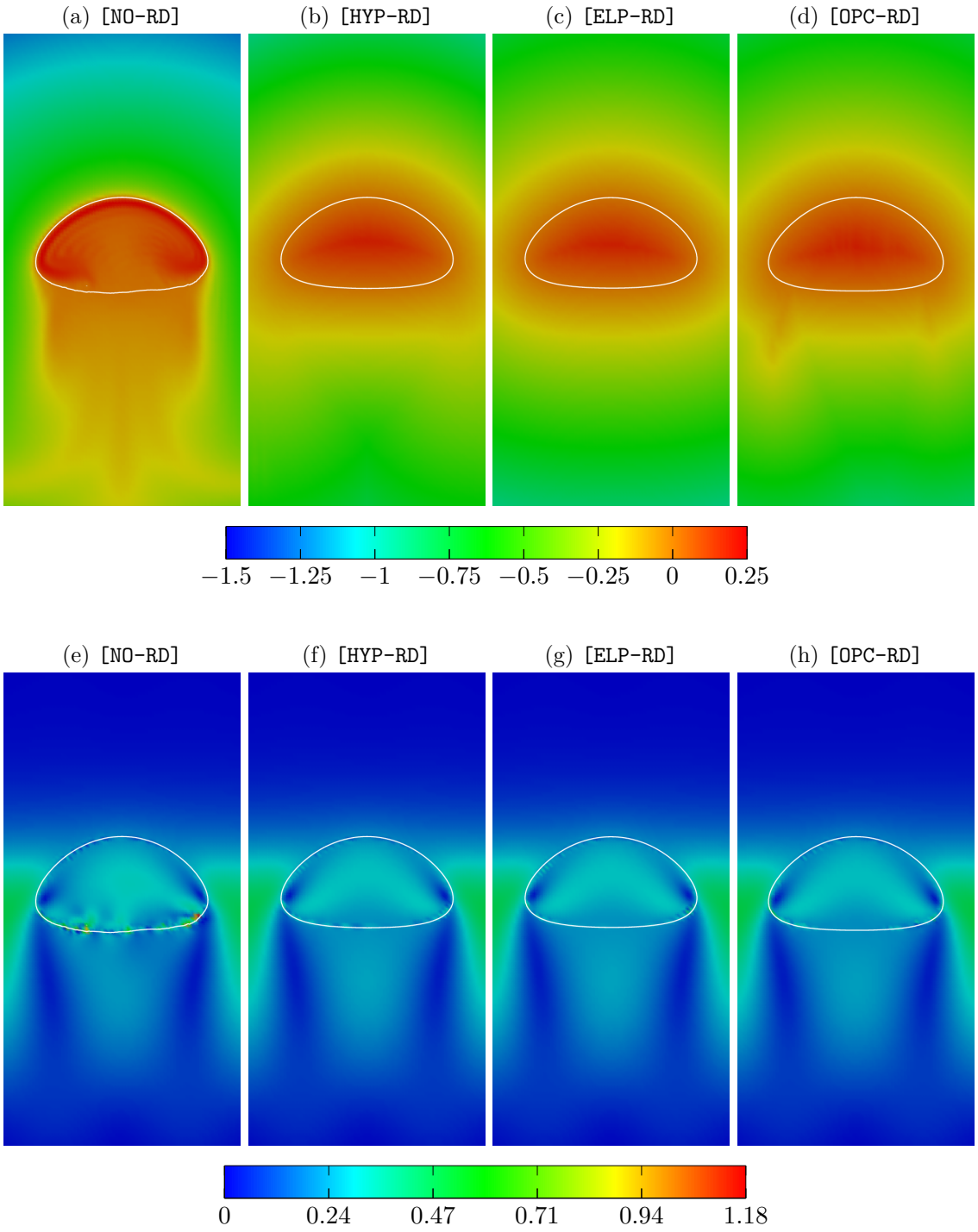

Figure 7.3.: Plots of level set functions (a)-(d) and velocity magnitudes (e)-(h) at final time $t = 3$ and on refinement level $\ell = 2$. The discrete interface is shown in white.

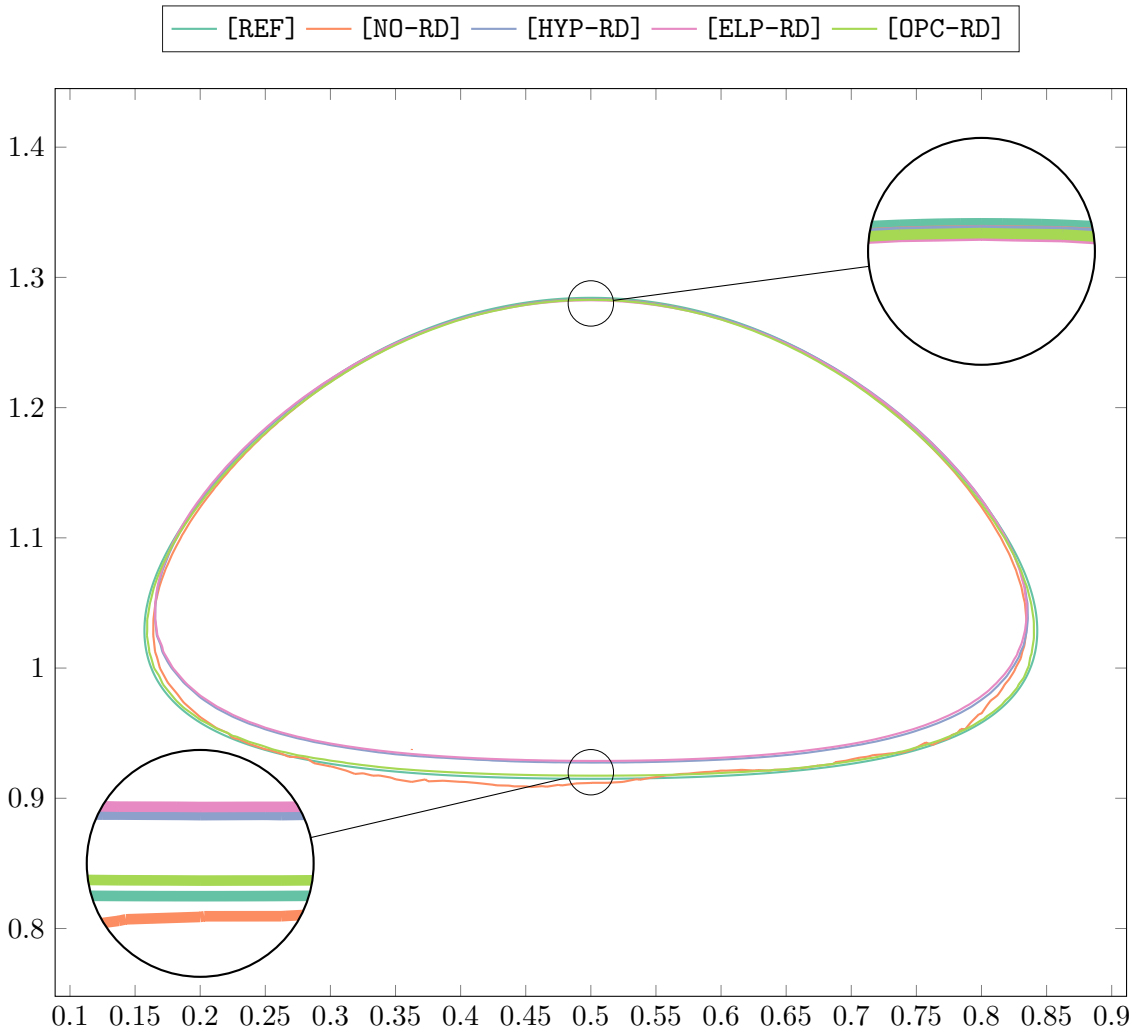

Figure 7.4.: Bubble shapes of `[NO-RD]`, `[HYP-RD]`, `[ELP-RD]` and `[OPC-RD]` at $t = 3$ and refinement level $\ell = 2$ plotted against the fine scale reference solution `[REF]`.

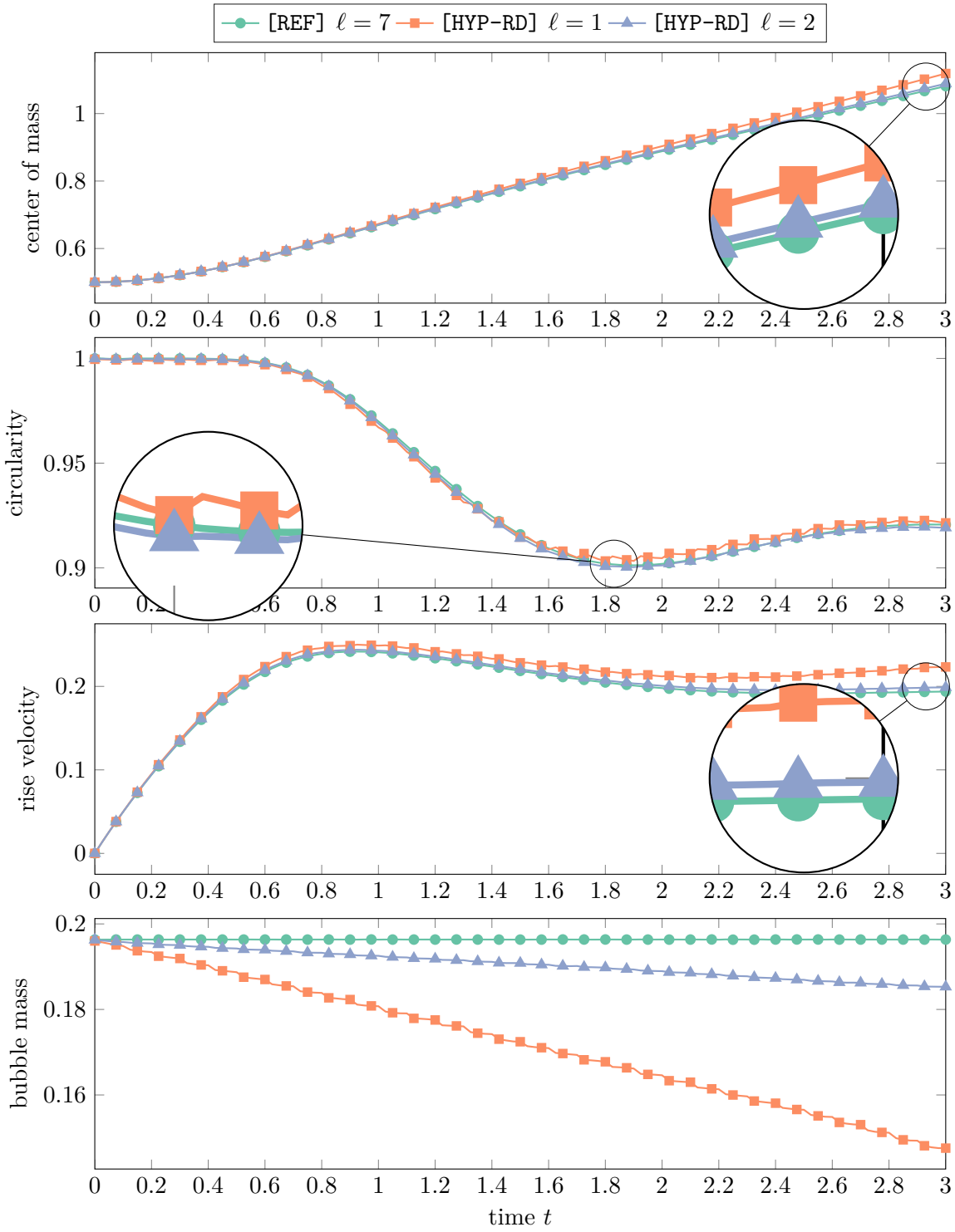

Figure 7.5.: Results of [HYP-RD] compared to the TP2D reference solution [REF].

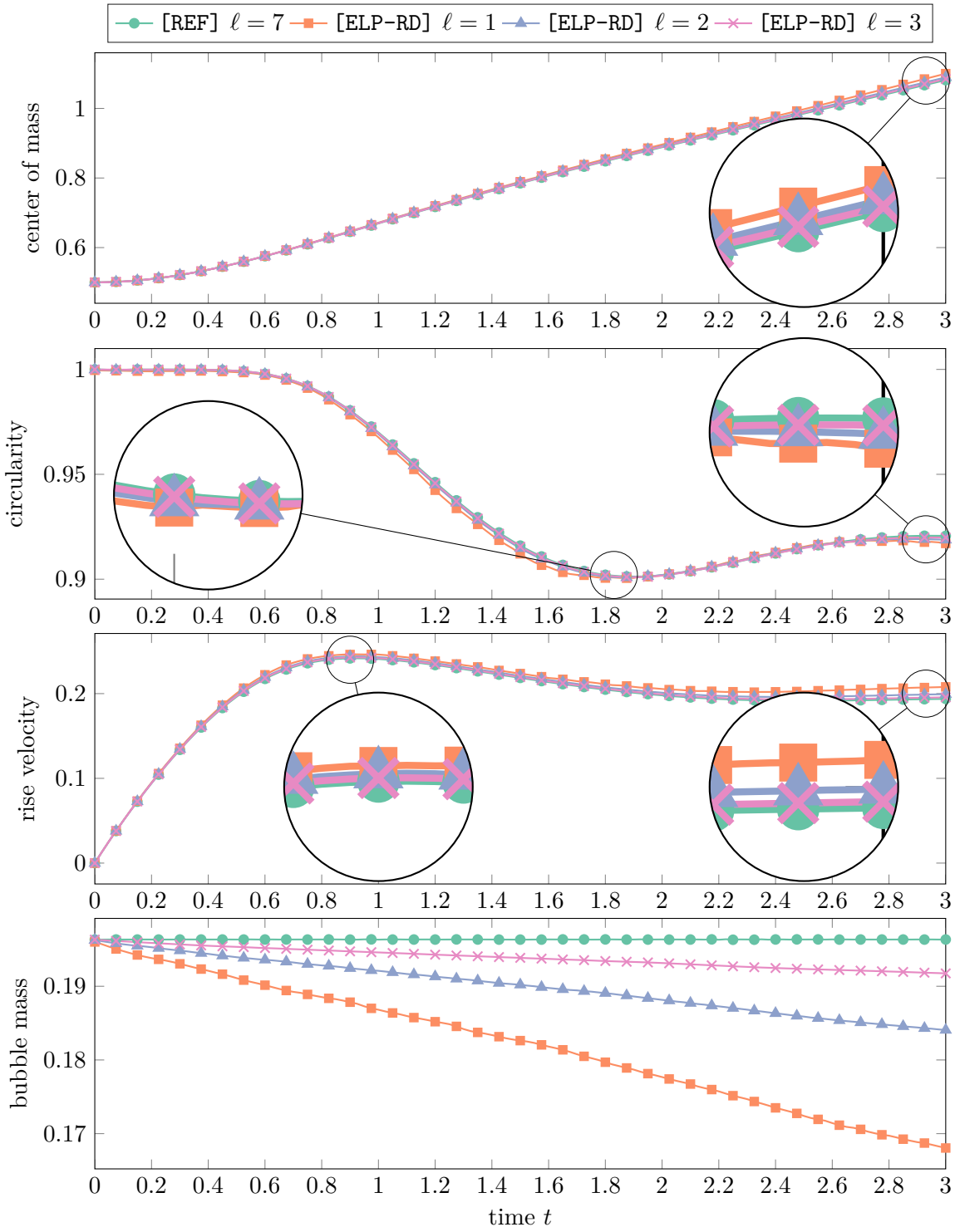

Figure 7.6.: Results of [ELP-RD] compared to the TP2D reference solution [REF].

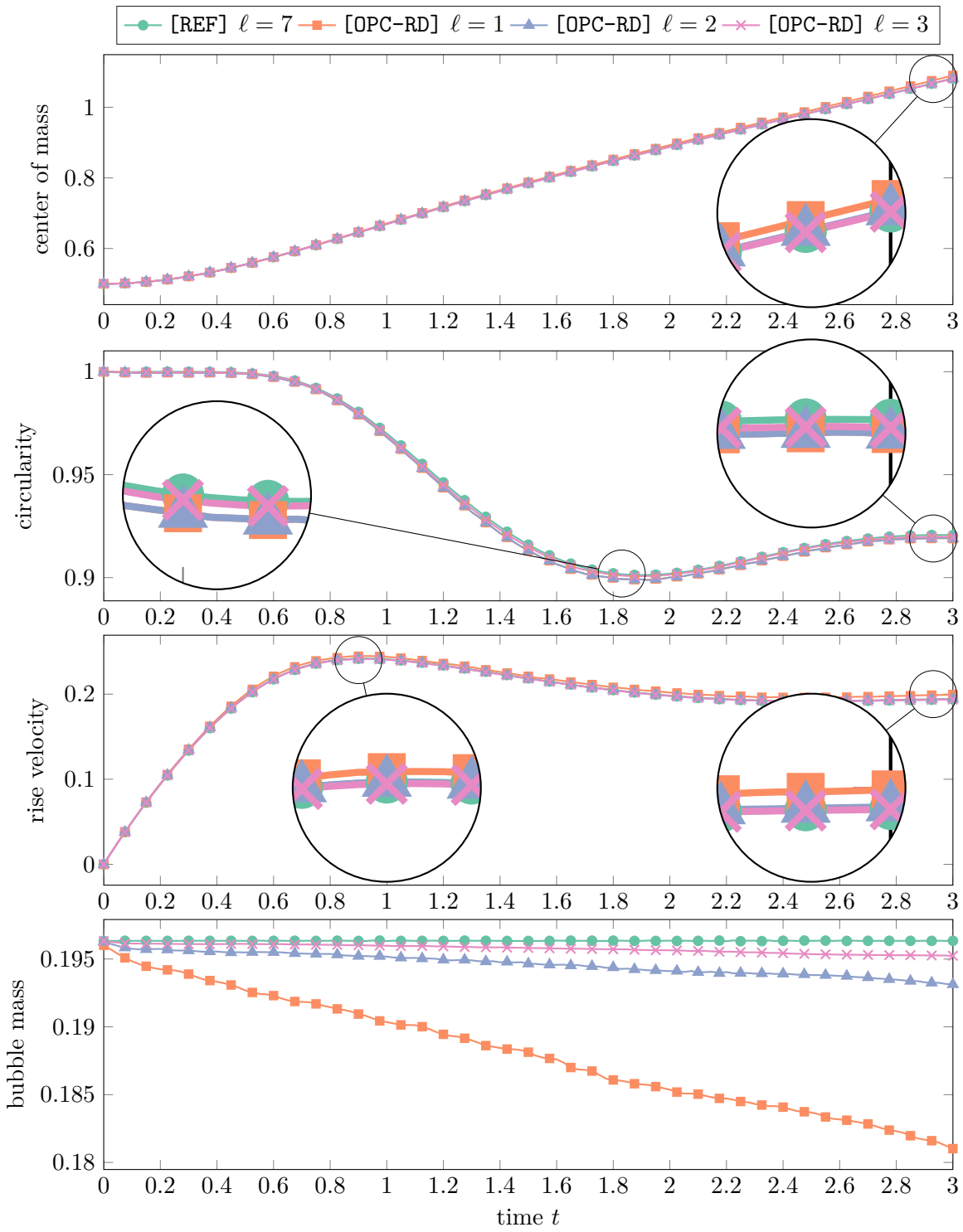

Figure 7.7.: Results of [OPC-RD] compared to the TP2D reference solution [REF].

Even though computationally more expensive, the optimal control approach for redistancing [OPC-RD] shows significant less loss of mass and best agreement with the benchmark reference solution [REF], which indicates that the monolithic problem formulation is advantageous. In particular the shape of the bubble almost matches the reference shape at refinement level $\ell = 2$, while clear deviations are visible for the two other approaches. The better accuracy may compensate for the higher computational efforts.

Let us now combine the efficient elliptic redistancing approach [ELP-RD] with the mass correction schemes [SH-MC] and [OSC-MC] presented in the previous chapter. The numerical results are depicted in Figures 7.8 and 7.9. Note that these results were obtained on the coarsest refinement level $\ell = 1$. Compared to the non-conservative schemes, the increase in accuracy is quite significant. [OSC-MC] seems to be slightly more accurate in terms of circularity and rise velocity, but is also computationally more expensive. However, the main advantage of local conservation did not really come into play in this test case.

In summary, the application of the elliptic redistancing scheme combined with the level set shifting approach yields a very efficient numerical scheme that significantly improves the overall accuracy. In simulations where local mass conservation plays a crucial role, the use of the more involved [OSC-MC] technique is worth the effort.

7.6.2. Test Case 2

This chapter concludes with numerical results for the challenging benchmark test case. It features large density and viscosity ratios and the surface tension is significantly decreased. The bubble shape becomes non-convex and thin filaments are developed which eventually break off [HTK+07]. The results of the three different groups participating in the benchmark did not show agreement in the filament regions, so that there is no clear reference solution to compare results to. This is why we only present the results of the [OSC-MC] approach combined with [ELP-RD] compared to the benchmark solutions in Fig. 7.10.

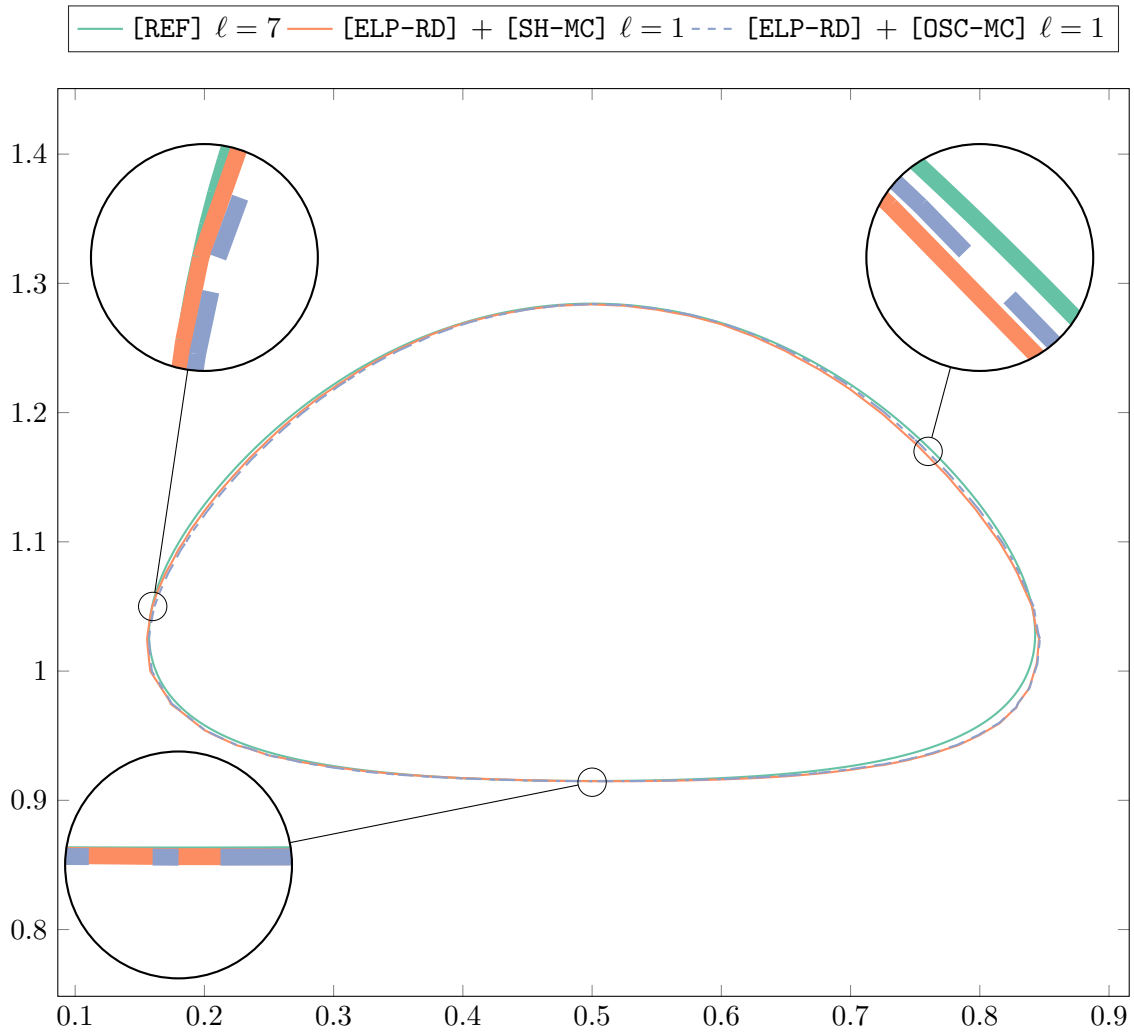

Figure 7.8.: Bubble shapes of [ELP-RD] + [SH-MC] and [ELP-RD] + [OSC-MC] at refinement level $\ell = 1$ compared to reference solution [REF].

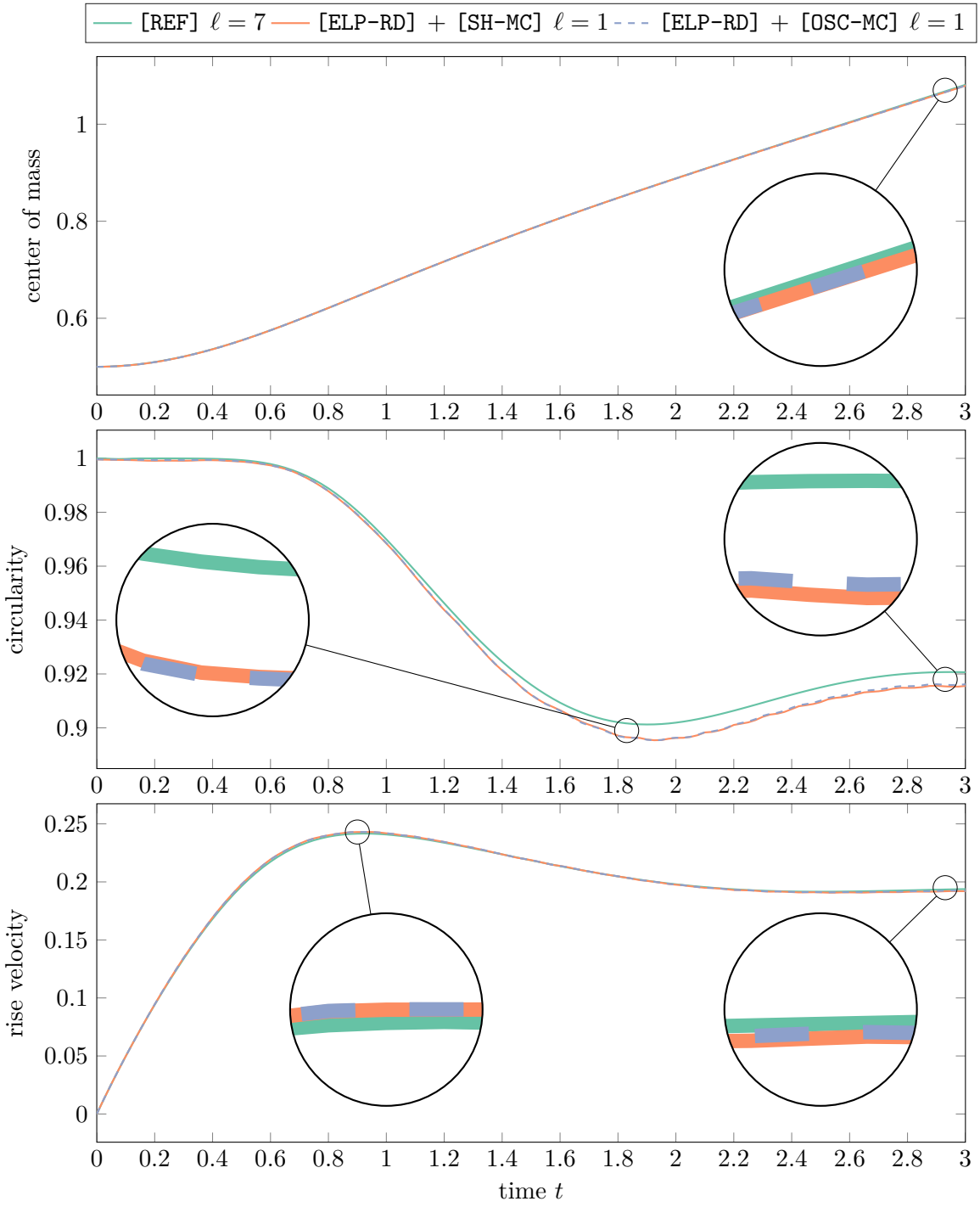

Figure 7.9.: Results of [ELP-RD] + [SH-MC] and [ELP-RD] + [OSC-MC] compared to the TP2D reference solution [REF].

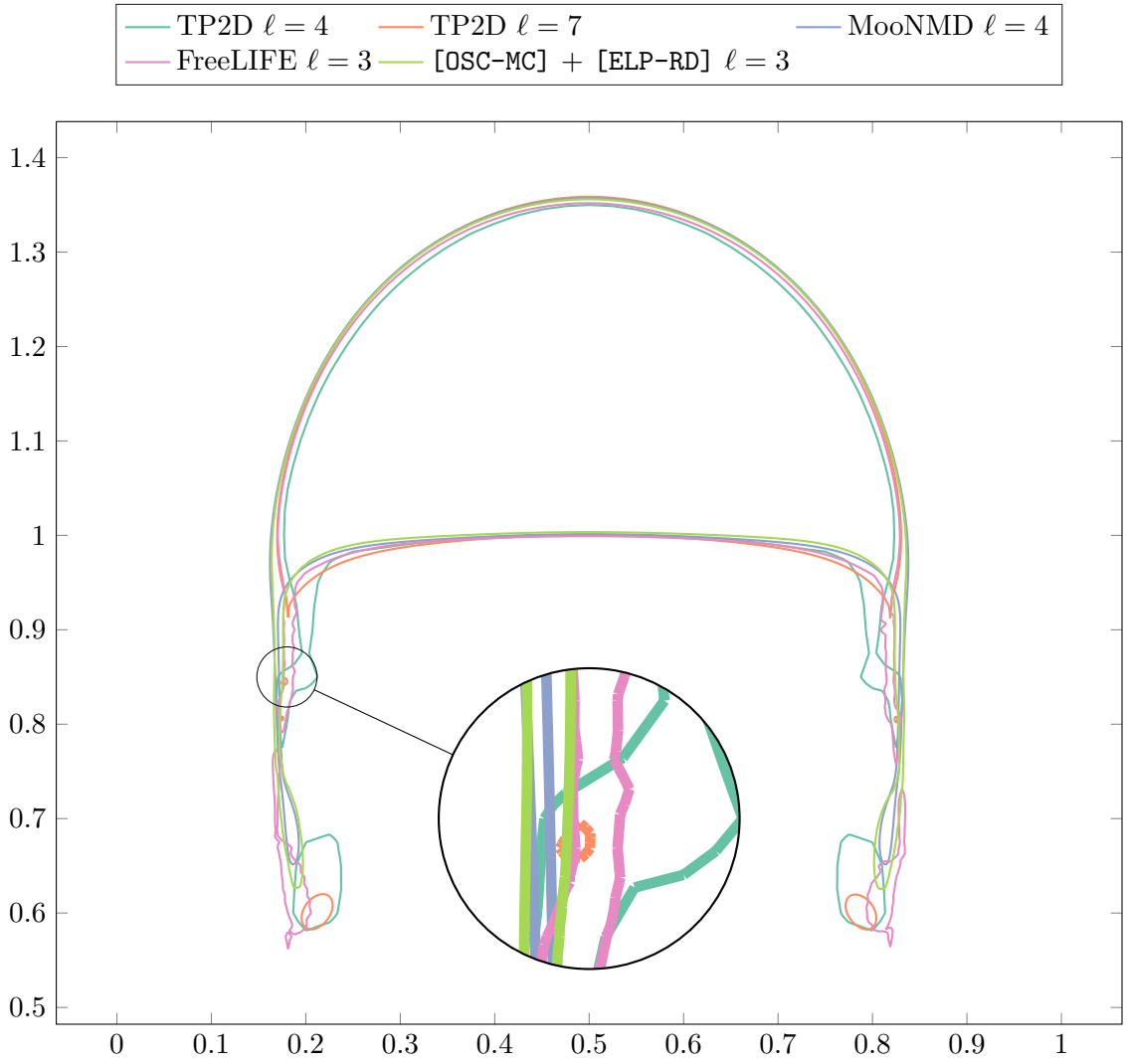

Figure 7.10.: Bubble shapes of benchmark codes and [OSC-MC] + [ELP-RD].

8 Summary and Outlook

This thesis was concerned with the development of numerical approaches to redistancing and conservation of mass in finite element methods for the level set transport equation.

8.1. Summary

The key components of the proposed numerical algorithms are as follows:

1. We have introduced a minimization-based PDE redistancing approach in the context of variational level set algorithms. The objective functional of the optimization problem is defined in terms of a potential function. The choice of the potential function determines the geometrical properties of the solution. Interface displacements are effectively prevented by a suitable penalization term.
   In the context of a finite element discretization, the problem can be solved without resorting to pseudo-time stepping so that no time step restrictions have to be considered. For suitable potential functions, the non-linear minimization problem reduces to the repeated solution of a steady diffusion-reaction equation.
   The proposed method is very robust, preserves the interface, offers the possibility to incorporate further design criteria into the objective functional and can easily be applied in the setting of a standard finite element discretization for elliptic PDEs, thus also allowing for unstructured meshes. The approach has already been extended to discontinuous Galerkin approximations in [UKO16]. Furthermore, in contrast to many hyperbolic redistancing schemes, it exhibits fast convergence and the choice of the regularization parameter has only little influence on accuracy and convergence behavior.
2. Next, we have presented a monolithic redistancing approach based on an optimal control problem. The level set transport equation is enriched by a source term and solved while simultaneously maintaining the signed distance function property as far as possible. By design of the source term, the interface cannot be artificially displaced on an analytical level.
   Using the discretize-then-optimize approach, the discrete system of first order optimality conditions is obtained and numerically solved using a suitable fixed-point iteration.

Even though this approach is more expensive in terms of computational costs, it offers several significant advantages. First, our numerical experiments indicate that the monolithic problem formulation leads to better interface accuracy compared to post-processing techniques. This is due to the fact that the optimal control problem does not require a stabilization technique, so that less artificial diffusion is induced. As for the elliptic redistancing approach, the objective functional can easily be extended to satisfy further design criteria.

3. Last but not least, we have presented an optimal control approach to enforce conservation of mass in the context of finite element level set methods. While most of the other conservative techniques are based on a combination of the level set approach with volume-of-fluid techniques, this approach employs a suitable corrective flux in a conservation law for the corresponding Heaviside function.
   We have considered two different control fluxes: the gradient of a scalar control function and a vector-valued control function. Even though the algebraic system for the latter case is of higher dimension than in the scalar control case, it can be solved more efficiently using iterative solution techniques.
   As for the previous optimal control problem, the numerical solution is based on the discretize-then-optimize technique. The obtained system of first order optimality conditions is linearized and a simple preconditioning scheme is applied. In contrast to many other approaches to mass correction, the optimal control scheme is conservative to machine precision. Furthermore, mass is corrected locally so that unphysical redistribution of mass is ruled out and high interface approximation accuracy is obtained.

8.2. Outlook

Future work will focus on improving the efficiency of the presented numerical schemes. For the considered optimal control problems, we solved the arising system of first order optimality conditions as a coupled system by application of direct solvers in the current implementation. A reduction in the overall computational efforts can be achieved using more sophisticated solution strategies. The development of reduced space problems for the non-linear optimal control problems, of improved preconditioning techniques and of problem-tailored descent methods (instead of solving the KKT system directly) appear to be promising directions for further research.

Another aspect that merits further research is the analysis of optimal penalty parameters in the considered optimization problems. We have already seen in numerical examples that non-constant choices may improve both accuracy and the conditioning of the linear systems to be solved. Furthermore, the potentials used to define the level set regularization term in the context of the redistancing approaches, are still not optimal. While single-well potentials may cause numerical oscillations in the vicinity of singularities (thus causing numerical instabilities), the double-well potential is robust. However, in regions with flat gradients the double-well potential may lead to constant solutions rather than to the desired signed distance function approximation. Hence, the development of an improved potential function could be pursued in future work.

The proposed methods are currently implemented only for the two-dimensional case. An extension to the three-dimensional case is possible without significant algorithmic modifications and appears to be a promising aspect of future work.

Last but not least, we envisage the application to more scientific and industrial problems. For example, the proposed redistancing schemes could be applied in image processing techniques such as mean curvature flow. The robustness and global nature of the elliptic redistancing approach are highly advantageous in this particular context. Furthermore, problems involving several non-connected domains, for example bubble flows, could significantly benefit from the good local conservation properties of the proposed optimal control approach.

A Appendix

This chapter will provide various fundamental results from calculus, linear algebra and functional analysis. Most of the definitions and theorems are taken from the referenced textbooks.

A.1. Finite Element Approximation

In this section we will provide essential definitions and results for the construction of suitable finite element spaces. From [EG04] and [QV08], we use the following definitions:

Definition A.1 (Domain, [EG04])
"In dimension 1, a domain is an open, bounded interval. In dimension $d \geq 2$, a domain is an open, bounded, connected set in $\mathbb{R}^d$ such that its boundary $\partial\Omega$ satisfies the following property: There are $\alpha > 0$, $\beta > 0$, a finite number R of local coordinate systems $x^{r'} = (x^{r\prime}, x_d^r)$, $1 \leq r \leq R$, where $x^{r\prime} \in \mathbb{R}^{d-1}$ and $x_d^r \in \mathbb{R}$, and R local maps φ^r that are Lipschitz on their definition domain $\{x^{r\prime} \in \mathbb{R}^{d-1};\ |x^{r\prime}| < \alpha\}$ and such that

$$\partial\Omega = \bigcup_{r=1}^{R} \{(x^{r\prime}, x_d^r);\ x_d^r = \varphi^r(x^{r\prime});\ |x^{r\prime}| < \alpha\},$$
$$\{(x^{r\prime}, x_d^r);\ \varphi^r(x^{r\prime}) < x_d^r < \varphi^r(x^{r\prime}) + \beta;\ |x^{r\prime}| < \alpha\} \subset \Omega, \qquad \forall r,$$
$$\{(x^{r\prime}, x_d^r);\ \varphi^r(x^{r\prime}) - \beta < x_d^r < \varphi^r(x^{r\prime});\ |x^{r\prime}| < \alpha\} \subset \mathbb{R}^d \setminus \overline{\Omega}, \qquad \forall r,$$

where $|x^{r\prime}| \leq \alpha$ means that $|x_i^{r\prime}| \leq \alpha$ for $1 \leq i \leq d-1$. For $m \geq 1$, Ω is said to be of class C^m (resp., piecewise of class C^m) if all the local maps φ^r are of class C^m (resp., piecewise of class C^m)." (direct quote from [EG04, Definition 1.46]).

Definition A.2 (Triangulation [QV08])
Let $\Omega \subset \mathbb{R}^d$, $d \in \{2, 3\}$ be an open, bounded and connected subset such that $\overline{\Omega}$ is the union of a finite number of polyhedra. A finite decomposition

$$\overline{\Omega} = \bigcup_{K \in \mathcal{T}_h} K, \tag{A.1}$$

is called *triangulation* of $\overline{\Omega}$, if:

$$\text{each } K \text{ is a nonempty polyhedron,} \tag{A.2a}$$
$$\text{for all } K_1, K_2 \in \mathcal{T}_h \text{ such that } K_1 \neq K_2\text{: } \operatorname{intr} K_1 \cap \operatorname{intr} K_2 = \emptyset, \tag{A.2b}$$
$$F = K_1 \cap K_2 \neq \emptyset \text{ for } K_1, K_2 \in \mathcal{T}_h,\ K_1 \neq K_2, \text{ is a common face of } K_1 \text{ and } K_2, \tag{A.2c}$$
$$\text{for all } K \in \mathcal{T}_h\text{: } h_K \coloneqq \operatorname{diam}(K) \leq h. \tag{A.2d}$$

A family of triangulations $\mathcal{T}_h$, $h > 0$, is called *regular*, if there is a constant $\sigma \geq 1$ such that

$$\max_{K \in \mathcal{T}_h} \frac{h_K}{\rho_K} \leq \sigma, \qquad \forall h > 0, \tag{A.3}$$

where $\rho_K \coloneqq \sup\{\operatorname{diam}(S) \ : \ S \text{ is a ball contained in } K\}$.

A.2. Level Set Function Properties

In this section we will summarize some essential properties and results for level set functions as defined in Chapter 4.

Definition A.3 (Distance function [AD99])
Let $M \subset \mathbb{R}^d$ be a set. The *distance function* of M is defined as

$$\operatorname{dist}(\mathbf{x}, M) \coloneqq \inf_{\mathbf{y} \in M} |\mathbf{x} - \mathbf{y}|. \tag{A.4}$$

Theorem A.4 (Differentiability of distance [AD99, Theorem 1 in Part 1])
"Let $M \subset \mathbb{R}^d$ be nonempty and closed and let $\mathbf{x} \in \mathbb{R}^d \setminus M$. Then, $\operatorname{dist}(\mathbf{x}, M)$ is differentiable at $\mathbf{x}$ if and only if there exists a unique $\mathbf{y} \in M$ such that $\operatorname{dist}(\mathbf{x}, M) = |\mathbf{x} - \mathbf{y}|$. In this case

$$\nabla \operatorname{dist}(\mathbf{x}, M) = \frac{\mathbf{x} - \mathbf{y}}{|\mathbf{x} - \mathbf{y}|} = \frac{\mathbf{x} - \mathbf{y}}{\operatorname{dist}(\mathbf{x}, M)}. \tag{A.5}$$

In particular, $|\nabla \operatorname{dist}(x, M)| = 1$ at any differentiability point $\mathbf{x} \in \mathbb{R}^d \setminus M$." (quote from [AD99, Theorem 1 in Part 1])

A.3. Functional Analysis

The following fundamental result shows a way to characterize the dual space of a Hilbert space $\{H, (\cdot,\cdot)_H\}$. In particular, we can identify H^* by H.

Theorem A.5 (Riesz Representation Theorem, [Trö10, Section 2.4])
"Let $\{H, (\cdot,\cdot)_H\}$ be a real Hilbert space. Then for any continuous linear functional $F \in H^*$ there exists a uniquely determined $f \in H$ such that $\|F\|_{H^*} = \|f\|_H$ and

$$F(v) = (f, v)_H \qquad \forall v \in H." \tag{A.6}$$

(direct quote from [Trö10, Section 2.4]).

The following lemma is commonly used in the stability and convergence analysis of initial-boundary value problems.

Lemma A.6 (Gronwall Lemma [QV08, Lemma 1.4.1])
"Let $F \in L^1(0,T)$ be a non-negative function, G and U be continuous functions on $[0,T]$. If U satisfies

$$u(t) \leq G(t) + \int_0^t F(\tau)U(\tau)\,\mathrm{d}\tau, \tag{A.7}$$

for all $t \in [0,T]$, then

$$U(t) \leq G(t) + \int_0^T F(s)G(s)\exp\left(\int_s^t F(\tau)\,\mathrm{d}\tau\right), \tag{A.8}$$

for all $t \in [0,T]$." (quote from [QV08, Lemma 1.4.1])

Theorem A.7 (Rademacher's Theorem [Eva98, Theorem 6 in Chapter 5.8])
Let $U \subset \mathbb{R}^d$ be open and $u : U \to \mathbb{R}$ a locally Lipschitz continuous function. Then u is differentiable almost everywhere in U.

Theorem A.8 (Trace Theorem [LT05, Theorem A.4])
Let $\Omega \subset \mathbb{R}^d$, $d \geq 2$, be a bounded domain with piecewise smooth boundary Γ. Then the *trace operator* $\gamma : C^1(\overline{\Omega}) \to C(\Gamma)$ may be extended to $\gamma : H^1(\Omega) \to L^2(\Gamma)$ defining the trace $\gamma v \in L^2(\Gamma)$ for all $v \in H^1(\Omega)$. Moreover, there is a constant C_Ω such that

$$\|\gamma v\|_{L^2(\Omega)(\Gamma)} \leq C_\Omega \|v\|_{H^1(\Omega)}, \qquad \forall v \in H^1(\Omega). \tag{A.9}$$

Theorem A.9 (Poincaré [EG04])
Let Ω be a bounded open set and $1 \leq p < \infty$. Then, there exists a constant $c_{p,\Omega}$ such that

$$\|v\|_{L^p(\Omega)} \leq c_{p,\Omega} \|\nabla v\|_{L^p(\Omega)}, \qquad \forall v \in W_0^{1,p}(\Omega). \tag{A.10}$$

The following theorem generalizes the proposition of Poincaré in Theorem A.9:

Theorem A.10 (Poincaré-Friedrichs [EG04, Ex. B.64, Cor. B.65, Lem. B.66])
Let Ω be a bounded connected open set and $v \in W^{1,p}(\Omega)$ for $1 \leq p < \infty$. Let E be a subset of Ω with non-zero d or $(d-1)$ measure and f be a linear form on $W^{1,p}(\Omega)$ defined by

$$f(v) \coloneqq \frac{1}{\operatorname{meas}(E)} \int_E v \, \mathrm{d}e. \tag{A.11}$$

Then

$$\|v - f(v)\|_{W^{1,p}(\Omega)} \leq c \|\nabla v\|_{L^p(\Omega)}, \qquad \forall v \in W^{1,p}(\Omega), \tag{A.12}$$

or for $W = \{v \in W^{1,p}(\Omega) \ : \ f(v) = 0\}$

$$\|v\|_{W^{1,p}(\Omega)} \leq c \|\nabla v\|_{L^p(\Omega)}, \qquad \forall v \in W. \tag{A.13}$$

Note that in the case of E having zero d measure but non-zero $(d-1)$ measure, the continuity of f is a consequence of the trace theorem [EG04, Thoerem B.52].

Theorem A.11 ([Trö10])
"Every continuous and convex functional $f : U \to \mathbb{R}$ on a Banach space U is *weakly lower semicontinuous*; that is, for any sequence $\{u_n\}_{n=1}^{\infty} \subset U$ such that $u_n \rightharpoonup u$ as $n \to \infty$ we have

$$\liminf_{n\to\infty} f(u_n) \geq f(u)." \tag{A.14}$$

(direct quote from [Trö10, Section 2.4])

In particular, the functional $f(u) = \|u\|$ on any Banach space and for any norm $\|\cdot\|$ is continuous and, by the triangle inequality convex. Therefore, by Theorem A.11 the norm functional is also weakly lower semicontinuous.

Definition A.12 (Differentiability in Banach Spaces [Trö10, Section 2.6])
Let $\{U, \|\cdot\|_U\}$, $\{V, \|\cdot\|\}_V$ be a Banach spaces and $\mathcal{U} \subset U$ nonempty and open. Let $F : \mathcal{U} \to V$ be a mapping.

(i) Let $u \in \mathcal{U}$ and $h \in U$ be given. The limit

$$\delta F(u, h) \coloneqq \lim_{t \searrow 0} \frac{1}{t} \big(F(u + th) - F(u)\big), \tag{A.15}$$

is called *directional derivative* of F at u in direction h (if it exists). The mapping

$$h \mapsto \delta F(u, h), \tag{A.16}$$

is called *first variation* of F if the limit exists for all directions h.

(ii) Assume that the first variation of F exists at $u \in \mathcal{U}$. If there exists a linear operator $A \in \mathscr{L}(U, V)$ such that

$$\delta F(u, h) = Ah, \qquad \forall h \in U, \tag{A.17}$$

then F is *Gâteaux differentiable* at u and $A \coloneqq F'(u)$ is the *Gâteaux derivative* of F at u.

(iii) If there exists a linear operator $A \in \mathscr{L}(U, V)$ at $u \in \mathcal{U}$ and a mapping $r(u, \cdot) : U \to V$ such that for all $u + h \in \mathcal{U}$

$$F(u + h) = F(u) + Ah + r(u, h), \tag{A.18}$$

and for $\|h\|_U \to 0$

$$\frac{\|r(u, h)\|_V}{\|h\|_U} \to 0, \tag{A.19}$$

then F is called *Fréchet differentiable* at u and $A \coloneqq F'(u)$ is called its *Fréchet derivative*.

Definition A.13 (Nemytskii Operators [Trö10, Section 4.3])
"Let $E \subset \mathbb{R}^m$, $m \in \mathbb{N}$, be a bounded and measurable set, and let $\psi = \psi(\mathbf{x}, \varphi) : E \times \mathbb{R} \to \mathbb{R}$ be a function. The mapping Φ given by

$$\Phi(\varphi) = \psi\big(\cdot, \varphi(\cdot)\big), \tag{A.20}$$

which assigns to a function $\varphi : E \to \mathbb{R}$ the function $z : E \to \mathbb{R}$, $z(\mathbf{x}) = \psi\big(\mathbf{x}, \varphi(\mathbf{x})\big)$ is called *Nemytskii operator* or *superposition operator*." (quote from [Trö10, Section 4.3] with adapted notation)

B Nomenclature

This chapter introduces the general notation used throughout this thesis. Commonly used variables are listed in Table B.1, operators in Table B.3 and sets and function spaces in Table B.4. The notation is based on the nomenclature used in the books [GP08] and [GR11].

Variable	Definition
d	space dimension
$\mathbf{x}$	space coordinates, $\mathbf{x} \in \mathbb{R}^d$, $\mathbf{x} = (x_1, x_2, \ldots, x_d)$
Ω	space domain, $\Omega \subset \mathbb{R}^d$, cf. Definition A.1
$\partial\Omega$	the boundary of Ω
$\mathbf{n}$	the (outward pointing) normal vector to the boundary
t	time
$(0, T)$	time domain
φ	level set function
q, $\mathbf{q}$	control variable (scalar or vector valued)
λ	Lagrange multiplier
$\mathbf{v}$	time independent velocity field
$\mathbf{u}$	time dependent velocity field
p	pressure
Ω_1, Ω_2	two subdomains of Ω such that $\overline{\Omega}_1 \cup \overline{\Omega}_2 = \overline{\Omega}$
Γ	the interface separating Ω_1 and Ω_2, i.e. $\Gamma = \overline{\Omega}_1 \cap \overline{\Omega}_2$
$\hat{\mathbf{n}}$	the (outward pointing) normal vector to the interface Γ

Table B.1.: General variables of interest.

Scalar quantities are printed in italic (z), whereas bold symbols are used for vector valued quantities ($\mathbf{z}$). The discrete counterpart of a variable z is usually denoted by an index h, e.g. z_h. Parameters associated with the discretization are listed in Table B.2.

Parameter	Meaning
h	mesh size parameter
Δt	time step size
δ, δ_K	SUPG stabilization parameter (on cell K)

Table B.2.: Discretization parameters.

Symbol	Definition
$\lvert\cdot\rvert$	absolute value of a scalar quantity; Euclidean norm of a vector valued quantity; measure of a set; length of a multi-index
$\mathrm{meas}_\ell(E)$	Lebesgue measure of $E \subset \mathbb{R}^d$, $\ell \leq d$
$\frac{\mathrm{d}}{\mathrm{d}t}u,\ \mathrm{d}_t u$	total time derivative of u
$\frac{\partial}{\partial t}u, \partial_t u,$	first order partial derivative of u w.r.t. time
$\frac{\partial^2}{\partial t^2}u,\ \partial_{tt}u$	second order partial derivative of u w.r.t. time
$\partial_i,\ \partial_{x_i}$	first order partial derivative of u w.r.t. x_i
$\partial_{ij},\ \partial_{x_i,x_j}$	second order partial derivative of u w.r.t. x_i and x_j
$\partial^\alpha u$	derivative w.r.t. multi-index $\alpha \in \mathbb{N}^d$, $\partial^\alpha u \coloneqq \partial_{\alpha_1}\big(\partial_{\alpha_2}(\cdots \partial_{\alpha_d} u)\big)$
$\partial_y^\ell u$	ℓ-th derivative of u w.r.t. y
∇u	gradient of u, $\nabla u \coloneqq (\partial_1 u, \partial_2 u, \ldots, \partial_d u)^\top$
$\underline{\nabla} u$	tangential derivative of u, cf. (7.43)
$\mathrm{div}(u), \nabla \cdot u$	divergence of u, $\nabla \cdot u \coloneqq \partial_1 u + \partial_2 u + \cdots + \partial_d u$
$\underline{\mathrm{div}}(u)$	tangential divergence of u, $\underline{\mathrm{div}}(u) = \underline{\nabla} \cdot u$
$\Delta u, \nabla \cdot \nabla u$	Laplace operator applied to u, $\Delta u \coloneqq \partial_{11} u + \partial_{22} u + \cdots + \partial_{dd} u$
$\underline{\Delta} u$	Laplace-Beltrami operator applied to u, cf. (7.42)
$[\![f]\!]_\Gamma$	jump across Γ: $[\![f]\!]_\Gamma(x) \coloneqq \lim_{h \searrow 0} \big(f(x - h\hat{\mathbf{n}}(x)) - f(x + h\hat{\mathbf{n}}(x)\big)$
$\mathcal{I}(f)$	interpolation operator (cf. Definition 3.11)
$\mathbf{u} \cdot \mathbf{v}$	Euclidean scalar product of $\mathbf{u}$ and $\mathbf{v}$, i.e. $\mathbf{u} \cdot \mathbf{v} = \sum_{i=1}^{d} u_i v_i$
$\det(A)$	determinant of A
$\mathrm{tr}(A)$	trace of A
$\mathrm{Ker}(A)$	kernel of A
$\mathrm{Im}(A)$	image of A
$\mathrm{H}(x)$	Heaviside function of x, i.e. $\mathrm{H}(x) = \begin{cases} 1, & \text{if } x \geq 0 \\ 0 & \text{if } x < 0 \end{cases}$

Table B.3.: Operators and other symbols.

Symbol	Definition
$\mathbb{R}^d$	vector space of real vectors of dimension d
$\mathbb{R}^{m,n}$	vector space of real matrices of dimension $m \times n$
$\mathscr{L}(U,V)$	vector space of bounded linear operators from U to V
V^*	dual space to topological space V
$C(\Omega)$	space of continuous functions on Ω
$C^k(\Omega)$	space of k times continuously differentiable functions on Ω
$\mathrm{Lip}(\Omega)$	space of Lipschitz-continuous functions in Ω
$L^p(\Omega)$	vector space of functions on Ω whose p-th power is Lebesgue integrable
$W^{k,p}(\Omega)$	Sobolev space, i.e. vector space of functions whose weak derivatives of order $\leq k$ are in $L^p(\Omega)$
$H^k(\Omega)$	Sobolev space for the special case $p = 2$, i.e. $H^k(\Omega) \coloneqq W^{k,p}(\Omega)$
$C^k(0,T;V)$	V-valued functions in C^k w.r.t. to time $t \in [0,T]$
$L^p(0,T;V)$	V-valued functions in L^p w.r.t. to time $t \in (0,T)$
$\mathbb{P}^k(K)$	vector space of polynomials of degree $\leq k$ on K
X_h^k	Lagrange finite element space of degree k (cf. 3.38)
$\{\psi_i\}_{i=1}^N$	set of basis functions of X_h^k
V_{div}	subspace of divergence-free functions of V, $V_{\mathrm{div}} \coloneqq \{v \in V \ : \ \mathrm{div}(v) = 0\}$

Table B.4.: Sets and function spaces.

Symbol	Definition
$\|\cdot\|_U$	norm of normed space U
$\|\cdot\|_{C^k(\Omega)}$	norm in $C^k(\Omega)$, $\|u\|_{C^k(\Omega)} \coloneqq \max\limits_{0\leq\|\alpha\|\leq k} \sup\limits_{\mathbf{x}\in\Omega} \|\partial^\alpha u(\mathbf{x})\|$
$\|\cdot\|_{L^p(\Omega)}$	norm in $L^p(\Omega)$, $\|u\|_{L^p(\Omega)} \coloneqq \left(\int_\Omega \|u\|^p \ \mathrm{d}\mathbf{x}\right)^{1/p}$
$\|\cdot\|_{H^k(\Omega)}$	semi-norm in $H^k(\Omega)$, $\|u\|_{H^k(\Omega)} \coloneqq \sum\limits_{\|\alpha\|=k} \|\partial^\alpha u\|_{L^2(\Omega)}$
$\|\cdot\|_{H^k(\Omega)}$	norm in $H^k(\Omega)$, $\|u\|_{H^k(\Omega)} \coloneqq \|u\|_{L^2(\Omega)} + \sum\limits_{\ell=1}^{k} \|u\|_{H^\ell(\Omega)}$
$\|\cdot\|_{\mathscr{L}(U,V)}$	operator norm: $\|A\|_{\mathscr{L}(U,V)} \coloneqq \sup\limits_{u\in U} \frac{\|Au\|_V}{\|u\|_U} = \sup\limits_{\|u\|_U=1} \|Au\|_V$
$\|u\|_{C^k(0,T;V)}$	norm in $C^k(0,T;V)$, $\|u\|_{C^k(0,T;V)} \coloneqq \max\limits_{t\in[0,T]} \|u(t)\|_V$
$\|u\|_{L^p(0,T;V)}$	norm in $L^p(0,T;V)$, $\|u\|_{L^p(0,T;V)} \coloneqq \left(\int_0^T \|u(t)\|_V^p \ \mathrm{d}t\right)^{1/p}$
$(u,v)_{L^2(\Omega)}$	scalar product in Hilbert space $L^2(\Omega)$, $(u,v)_{L^2(\Omega)} \coloneqq \int_\Omega uv \ \mathrm{d}\mathbf{x}$
$(u,v)_{H^1(\Omega)}$	scalar prodcut in $H^1(\Omega)$, $(u,v)_{H^1(\Omega)} \coloneqq \int_\Omega (uv + \nabla u \cdot \nabla v) \ \mathrm{d}\mathbf{x}$

Table B.5.: Inner products, norms, semi-norms and duality pairings.

Bibliography

[AB73] Anderson, Ned ; Björck, Åke: A new high order method of regula falsi type for computing a root of an equation. In: *BIT Numerical Mathematics* 13 (1973), Nr. 3, 253–264. http://dx.doi.org/10.1007/BF01951936. – DOI 10.1007/BF01951936. – ISSN 1572–9125

[AD99] Ambrosio, Luigi ; Dancer, Norman: *Calculus of variations and partial differential equations*. Springer, 1999. http://dx.doi.org/10.1007/978-3-642-57186-2. DOI 10.1007/978–3–642–57186–2

[ADB11] Ausas, Roberto F. ; Dari, Enzo A. ; Buscaglia, Gustavo C.: A geometric mass-preserving redistancing scheme for the level set function. In: *International Journal for Numerical Methods in Fluids* 65 (2011), Nr. 8, 989–1010. http://dx.doi.org/10.1002/fld.2227. – DOI 10.1002/fld.2227. – ISSN 1097–0363

[Alt12] Alt, Hans W.: *Lineare Funktionalanalysis - Eine anwendungsorientierte Einführung*. Springer Berlin Heidelberg, 2012. http://dx.doi.org/10.1007/978-3-642-22261-0. DOI 10.1007/978–3–642–22261–0

[APB00] Angelis, E. de ; Preziosi, L. ; Bellomo, N.: Advection-diffusion models for solid tumour evolution in vivo and related free boundary problems. In: *Mathematical Models & Methods in Applied Sciences* 10 (2000), Nr. 3, 379. http://search.ebscohost.com/login.aspx?direct=true&db=egs&AN=6620050&site=ehost-live. – ISSN 02182025

[Bän01] Bänsch, Eberhard: Finite element discretization of the Navier–Stokes equations with a free capillary surface. In: *Numerische Mathematik* 88 (2001), Nr. 2, 203–235. http://dx.doi.org/10.1007/PL00005443. – DOI 10.1007/PL00005443. – ISSN 0945–3245

[Bas12] Basting, Christopher: *Enforcing the Eikonal equation as a constraint in finite element level set methods*, University of Erlangen-Nürnberg, Diplomarbeit, 2012

[Bas16] Basting, Steffen: *An interface fitted finite element method for multiphysics simulations*, University of Erlangen-Nürnberg, Diss., 2016

[BGL05] Benzi, Michele ; Golub, Gene H. ; Liesen, Jörg: Numerical solution of saddle point problems. In: *ACTA NUMERICA* 14 (2005), 1–137. http://dx.doi.org/10.1017/S0962492904000212. – DOI 10.1017/S0962492904000212

[BGS04] Bochev, Pavel B. ; Gunzburger, Max D. ; Shadid, John N.: Stability of the {SUPG} finite element method for transient advection–diffusion problems.

In: *Computer Methods in Applied Mechanics and Engineering* 193 (2004), Nr. 23–26, 2301 - 2323. http://dx.doi.org/10.1016/j.cma.2004.01.026. – DOI 10.1016/j.cma.2004.01.026. – ISSN 0045–7825

[BH04] Burman, Erik ; Hansbo, Peter: Edge stabilization for Galerkin approximations of convection–diffusion–reaction problems. In: *Computer Methods in Applied Mechanics and Engineering* 193 (2004), Nr. 15–16, 1437 - 1453. http://dx.doi.org/10.1016/j.cma.2003.12.032. – DOI 10.1016/j.cma.2003.12.032

[BK13] Basting, Christopher ; Kuzmin, Dmitri: A minimization-based finite element formulation for interface-preserving level set reinitialization. In: *Computing* 95 (2013), Nr. 1, 13-25. http://dx.doi.org/10.1007/s00607-012-0259-z. – DOI 10.1007/s00607–012–0259–z. – ISSN 0010–485X

[BK14] Basting, Christopher ; Kuzmin, Dmitri: Optimal control for mass conservative level set methods. In: *Journal of Computational and Applied Mathematics* 270 (2014), 343 - 352. http://dx.doi.org/10.1016/j.cam.2013.12.040. – DOI 10.1016/j.cam.2013.12.040. – ISSN 0377–0427

[BKS16] Basting, Christopher ; Kuzmin, Dmitri ; Shadid, John N.: Optimal control for reinitialization in finite element level set methods. In: *International Journal for Numerical Methods in Fluids* (2016). http://dx.doi.org/10.1002/fld.4348. – DOI 10.1002/fld.4348. – ISSN 1097–0363

[Bur10] Burman, Erik: Consistent SUPG-method for transient transport problems: stability and convergence. In: *Computer Methods in Applied Mechanics and Engineering* 199 (2010), Nr. 17–20, 1114 - 1123. http://dx.doi.org/10.1016/j.cma.2009.11.023. – DOI 10.1016/j.cma.2009.11.023. – ISSN 0045–7825

[BW13] Basting, Steffen ; Weismann, Martin: A hybrid level set–front tracking finite element approach for fluid–structure interaction and two-phase flow applications. In: *Journal of Computational Physics* 255 (2013), 228 - 244. http://dx.doi.org/10.1016/j.jcp.2013.08.018. – DOI 10.1016/j.jcp.2013.08.018. – ISSN 0021–9991

[Cho93] Chopp, David L.: Computing minimal surfaces via level set curvature flows. In: *Journal of Computational Physics* 106 (1993), Nr. 1, 77 - 91. http://dx.doi.org/10.1006/jcph.1993.1092. – DOI 10.1006/jcph.1993.1092. – ISSN 0021–9991

[Cho01] Chopp, David L.: Some improvements of the fast marching methods. In: *SIAM Journal on Scientific Computing* 23 (2001), 230-244. http://dx.doi.org/10.1137/S106482750037617X. – DOI 10.1137/S106482750037617X

[CIL92] Crandall, Michael G. ; Ishii, Hitoshi ; Lions, Pierre-Louis: User's guide to viscosity solutions of second order partial differential equations. In: *Bull. Amer. Math. Soc.* 27 (1992), 1-67. http://dx.doi.org/10.1090/S0273-0979-1992-00266-5. – DOI 10.1090/S0273–0979–1992–00266–5

[CT08] Cheng, Li-Tien ; Tsai, Yen-Hsi: Redistancing by flow of time dependent Eikonal equation. In: *Journal of Computational Physics* 227 (2008), Nr. 8, 4002 - 4017. http://dx.doi.org/10.1016/j.jcp.2007.12.018. – DOI 10.1016/j.jcp.2007.12.018. – ISSN 0021–9991

[DH03] Donea, J. ; Huerta, A.: *Finite element methods for flow problems*. Wiley, 2003. – ISBN 9780471496663

[DHO+14] Denner, Fabian ; Heul, Duncan R. d. ; Oud, Guido T. ; Villar, Millena M. ; Silveira Neto, Aristeu da ; Wachem, Berend G.: Comparative study of mass-conserving interface capturing frameworks for two-phase flows with surface tension. In: *International Journal of Multiphase Flow* 61 (2014), 37 - 47. http://dx.doi.org/10.1016/j.ijmultiphaseflow.2013.12.011. – DOI 10.1016/j.ijmultiphaseflow.2013.12.011. – ISSN 0301–9322

[DMAW98] D. M. Anderson, G. B. M. ; Wheeler, A. A.: Diffuse-interface methods in fluid mechanics. In: *Annual Review of Fluid Mechanics* 30 (1998), xiii-691. http://dx.doi.org/10.1146/annurev.fluid.30.1.139. – DOI 10.1146/annurev.fluid.30.1.139

[Dob10] Dobrowolski, Manfred: *Angewandte Funktionalanalysis*. Springer Berlin Heidelberg, 2010. http://dx.doi.org/10.1007/978-3-642-15269-6. DOI 10.1007/978–3–642–15269–6

[DPE12] Di Pietro, Daniele A. ; Ern, Alexandre: *Mathematical aspects of discontinuous galerkin methods*. Springer, 2012. http://dx.doi.org/10.1007/978-3-642-22980-0. DOI 10.1007/978–3–642–22980–0

[DPLFP06] Di Pietro, Daniele A. ; Lo Forte, Stefania ; Parolini, Nicola: Mass preserving finite element implementations of the level set method. In: *Applied Numerical Mathematics* 56 (2006), Nr. 9, 1179 - 1195. http://dx.doi.org/10.1016/j.apnum.2006.03.003. – DOI 10.1016/j.apnum.2006.03.003. – ISSN 0168–9274

[DT80] *Kapitel* A finite element method for the simulation of a Rayleigh-Taylor instability. In: Dervieux, A. ; Thomasset, F.: *Approximation methods for Navier-Stokes problems*. Berlin, Heidelberg : Springer Berlin Heidelberg, 1980. – ISBN 978–3–540–38550–9, 145–158

[Dzi90] Dziuk, G.: An algorithm for evolutionary surfaces. In: *Numerische Mathematik* 58 (1990), Nr. 1, 603–611. http://dx.doi.org/10.1007/BF01385643. – DOI 10.1007/BF01385643. – ISSN 0945–3245

[EG04] Ern, Alexandre ; Guermond, Jean-Luc: *Theory and practice of finite elements*. Springer New York, 2004. http://dx.doi.org/10.1007/978-1-4757-4355-5. DOI 10.1007/978–1–4757–4355–5

[EG14] Esser, Patrick ; Grande, Jörg: An accurate and robust finite element level set redistancing method. In: *IMA Journal of Numerical Analysis* (2014). http://dx.doi.org/10.1093/imanum/dru052. – DOI 10.1093/imanum/dru052

[EGK11] Eck, C. ; Garcke, H. ; Knabner, P.: *Mathematische Modellierung*. Springer, 2011. – 1–523 S. http://dx.doi.org/10.1007/978-3-642-18424-6. DOI 10.1007/978–3–642–18424–6

[EMC07] Elias, Renato N. ; Martins, Marcos A. D. ; Coutinho, Alvaro L. G. A.: Simple finite element-based computation of distance functions in unstructured grids. In: *International Journal for Numerical Methods in Engineering* 72 (2007), Nr. 9, 1095–1110. http://dx.doi.org/10.1002/nme.2079. – DOI 10.1002/nme.2079. – ISSN 1097–0207

[Eva98] Evans, Lawrence C.: *Partial differential equations*. Graduate Studies in Mathematics. Oxford University Press, 1998

[Gal11] Galdi, G. P.: *An introduction to the mathematical theory of the Navier-Stokes equations*. Springer New York, 2011. http://dx.doi.org/10.1007/978-0-387-09620-9. DOI 10.1007/978–0–387–09620–9

[GMT07] Ganesan, Sashikumaar ; Matthies, Gunar ; Tobiska, Lutz: On spurious velocities in incompressible flow problems with interfaces. In: *Computer Methods in Applied Mechanics and Engineering* 196 (2007), Nr. 7, 1193 - 1202. http://dx.doi.org/10.1016/j.cma.2006.08.018. – DOI 10.1016/j.cma.2006.08.018. – ISSN 0045–7825

[GP08] Guermond, Jean-Luc ; Popov, Bojan: L1-minimization methods for Hamilton–Jacobi equations: the one-dimensional case. In: *Numerische Mathematik* 109 (2008), Nr. 2, 269-284. http://dx.doi.org/10.1007/s00211-008-0142-1. – DOI 10.1007/s00211–008–0142–1. – ISSN 0029–599X

[GR11] Gross, Sven ; Reusken, Arnold: *Numerical methods for two-phase incompressible flows*. Springer, 2011. http://dx.doi.org/10.1007/978-3-642-19686-7. DOI 10.1007/978–3–642–19686–7

[Har77] Harten, Amiram: The artificial compression method for computation of shocks and contact discontinuities. I. Single conservation laws. In: *Communications on Pure and Applied Mathematics* 30 (1977), Nr. 5, 611–638. http://dx.doi.org/10.1002/cpa.3160300506. – DOI 10.1002/cpa.3160300506. – ISSN 1097–0312

[HMS06] Hogea, Cosmina S. ; Murray, Bruce T. ; Sethian, James A.: Simulating complex tumor dynamics from avascular to vascular growth using a general level-set method. In: *Journal of Mathematical Biology* 53 (2006), Nr. 1, 86-134. http://dx.doi.org/10.1007/s00285-006-0378-2. – DOI 10.1007/s00285–006–0378–2

[HMS08] Hartmann, Daniel ; Meinke, Matthias ; Schröder, Wolfgang: Differential equation based constrained reinitialization for level set methods. In: *Journal of Computational Physics* 227 (2008), Nr. 14, 6821 - 6845. http://dx.doi.org/10.1016/j.jcp.2008.03.040. – DOI 10.1016/j.jcp.2008.03.040. – ISSN 0021–9991

[HMS10] Hartmann, Daniel ; Meinke, Matthias ; Schröder, Wolfgang: The constrained reinitialization equation for level set methods. In: *Journal of Computational Physics* 229 (2010), Nr. 5, 1514 - 1535. http://dx.doi.org/http://doi.org/10.1016/j.jcp.2009.10.042. – DOI http://doi.org/10.1016/j.jcp.2009.10.042. – ISSN 0021–9991

[HN81] Hirt, C.W ; Nichols, B.D: Volume of fluid (VOF) method for the dynamics of free boundaries. In: *Journal of Computational Physics* 39 (1981), Nr. 1, 201 - 225. http://dx.doi.org/10.1016/0021-9991(81)90145-5. – DOI 10.1016/0021–9991(81)90145–5. – ISSN 0021–9991

[HTK+07] Hysing, S. ; Turek, S. ; Kuzmin, D. ; Parolini, N. ; Burman, E. ; Ganesan, S. ; Tobiska, L.: Proposal for quantitative benchmark computations of bubble dynamics / Dortmund University of Technology. Version: 2007. http://www.featflow.de/media/bubble/HysingTurekKuzminParoliniBurmanGanesanTobiska2007.pdf. 2007. – Forschungsbericht

[Hym84] Hyman, James M.: Numerical methods for tracking interfaces. In: *Physica D: Nonlinear Phenomena* 12 (1984), Nr. 1, 396 - 407. http://dx.doi.org/10.1016/0167-2789(84)90544-X. – DOI 10.1016/0167–2789(84)90544–X. – ISSN 0167–2789

[Hys07] Hysing, Shu-Ren: *Numerical simulations of immiscible fluids with FEM level set techniques*, University of Dortmund, Diss., 2007

[JCT07] Jung, Y. ; Chu, K. T. ; Torquato, S.: A variational level set approach for surface area minimization of triply-periodic surfaces. In: *J. Comput. Phys.* 223 (2007), Mai, Nr. 2, 711–730. http://dx.doi.org/10.1016/j.jcp.2006.10.007. – DOI 10.1016/j.jcp.2006.10.007. – ISSN 0021–9991

[JN11] John, Volker ; Novo, Julia: Error analysis of the SUPG finite element discretization of evolutionary convection-diffusion-reaction equations. In: *SIAM J. Numer. Anal.* 49 (2011), 1149-1176. http://dx.doi.org/10.1137/100789002. – DOI 10.1137/100789002

[KA03] Knabner, P. ; Angermann, L.: *Numerical methods for elliptic and parabolic partial differential equations*. Springer, 2003 (Texts in Applied Mathematics Series). http://dx.doi.org/10.1007/b97419. DOI 10.1007/b97419. – ISBN 9781441930040

[KAFB11] Kees, C.E. ; Akkerman, I. ; Farthing, M.W. ; Bazilevs, Y.: A conservative level set method suitable for variable-order approximations and unstructured meshes. In: *Journal of Computational Physics* 230 (2011), Nr. 12, 4536 - 4558. http://dx.doi.org/10.1016/j.jcp.2011.02.030. – DOI 10.1016/j.jcp.2011.02.030. – ISSN 0021–9991

[KB13] Knabner, Peter ; Barth, Wolf: *Lineare Algebra*. Bd. 1. Springer Berlin Heidelberg, 2013. http://dx.doi.org/10.1007/978-3-642-32186-3. DOI 10.1007/978–3–642–32186–3

[KH15] Kuzmin, Dmitri ; Hämäläinen, Jari: *Finite element methods for computational fluid dynamics: A practical guide*. SIAM, 2015 (Computational science and engineering). http://bookstore.siam.org/cs14/

[KLR+12] Kirby, Robert C. ; Logg, Anders ; Rognes, Marie E. ; Terrel, Andy R. ; Mardal, Kent-Andre ; Wells, Garth N. ; Ølgaard, Kristian B. ; Knepley, Matthew G. ; Scott, L. R. ; Hake, Johan ; Logg, Anders (Hrsg.) ; Mardal, Kent-Andre (Hrsg.) ; Wells, Garth (Hrsg.): *The FEniCS book - Automated solution of differential equations by the finite element method*. Bd. 84. Springer Berlin Heidelberg, 2012. http://dx.doi.org/10.1007/978-3-642-23099-8. DOI 10.1007/978–3–642–23099–8

[Kuz10] Kuzmin, D.: *A guide to numerical methods for transport equations*. http://www.mathematik.uni-dortmund.de/~kuzmin/cfdbook.html. Version: 2010

[Kuz13] Kuzmin, Dmitri: An optimization-based approach to enforcing mass conservation in level set methods. In: *Journal of Computational and Applied Mathematics* (2013), -. http://dx.doi.org/10.1016/j.cam.2013.09.009. – DOI 10.1016/j.cam.2013.09.009. – ISSN 0377–0427

[LD09] Lesage, Anne-Cecile ; Dervieux, Alain: Conservation correction by dual level set. Version: 2009. http://hal.inria.fr/inria-00430191. 2009. – Rapport de recherche. – 29 S.

[LT05] Larsson, Stig ; Thomée, Vidar: *Partielle Differentialgleichungen und numerische Methoden*. Springer Berlin Heidelberg, 2005 http://www.springerlink.com/content/978-3-540-20823-5/. – ISBN 9783540208235

[LXGF10] Li, Chunming ; Xu, Chenyang ; Gui, Changfeng ; Fox, M.D.: Distance regularized level set evolution and its application to image segmentation. In: *Image Processing, IEEE Transactions on* 19 (2010), dec., Nr. 12, 3243 -3254. http://dx.doi.org/10.1109/TIP.2010.2069690. – DOI 10.1109/TIP.2010.2069690. – ISSN 1057–7149

[MBD06] Mut, Fernando ; Buscaglia, Gustavo C. ; Dari, Enzo A.: A new mass-conserving algorithm for level set redistancing on unstructured meshes. In: *Journal of Applied Mechanics* 73 (2006), S. 1011–1016

[OF03] Osher, S. ; Fedkiw, R.: *Applied Mathematical Sciences*. Bd. 153: *Level set methods and dynamic implicit surfaces*. Springer, 2003. – 273 S. http://dx.doi.org/10.1007/b98879. DOI 10.1007/b98879

[OK05] Olsson, Elin ; Kreiss, Gunilla: A conservative level set method for two phase flow. In: *Journal of Computational Physics* 210 (2005), Nr. 1, 225 - 246. http:

//dx.doi.org/10.1016/j.jcp.2005.04.007. – DOI 10.1016/j.jcp.2005.04.007. – ISSN 0021–9991

[OKZ07] Olsson, Elin ; Kreiss, Gunilla ; Zahedi, Sara: A conservative level set method for two phase flow II. In: *Journal of Computational Physics* 225 (2007), Nr. 1, 785 - 807. http://dx.doi.org/10.1016/j.jcp.2006.12.027. – DOI 10.1016/j.jcp.2006.12.027. – ISSN 0021–9991

[OS88] Osher, Stanley ; Sethian, James A.: Fronts propagating with curvature-dependent speed: Algorithms based on Hamilton-Jacobi formulations. In: *Journal of Computational Physics* 79 (1988), Nr. 1, 12 - 49. http://dx.doi.org/10.1016/0021-9991(88)90002-2. – DOI 10.1016/0021–9991(88)90002–2. – ISSN 0021–9991

[Par04] Parolini, Nicola: *Computational fluid dynamics for naval engineering problems*. Lausanne, École polytechnique fédérale de Lausanne, Diss., 2004. http://dx.doi.org/10.5075/epfl-thesis-3138. – DOI 10.5075/epfl–thesis–3138

[PMO+99] Peng, Danping ; Merriman, Barry ; Osher, Stanley ; Zhao, Hongkai ; Kang, Myungjoo: A PDE-based fast local level set method. In: *Journal of Computational Physics* 155 (1999), Nr. 2, 410 - 438. http://dx.doi.org/10.1006/jcph.1999.6345. – DOI 10.1006/jcph.1999.6345. – ISSN 0021–9991

[PSVW05] Pijl, S. P. d. ; Segal, A. ; Vuik, C. ; Wesseling, P.: A mass-conserving level-set method for modelling of multi-phase flows. In: *International Journal for Numerical Methods in Fluids* 47 (2005), Nr. 4, 339–361. http://dx.doi.org/10.1002/fld.817. – DOI 10.1002/fld.817. – ISSN 1097–0363

[QV08] Quarteroni, Alfio ; Valli, Alberto: *Numerical approximation of partial differential equations*. Springer, 2008 http://www.springer.com/mathematics/analysis/book/978-3-540-85267-4

[Reu13] Reusken, Arnold: A finite element level set redistancing method based on gradient recovery. In: *SIAM Journal on Numerical Analysis* 51 (2013), Nr. 5, 2723-2745. http://dx.doi.org/10.1137/120895433. – DOI 10.1137/120895433

[RL11] Reusken, Arnold ; Loch, Eva: *On the accuracy of the level set SUPG method for approximating interfaces*. http://publications.rwth-aachen.de/record/47338. Version: 2011

[RS00] Russo, Giovanni ; Smereka, Peter: A remark on computing distance functions. In: *Journal of Computational Physics* 163 (2000), Nr. 1, 51 - 67. http://dx.doi.org/10.1006/jcph.2000.6553. – DOI 10.1006/jcph.2000.6553. – ISSN 0021–9991

[Set96a] Sethian, J. A.: A fast marching level set method for monotonically advancing fronts. In: *Proceedings of the National Academy of Sciences of the United States of America* 93 (1996), S. 1591–1595

[Set96b] Sethian, James A.: Theory, algorithms, and applications of level set methods for propagating interfaces. In: *Acta Numerica* 5 (1996), 1, 309–395. http://dx.doi.org/10.1017/S0962492900002671. – DOI 10.1017/S0962492900002671. – ISSN 1474–0508

[Set99a] Sethian, J.: Fast marching methods. In: *SIAM Review* 41 (1999), Nr. 2, 199-235. http://dx.doi.org/10.1137/S0036144598347059. – DOI 10.1137/S0036144598347059

[Set99b] Sethian, J.A.: *Level set methods and fast marching methods: Evolving interfaces in computational geometry, fluid mechanics, computer vision, and materials science*. Cambridge University Press, 1999 http://math.berkeley.edu/~sethian/2006/Publications/Book/2006/book_1999.html

[Smo01] Smolianski, Anton: *Numerical modeling of two-fluid interfacial flows*, University of Jyväskylä, Diss., 2001

[SOW05] Smith, Kurt A. ; Ottino, Julio M. ; Warren, Patrick B.: Simple representation of contact-line dynamics in a level-set model of an immiscible fluid interface. In: *Industrial & Engineering Chemistry Research* 44 (2005), Nr. 5, 1194-1198. http://dx.doi.org/10.1021/ie0498605. – DOI 10.1021/ie0498605

[SP00] Sussman, Mark ; Puckett, Elbridge G.: A coupled level set and volume-of-fluid method for computing 3D and axisymmetric incompressible two-phase flow. In: *Journal of Computational Physics* 162 (2000), Nr. 2, 301 - 337. http://dx.doi.org/http://dx.doi.org/10.1006/jcph.2000.6537. – DOI http://dx.doi.org/10.1006/jcph.2000.6537. – ISSN 0021–9991

[SSO94] Sussman, Mark ; Smereka, Peter ; Osher, Stanley: A level set approach for computing solutions to incompressible two-phase flow. In: *Journal of Computational Physics* 114 (1994), 146-159. http://dx.doi.org/10.1006/jcph.1994.1155. – DOI 10.1006/jcph.1994.1155

[TE00] Tornberg, Anna-Karin ; Engquist, Björn: A finite element based level-set method for multiphase flow applications. In: *Computing and Visualization in Science* 3 (2000), 93-101. http://dx.doi.org/10.1007/s007910050056. – ISSN 1432–9360

[Tor00] Tornberg, Anna-Karin: *Interface tracking methods with application to multiphase flows*, Royal Instituyte of Technology, Department of Numerical Analysis and Computing Science, Diss., 2000. http://www.nada.kth.se/utbildning/forsk.utb/avhandlingar/dokt/tornberg000512.pdf

[Trö10] Tröltzsch, Fredi: *Optimal control of partial differential equations*. American Mathematical Society, 2010 (Graduate Studies in Mathematics). http://bookstore.ams.org/gsm-112/. – ISBN 0821849042

[Tsi94] Tsitsiklis, J. N.: Efficient algorithms for globally optimal trajectories. In: *Proceedings of 1994 33rd IEEE Conference on Decision and Control* Bd. 2, 1994, 1368-1373 vol.2

[Tur99] Turek, Stefan: *Efficient solvers for incompressible flow problems: an algorithmic and computational approach*. Bd. 6. Springer-Verlag, Berlin, 1999 http://www.springer.com/cn/book/9783642635731

[UKO16] Utz, Thomas ; Kummer, Florian ; Oberlack, Martin: Interface-preserving level-set reinitialization for DG-FEM. In: *International Journal for Numerical Methods in Fluids* (2016), n/a–n/a. http://dx.doi.org/10.1002/fld.4344. – DOI 10.1002/fld.4344. – ISSN 1097–0363

[Vex12] Vexler, B.: *Optimierung mit partiellen Differentialgleichungen*. Vorlesungsskriptum, 04 2012

[Vin10] Vinter, Richard: *Optimal control*. Birkhäuser Boston, 2010. http://dx.doi.org/10.1007/978-0-8176-8086-2. DOI 10.1007/978–0–8176–8086–2

[Vog06] Vogt, W.: *Adaptive Verfahren zur numerischen Quadratur und Kubatur*. Preprint No. M 1/06, IfMath TU Ilmenau. https://www.tu-ilmenau.de/math/forschung/preprints/. Version: 2006

[VSC11] Ville, Laurence ; Silva, Luisa ; Coupez, Thierry: Convected level set method for the numerical simulation of fluid buckling. In: *International Journal for Numerical Methods in Fluids* 66 (2011), Nr. 3, 324–344. http://dx.doi.org/10.1002/fld.2259. – DOI 10.1002/fld.2259. – ISSN 1097–0363

[Wer09] Werner, Dirk: *Einführung in die höhere Analysis*. Springer Berlin Heidelberg, 2009. http://dx.doi.org/10.1007/978-3-540-79696-1. DOI 10.1007/978–3–540–79696–1

[Zal79] Zalesak, Steven T.: Fully multidimensional flux-corrected transport algorithms for fluids. In: *Journal of Computational Physics* 31 (1979), Nr. 3, 335 - 362. http://dx.doi.org/10.1016/0021-9991(79)90051-2. – DOI 10.1016/0021–9991(79)90051–2. – ISSN 0021–9991

[Zho97] Zhou, Guohui: How accurate is the streamline diffusion finite element method? In: *Mathematics of Computation* 66 (1997), Nr. 217, pp. 31-44. http://www.jstor.org/stable/2153641. – ISSN 00255718